

REMOVAL OF PARTICLES FROM WATER BY DISPERSED AIR FLOTATION

D. Reay

REMOVAL OF FINE PARTICLES FROM WATER  
BY DISPERSED AIR FLOTATION

BY

David Reay

Thesis submitted to the Faculty of Graduate Studies and Research  
in partial fulfilment of the requirements  
for the degree, of Doctor of Philosophy

Department of Chemical Engineering  
McGill University

August 1973

Ph.D.

Chemical Engineering

David Reay

REMOVAL OF FINE PARTICLES FROM WATER  
BY DISPERSED-AIR FLOTATION

Abstract

Flotation rates of very fine glass beads and of styrene divinylbenzene latex particles have been measured as a function of particle size and bubble size using bubbles of diameter less than 100 microns. The flotation rate of glass beads depends strongly on both particle size and bubble size. The observed rate versus size relationships agree quite well with the predictions of a simple hydrodynamic collision model. With latex particles, the effect of bubble size is similar to that found for glass beads but the effect of particle size is very much smaller, particularly at smaller bubble sizes. The latter result can be explained if the simple hydrodynamic model is corrected to take account of electrical attraction between particles and bubbles. More sophisticated hydrodynamic models which ignore electrical forces give no better agreement than the simple model.

A technique is developed for calculating collision efficiency while taking unsteady state drag forces into account. A criterion is derived for predicting when these forces can be neglected without serious error.

On both economic and environmental grounds the large surfactant requirement is shown to be the main reason why froth flotation cannot be used widely for non-selective removal of fine hydrophilic particles from water. A new process called effervescent flotation, which uses surfactant concentrations below one part per million, is proposed and is found to work efficiently.

David Reay

ELIMINATION DE FINES PARTICULES EN SUSPENSIONDANS L'EAU AU MOYEN DE LA FLOTATION PAR AIR DISPERSÉRésumé

Les vitesses de flotation de billes de verre très fines et de particules de latex de divinylbenzene-styrene ont été mesurées en fonction de la dimension des particules et des bulles, en utilisant des bulles de diamètre inférieur à 100 microns. La vitesse de flotation des billes de verre dépend fortement à la fois de la dimension des particules et de celle des bulles. Les relations observées entre la vitesse et les dimensions sont en accord satisfaisant avec les prédictions d'un modèle hydrodynamique simple de collisions. Pour les particules de latex l'effet de la dimension des bulles est semblable à celui trouvé pour les bulles de verre mais l'effet de la dimension des particules est beaucoup plus faible, en particulier pour de très petites bulles. Ce dernier résultat peut être expliqué en corrigeant le modèle hydrodynamique simple de façon à tenir compte des attractions électriques entre particules et bulles. Des modèles hydrodynamiques plus compliqués qui ignorent les forces électriques ne donnent pas un meilleur accord que le modèle simple.

Une methode est mise au point pour le calcul de l'efficacit  des collisions en tenant compte des forces de train e en r gime non stationnaire. Un crit re indiquant jusqu'  quel point l'on peut negliger ces forces est d duit.

Du point de vue  conomique et pour des considerations  cologiques on montre que la n cessit  d'utiliser de grandes quantit s d'agent surfactant est la raison principale qui emp che l'utilisation fr quente de la flotation par mousse pour l' limination non s lective de fines particules hydrophiles en suspension dans l'eau. Un nouveau proc d  appel  flotation par effervescence est propos ; il utilise des concentrations en agent surfactant inf rieures   1 ppm et fonctionne efficacement.

ACKNOWLEDGEMENTS

I wish to acknowledge with gratitude the help I have received from the following people:

My wife Pauline, who helped to analyse the data from the batch cell experiments, assisted me with the illustrations and gave me love, companionship and encouragement at all times;

My supervisor, Dr. G.A. Ratcliff, who supported and encouraged me in this work, and whose shrewd and thoughtful analysis of my ideas was a very important contribution;

Dr. Roland Clift, who supplied the NERSON numerical integration subroutine used in the work reported in Chapters 8 and 11; and Mr. Rashid Maqsood, who supplied programming assistance for that section of the work;

Drs. John Grace and Marty Weber and my fellow graduate student David Fung who, together with Dr. Clift, gave me the benefit of many valuable discussions;

Mr. Bill Hoogendoorn, who spent a great deal of time helping me to rectify the electronic malfunctions of the Celloscope particle counter;

Dr. H.L. Goldsmith of the University Medical Clinic, who allowed me to use his cinéphotomicrography equipment for the work reported in Chapter 6; and Mr. Simon Yu, who assisted me with its operation;

Mr. Andy Homola of the Pulp and Paper Research Institute of Canada, Physical Chemistry Section, who allowed me to use the Zeiss cytospherometer for the zeta potential measurements and who

assisted me with its operation.

I wish also to acknowledge with gratitude the financial support I have received over the past three years from the National Research Council of Canada in the form of a Post Industrial Experience Research Fellowship.

CONTENTS

	<u>Page</u>
ACKNOWLEDGEMENTS	i
CONTENTS	<del>iii</del>
LIST OF FIGURES	viii
LIST OF TABLES	xi
LIST OF EXHIBITS	xii
1. <u>INTRODUCTION</u>	1
1.1 Situations Requiring Removal of Fine Particles from Water	1
1.2 Particle Removal Processes	2
1.3 Objectives of this Project	4
1.4 Closure	5
2. <u>BACKGROUND SURFACE CHEMISTRY AND HYDRODYNAMICS</u>	6
2.1 Electrical Properties of a Solid-Liquid Interface	6
2.2 Surfactants	9
2.3 Adsorption of Ionic Surfactants by Solid Particles	10
2.4 Froth Stability	15
2.5 Motion of Small Bubbles in Surfactant Solutions	17
2.6 Closure	22
3. <u>REVIEW OF PREVIOUS WORK: EXPERIMENTAL STUDIES</u>	23
3.1 Introduction	23
3.2 Effect of Particle Size on Flotation Rate	26
3.3 Effect of Bubble Size on Flotation Rate	28
3.4 Closure	29

	<u>Page</u>
4. <u>REVIEW OF PREVIOUS WORK: THEORETICAL MODELS</u>	30
4.1 Particles not Affected by Brownian Motion	30
4.1.1 Introduction	30
4.1.2 Collision Models	32
4.1.3 Attachment Models	41
4.2 Sub-micron Particles	42
4.3 Closure	42
5. <u>A PRELIMINARY MODEL OF FINE PARTICLE COLLECTION BY SMALL BUBBLES</u>	43
5.1 Introduction	43
5.2 Collision Regime	44
5.3 Diffusion Regime	52
5.4 Comparison of Efficiencies	54
5.5 Alternative Flow Patterns	57
5.5.1 Hadamard-Rybczinski Flow	57
5.5.2 Potential Flow	58
5.6 Closure	61
6. <u>THE CINEPHOTOMICROGRAPHY EXPERIMENTS</u>	62
6.1 Introduction	62
6.2 Equipment and Procedure	62
6.3 Results	68
6.4 Closure	77
7. <u>THE BATCH CELL EXPERIMENTS</u>	78
7.1 Introduction	78
7.2 Equipment	78
7.3 Materials	84
7.4 Preliminary Tests	90

	<u>Page</u>
7.4.1 Settling of Glass Beads	90
7.4.2 Coagulation During Flotation	91
7.4.3 Coagulation of Samples	92
7.4.4 Coagulation During Analysis	93
7.4.5 Coagulation of Latex Prior to Flotation	93
7.4.6 Gas Hold-up in Liquid	93
7.4.7 Variation of Liquid Height with Time	94
7.4.8 Loss of Surfactant with Time	95
7.4.9 Mixing	96
7.4.10 Effect of Stirring on Bubble Size	96
7.5 Experimental Procedure for Flotation Runs	99
7.5.1 Glass Beads	99
7.5.2 SDB Latex	101
7.6 Results	102
7.7 Discussion of Results	119
7.8 Miscellaneous Flotation Runs	120
7.9 Closure	122
8. <u>THE VISCOUS INTERACTION MODEL</u>	124
8.1 Introduction	124
8.2 Development of the Model	125
8.3 Application to Glass Bead Flotation	134
8.4 Application to SDB Latex Flotation;	138
8.5 Closure	148
9. <u>THE BUBBLE SWARM MODEL</u>	149

	<u>Page</u>
10. <u>THE ELECTRICAL ATTRACTION HYPOTHESIS</u>	153
11. <u>A CRITERION FOR SAFE NEGLECT OF UNSTEADY STATE DRAG TERMS IN THE CALCULATION OF COLLISION EFFICIENCY</u>	164
11.1 Introduction	164
11.2 Derivation of the Criterion	165
11.3 Computation of Collision Efficiency Including Unsteady State Drag Terms	171
11.4 Testing of the Criterion	178
11.5 Closure	180
12. <u>ECONOMICS OF DISPERSED AIR FLOTATION</u>	182
12.1 Introduction	182
12.2 Coagulation-Sedimentation	183
12.3 Electroflotation	183
12.4 Flotation with Bubbles Generated at a Porous Distributor	187
12.5 Closure	189
13. <u>EFFERVESCENT FLOTATION</u>	190
13.1 Introduction	190
13.2 Experiment	192
13.3 Discussion	192
13.4 Closure	195
14. <u>CONCLUSIONS</u>	196
15. <u>CLAIMS TO ORIGINAL WORK</u>	199
16. <u>SUGGESTIONS FOR FURTHER RESEARCH</u>	200
NOMENCLATURE	202
REFERENCES	212

APPENDICES

A.	<u>Celloscope Particle Counter</u>	217
A.1.	The Basic Principle	217
A.2	The Instrument	219
A.3	Calibration	225
A.4	Particle Coincidence	231
A.5	Operating Precautions	232
A.6	Repeatability of Counts	233
A.7	Time Required for Analysis	234
B.	<u>Sample Run</u>	235
C.	<u>Force Coefficients in the Viscous Interaction Model</u>	241
C.1	Motion Perpendicular to Line of Centres	241
C.2	Motion Along Line of Centres	242
D.	<u>Computer Programs</u>	251
D.1	The Viscous Interaction Model	251
D.1.1	Backward Integration	251
D.1.2	Forward Integration	252
D.2	Collision Efficiency Calculation with Unsteady State Drag Terms Included	252
E.	<u>Fluid Velocities and Accelerations</u>	260
E.1	Stokes Flow	260
E.2	Potential Flow	262

LIST OF FIGURES

	<u>Page</u>
2.1 Double layer structure at a solid-liquid interface	7
2.2 Adsorption of cationic surfactant on silver iodide	11
2.3 Orientation of surfactant ions on silver iodide surface.	
(a) below point of zero charge	
(b) above point of zero charge	12
2.4 Adsorption of cationic surfactant on polystyrene latex	14
2.5 Correlation of $Y = U/U_{st}$ with Eotvos number	20
2.6 Correlation of $Y = U/U_{st}$ with half-angle $\theta$ subtended by mobile portion of bubble surface	21
4.1 Approach of a particle to a collector	33
4.2 Grazing trajectory	33
4.3 Variation of collision efficiency with Stokes number in Stokes and potential flow (Fint-Howarth model)	37
5.1 Trajectory of particles approaching a bubble	45
5.2 Collision efficiency $E_1$ as a function of $r/R_b$ and $\rho_p/\rho_f$ with Stokes <sup>1</sup> flow (preliminary model)	51
5.3 Collection efficiency $E$ as a function of particle diameter with $D_b = 75$ microns, $\rho_p/\rho_f = 2.5$ and Stokes flow (preliminary model)	56
5.4 Collision efficiency $E_1$ as a function of $r/R_b$ and $\rho_p/\rho_f$ with Hadamard-Rybczinski flow (preliminary model)	59
5.5 Collision efficiency $E_1$ as a function of $r/R_b$ and $\rho_p/\rho_f$ with potential flow (preliminary model)	60
6.1 Miniature flotation cell	63
6.2 Arrangement of cinéphotomicrography equipment (viewed from above)	64
6.3 X versus $d_p$	70

	<u>Page</u>
6.4	Y versus $d_p$ (log-log) 73
6.5	Y versus $d_p$ (linear) 74
6.6	Bubble carrying one particle 76
6.7	Bubble carrying two particles 76
7.1	Batch cell flotation rig; flowsheet 80
7.2	(a) Batch cell; side view
	(b) Batch cell; top view 81
7.3	Batch cells; bubble size distributions (taken from Kalman (7) and Kaufman (45)) 82
7.4	Run G1; $\log P/P_0$ versus time 104
7.5	Run G2; $\log P/P_0$ versus time 105
7.6	Run G3; $\log P/P_0$ versus time 106
7.7	Run G4; $\log P/P_0$ versus time 107
7.8	Run G5; $\log P/P_0$ versus time 108
7.9	Run L1; $\log P/P_0$ versus time 109
7.10	Run L2; $\log P/P_0$ versus time 110
7.11	Run L3; $\log P/P_0$ versus time 111
7.12	Run L4; $\log P/P_0$ versus time 112
7.13	Run L5; $\log P/P_0$ versus time 113
7.14	Glass bead runs; $\log k$ versus $\log d_p$ 114
7.15	SDB latex runs; $\log k$ versus $\log d_p$ 115
7.16	Effects of surfactant and frother concentrations on flotation rate 121
8.1	Viscous interaction model 126
8.2	Viscous interaction model; particle trajectory relative to bubble 132
8.3	Viscous interaction model; rotation of particle and bubble 133

	<u>Page</u>
8.4	Viscous interaction model; collision efficiency versus $d_p/D_b$ for $\rho_p/\rho_f = 2.5$ 135
8.5	Viscous interaction model; comparison of predictions with batch cell glass bead results 137
8.6	Viscous interaction model; comparison of predicted collision efficiency versus bubble size curve with cinéphotomicrography results 139
8.7	Viscous interaction model; comparison of predicted collision efficiency versus particle size curve with cinéphotomicrography results 140
8.8	Viscous interaction model; comparison of predictions with batch cell SDB latex results 141
9.1	Bubble swarm model; $E_1$ versus $r_p/R_b$ 151
10.1	Preliminary model with electrical attraction correction; comparison of predictions with batch cell SDB latex data 160
11.1	Search procedure for locating grazing trajectory 177
11.2	Comparison of collision efficiencies with and without unsteady state drag terms included 179
11.3	Excess pressure at the surface of a sphere; comparison of Stokes and potential flow 181
13.1	Rate of removal of SDB latex particles from water by effervescent flotation. 193
13.2	Particles removed by effervescent flotation (a) no surfactant (b) 0.8 ppm of EHDA-Br 194
A.1	Particle in orifice 218
A.2	Celloscope particle counter; basic schematic 220
A.3	Celloscope particle counter; ancillary instruments 222
A.4	Celloscope particle counter; external view 226
A.5	Celloscope particle counter; log V versus C 227

LIST OF TABLES

		<u>Page</u>
6.1	Particle collection as a function of bubble size	69
6.2	Size distributions of collected particles (A) and particles in suspension (B)	72
6.3	Agglomeration of particles in suspension	72
7.1	Glass bead settling test	91
7.2	Gas hold-up in batch cells	94
7.3	Effect of stirring on bubble size	98
7.4	Batch cell runs; experimental conditions	103
7.5	Glass bead runs; experimental values of $n$ in the relation $E \propto 1/D_b^n$	118
8.1	Viscous interaction model; forward integration results	143
10.1	Preliminary model with electrical attraction correction; collision efficiencies for SDB latex particles	159
B.1	Sample run; total count versus time	236
B.2	Sample run; analysis of size distribution and total count data	239
C.1	Equivalence of force coefficients	246
C.2	Perpendicular force coefficients; parameters for cubic approximation	247
C.3	Parallel force coefficients; parameters for quartic approximation	250

LIST OF EXHIBITS

		<u>Page</u>
7.1	Equipment for batch cell runs	79
7.2	Material for batch cell runs	85
7.3	Glass bead size distribution	86
7.4	Styrene divinylbenzene latex size distribution	87
B.1	Sample run; size distributions of samples	237
D.1	Viscous interaction model; computer program for backwards integration	254
D.2	Viscous interaction model; sample output with backwards integration	255
D.3	Viscous interaction model; computer program for forward integration	256
D.4	Viscous interaction model; sample output with forward integration	257
D.5	Collision efficiency with unsteady state drag terms; computer program	258
D.6	Collision efficiency with unsteady state drag terms; sample output	259

## 1. INTRODUCTION

### 1.1 Situations Requiring Removal of Fine Particles from Water

The following are examples of situations where a separation is required between water and suspended particles which are too fine to settle at an appreciable rate or to be filtered out economically using conventional filter fabrics.

- (a) Removal of fine suspended solids from industrial and municipal waste streams.
- (b) Removal of fine clay particles and micro-organisms from turbid natural surface water to make it potable after chlorination.
- (c) Recovery of single cell protein and algae from culture media.
- (d) Recovery of trace quantities of valuable metals from ores by leaching and precipitation as insoluble salts.
- (e) Precipitation of traces of toxic metals from industrial waste streams.

The particles may range from sub-micron colloids up to a maximum diameter of the order of 20 microns. Particle concentrations are generally several hundred milligrams per litre in cases (a) to (c) above, but may be less than 10 mg/l. in (d) and (e). In cases (a) and (e) where the effluents are discharged to receiving waters the legal requirements to be met by the treated effluents are typically 20 mg/l. maximum for suspended solids and 0.5 mg./l. maximum for toxic metals (1).

treatment process may have to remove more than 95% of the suspended particles. In the other cases lower particle removal efficiencies may suffice.

## 1.2 Particle Removal Processes

The conventional processes for separating fine particles from water are coagulation and dissolved air flotation (2). Typically, these achieve 80 to 90% removal of particulates and may have to be followed by filtration through a bed of finely-graded sand to meet discharge standards. Both require the addition of a flocculant such as lime or alum to neutralise the charge on the particles and to precipitate a floc, e.g. insoluble  $\text{Al}(\text{OH})_3$ , in which the agglomerated particles are trapped. Polyelectrolytes may also be added to provide cross-linking between flocs. In coagulation the particle-laden floc is separated by settling in a large sedimentation basin with a typical residence time of 30 to 60 minutes. In dissolved air flotation air is dissolved in the feed under 4 to 5 atmospheres pressure; when the pressure is released the air precipitates out on and inside the particle-laden flocs and raises their buoyancy. They float up to the surface and are skimmed off. Residence times are low (10 to 20 minutes) so the equipment is compact, but to provide adequate dissolved air a substantial portion of the clarified effluent must be recycled, compressed, saturated with air and mixed with fresh feed. Both coagulation and dissolved air flotation have been used for many years and several more or less empirical design procedures have been developed. They both produce a lime or alum sludge which may present a solid waste disposal problem.

Filtration through a sand bed may be used by itself if the initial particle concentration is low enough. Eventually, the bed becomes so clogged with particles that the available pressure head is unable to sustain an adequate flow and the bed must be cleaned by backwashing with clarified effluent. Either another bed must be supplied in parallel to maintain continuous operation or else adequate buffer storage capacity must be supplied upstream. Capacity must also be provided for storage of backwash water before use. Sand bed filtration has been used for over a hundred years.

In contrast, the use of dispersed air flotation for fine particle removal has been confined largely to the laboratory so far. Most of the work on it has been done in the last ten years, there are no well-established design guidelines and the first large-scale application was only reported in 1968 (3). In this process the particles are adsorbed on small, rising air bubbles, typically of diameters up to 0.1 mm. These bubbles may be generated either by electrolysis (in which case the name "electroflotation" is often used) or by forcing air through a porous plate or through spargers. As they rise through the water they contact particles either through collision or through Brownian diffusion, depending on particle size. At the top they form a scum or froth which can be skimmed off. For particle-bubble attachment to occur the particles must be at least partly hydrophobic. If they are not already in this state in the feed to the flotation unit they must be made so by adding a suitable surfactant.

At first sight this process looks like a straightforward adaptation of the froth flotation process used for about fifty years in mineral dressing, but in fact there are some important physical differences and these will be brought out in subsequent chapters. Laboratory studies with a continuous flow unit (7) indicate that 80 to 90% removal is attainable with 15 to 20 minutes residence time, so performance is roughly comparable with that of dissolved air flotation. Capital costs should be lower since there is no recycling and compression of clarified effluent. Capital costs should also be lower than for coagulation or sand bed filtration since there is no need for a large sedimentation tank or for backwashing. On the other hand, operating costs may be higher for dispersed air flotation if surfactant has to be added. These economic aspects are explored more fully in Chapter 12.

### 1.3 Objectives of this Project

Most research on solid-liquid separation by dispersed air flotation has been directed towards studying the sensitivity of flotation rate to chemical variables such as pH, ionic strength, surfactant type and the chemical nature of the particles. Very little work has been done on the effects of physical variables, yet it is important to know these effects if engineering design and scale-up from laboratory tests is to be done in a scientific manner. This project's attention is focussed on two of the most important physical variables, particle size and bubble size; its objectives are to formulate a theoretical model of bubble-particle interactions which enables

predictions to be made concerning the sensitivity of flotation rate to these variables, and then to test these predictions by measuring flotation rates in laboratory apparatus using particles and bubbles of various sizes.

The practical significance of the project is as follows:

- (a) If particle size is found to have a large effect then it may be possible to control upstream processing, e.g. precipitation conditions, in order to produce a particle size with good flotation characteristics. Alternatively, particle size modification could be carried out in the flotation cell itself, e.g. by coagulation. Reliable quantitative knowledge of the effect of particle size on flotation rate is needed in order to evaluate such alternatives.
- (b) Bubble size is an independent variable under the direct control of the process designer. Furthermore, the cost of the bubble-generating equipment is likely to be a major part of the overall cost of the flotation unit. Hence, any design prepared without a quantitative knowledge of the effect of bubble size on flotation rate is likely to be sub-optimal.

#### 1.4 Closure

The next chapter reviews some topics in surface chemistry and hydrodynamics which are fundamental to a proper understanding of dispersed air flotation.

## 2. BACKGROUND SURFACE CHEMISTRY AND HYDRODYNAMICS

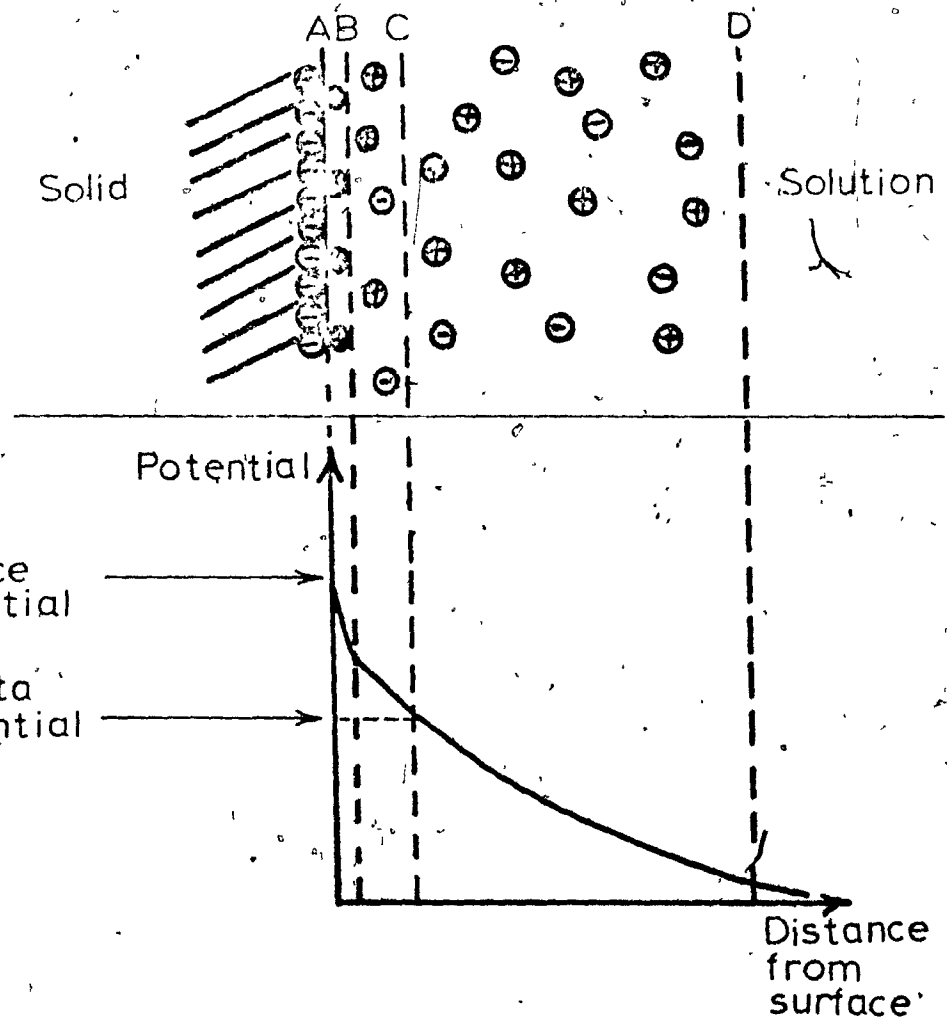
### 2.1 Electrical Properties of a Solid-Liquid Interface

Most solid particles acquire an electrical charge when immersed in water due to one of the following effects.

- (a) Ionization of surface groups, e.g.  $\text{-COOH} \rightarrow \text{COO}^- + \text{H}^+$   
 $\text{-NH}_2 + \text{H}_2\text{O} \rightarrow \text{NH}_3^+ + \text{OH}^-$
- (b) Adsorption of ions from solution. This usually gives the particle a negative charge since anions tend to be less hydrated in solution than cations and so can get closer to the solid surface.
- (c) Loss of ions from the solid surface. For example, AgI may release either  $\text{Ag}^+$  or  $\text{I}^-$  into solution depending on the existing concentration of these ions in solution.

The charge thus created is partly neutralized by a fairly strongly held layer of ions of opposite charge (counter-ions) called the Stern layer (AB in Fig.2.1). These are held partly by electrostatic attraction and partly by Van der Waals forces. The residual potential at plane B is neutralized by a diffuse layer BD which contains ions of both signs but has a preponderance of counter-ions. When the particle moves relative to the surrounding liquid the hydrodynamic shear plane C is a little way outside the Stern layer. The potential of plane C is called the zeta potential. This can be measured since it is proportional to the velocity of the particle in an applied electric field (the electrophoretic mobility). It is not proportional to the surface charge but it is closely related to it.

Figure 2.1  
DOUBLE LAYER STRUCTURE AT A SOLID-LIQUID INTERFACE



The following actions reduce the zeta potential.

- (a) Increasing the ionic strength of the solution. This increases the adsorption of counter-ions in the Stern layer.
- (b) Adding a small quantity of an electrolyte containing multi-valent counter-ions. Their neutralizing effect increases greatly with their charge.
- (c) Adding a small quantity of a surface-active counter-ion. Van der Waals adsorption forces are very strong for surfactants, so again this markedly increases the number of counter-ions in the Stern layer.
- (d) Reducing the surface potential by adjusting the concentration in solution of those ions which determine the surface potential. For example, the pH could be changed if  $H^+$  or  $OH^-$  is potential-determining.

If any of these actions is carried far enough, the adsorbed counter-ions more than balance the surface charge and the sign of the zeta potential is reversed.

Zeta potential is closely related to the stability of a suspension since it is a measure of the electrostatic repulsion between two particles which come close together. Riddick and Ravina (87) present data on the stability of an aqueous suspension of silica particles (average diameter 1.1 microns, average z.p. in distilled water - 30 mV) as a function of zeta potential, with zeta potential changes made by adding electrolyte.

	<u>z.p. (mV)</u>
maximum agglomeration	0 to 3
strong agglomeration	5 to 5
threshold of agglomeration	-10 to -15
threshold of delicate dispersion	-16 to -30
moderate stability	-31 to -40
good stability	-41 to -100

## 2.2 Surfactants

Surfactants are long-chain hydrocarbon molecules or ions with a polar group at one end to give them a limited solubility in water. They have a high free energy in solution due to repulsion between the hydrocarbon chain and the surrounding water-molecules, so if an air-water or solid-water interface is present they congregate at the interface in order to reduce the free energy of the system. As the hydrocarbon chain length increases the solubility in water decreases and the driving force for adsorption at the interface increases.

If the surfactant is an ion the driving force for adsorption on particles also depends on the particle charge. If the particles and surfactant ions have opposite charges the adsorption is strengthened by electrostatic attraction, probably into the Stern layer. If they have the same charge electrostatic repulsion weakens the driving force for adsorption and may even prevent adsorption completely, depending on the magnitude of the particle charge and the hydrocarbon chain length. If the surfactant forms a chemical bond with the particle

surface this also increases the strength of adsorption. An example is the adsorption of xanthate ion on sulphide minerals.

Adsorption of surfactant gives the particle some hydrophobic character since at least part of the hydrocarbon chain is still exposed to water. This makes the particle floatable, because by becoming attached to an air bubble it can replace part of the solid-water interface by a solid-air interface and thereby reduce the system free energy further.

Best flotation results are obtained when the surfactant is strongly adsorbed by the particles, with the natural tendency to adsorption reinforced either by electrostatic attraction or chemical bonding. A surfactant added to make the particles hydrophobic is termed a "collector".

### 2.3 Adsorption of Ionic Surfactants by Solid Particles

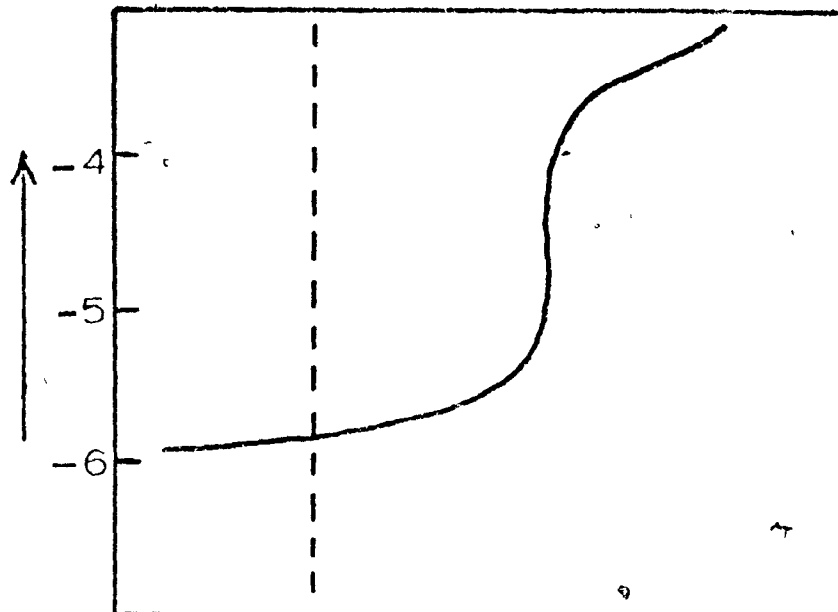
The various stages involved in the adsorption of ionic surfactants by charged inorganic solids when no chemical reactions occur are illustrated by the work of Jaycock and Ottewill (69). They measured the adsorption of dodecylpyridium bromide by negatively-charged silver iodide particles at a series of increasing surfactant concentrations and also measured the floatability and zeta potential of the particles at each surfactant concentration. Their results are presented schematically in Figure 2.2.

Adsorption increased steadily and flotation increased quite rapidly up to the point of zero charge, which occurred at a surfactant concentration of  $4.5 \times 10^{-5}$  M. In this region the surfactant

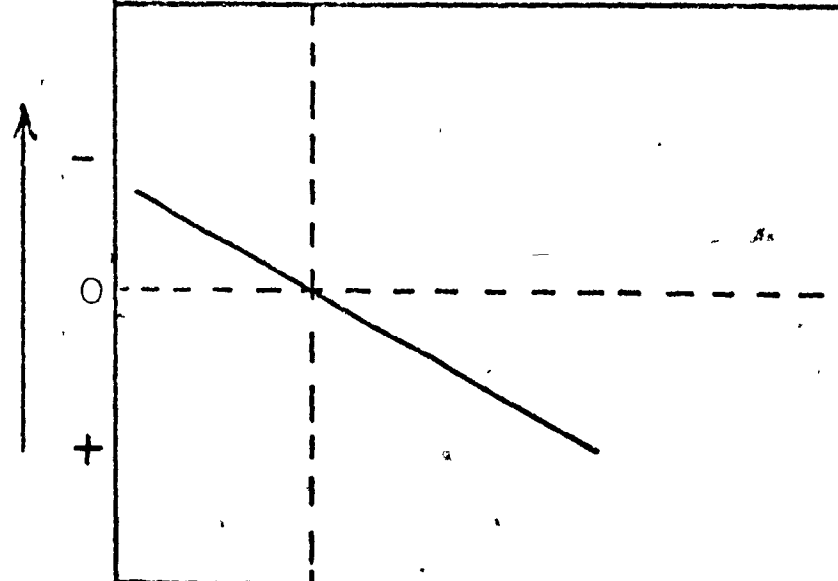
Figure 2.2

ADSORPTION OF CATIONIC SURFACTANT ON SILVER IODIDE

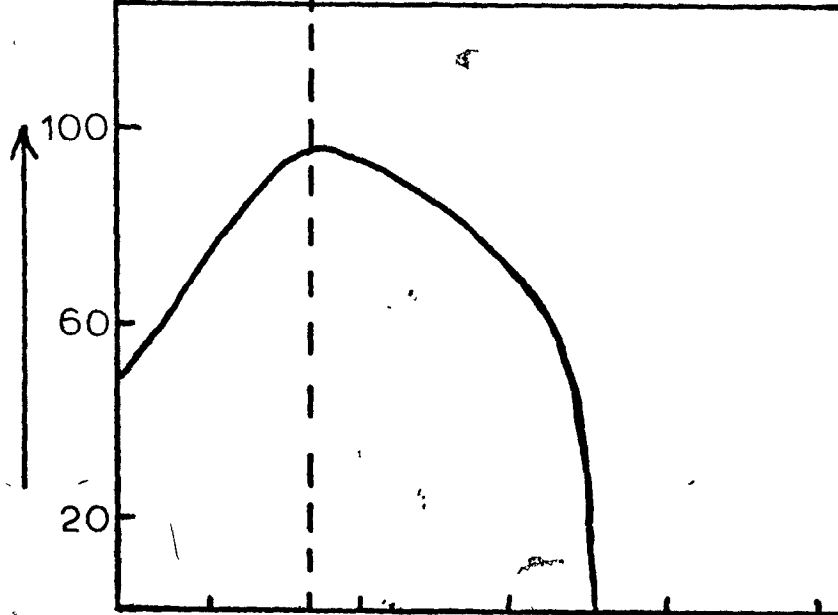
Log  
surfactant  
adsorbed  
per gm.



Zeta  
potential



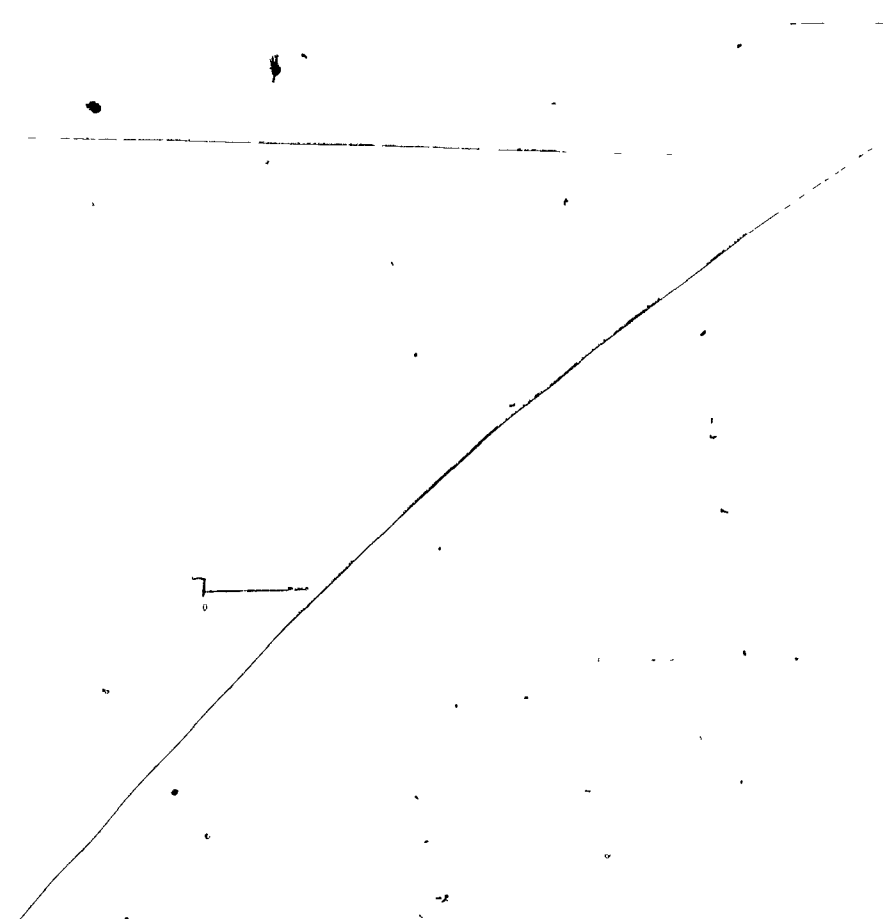
%  
Floated



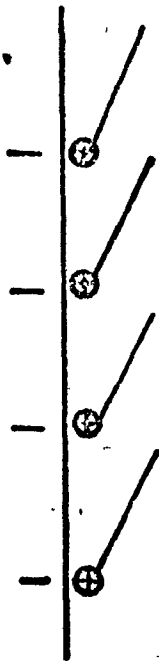
Log molar surfactant  
concentration

Figure 2.3  
ORIENTATION OF SURFACTANT IONS ON SILVER IODIDE SURFACE.

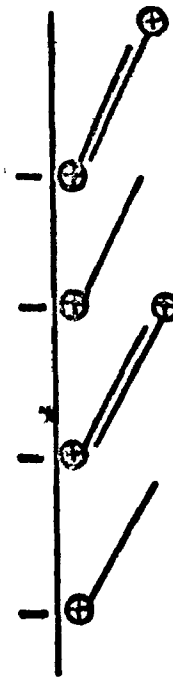
- (A) BELOW POINT OF ZERO CHARGE
- (B) ABOVE POINT OF ZERO CHARGE



(a)



(b)



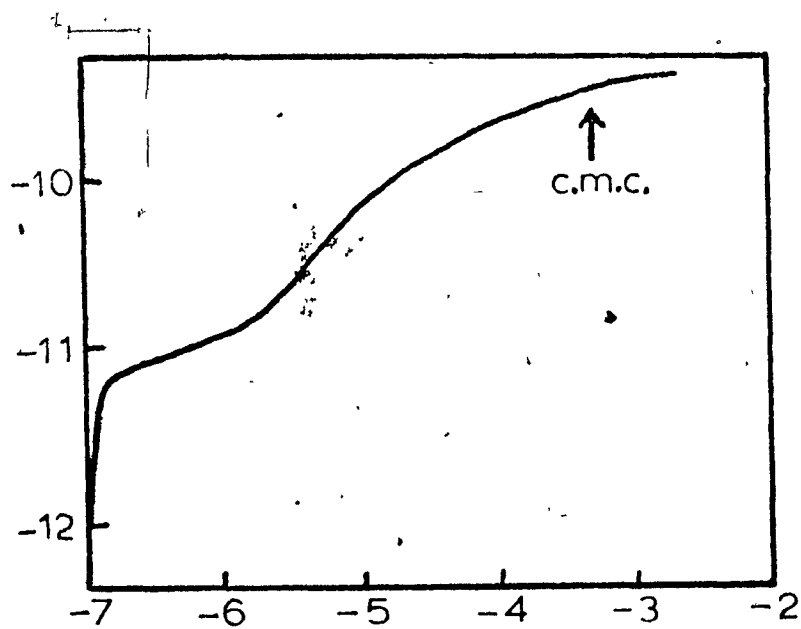
ions were pictured as lying at a small angle to the solid surface (Fig.2.3a). They are not flat because water has an ice-like structure adjacent to a solid surface. Beyond the zero point of charge adsorption continued to increase steadily but flotation decreased. In this region they argued that the additional surfactant ions were being held by Van der Waals attraction between hydrocarbon chains with the polar groups of the additional ions pointing outwards (Fig.2.3b). Thus, the hydrophobicity of the surface would begin to decrease after the point of zero charge had been passed, which accounted for the decrease in floatability. Eventually, at a surfactant concentration just above  $10^{-3}$  M there was a sudden increase in adsorption and floatability dropped to zero. They hypothesised that this corresponded to micelle formation.

Adsorption on latex particles follows a different type of isotherm, as shown by the work of Connor and Ottewill (56). Figure 2.4 shows in schematic form the isotherm obtained by them for the adsorption of hexadecyltrimethylammonium ions on polystyrene latex. The surface of latex particles is largely hydrocarbon with a small percentage of the area containing carboxyl groups which ionise to give the particles a negative charge at intermediate pH. It required only a very small surfactant concentration (about  $10^{-7}$  M) to neutralise the charge on the particles. These initially-adsorbed surfactant ions were held by both electrostatic attraction and Van der Waals bonding of their chains to the hydrocarbon surface. They could not be washed off with distilled water. As the surfactant

---

Figure 2.4  
ADSORPTION OF CATIONIC SURFACTANT ON POLYSTYRENE LATEX

Log moles  
adsorbed  
per cm<sup>2</sup>



Log molar  
surfactant  
concentration

concentration was raised beyond the point of zero charge the amount adsorbed increased much more slowly than before because the Van der Waals attraction between surfactant ion chains and the hydrocarbon surface was now opposed by electrostatic repulsion. These later ions could be washed off quite easily with distilled water. In this region the adsorbed ions were still pictured as isolated chains lying almost flat on the surface, so floatability should still be quite high although not as high as at the point of zero charge. As the surfactant concentration rises above  $10^{-5}$  M there is an increase in the slope of the isotherm. In this region it was thought that association of hydrocarbon chains on the particle surface was beginning to occur. Eventually, at the critical micelle concentration the surface was saturated with close-packed vertically oriented ions and no further adsorption could occur. In this condition (reached between  $10^{-4}$  M and  $10^{-3}$  M) the particles would be hydrophilic and unfloatable. In the region of increased slope leading up to this point the floatability must be continually decreasing as the orientation of the surfactant hydrocarbon chains becomes more vertical.

#### 2.4 Froth Stability

The lifetime of an undisturbed froth depends mainly on two factors:

- (a) The rate of drainage of liquid from the interstices between bubbles.
- (b) The rate of thinning and eventual collapse of the film of liquid separating adjacent bubbles.

If both rates are slow the froth will have a long life and will appear stable.

The first factor depends on the bubble size. Wace, et al. (53) have shown experimentally that the drainage rate is inversely proportional to the square of the bubble diameter, in direct analogy with the flow of liquids through packed beds.

The second factor depends on the surface viscosity. The greater the surface viscosity the greater will be the resistance to thinning (81).

If the collector is adsorbed strongly at the air-water interface, as is the case with fatty acid and amine collectors, it stabilizes the froth by influencing both factors. High surfactant concentration at the interface increases the surface viscosity greatly if the surfactant is not very soluble in water, and the lowering of surface tension caused by the surfactant tends to reduce the bubble size by reducing the buoyancy force needed to detach a bubble from the distributor. However, if the distributor is a porous frit a much more effective way of reducing the bubble size is to add 0.1 to 0.5 per cent of a short-chain alcohol such as ethanol or isopropanol to the water (59). The small, fast-moving alcohol molecules adsorb at the interface while the bubble is being formed and act by preventing coalescence between bubbles growing at adjacent sites. Porous frit distributors give very stable foams when the water above them contains about 40ppm of a long-chain collector and 0.5 vol. per cent of isopropanol; such a system was used in this project for the experimental work to be reported in Chapter 7.

In ore flotation the bubbles are large and stirring is vigorous. The froth would be rather unstable if collectors were used alone, so normally a "frother" is also added. These are usually long-chain alcohols such as terpineol which form molecular penetration complexes with the adsorbed film of collector (81). This increases the rigidity of the film greatly. Short-chain alcohols cannot form complexes with long-chain collectors (62).

### 2.5 Motion of Small Bubbles in Surfactant Solutions

The terminal velocity  $U$  of a rigid sphere of diameter  $D$  and density  $\rho_1$  moving through a fluid of density  $\rho_2$  and viscosity  $\mu$  under the influence of gravity at a Reynolds number  $Re$  less than 0.5 is given by Stokes' Law as

$$U_{st} = \frac{g D^2 |\Delta \rho|}{18 \mu} \quad \text{where } \Delta \rho = \rho_1 - \rho_2$$

If the sphere is not a solid but a second fluid of viscosity  $\mu_1$  immiscible with the first and both fluids are pure then the terminal velocity  $U_H$  is given by the Hadamard-Rybczinski equation

(54) as:

$$U_H = \frac{g D^2 |\Delta \rho|}{6 \mu} \cdot \left( \frac{1 + \gamma}{2 + 3\gamma} \right) \quad \text{where } \gamma = \frac{\mu_1}{\mu}$$

If the sphere is an air bubble and the medium is water  $\gamma \approx 0$  and

$U_H = \frac{g R^2 |\Delta \rho|}{3 \mu} = 1.5 U_{st}$ . The Stokes case has a zero velocity boundary condition at the sphere surface whereas the Hadamard-Rybczinski case

has continuity of tangential stress as the boundary conditions resulting in a moving surface and internal circulation in the fluid sphere. This circulation has been observed experimentally in very pure systems (51).

If a fluid sphere is moving through a medium containing traces of a surface active substance the surfactant will be adsorbed at the sphere surface and swept to the back of the sphere. If the fluid sphere is moving fast enough the front of its surface will contain less surfactant than the back and a surface tension gradient will be set up. This gradient sets up a tangential stress which tends to retard surface motion and internal circulation. Photographs taken by Savic (51) show that in fact the surfactant accumulates in a stagnant cap at the back of the fluid sphere. Circulation persists forward of the cap but is non-existent inside it.

In such a situation the terminal velocity  $U$  of the sphere will be intermediate between  $U_H$  and  $U_{st}$ . Let  $Y = U/U_{st}$ . Then for an air bubble in water  $Y$  will be 1.5 when there is no surfactant in the system and 1.0 when there is enough surfactant for the stagnant cap to completely cover the bubble surface. In the latter case the bubble will behave hydrodynamically as though it is a rigid sphere.

The Eotvos number  $Eo = \frac{g D^2 |\Delta\rho|}{\Delta\sigma}$  is a convenient dimensionless group against which to correlate  $Y$ .  $\Delta\sigma$  is the difference in surface tension between the front and rear stagnation points of the bubble.  $Eo$  characterises the ratio of the gravitational force promoting internal circulation to the surface force retarding it, so we expect  $Y$  to be an increasing function of  $Eo$ . We also expect that the smaller the bubble the smaller will be  $Y$  and the closer will be the approach to rigid sphere behavior.

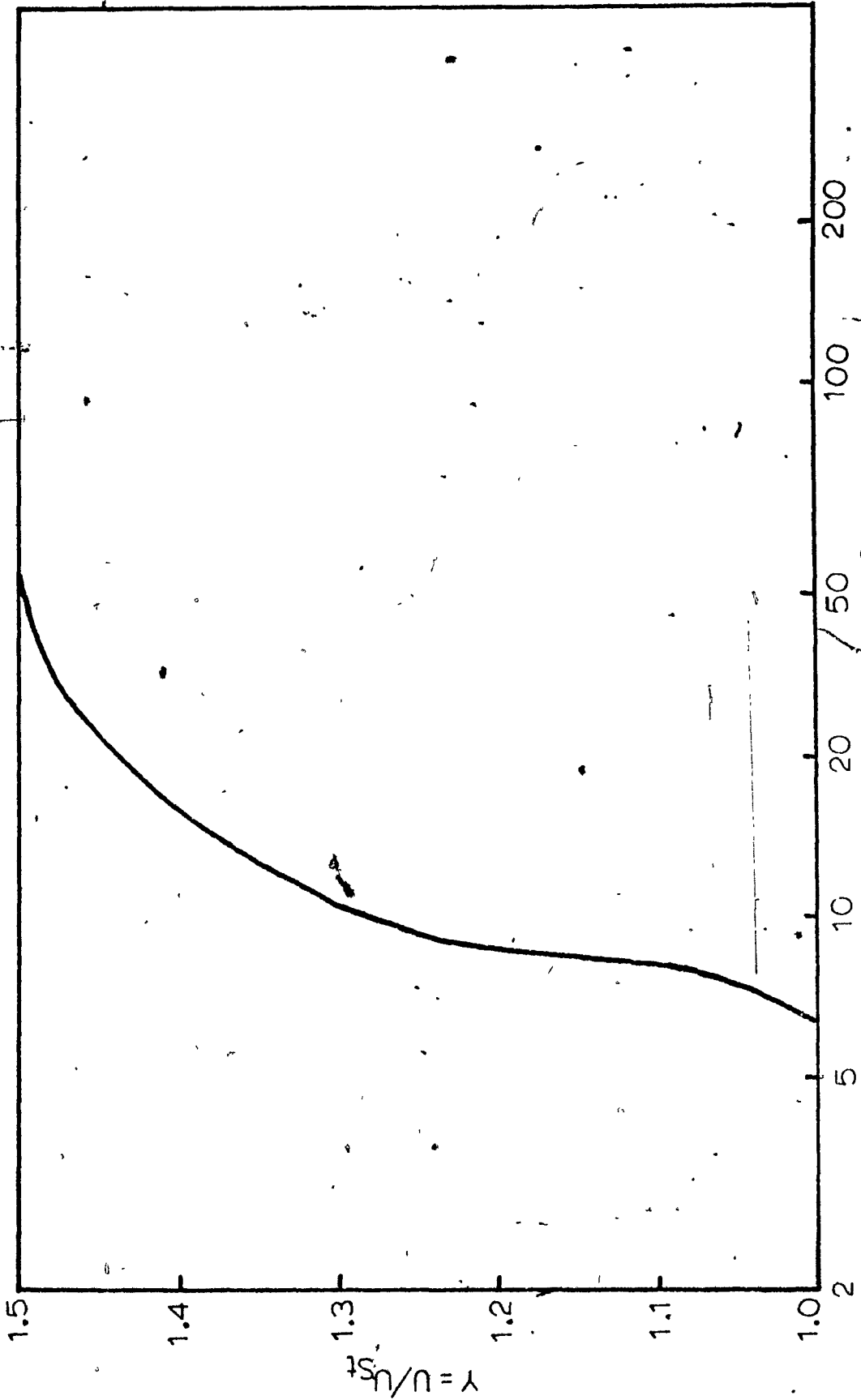
Figure 2.5 is the correlation of  $Y$  with  $E_o$  obtained by Clift, Grace and Weber (60) from the calculations of Davis and Acrivos (52). These calculations are in rough agreement with the experimental data of Bond and Newton (61). Figure 2.6 is the correlation of  $Y$  with the half angle  $\theta$  subtended by the mobile portion of the bubble surface; it also comes from the calculations of Davis and Acrivos.

We are interested in air bubbles of diameter up to 100 microns rising in water. The water will normally contain strong surfactants at concentrations of the order of 20 to 40 ppm, which will reduce the surface tension of water by 5 to 10 dynes/cm. (81). Taking  $\Delta\sigma = 10$  dynes/cm.,  $D_b = 0.01$  cm.,  $|\Delta\rho| = 1$  gm./ml. and  $g = 981$  cm./sec.<sup>2</sup> gives  $E_o \approx 10^{-2}$ . From Figures 2.5 we find  $Y = 1.0$  and from Figure 2.6 we find  $\theta = 0$ . Therefore, the stagnant layer of surfactant ions covers the entire bubble surface; the surface of the bubble is rigid and we have Stokes flow around the bubble.

Bubble diameters as large as 0.3 cm. are common in mineral flotation. This gives  $E_o \approx 10$ ,  $Y = 1.3$  and  $\theta = 110^\circ$ . Of course, the calculations on which Figs. 3.5 and 3.6 are based are not valid for such large bubbles because their Reynolds numbers will be much greater than unity, but nevertheless it will be true that a substantial part of the surface of mineral flotation bubbles will be mobile. The flow pattern around such bubbles will be described best by potential flow (54).

Figure 2.5

CORRELATION OF  $\gamma = U/U_{st}$  WITH EOTVOS NUMBER

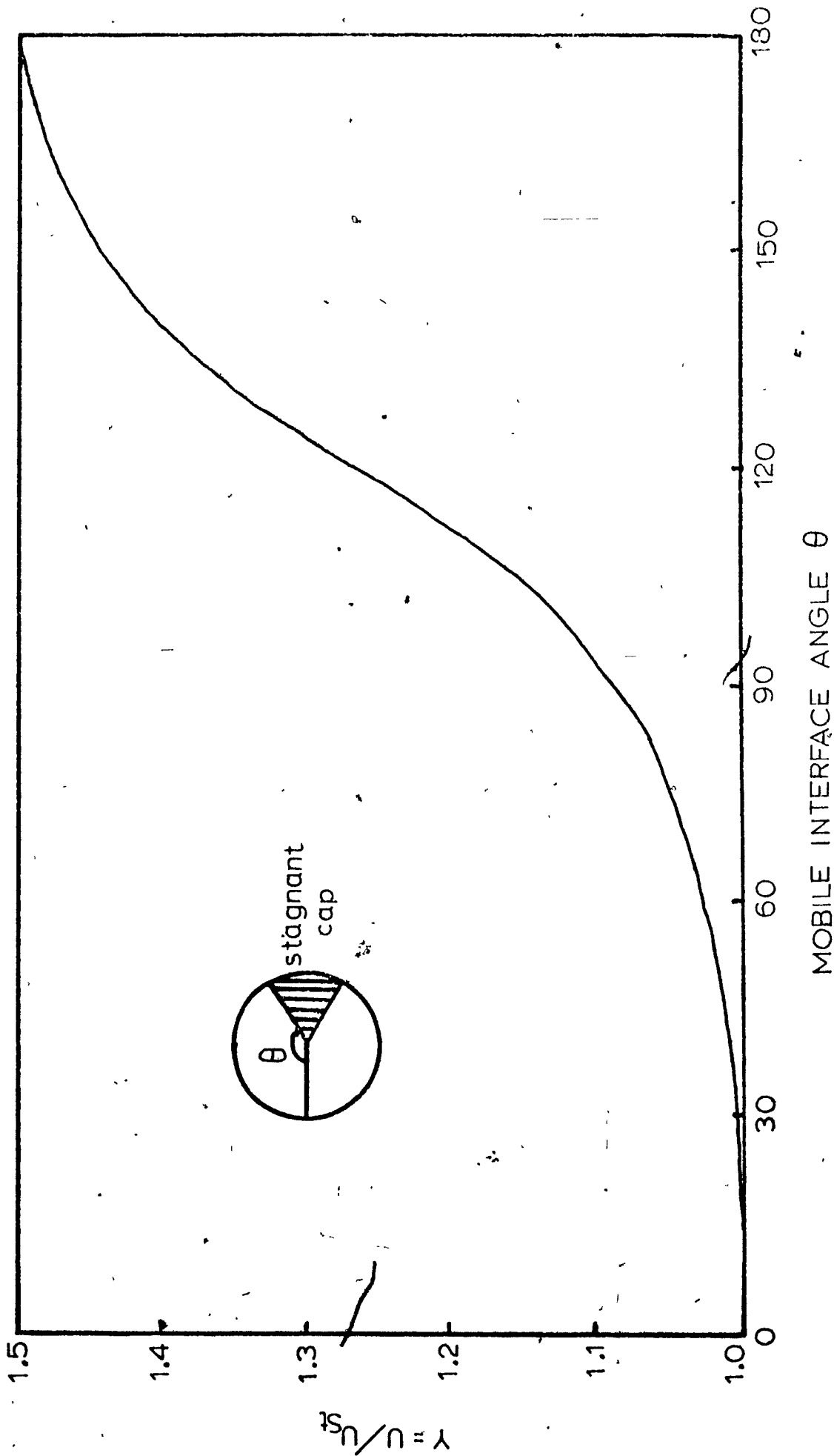


EÖTVÖS NUMBER  $Eo = \frac{g d^3 \Delta \rho}{\Delta \sigma}$



Figure 2.6

CORRELATION OF  $Y = U/U_{st}$  WITH HALF-ANGLE  $\theta$  SUBTENDED  
BY MOBILE PORTION OF BUBBLE SURFACE



## 2.6 Closure

In this chapter some aspects of surface chemistry which are important in dispersed air flotation have been reviewed briefly. The motion of small bubbles in water containing surfactants has also been described and it has been concluded that bubbles of diameter up to 100 microns are small enough to behave like rigid spheres. In the next chapter a review will be presented of previous experimental work pertinent to our objective of establishing the relations between flotation rate, particle size, and bubble size.

### 3. REVIEW OF PREVIOUS WORK: EXPERIMENTAL STUDIES

#### 3.1 Introduction

Dispersed air flotation is one of a group of processes called adsorptive bubble separation processes, in which a component is removed from solution or suspension by selective adsorption at an air-water interface. In this it differs from dissolved air flotation where the bubbles are trapped mechanically inside or underneath flocculated clusters of particles. Adsorptive bubble separation processes are the subject of a recent book edited by Lemlich (8) and of excellent review articles by Karger and DeVivo (9) and Somasundaran (10). In the present review only those studies relevant to the objectives of this project will be highlighted.

The first problem confronting any review of this field is that of nomenclature. All authors agree that a primary classification of adsorptive bubble separation processes can be made according to the nature of the species removed from water. Thus, names such as ion flotation, colloid flotation, microflotation, precipitate flotation and mineral flotation are self-explanatory. There, however, agreement ends and any secondary classification depends on the purpose for which the classification is being made. Karger et al. (11) sub-divide according to whether or not a foam is generated to carry off material raised to the surface of the bulk liquid; Rubin (12) sub-divides according to whether a low or a high air rate is used (without ever defining "low" and "high") and Somasundaran (10), in a review oriented mainly towards surface chemistry, sub-divides according to whether

the particles are naturally hydrophobic or have to be made so by adding a surfactant.

We wish to focus attention on the processes by which bubble-particle contact is achieved. Studies reported in the literature may be classified according to whether adsorption of particles takes place from the bulk liquid on to bubbles rising through that liquid or from liquid draining back through the foam. It seems logical to call the first situation "flotation" and the second "foam separation". These definitions represent two extremes of a continuum rather than a rigid demarcation. The present dissertation is concerned only with flotation as defined above. Included within our definition of flotation is, for example, the work of Sebba on ion flotation (13), that of Cassell et al. on flotation of sub-micron colloids (14), that of Rubin and co-workers on flotation of micro-organisms (15-17), that of Kalman and Ratcliff (6,7), of Pinfold and co-workers (18-22) and of Rubin (12) on flotation of precipitates, that of DeVivo and Karger on flotation of clay particles (23) and also Saint Gobain's commercially successful Electroflotation process for effluent treatment (3-5). All the above workers used small bubbles (average diameter less than 100 microns), low air rates (less than 1 ml. per min. per  $\text{cm}^2$  cell area) and a very small foam head above the bulk liquid. They were working at the flotation end of the flotation-foam separation continuum. Grieves and his co-workers (24-31) always use larger bubbles (200 to 700 microns diameter), larger air rates (4 to 12 ml. per min. per  $\text{cm}^2$  cell area) and a substantial foam head, so their work is intermediate between

flotation and foam separation. In such cases the work reported in this dissertation is applicable to the primary separation by flotation in the pool of bulk liquid but not necessarily to the subsequent enrichment by drainage through the foam column.

Mineral flotation (32) is included in our definition, but because of the large size of the particles there are some important physical differences in flotation technique compared to processes specifically designed for floating fine particles. The mineral particles produced by grinding ores can be as large as 200 microns in diameter. Vigorous stirring is needed to keep these in suspension whereas the cells used for floating fine particles are unstirred. In addition, large particles need large bubbles to lift them, and since mineral pulps typically contain 30 to 40 wt.% solids each bubble has to lift many particles. Usually the air is introduced by downdraught through the impeller and flung out into the liquid where it forms bubbles up to 3 mm. in diameter. Under these conditions very small particles of the size range we are interested in are regarded as notoriously difficult to float and strenuous efforts are made in the design of grinding circuits to minimize their production. The flow pattern around these large bubbles will be quite different from that around the very small bubbles used for floating fines and the large particles will have much more inertia than the small particles. Therefore, although most of the work done on the surface chemistry of mineral flotation is directly applicable to the flotation of fines the effects of physical variables may not be the same in the two systems.

### 3.2 Effect of Particle Size on Flotation Rate

In the past a typical laboratory study on the dispersed air flotation of fine particles has consisted of bubbling air through a small batch cell, withdrawing samples at regular intervals, analysing the samples for particle concentration by chemical or turbidimetric methods and plotting a curve of per cent removal versus time. Given a suitable surfactant and pH it appears that precipitates of particle size 10 to 20 microns can be floated rapidly with better than 95% removal in ten minutes or less (7,25). Flotation rate is increased both by increased temperature of precipitation and increased time lag between precipitation and start of flotation, both of which tend to increase particle size (19). Micro-organisms of diameter of the order of 1 to 2 microns can be floated at an appreciable rate only if the pH is near their isoelectric point, i.e. where they are likely to agglomerate (17). Adding alum and adjusting the pH to give a gelatinous floc of  $\text{Al}(\text{OH})_3$  improves the flotation rate and enables high removals to be obtained over a much wider pH range (15-17). It has been hypothesized that the micro-organisms become enmeshed in the growing floc and that it is the floc which becomes attached to the bubbles, either by adsorption or by providing a mechanical barrier to the rise of the bubbles. Sub-micron particles such as polystyrene latex can only be floated by adding alum and precipitating an  $\text{Al}(\text{OH})_3$  floc (14).

From the above evidence it appears that flotation rate must increase quite rapidly with increasing particle size. In this context there is a result given by DeVivo and Karger (23) which is

puzzling. They floated finely-ground kaolin and montmorillonite using two different cells. Cell A employed bubbles of diameter 200 microns, flow rate 2.7 ml. per min. per  $\text{cm}^2$  cell area and a very small foam head. Cell B employed bubbles of diameter 2 mm., flow rate 27 ml. per min. per  $\text{cm}^2$  cell area and a substantial foam head. The particle sizes are not given, but it was stated that the montmorillonite appeared finer than the kaolin. In the uncoagulated state the kaolin floated the faster of the two, as expected. The particles were then coagulated by adding  $\text{Na}_2\text{SO}_4$  to reduce their zeta potential to zero. In this state the flotation rates in cell A were increased substantially, as expected, but in cell B there was an unexpected fall in the flotation rates of both types of particle. There has been no satisfactory explanation of this result.

The only systematic studies of the effect of particle size on flotation rate have been in the mineral flotation field. No clear-cut relation has emerged. If the first order flotation rate constant is  $k$  and the particle diameter is  $d_p$  then Morris (33) found  $k \propto \ln d_p$ ; Bushell (34) found  $k$  independent of  $d_p$ ; Tomlinson and Fleming (35) found  $k \propto d_p^2$  for easily floated minerals and  $k \propto d_p$  for poorly floated minerals; Gaudin et al. (36) found  $k$  to be independent of  $d_p$  for  $d_p = 1$  to 4 microns and  $k \propto d_p$  for  $d_p = 4$  to 20 microns. The two latter investigations are probably the most reliable since they were carried out in specially designed laboratory cells under controlled conditions. The other two studies were performed on full-scale plants where control of variables would be much more difficult. Only Tomlinson and Fleming reported the bubble size used

in their experiments (0.3 to 1.6 mm., average 0.8 mm.). The other studies probably had similar bubble sizes since their air was introduced by downdraught through an impeller. In all cases the cells were stirred vigorously and the flotation pulps were comparatively concentrated. For the reasons discussed in the previous section their applicability to dilute suspensions of fine particles using small bubbles in an unstirred cell is doubtful.

The above investigations all found that flotation rate followed first order kinetics well. The experiments of Suwanasing (37), using similar equipment to Tomlinson and Fleming, gave a better fit to second order kinetics. The second order rate constant was found to increase linearly with  $d_p$  for galena and to be independent of  $d_p$  for silica. This highlights further the confusing state of experimental data in this field.

### 3.3 Effect of Bubble Size on Flotation Rate

It is generally accepted that as long as the particles are not too heavy or the pulps too concentrated then for a given air rate the flotation rate will increase as the bubble size is decreased due to the smaller bubbles sweeping out a greater volume of liquid. A subsidiary function of the frothers (long chain alcohols) used in mineral flotation is to reduce the bubble size (37). The results of DeVivo and Karger on uncoagulated clay particles cited earlier (23) indicate that their low air rate cell (bubble diameter 200 microns) gave roughly the same flotation rate as their high air rate cell (bubble diameter 2 mm.), even though the air rate in the latter was

ten times higher than in the former. This suggests that within this range of bubble sizes the flotation rate is inversely proportional to bubble diameter, as would be predicted simply by comparing swept volumes. (Swept volume =  $3GL/2D_b$ , where  $G$  = air rate,  $L$  = bubble path length and  $D_b$  = bubble diameter). There have been no other experimental studies on the effect of bubble size on flotation rate.

### 3.4 Closure

This chapter has reviewed the available experimental data regarding the effects of particle size and bubble size on flotation rate. The data on the effect of particle size were all obtained under mineral flotation conditions of large bubbles and, frequently, large particles. There is reason to believe that they are not applicable when the bubbles and particles are very small as in the use of dispersed air flotation for effluent treatment. Furthermore, the data from different studies are often contradictory, which suggests that the parameters governing the relation between flotation rate and particle size have not been identified correctly. The effect of bubble size on flotation rate has not been studied directly, although it is known that flotation rates are enhanced by reducing the bubble size.

The next chapter reviews attempts which have been made to formulate theoretical models of bubble-particle interactions in flotation.

4. REVIEW OF PREVIOUS WORK: THEORETICAL MODELS

4.1 Particles not Affected by Brownian Motion

4.1.1 Introduction

When the particles are large enough to have no appreciable Brownian motion a complete theoretical model of their capture by bubbles will involve:

- (a) an account of the interplay of those forces (primarily hydrodynamic and gravitational) which determine the trajectory of a particle as it approaches a bubble;
- (b) an account of the interplay of those forces (primarily surface-molecular and electrical) which determine whether a particle whose trajectory has brought it close to the bubble surface will form a stable bond with the bubble.

The above distinction is somewhat artificial in that in reality there will be an overlap region in which both type (a) and type (b) forces are important. However, the division into two non-interacting zones is normally made in order to simplify analysis of the situation. The range of action of the surface forces is known to be of the order of fractions of a micron (73), so for many purposes the boundary between zones can be considered to coincide with the bubble surface. The situation is expressed mathematically by writing

$$E = E_1 \times E_2 \quad (3.1)$$

where  $E$  = collection efficiency, i.e. the fraction of particles whose centres initially lie in the bubble's path which are actually collected by the bubble;

$E_1$  = collision efficiency, i.e. the fraction of particles whose centres initially lie in the bubble's path which actually come in contact with the bubble;

and  $E_2$  = attachment efficiency, i.e. the fraction of particles contacting the bubble which actually form a stable attachment to it.

The forces in zone (a) are considered to determine  $E_1$  and those in zone (b) to determine  $E_2$ . The flotation rate is proportional to the collection efficiency  $E$ .

Derjaguin and Dukhin (74) postulate the existence of an intermediate zone of thickness 1 to 10 microns consisting of a diffusional boundary layer on the bubble. It is claimed to arise with bubbles of diameter 1 mm. or larger. Such bubbles rise so rapidly that a considerable degree of surface circulation exists despite the retarding effect of adsorbed surfactant. Fresh surface is continually being created at the front of the bubble and this new surface has the surfactant concentration of the bulk liquid. There is a large driving force for adsorption of more surfactant ions on the freshly-created surface and this gives rise to a strong diffusional flux of surfactant ions towards the bubble. As a consequence it is claimed that strong diffusiophoretic and electrophoretic forces exist which dominate the particle's motion in this zone. However, our bubbles are so small that their surface is covered completely by a stagnant monolayer of adsorbed surfactant and no surface circulation

is possible (see Chapter 3, section 3.4). Therefore, there will be no flux of surfactant ions towards the bubble surface and no intermediate zone will exist.

#### 4.1.2 Collision Models

When viewed as a collision between two spheres flotation differs from raindrop coalescence and spray dedusting only in that the two spheres are of markedly different densities and may move in opposite directions under the influence of gravity. Collisions between falling raindrops have been studied intensively by meteorologists in an attempt to explain observed rates of raindrop growth, while the work on spray dedusting was stimulated by the mining industries' need to suppress dust in mines. Work up to 1962 was summarised by Herne (75).

The physical situation is depicted in Figure 4.1. Hydrodynamic drag tends to sweep the particle around the collector sphere following the fluid streamlines, but particle inertia tends to make the particle continue in a straight line towards the collector. The result is a particle trajectory deviating from the fluid streamlines. Gravity tends to reinforce the effect of particle inertia if the collector is moving downwards relative to the collector and opposes it if the particle is moving upward relative to the collector.

The usual procedure is to assume that the drag on the particle follows Stokes' Law and to write the equation of motion of the particle as:

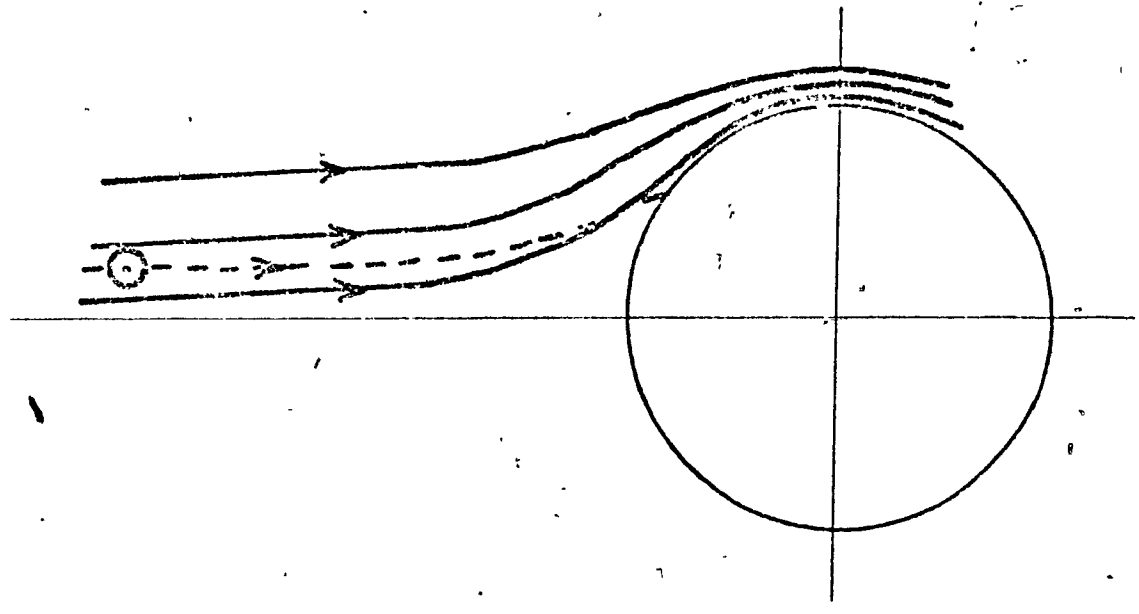
Figure 4.1 and Figure 4.2

4.1 APPROACH OF A PARTICLE TO A COLLECTOR

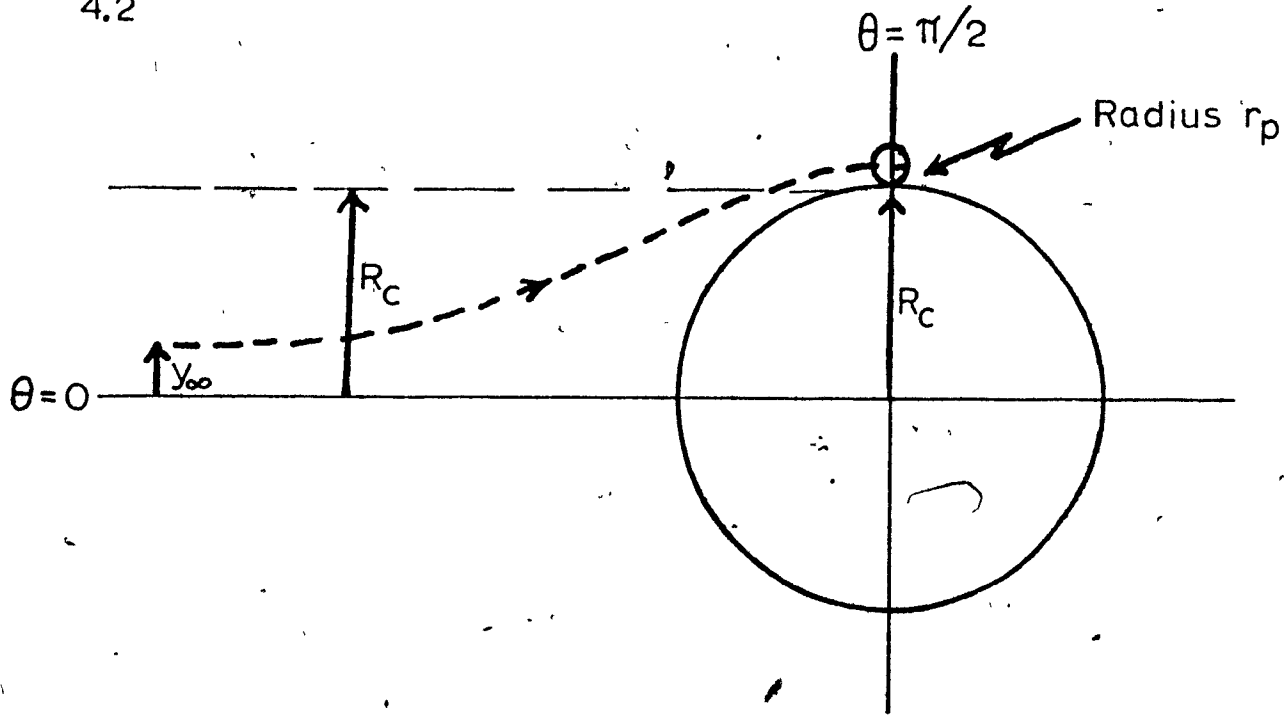
4.2 GRAZING TRAJECTORY



4.1



4.2



$$\text{St} \frac{du_p^*}{dt^*} = - (u_p^* - u_f^* - u_{pt}^*) \quad (4.1)$$

where  $\frac{u_p^*}{p}$  = dimensionless particle velocity  
 $\frac{u_f^*}{f}$  = dimensionless fluid velocity  
 $\frac{u_{pt}^*}{pt}$  = dimensionless particle terminal velocity under gravity

$$\text{St} = \frac{2\rho_p U r_p^2}{9\mu R_c}$$

$\rho_p$  = particle density

$\mu$  = fluid viscosity

$r_p$  = particle radius

$R_c$  = collector radius

$U$  = fluid velocity an infinite distance from the collector.,

$U$  is the reference velocity for  $\frac{u_p^*}{p}$ ,  $\frac{u_f^*}{f}$  and  $\frac{u_{pt}^*}{pt}$ . A trajectory is calculated by selecting a starting point far away from the collector and then integrating equation 4.1 numerically. A particular flow pattern round the collector, for example Stokes flow or potential flow, has to be assumed; this gives the spatial variation of  $\frac{u_f^*}{f}$ . The distance of the starting point from the collector's axis is varied until a trajectory is found on which the particle just grazes the collector (Fig.4.2). On this trajectory the particle's centre crosses the equatorial plane at a dimensionless distance  $(r_p + R_c)/R_c = (1 + r_p^*)$  from the collector's centre. If this trajectory is a distance  $y_\infty$  from the collector's axis at an infinite distance from the collector then the collision efficiency  $E_1 = \left(\frac{y_\infty}{R_c}\right)^2$ , since all trajectories within this one will result in the particle contacting the collector.

It is apparent from equation 4.1 and the boundary condition that  $E_1$  will be a function of the three dimensionless groups,  $St$ ,  $u_{pt}^*$  and  $r_p^*$ . The Stokes number  $St$  characterises the ratio of particle inertia to viscous drag on the particle. Obviously,  $E_1$  is an increasing function of  $St$  and  $r_p^*$ . The variation of  $E_1$  with  $u_{pt}^*$  will depend on the direction of motion of the particle relative to the collector. Langmuir (76) showed that if gravity is ignored and  $r_p^*$  is so small that it can be neglected there is a minimum value of  $St$  below which  $E_1$  is zero. It was shown later by Michael and Norey (47) that if gravity is taken into account and  $u_{pt}^*$  is positive then there is no such limit.

Two attempts have been made to apply this approach to flotation. Derjaguin and Dukhin (74) ignored gravity and predicted incorrectly that there was a limiting value of particle diameter below which no collisions could occur. For particles of density 2 gm./ml. and bubbles of diameter 0.08 cm. they predicted this limit to be a particle diameter of 40 microns. There is a great deal of data testifying to the fact that particles much smaller than 40 microns can be recovered by 0.08 cm. diameter bubbles (see, for example, ref. 35).

Flint and Howarth (42) allowed for the effect of gravity but neglected  $r_p^*$ . This is equivalent to saying that a particle only collides with a bubble if the trajectory of the centre of the particle grazes the bubble surface, which can only be correct if the particle is very small relative to the bubble. Figure 4.3 shows their curves

of  $E_1$  versus  $St$  and  $u_{pt}^*$  for both Stokes and potential flow round the bubble. Below  $St = 0.1$ ,  $E_1$  is almost independent of  $St$ . The limiting value of  $E_1$  at  $St = 0$  was deduced by them to be  $E_1 = \frac{u_{pt}^*}{1 + u_{pt}^*}$  irrespective of whether the flow round the bubble was Stokes or potential. However, this expression for the limiting  $E_1$  is critically dependent on their assumption that  $r_p^*$  can be neglected. If this assumption is removed the grazing trajectory is defined by  $r^* = 1 + r_p^* = \lambda$  at  $\theta = \pi/2$ . Working through their derivation with  $r^* = \lambda$  instead of  $r^* = 1$  we obtain the following expressions for the limiting  $E_1$  at  $St = 0$ :

(a) for potential flow round the bubble at  $St = 0$

$$E_1 = \lambda^2 - \frac{1}{\lambda(1 + u_{pt}^*)} \quad (4.2)$$

(b) for Stokes flow round the bubble at  $St = 0$

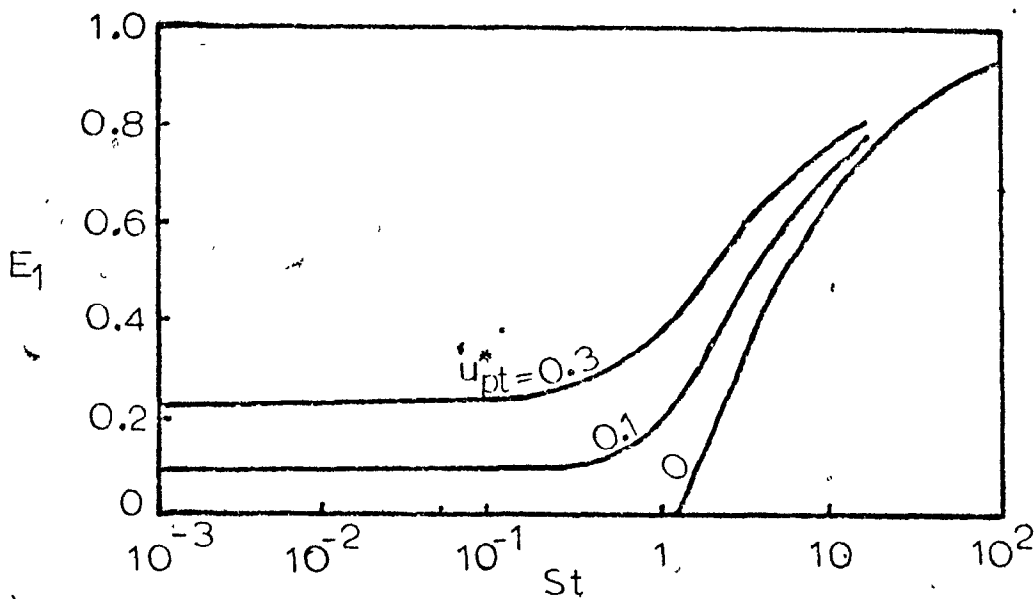
$$E_1 = \lambda^2 - \frac{3\lambda^2 - 1}{2\lambda(1 + u_{pt}^*)} \quad (4.3)$$

A second criticism of their work is that when water is the medium it is not accurate in general to assume that the drag on the particle obeys Stokes' Law. When a particle is accelerating relative to a fluid, which it is here since it deviates from streamlines, the instantaneous drag on the particle is only equal to the steady state (Stokes' Law) drag at that velocity if the fluid inertia is vanishingly small. With a fluid of non-zero inertia the flow pattern

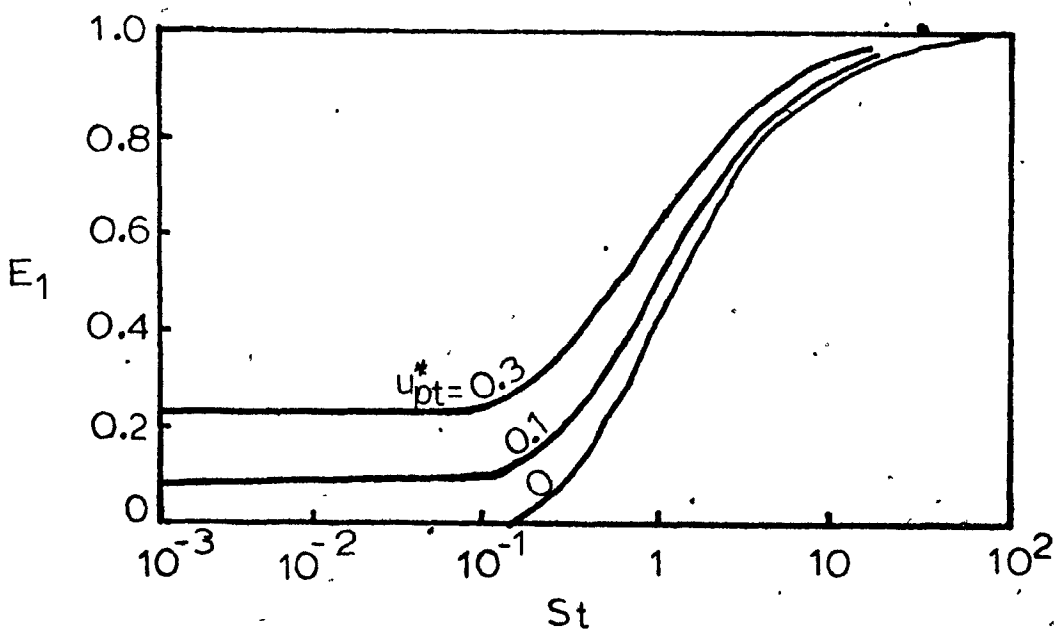
Figure 4.3

VARIATION OF COLLISION EFFICIENCY WITH STOKES NUMBER IN  
STOKES AND POTENTIAL FLOW (FLINT-HOWARTH MODEL)

# STOKES FLOW



# POTENTIAL FLOW



round the accelerating particle has not had time to adjust itself to the steady state pattern for a given velocity before the velocity has moved on to a new value. When the fluid density is very small (air, for example) or the particle acceleration relative to the fluid is very small ( $St \ll 1.0$  with water as the medium, as will be shown in Chapter 11) the steady state drag is a good approximation and equation 4.1 is valid. When the medium is water and  $St > 1.0$ , which is the case for the greater part of Flint and Howarth's theoretical curves, assumption of the steady state drag will seriously underestimate the actual drag on the particle and result in overestimated collision efficiencies. This is explored in greater depth in Chapter 11. Flint and Howarth did observe some trajectories experimentally and concluded on the basis of good agreement with theoretical trajectories that use of the steady state drag was sufficiently accurate. However, all their experimental data were obtained at  $St < 0.1$  so their claim cannot be accepted.

Recent work on raindrop collisions has concentrated on three refinements to earlier models.

- (a) Allowance for the fact that a particle of finite size will perturb the flow field round the collector (63,78).
- (b) Allowance for viscous resistance to thinning of the film of fluid separating particle and collector when they are close together (63).
- (c) More sophisticated representations of the flow field round the collector (78). This is important at collector Reynolds number  $Re_c > 1$ , and also at  $Re_c < 1$  if the particle is approaching the collector from the

downstream side.

The work of Hocking and Jonas (63) wraps (a) and (b) together by making use of recently-developed solutions to the Navier-Stokes equation for flow past a pair of spheres. It is only valid for  $Re \ll 1$ . This approach is applied to flotation in Chapter 8. Refinement (c) is not worth applying to flotation with small bubbles because we have  $Re_c < 1$  and approach from the upstream side.

In the spray dedusting field Zebel has considered the effect of electrical charges on the particles and collector drops (79). Electrical effects have also been considered in models of aerosol filtration, where the collector is a cylindrical fibre (80). They have not been taken into account in flotation models because very little is known about the electrical properties of bubbles. Davies and Rideal (81) state that pure water has a surface potential of  $-0.1$  to  $-0.2$  mV, indicating a preferential orientation of water molecules at the interface, but undoubtedly this will be altered by the presence of surfactants. Chapter 10 outlines a possible approach to including electrical forces in flotation collision efficiency calculations.

Collision models have been developed recently for filtration of water through a sand bed (82,83,41). Since in this case the collector is a solid it is likely that London - van der Waals forces of attraction between collector and particle will be important; these have been taken into account by Spielman and Goren (83). However, they are unlikely to be important when the collector is a bubble.

There is one type of collision model which is totally different from those discussed above and it must be mentioned briefly because it has some currency in mineral dressing circles. It was introduced by Philippoff (77) and developed further by Evans (67). It focusses on the deformation of the bubble surface caused by the impact of the particle. If the bubble surface is treated as an elastic skin it is easily shown that the restoring force is proportional to the deformation, so the motion of the penetrating particle is simple harmonic. The contact time  $t_c$ , defined as half the period of the simple harmonic motion, is calculated to be  $\sqrt{\frac{\pi m}{2\sigma}}$  or  $\frac{\pi h_{\max}}{V}$ , where  $m$  is the mass of the particle,  $\sigma$  the surface tension,  $h_{\max}$  the maximum deformation of the surface and  $V$  the normal velocity of approach of the particle. Attachment is supposed to take place if the contact time exceeds some magic but unspecified value. Consider two cases.

- (a) 0.3 mm. galena particle, 3 mm. bubble rising at 25 cm./sec.

Taking  $\sigma = 60$  dynes/cm. and  $V$  equal to the bubble rising velocity we obtain  $t_c = 1.2 \times 10^{-3}$  secs. and

$$h_{\max} = 0.09 \text{ mm.} = \frac{D_b}{30}$$

- (b) 10 micron glass beads, 100 micron bubble rising at its terminal velocity of 0.5 cm./sec. Again take  $\sigma = 60$  dynes/cm. and take  $V = 0.5$  cm./sec., i.e. we are considering the maximum deformation case where the particle is on the bubble's axis of motion. We

$$\text{obtain } t_c = 6 \times 10^{-6} \text{ secs. and } h_{\max} = 0.01 \mu = \frac{D_b}{10,000}$$

Therefore, while this model may have some use with large bubbles and particles large enough for their motion to be almost rectilinear, it is not applicable to small bubbles and small particles. In our case the bubbles hardly deform at all and to the particles they appear as rigid spheres.

#### 4.1.3 Attachment Models

Very little work has been done on the attachment process. By pursuing an analogy between particle-bubble attachment and the heterocoagulation of unlike colloidal particles Derjaguin and Dukhin (74) were able to adapt heterocoagulation theory to predict  $\frac{\epsilon \gamma^2}{A} < 3$  as the criterion for attachment to take place, where  $\epsilon$  is the dielectric constant of the medium,  $\gamma$  is the particle's double layer thickness and  $\zeta$  its zeta potential and A is the Hamaker constant for the hetero-system. None of the above parameters is affected significantly by particle size or bubble size when the particles are larger than one micron in diameter.

The only experimental work on attachment efficiency is that of Whelan and Brown (48) who photographed the collisions of large pyrite, galena and coal particles with the large bubbles. They found the attachment efficiency to be an increasing function of the normal velocity of impact.

#### 4.2 Sub-Micron Particles

No work has been done on the collection of sub-micron particles by bubbles, but the scavenging of sub-micron particles by water drops and fibrous filters has received attention (46,85). The approach is to apply the thin concentration boundary layer theory developed for mass transfer and to use the Stokes-Einstein equation to obtain the diffusivity of the particles. We shall apply this method to the flotation case in Chapter 5, section 5.3.

Cookson (86) and Yao et al. (41) have measured the removal of sub-micron particles from water flowing through a packed bed. They found the predictions of the above type of model to be in agreement with their experimental data provided Pfeffer's correction (68) for the influence of neighbouring spheres was applied.

#### 4.3 Closure

This chapter has reviewed the models of bubble-particle collisions which have been proposed to date. In general, they have been developed with large bubbles and mineral dressing applications in mind. Only the Flint-Howarth model purports to be applicable also to small bubbles and its defects have been pointed out. In the next chapter a simple collision model is developed specifically for the case of small bubbles and small particles.

5. A PRELIMINARY MODEL OF FINE PARTICLE COLLECTION  
BY SMALL BUBBLES

5.1 Introduction

To model the collection of fine particles by small bubbles we note first of all that particles larger than 2 to 3 microns in diameter will not be affected significantly by Brownian motion and will contact the bubble only if their hydrodynamically-determined trajectories come within one particle radius  $r_p$  of the bubble surface. In this region, which we call the collision regime, the collection efficiency  $E$  should increase with increasing  $r_p$  due to the geometric fact that the trajectory of a larger particle need not come so close to the bubble for the particle and bubble surfaces to touch. Sub-micron particles will reach the bubble mainly by Brownian diffusion. In this regime  $E$  should decrease with increasing  $r_p$  since larger particles diffuse more slowly. Hence, in the intermediate region where both mechanisms contribute significantly to particle capture we expect  $E = f(r_p)$  to have a minimum. The existence of such a minimum has been confirmed experimentally for aerosol filtration (85) and for liquid filtration (41) in which similar mechanisms are operative.

Our treatment of the collision regime has an important conceptual difference from that of Flint and Howarth (42). As was mentioned in Chapter 4, their boundary conditions imply that a collision is only considered to occur if the trajectory of the centre of the particle grazes the bubble surface, whereas we define a collision as occurring when the surface of the particle grazes the bubble surface.

## 5.2 Collision Regime

Let

$$E = E_1 \times E_2$$

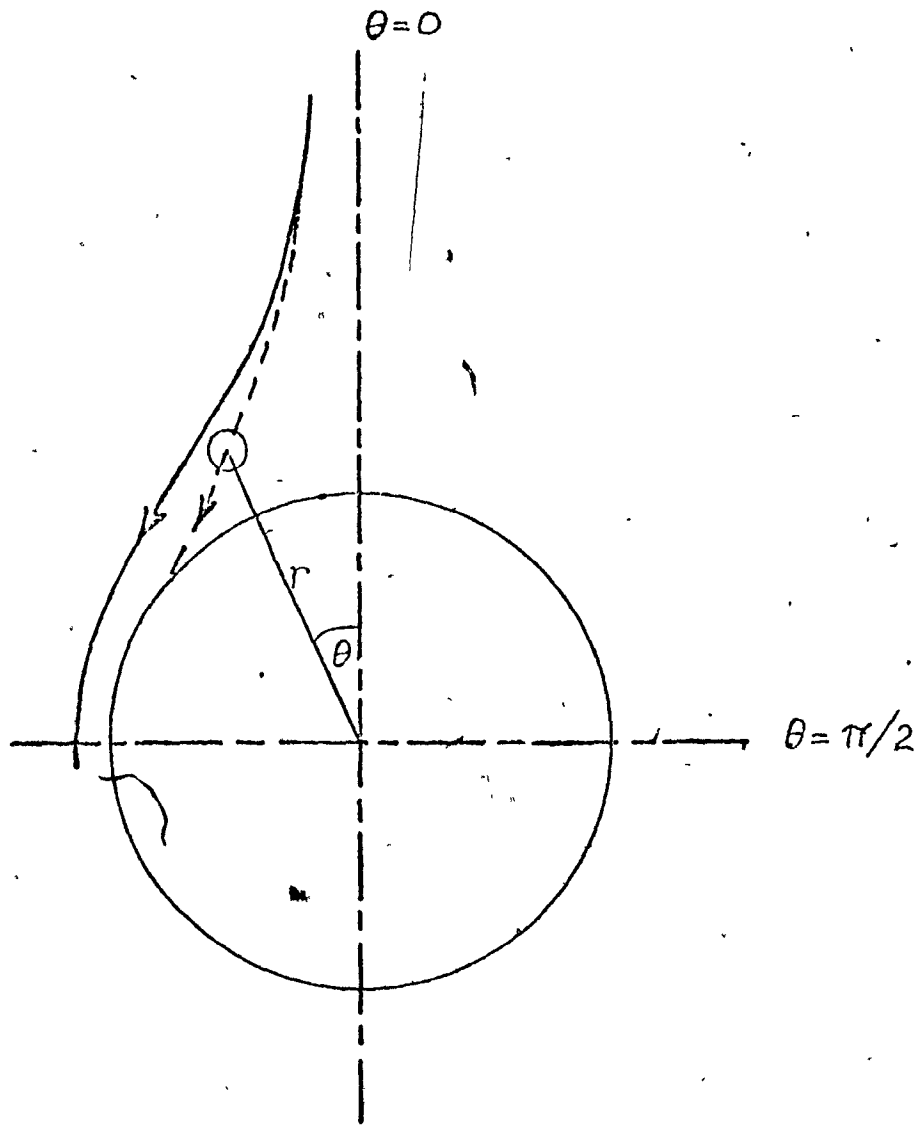
where  $E_1$  = collision efficiency, i.e. the fraction of particles in the bubble's path which actually collide with the bubble, and  $E_2$  = attachment efficiency, i.e. the fraction of particles colliding with the bubble which actually stick to it.

It seems likely that  $E_2$  will depend mainly on the chemical natures of the particle surface, the bubble surface and the thin film of liquid draining from between them. Therefore, as an initial hypothesis, let us assume that the effects of particle size and bubble size on  $E$  are given by their effects on  $E_1$ .

Consider a spherical bubble of radius  $R_b$  rising vertically at constant velocity  $U_b$ . Take coordinates  $(r, \theta)$  centred at the center of the bubble and moving with the bubble.  $\theta = 0$  is the vertical axis. Figure 5.1 shows a typical particle trajectory. Consider the limiting trajectory in which the particle just grazes the bubble at  $\theta = \pi/2$ . Let this trajectory be a distance  $y_\infty$  from  $\theta = 0$  at  $r = \infty$ . All particles whose centres are initially closer to  $\theta = 0$  than  $y_\infty$  will collide with the bubble, and if the particles are uniformly distributed in the liquid we have  $E = (y_\infty/R_b)^2$ . In the general case particle trajectories must be calculated by a step-by-step numerical solution of the particle's equation of motion and the grazing trajectory found by trial and error. However, for the special case of small particles and small, slowly rising bubbles encountered in effluent treatment, a simple analytical solution is possible.

Figure 5.1

TRAJECTORY OF PARTICLE APPROACHING A BUBBLE



— FLUID STREAMLINES  
- - - PARTICLE TRAJECTORY ( $\rho_p > \rho_f$ )

We make the following assumptions.

- (1) The flow pattern around the front of the bubble is given by the Stokes solution for creeping flow around a rigid sphere. It was shown in Chapter 2, Section 2.5, that this is a reasonable assumption for bubbles of diameter up to 0.1 mm. rising at their terminal velocity in water which has not been rigorously purified to eliminate surfactants.
- (2) Electrical interactions between particle and bubble have a negligible effect on the particle trajectory.
- (3) Any particles collected are immediately swept or rolled to the back of the bubble so that the full front surface is always clear. Photographic evidence cited in Chapter 6 shows this to be true.
- (4) The motion of the bubble is not affected by the presence of the particles.
- (5) The fluid velocity used in computing the drag on a particle is the velocity which would exist at the point occupied by the centre of the particle if the particle were absent.

Obviously, these last two assumptions are strictly valid only at  $r_p/R_b = 0$  and become less valid as  $r_p/R_b$  increases.

Ignoring unsteady state drag terms and taking upwards as positive, the particle's equation of motion is:

$$\frac{4}{3}\pi r_p^3 \rho_p \frac{du_p}{dt} - 6\pi \mu_f r_p (u_p - u_f) - \frac{4}{3}\pi r_p^3 (\rho_p - \rho_f)g - 6\pi \mu_f r_p (u_p - u_f - u_{pt}) \quad (5.1)$$

where  $u_p$  = instantaneous particle velocity relative to bubble  
 $u_f$  = instantaneous fluid velocity relative to bubble  
 $u_{pt}$  = particle terminal falling velocity  
 $\rho_p$  = particle density  
 $\rho_f$  = fluid density  
 $\mu_f$  = fluid viscosity  
 $t$  = time.

Introduce dimensionless quantities:

$$\frac{u_p^*}{U_b} = \frac{u_p}{U_b}, \quad \frac{u_f^*}{U_b} = \frac{u_f}{U_b}, \quad \frac{u_{pt}^*}{U_b} = \frac{u_{pt}}{U_b},$$

$$t^* = \frac{U_b t}{R_b}, \quad St = \frac{2\rho_p U_b r_p^2}{9\mu_f R_b} = \frac{1}{9} \left(\frac{\rho_p}{\rho_f}\right) \left(\frac{r_p}{R_b}\right)^2 Re_b$$

where  $U_b$  = bubble rising velocity  
 and  $Re_b = \frac{2\rho_f U_b R_b}{\mu_f}$  = bubble Reynolds number.

Equation (5.1) becomes:

$$St \frac{du_p^*}{dt^*} = - (u_p^* - u_f^* - u_{pt}^*)$$

$$\therefore u_p^* = u_f^* + u_{pt}^* - St \frac{du_p^*}{dt^*} \quad (5.2)$$

Most of the interaction between bubble and particle occurs within a distance  $R_b$  of the bubble surface, i.e. for a time of order  $R_b/U_b$ , during which  $O(u_p)$  increases from at least  $(-U_b - u_{pt})$  to at most  $(-u_{pt})$ . Therefore,  $O(\frac{du_p^*}{dt^*}) < 1$ . For bubble of diameter up to 100 microns rising at their Stokes terminal velocity in water ( $Re_b < 0.5$ ) and particle diameters up to 20 microns, we have  $St < 10^{-2}$  for reasonable values of  $\rho_p$ .  $u_p^*$  and  $u_f^*$  are generally at least an order of magnitude larger than  $St(\frac{du_p^*}{dt^*})$ .  $u_{pt}^*$  may or may not be of the same order of magnitude as  $u_p^*$  and  $u_f^*$ , depending on the values of  $r_p$  and  $\rho_p$ . Therefore, it seems reasonable to neglect the final term on the right-hand side of equation 5.2 and write

$$\underline{u}_p^* = \underline{u}_f^* + \underline{u}_{pt}^*$$

$$\underline{u}_p = \underline{u}_f + \underline{u}_{pt} \tag{5.3}$$

Thus, gravity is the only factor which may cause the particle's trajectory to deviate significantly from the fluid streamlines. Particle inertia has no significant effect because the particle adjusts almost instantaneously to changes in the fluid flow around it. ( $St$  can be considered as the ratio of particle relaxation time  $\frac{2\rho_p r_p^2}{9\mu_f}$  to the characteristic time  $R_b/U_b$  for changes in the fluid flow.) This contrasts with the situation in aerosol capture (40, 45-47) and in mineral flotation (42), where particle inertia is the dominant factor causing deviation from streamlines. It means that in the present case the particle's equation of motion (5.2) can be approximated closely by the algebraic equation (5.3); this is what

makes possible an analytical solution for the collection efficiency. Also, since  $(u_p - u_f)$  is virtually constant and equal to  $u_{pt}$ , the relative acceleration between particle and fluid is negligible, which suggests that our neglect of the unsteady state drag terms is justified. A more rigorous justification will be presented in Chapter 11 in a generalized treatment of particle capture processes.

Considering the radial components of these velocities we have

$$u_{pr} = u_{fr} + u_{pt} \cos \theta \quad (5.4)$$

$$\approx U_b \cos \theta \left[ 1 + u_{pt}^* - \frac{3}{2} \left(\frac{R_b}{r}\right) + \frac{1}{2} \left(\frac{R_b}{r}\right)^3 \right] \quad (5.5)$$

where we have used the creeping flow solution for  $u_{fr}$  (see Appendix E).

The rate at which particles collide with the bubble is given by the flow  $N'$  of particles across the hemispherical surface defined by  $r = R_b + r_p$  and  $|\theta| \leq \pi/2$ . If there are  $c_p$  particles per unit volume uniformly distributed in the liquid, we have

$$N' = -2c_p \int_0^{\pi/2} (u_{pr})_{r=R_b+r_p} \cdot \pi(R_b+r_p) \sin \theta \cdot (R_b+r_p) d\theta$$

The flow of particles through the cylindrical volume swept out by the bubble is  $N = -\pi R_b^2 (U_b + u_{pt}^*) c_p = -\pi R_b^2 U_b (1 + u_{pt}^*) c_p$ . Therefore, collision efficiency  $E_1 = N'/N$ .

$$= \frac{2(1 + \frac{r_p}{R_b})^2}{U_b (1 + u_{pt}^*)} \int_0^{\pi/2} (u_{pr})_{r=R_b+r_p} \cdot \sin \theta d\theta \quad (5.6)$$

Substituting for  $u_{pr}$  from Equation (5.5) and putting  $r = R_b + r_p$  gives

$$E_1 = \frac{K^2}{1 + u_{pt}^*} \left( 1 + u_{pt}^* - \frac{3}{2K} + \frac{1}{2K^3} \right) \quad (5.7)$$

where  $K = 1 + r_p/R_b$ .

A little algebraic manipulation shows equation 5.7 to be exactly equivalent to equation 4.3, the Flint-Howarth Stokes flow case taken to the limit of zero Stokes number and corrected for non-zero particle radius. (In equation 4.3  $\lambda$  was used instead of  $K$  to avoid confusion with Flint and Howarth's use of  $K$  for Stokes number.)

Since both particle and bubble obey Stokes Law, we have

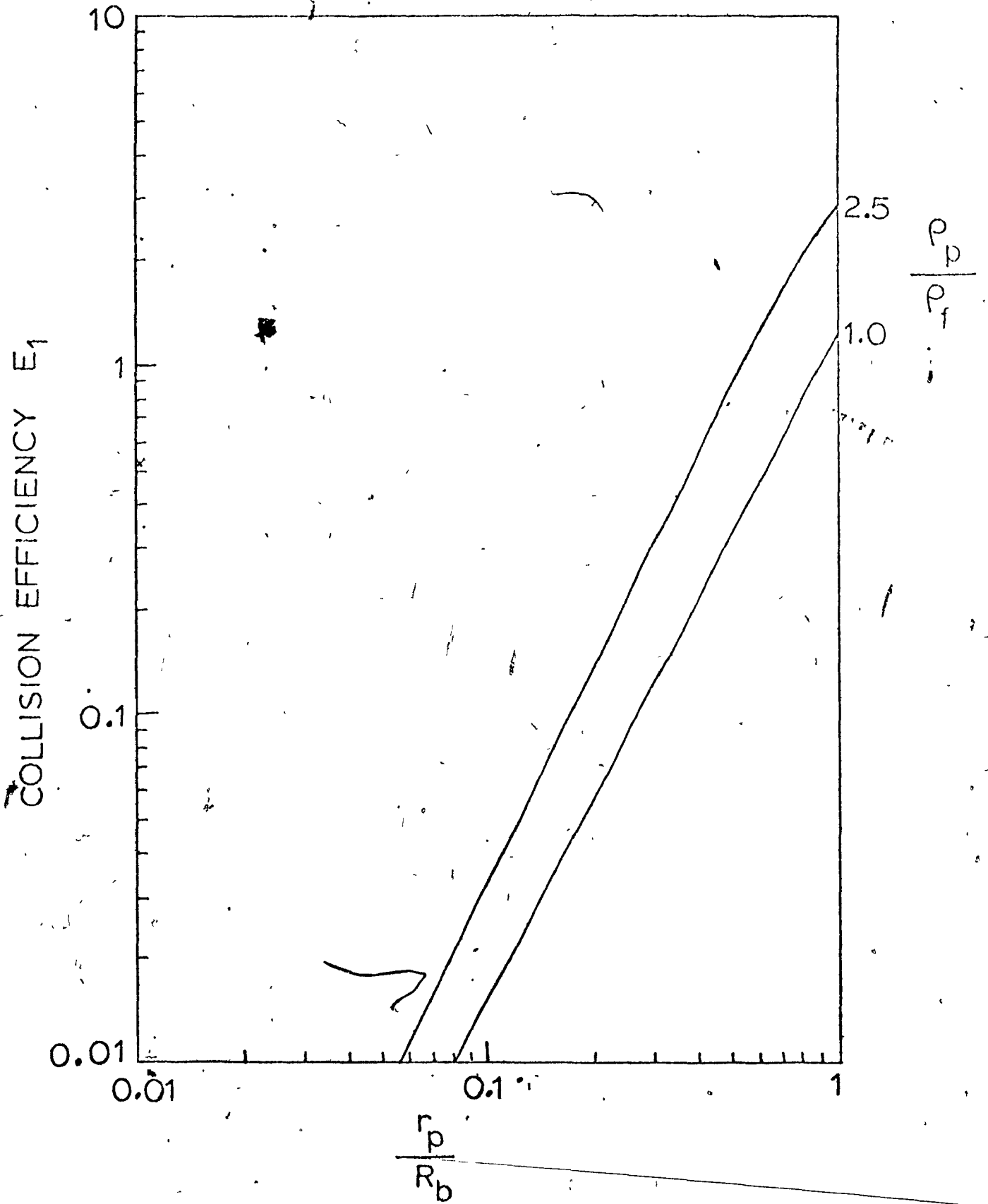
$$u_{pt}^* = \left( \frac{r_p}{R_b} \right)^2 \left( \frac{\rho_p}{\rho_f} - 1 \right) = (K - 1)^2 \left( \frac{\rho_p}{\rho_f} - 1 \right) \quad (5.8)$$

Therefore,

$$E_1 = f \left( \frac{r_p}{R_b}, \frac{\rho_p}{\rho_f} \right).$$

Figure 5.2 shows the theoretical relations between  $E_1$  and  $r_p/R_b$  predicted from Equations (5.7) and (5.8) for  $\rho_p/\rho_f = 1.0$  and 2.5. They are fitted very well by the straight line approximations  $E_1 = 1.25 (r_p/R_b)^{1.9}$  for  $\rho_p/\rho_f = 1.0$  and  $E_1 = 3.6 (r_p/R_b)^{2.05}$  for  $\rho_p/\rho_f = 2.5$ . Therefore,  $E_1$  is roughly proportional to  $(r_p/R_b)^2$  over this density range, which covers most practical situations. Since the volume swept out by a bubble is proportional to  $R_b^2$ , the average number of particles picked up by a bubble, assuming constant  $E_2$ , should be roughly independent of bubble size and the flotation

Figure 5.2  
COLLISION EFFICIENCY  $E_1$  AS A FUNCTION OF  $r_p/R_b$  AND  $\rho_p/\rho_f$   
WITH STOKES FLOW (PRELIMINARY MODEL)



rate should be proportional to bubble frequency. Therefore, for a given air rate, the flotation rate should be proportional to  $1/R_b^3$ , which provides a powerful incentive to make the bubbles as small as possible. Of course, this must be balanced against the extra cost of generating smaller bubbles in the case of spargers and porous plates.

The collision efficiencies  $E_1$  plotted in Figure 5.2 can be regarded as an upper limit on the collection efficiency  $E$  corresponding to an attachment efficiency  $E_2 = 1.0$ . If  $E_2$  is less than 1.0 and does not depend on  $r_p$  and  $R_b$ , the collection efficiency lines will be lower than the collision efficiency lines but will have the same slope. The results of Whelan and Brown (48) show that at least for mineral particles and large bubbles  $E_2$  is certainly less than 1.0.

### 5.3 Diffusion Regime

To model this regime we express the particle diffusivity by the Stokes-Einstein relation  $\mathcal{D} = kT/6\pi\mu_f r_p$  where  $k =$  Boltzmann constant and  $T =$  absolute temperature. This is then inserted in existing theoretical expressions for mass transfer to spheres.

For creeping flow around a sphere, thin concentration boundary layer theory (49) yields

$$Sh \approx Pe^{1/3} \quad (5.9)$$

where Sherwood number  $Sh = 2R_b k_p / \mathcal{D}$ , Peclet number  $Pe = 2R_b U_b / \mathcal{D}$  and  $k_p =$  particle mass transfer coefficient. Equation (5.9) is a very good approximation for  $Pe > 10^3$ . Let  $c_p$  be the concentration of particles in the bulk liquid and  $c_{ps}$  the concentration of unadsorbed

particles in the layer adjacent to the bubble surface. If the particles are adsorbed rapidly by the bubble  $c_{ps} \rightarrow 0$ , while if they are only slowly adsorbed  $c_{ps} \rightarrow c_p$ . The net flow of particles to the bubble surface in unit time is  $N'' = 4\pi R_b^2 k (c_p - c_{ps})$ . In unit time the bubble sweeps out a volume  $\pi R_b^2 U_b$  containing  $N = \pi R_b^2 U_b c_p$  particles. The collection efficiency

$$E = \frac{N''}{N} = \frac{4k (c_p - c_{ps})}{U_b c_p} = \frac{4Sh}{Pe} \quad f = \frac{4f}{Pe^{2/3}} \quad (5.10)$$

where  $f = \frac{c_p - c_{ps}}{c_p}$  is the dimensionless driving force for mass transfer. For strong adsorption  $f \rightarrow 1$  and for weak adsorption  $f \rightarrow 0$ . It seems plausible that, like the attachment efficiency  $E_2$  in the collision regime,  $f$  will depend mainly on the chemical natures of the particle surface, the bubble surface and the liquid phase. We make the hypothesis that  $f$  is independent of  $R_b$ ,  $r_p$  and  $\rho_p$ .

Expressing  $U_b$  as the Stokes terminal velocity and inserting the Stokes-Einstein relation for  $\mathcal{D}$ , we obtain:

$$E = \frac{4f}{R_b} \left( \frac{3kT}{8\pi g r_p} \right)^{2/3} \quad (5.11)$$

Taking  $T = 298^\circ K$ ,  $k = 1.38 \times 10^{-16}$  ergs  $^\circ K^{-1}$  molecule $^{-1}$ ,  $g = 981$  cm. sec. $^{-2}$  and expressing  $R_b$  and  $r_p$  in cm. we have

$$E = \frac{1.17 \times 10^{-11}}{R_b^{2/3} r_p} \times f \quad (5.12)$$

The following points should be noted:

- (1) Again we have  $E \propto 1/R_b^2$ , so this relation is predicted over the complete range of particle sizes when we have creeping flow round the bubble.
- (2)  $E$  is independent of particle density.
- (3) For this regime we have calculated the collection efficiency  $E$  rather than the collision efficiency  $E_1$  because the laws of diffusion refer to the net transfer of particles.
- (4) From Fick's first law of diffusion the particle mass transfer coefficient  $k_p \approx D/\delta$ , where  $\delta$  is the average thickness of the concentration boundary layer. Hence

$$\frac{\delta}{2R_b} \approx \frac{1}{Sh} = \frac{1}{Pe^{1/3}} = \frac{1}{2} \sqrt{\frac{E}{f}} = \frac{3.42 \times 10^{-6}}{2R_b r_p^{1/3}}$$

$$\text{Therefore, } \delta \approx \frac{3.42 \times 10^{-6}}{r_p^{1/3}} \text{ cm.} \approx \frac{4.45 \times 10^{-6}}{(2r_p)^{1/3}} \text{ cm.}$$

For the concentration boundary layer approach to be valid, we must have  $\delta \gg 2r_p$ . Therefore, Equations (5.10) to (5.12) can only be applied when the particle diameter is less than 0.2 microns ( $\delta \approx 1.6$  microns).

#### 5.4 Comparison of Efficiencies

So far we have calculated collision efficiencies for particles with diameters greater than 3 microns and collection efficiencies for particles with diameters less than 0.2 microns,

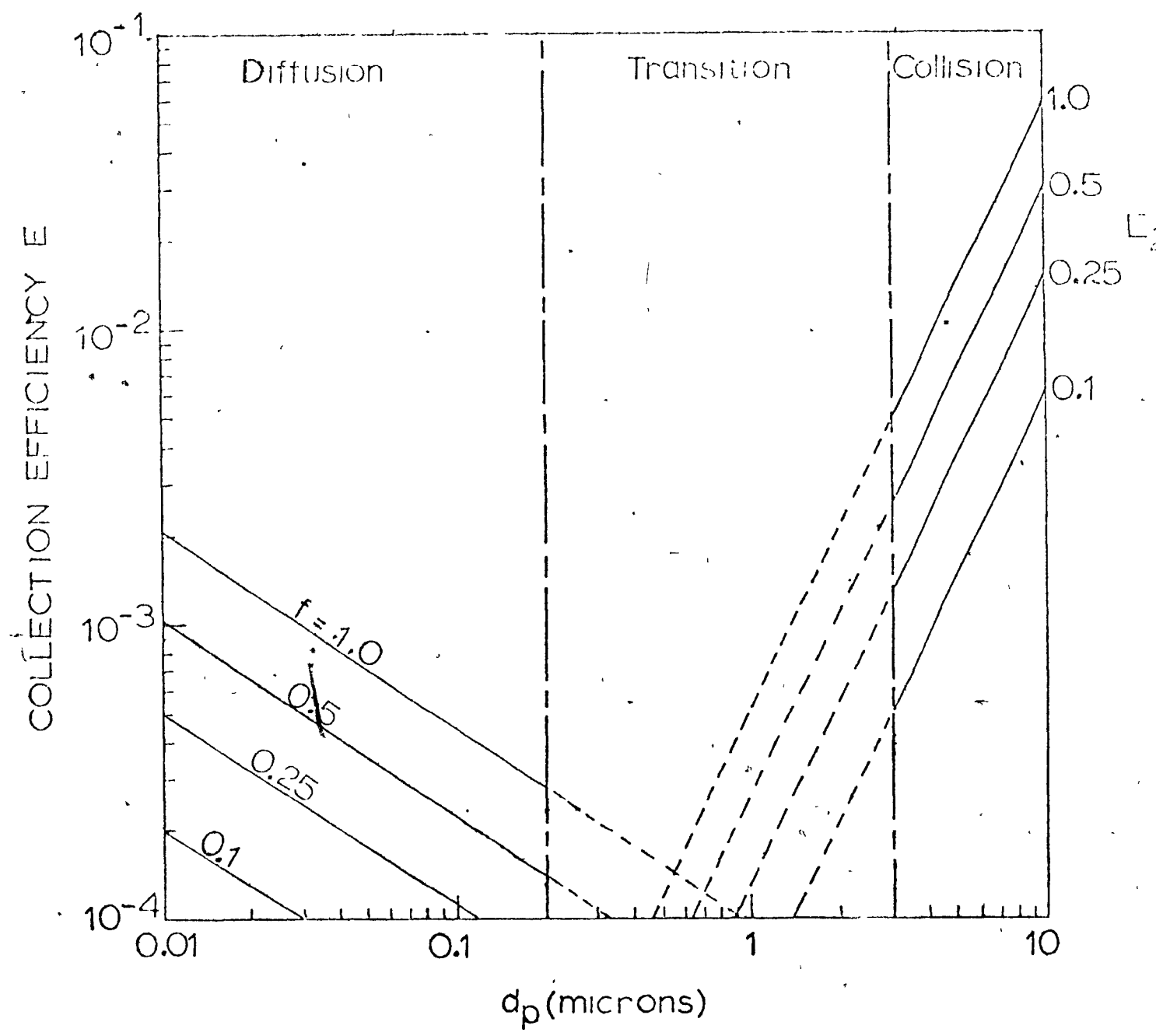
Figure 5.3 compares collection efficiencies for the two regimes for a bubble diameter of 75 microns,  $\rho_p/\rho_f = 2.5$ , a range of values of  $E_2$  in the collision regime and a range of values of  $f$  in the diffusion regime. For equal values of  $E_2$  and  $f$  the predicted efficiency is an order of magnitude higher in the collision regime than in the diffusion regime. Therefore, the flotation of sub-micron particles should be improved substantially if they can be agglomerated into flocs big enough to be in the collision regime. This explains Fung's observations on the flotation of ferric oxide (50). He found that sub-micron particles of colloidal ferric oxide in  $10^{-4}M$  surfactant solution floated very poorly, but when visible flocs were formed by raising the pH to the isoelectric point flotation became very rapid.

Coupling of the collision and diffusion mechanisms in the transition region is a complex matter which we have not resolved yet. However, this is unlikely to be important for practical purposes. The efficiency there is so low that if the particles in the feed are in this size range, one would certainly try to flocculate them into the collision regime. If the particles are initially in the diffusion regime, the theory suggests that they must be flocculated beyond the transition region, otherwise flotation performance may actually be worse.

Figure 5.3

COLLECTION EFFICIENCY E AS A FUNCTION OF PARTICLE DIAMETER  
WITH  $D_b = 75$  MICRONS,  $\rho_p / \rho_f = 2.5$  AND STOKES FLOW  
(PRELIMINARY MODEL)

S



### 5.5 Alternative Flow Patterns

So far it has been assumed that the flow pattern around the bubble is that of creeping flow. However, the methodology developed in Section 5.2 for the collision regime is capable of giving an analytical expression for the collision efficiency for any flow pattern having a simple analytical expression for  $u_{fr}$ .  $u_{fr}$  is inserted in equation (5.4) to give  $u_{pr}$ , which is then integrated in equation (5.6) to give  $E_1$ . The method will be applied here to Hadamard-Rybczinski flow and to potential flow.

#### 5.5.1 Hadamard-Rybczinski Flow

This flow pattern describes the flow in and around a bubble or drop (dispersed phase d) moving in a continuous medium (phase c) when there is no retardation of the i-interface by surfactants, i.e. the surface of the bubble or drop can move freely. It has been discussed already in Chapter 2, Section 2.5.

The Hadamard-Rybczinski stream function is

$$\psi = \frac{1}{2} u_b \sin^2 \theta \left[ r^2 + \frac{R_b}{2(1+X)} \left\{ X \frac{R_b^2}{r} - (2+3X)r \right\} \right]$$

where  $X = \frac{\mu_d}{\mu_c} = \frac{\mu_{air}}{\mu_{water}}$  in this case, i.e.  $\approx 0$ .

$$\therefore \psi = \frac{1}{2} u_b r^2 \sin^2 \theta \left( 1 - \frac{R_b}{r} \right)$$

$$\therefore u_{fr} = \frac{1}{r^2 \sin \theta} \frac{\partial \psi}{\partial \theta} = u_b \cos \theta \left( 1 - \frac{R_b}{r} \right) \quad (5.13)$$

Let  $K = \frac{R_b + r_b}{R_b}$  as before.

Then, inserting this expression for  $u_{fr}$  in equation (5.4) to obtain  $u_{pr}$  and integrating equation (5.6) we obtain

$$E_1 = \frac{K^2}{1 + u_{pt}^*} \left( 1 + u_{pt}^* - \frac{1}{K} \right) \quad (5.14)$$

Figure 5.4 shows  $E_1 = f\left(\frac{r}{R_b}\right)$  for  $\frac{\rho_p}{\rho_f} = 2.5$  and 1.0 as calculated from equation (5.14). The lines are slightly more curved than for Stokes flow, so in both cases it has been necessary to simulate them by three straight lines instead of by a single straight line. As  $r/R_b$  increases the slopes increase from 1.1 to 1.5 for  $\rho_p/\rho_f = 2.5$  and from 1.0 to 1.4 for  $\rho_p/\rho_f = 1.0$ .

### 5.5.2 Potential Flow

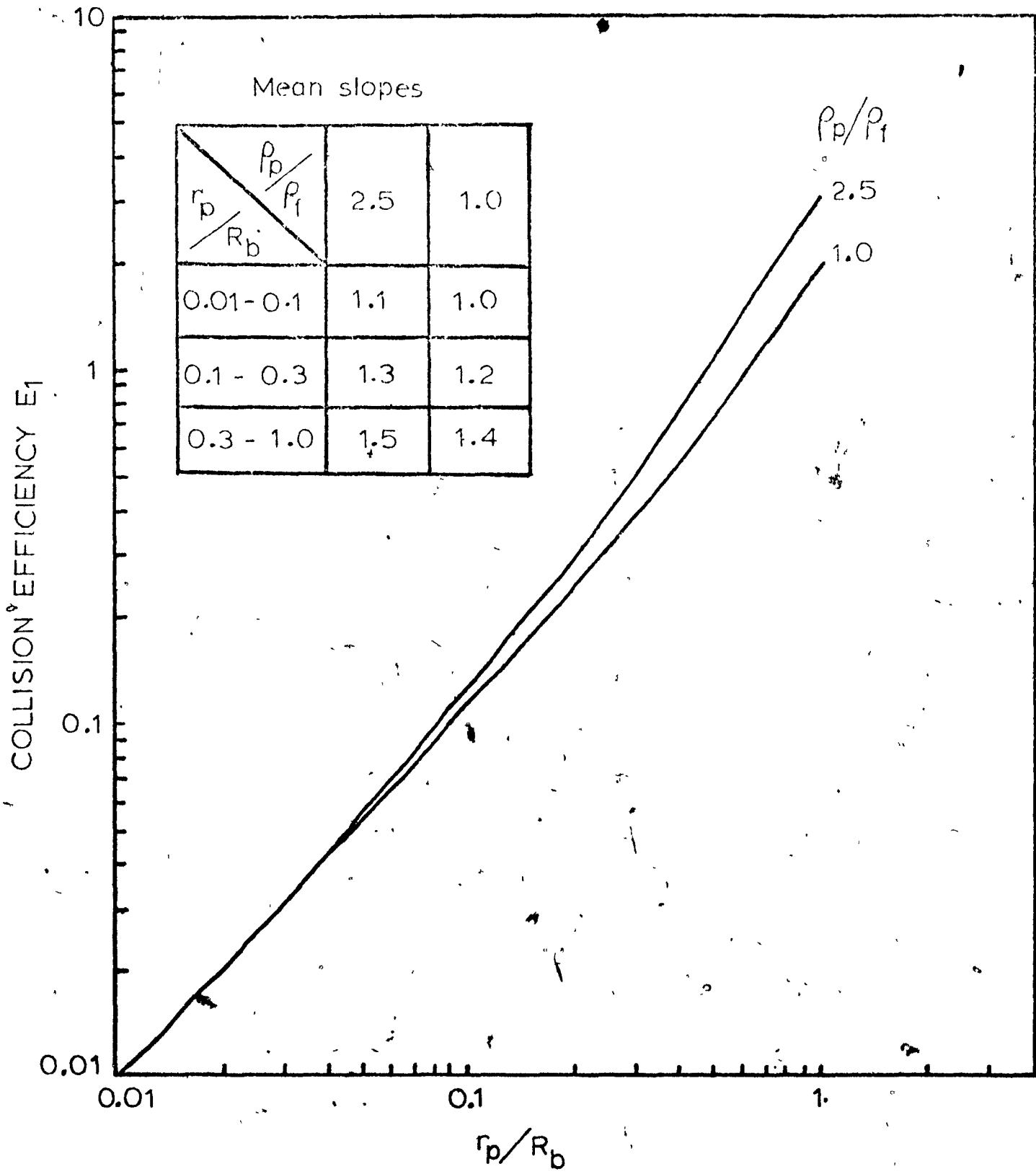
The flow pattern round the front of bubbles of diameter greater than 1 mm. is known to approximate potential flow whether surfactant is present or not (54). Although this study is concerned mainly with bubbles much smaller than this it is of interest to evaluate  $E_1$  for this case since sparger pipes and mechanical aerators tend to produce bubbles of this order of magnitude. A 1 mm. diameter bubble rises at roughly 12 cm./sec. in water containing surfactant at the sort of concentrations used in flotation (48), so for particles of diameter less than 20 microns we still have  $St < 10^{-2}$  and the methodology of section 5.2 is applicable.

For potential flow  $u_{fr} = U_b \cos \theta \left[ 1 - \left(\frac{R_b}{r}\right)^3 \right]$ .

This leads to  $E_1 = \frac{K^2}{1 + u_{pt}^*} \left( 1 + u_{pt}^* - \frac{1}{K^3} \right) \quad (5.15)$

Figure 5.4

COLLISION EFFICIENCY  $E_1$  AS A FUNCTION OF  $r_p/R_b$  AND  $\rho_p/\rho_f$   
WITH HADAMARD-RYBCZINSKI FLOW (PRELIMINARY MODEL)



COLLISION EFFICIENCY  $E_1$

10

1

0.1

0.01

0.01

0.1

1

$r_p/R_b$

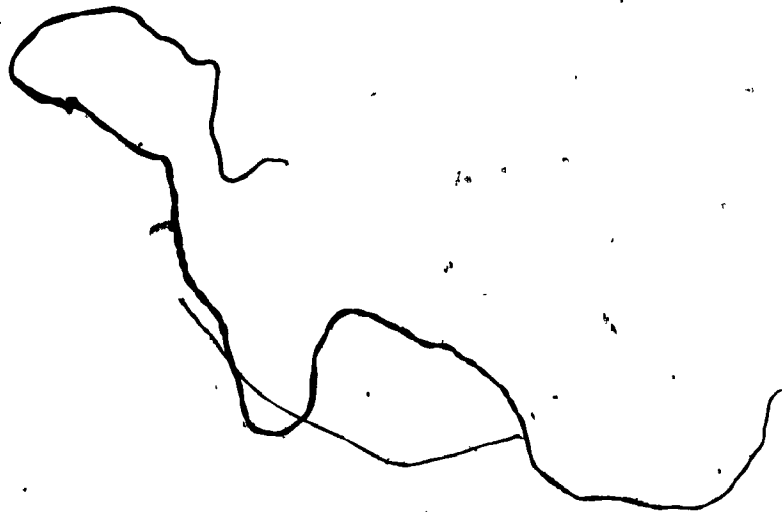
$\rho_p/\rho_f$

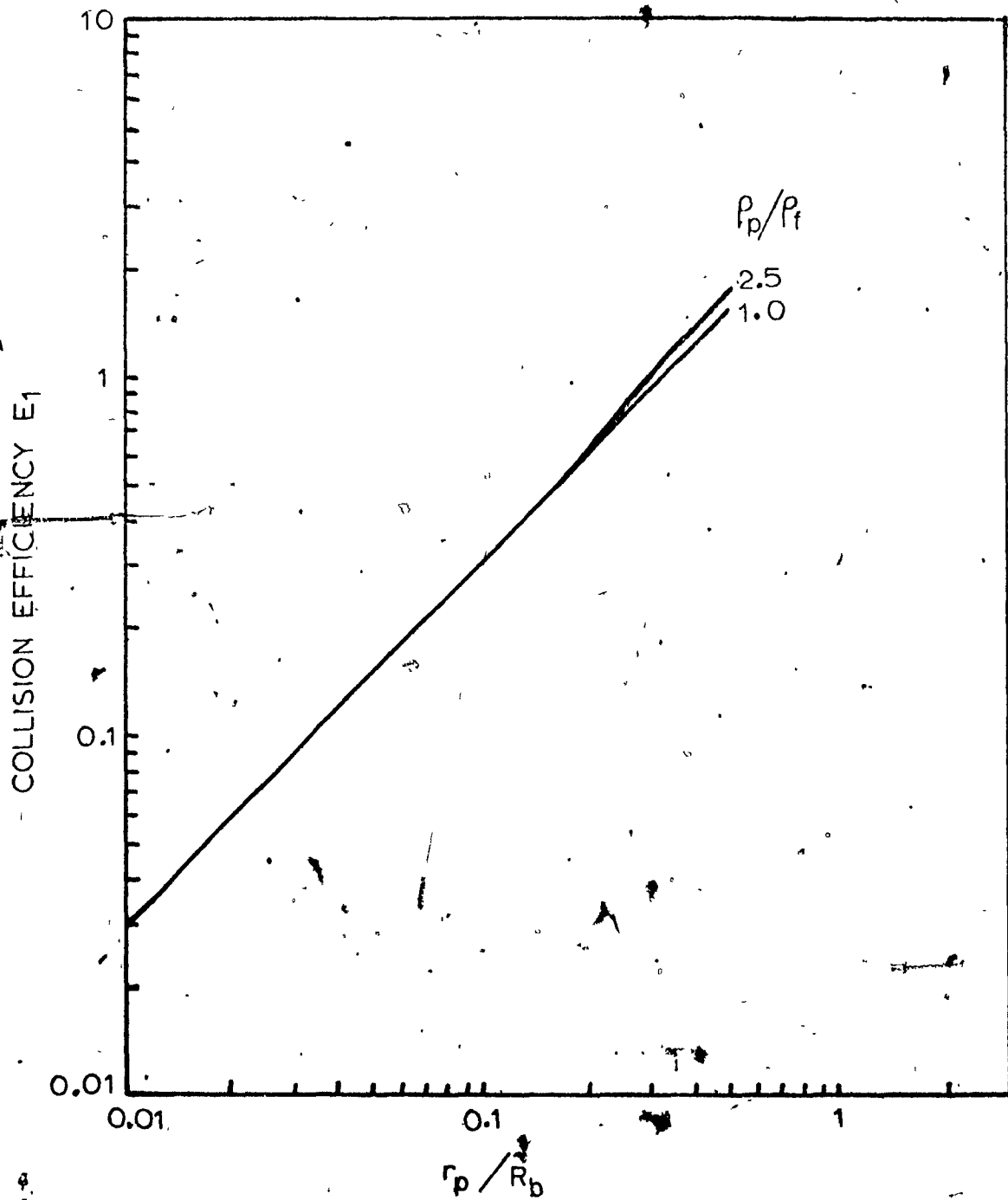
2.5

1.0

Figure 5.5

COLLISION EFFICIENCY  $E_1$  AS A FUNCTION OF  $r_p/R_b$  AND  $\rho_p/\rho_f$ ,  
WITH POTENTIAL FLOW (PRELIMINARY MODEL)





Algebraic manipulation shows equation 5.15 to be exactly equivalent to equation 4.2, the Flint-Howarth potential flow case taken to the limit of zero Stokes number and corrected for non-zero particle radius (again with  $K = \lambda$ ). Figure 5.5 shows  $E_1 = f\left(\frac{r}{R_b}\right)$  for  $\frac{\rho_p}{\rho_f} = 2.5$  and 1.0.  $E_1 = 3.0 \left(\frac{r}{R_b}\right)$  gives a good approximation regardless of  $\frac{\rho_p}{\rho_f}$ . The average number of particles collected per bubble is predicted to be proportional to  $R_b$ , and for a given air rate flotation rate, is predicted to be proportional to  $1/R_b^2$ . The absolute level of  $E_1$  is an order of magnitude higher than for Stokes flow because of the sharper curvature of the streamlines. The linear relation predicted for  $E_1 = f\left(\frac{r}{R_b}\right)$  agrees well with the experimental results obtained by Gaudin et al. (36) for fine particles and large bubbles.

### 5.6 Closure

In this chapter a simple hydrodynamic model of the capture of small particles by small bubbles has been developed. The next chapter presents some experimental data on the flotation of glass beads. These data permit a crude test of the model's predictions regarding the effects of particle size and bubble size on collection efficiency in the collision regime.

## 6. THE CINEPHOTOMICROGRAPHY EXPERIMENTS

### 6.1 Introduction

The original intention as far as experimental work was concerned was to go directly to the batch cell experiments described in the next chapter. However, these had to be postponed for almost a year due to late delivery of the Celloscope particle counter. Part of this time was used to observe the flotation process on a microscopic scale by taking high speed ciné films through a microscope. The films gave a qualitative insight into what occurs in a flotation cell and enabled some crude quantitative data to be obtained on the effects of particle size and bubble size on collection efficiency.

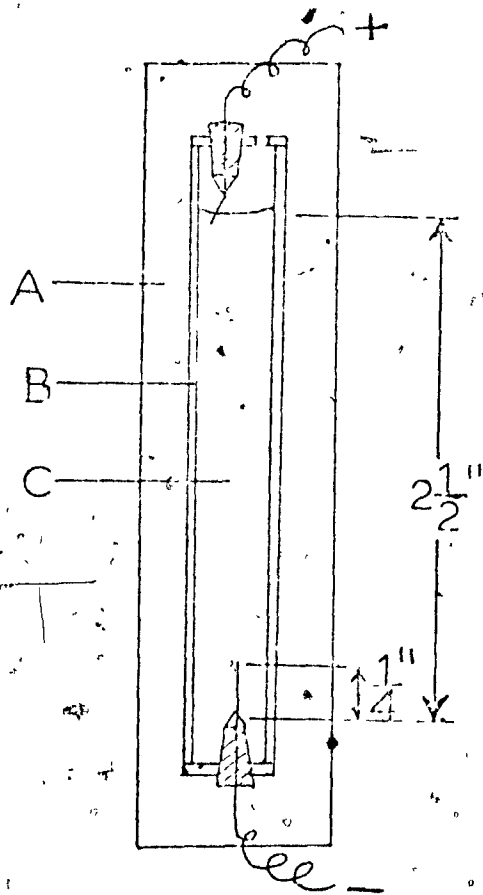
### 6.2 Equipment and Procedure

A small rectangular flotation cell was built of Plexiglas and mounted on a microscope slide as shown in Figure 6.1. The cell contained 2 g./l. of glass spheres of nominal diameter 1 to 20 microns and density 2.5 g./ml. suspended in a  $10^{-4}$  molar solution of a cationic surfactant, ethylhexadecyldimethylammonium bromide, in distilled water. The solution also contained 150 ppm of  $\text{Na}_2\text{SO}_4$  to give it adequate conductivity. The glass spheres were No.4000 Microbeads supplied by Cataphote Corporation, nominal diameter 1-30 microns, from which the +20 micron fraction had been removed by sieving in an Allen-Bradley Sonic Sifter. (Nominal hole diameter 20 microns, actual hole diameters 18-22 microns). Measurements with a Zeiss cytospherometer at the Pulp and Paper Research Institute showed the beads to

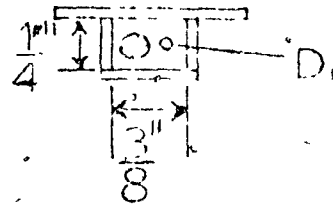
Figure 6.1

MINIATURE FLOTATION CELL

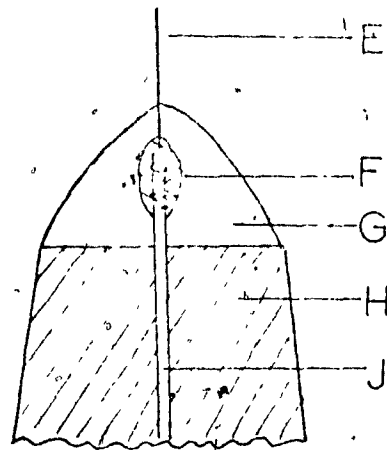
Vertical section



Top view

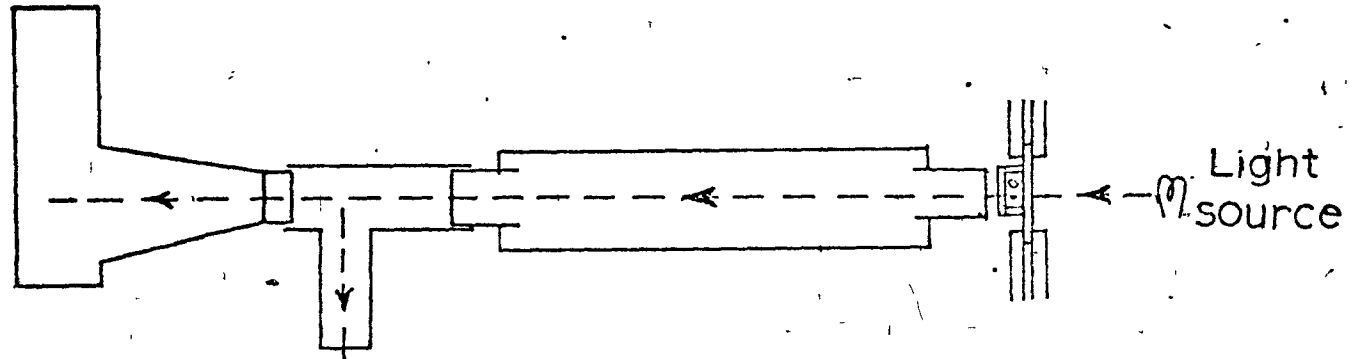


Section through electrode



- A. Microscope slide.
- B.  $\frac{1}{16}$ " Plexiglas.
- C. Solution with glass beads in suspension.
- D. Vent.
- E. Platinum thermocouple wire, diameter 0.002".
- F. Solder.
- G. Silicone sealant.
- H. Cork.
- J. Steel wire, diameter  $\frac{1}{32}$ ".

Figure 6.2  
ARRANGEMENT OF CINÉPHOTOMICROGRAPHY EQUIPMENT (VIEWED  
FROM ABOVE)



High-speed camera

Beam splitter

Compound microscope

Flotation cell clamped in travelling stage

Light source

have a zeta potential of  $-24$  mV in pure water and zero in the cell solution. A steady stream of hydrogen bubbles was generated at the bottom electrode by applying a potential difference of 10 volts across the electrodes with a Harrison voltage generator. Bubbles were generated simultaneously at many sites along the electrode so a broad spectrum of bubble sizes was obtained.

The slide with the cell mounted on it was designed to fit on a vertical travelling microscope stage normally used for medical research at the Montreal General Hospital (39). The stage could be moved up or down at speeds up to  $0.4$  cm./sec. by means of a variable speed motor acting through a gear drive. When in position on the stage the cell was viewed through a horizontal microscope giving 200X magnification. From the microscope the image passed through a beam splitter which gave two identical images. One image was observed by the experimenter while the other was filmed by a Hycam high speed cine camera. Figure 6.2 shows the overall arrangement. A special shutter was used on the camera which only exposed each frame for one-tenth of the time it was in position; for example, when the film speed was 125 frames per second, the exposure time was  $1/1250$  sec..

The objective of the experiments was to film two types of sequence. For type A the stage was stationary, the microscope focussed on the meniscus and the arrival of the bubbles at the meniscus filmed at 125 frames per second. The film was projected on a screen and the sizes of the bubbles and of the particles attached to them were measured. This gave the following information.

- (a) The average number of particles collected per bubble as a function of bubble size. According to our theoretical analysis, this should be almost independent of bubble size up to a bubble diameter of 100 microns.
- (b) The size distribution of the collected particles.

For a type B sequence no bubbles were generated. Initially the microscope was again focussed on the meniscus but this time the stage was given an upward velocity of 0.1 cm./sec. so that the field of view travelled down the cell from the meniscus to the bottom electrode. The sequence was filmed at 40 frames per second. By projecting this film on a screen, the size distribution of the particles in the suspension was obtained. For any narrow size fraction the ratio (particles collected/particles in suspension) will be proportional to the collection efficiency  $E$  of that fraction. Hence, by comparing the size distributions obtained in the type A and type B sequences, a curve of  $E = f(r_p)$  can be constructed. Our simple collision theory predicts  $E \propto r_p^{2.05}$  for a particle density of 2.5 gm./ml.

It was recognized that since the larger particles had an appreciable settling rate, the particle concentration and size distribution in the suspension would be a function of time. To allow for this the filming of all sequences was started at the same time (2 min. 53 sec.) after agitating the cell contents. Repeated type B runs showed that this gave fairly reproducible suspensions (Table 6.2). All sequences were about one minute long.

The main experimental difficulties were as follows:

1. The travelling stage, microscope and high-speed ciné camera were in constant use for an active medical research program and so were only available occasionally for flotation work. This was partly balanced by having an experienced operator at hand when the equipment was available.
2. At 200X magnification the depth of focus of the microscope is very narrow. Within 2 min<sup>s</sup>. 53 secs. a focal plane had to be located containing sufficient bubbles in focus for analysis of the film to be worthwhile. This was very difficult to judge since the bubbles were moving very rapidly when viewed through the microscope. In fact, only two successful type A sequences were filmed.
3. When the films were projected on a screen the bubble and particle outlines had varying degrees of sharpness depending on how close they were to the focal plane. The decision on which bubbles and particles to measure and which to reject as being too fuzzy was to some extent subjective. The criterion adopted was to include an image if, despite some fuzziness, it could be assigned unambiguously to one of the size ranges in use and to reject it if there was some doubt.

Because of these problems the number of bubbles and particles actually observed and measured was quite small. Nevertheless, it was obvious that collection efficiency increased strongly with increasing

particle size and decreasing bubble size and a rough check could be made on the preliminary model developed in Chapter 5.

### 6.3 Results

Table 6.1 presents the results from the two type A sequences filmed. The bubble size distributions are quite different, probably due to focussing on different planes in the cell, and the average bubble size is one-third larger in A2 than in A1. In spite of this the average number of particles per bubble is 0.42 in both cases. If we take the two sequences together  $\Sigma p_c / \Sigma b$  appears to a first approximation to be independent of bubble size, at least up to a bubble diameter of 100 microns. This is in line with the theoretical prediction made assuming Stokes flow. The higher value for bubbles larger than 100 microns may be due to the flow at the front of the bubble deviating appreciably from Stokes flow and starting to move towards potential flow. It is striking that a 90 micron bubble should collect no more particles than a 30 micron bubble even though it sweeps out nine times the liquid volume.

The function

$$X = \frac{\text{average number of particles per bubble}}{\text{cross-sectional area of bubble}} = \frac{(\Sigma p_c / \Sigma b)}{\frac{1}{4} \pi D_b^2}$$

is proportional to the collection efficiency E. Therefore, according to the collision theory developed in Section 5.2, X should be proportional to  $1/D_b^{2.05}$  for particles of density 2.5 gm./ml.. Figure 6.3 is a log-log plot of X versus  $D_b$ . A straight line of slope -2.05 fits

TABLE 6.1

Bubble diameter $D_b$ (microns)	Sequence A1			Sequence A2			$\frac{\sum p_c}{\sum b}$	$X = \frac{(\frac{\sum p_c}{\sum b}) \times 10^4}{\pi D_b^2 / 4}$ (microns <sup>-2</sup> )
	No. of bubbles = b	No. of particles = $p_c$	$\frac{p_c}{b}$	No. of bubbles = b	No. of particles = $p_c$	$\frac{p_c}{b}$		
20-39	43	16	0.38	38	21	0.55	0.46	6.50
40-59	47	21	0.45	48	11	0.23	0.34	1.73
60-79	15	7	0.47	31	14	0.45	0.46	1.19
80-99	1	0	0	17	7	0.41	0.39	0.613
100+	2*	1	0.50	15**	9	0.60	0.59	0.431***
Total	108	45	0.42	149	62	0.42	0.42	

\*average 124 microns

\*\*average 133 microns

\*\*\*based on average  $D_b = 132$  microns

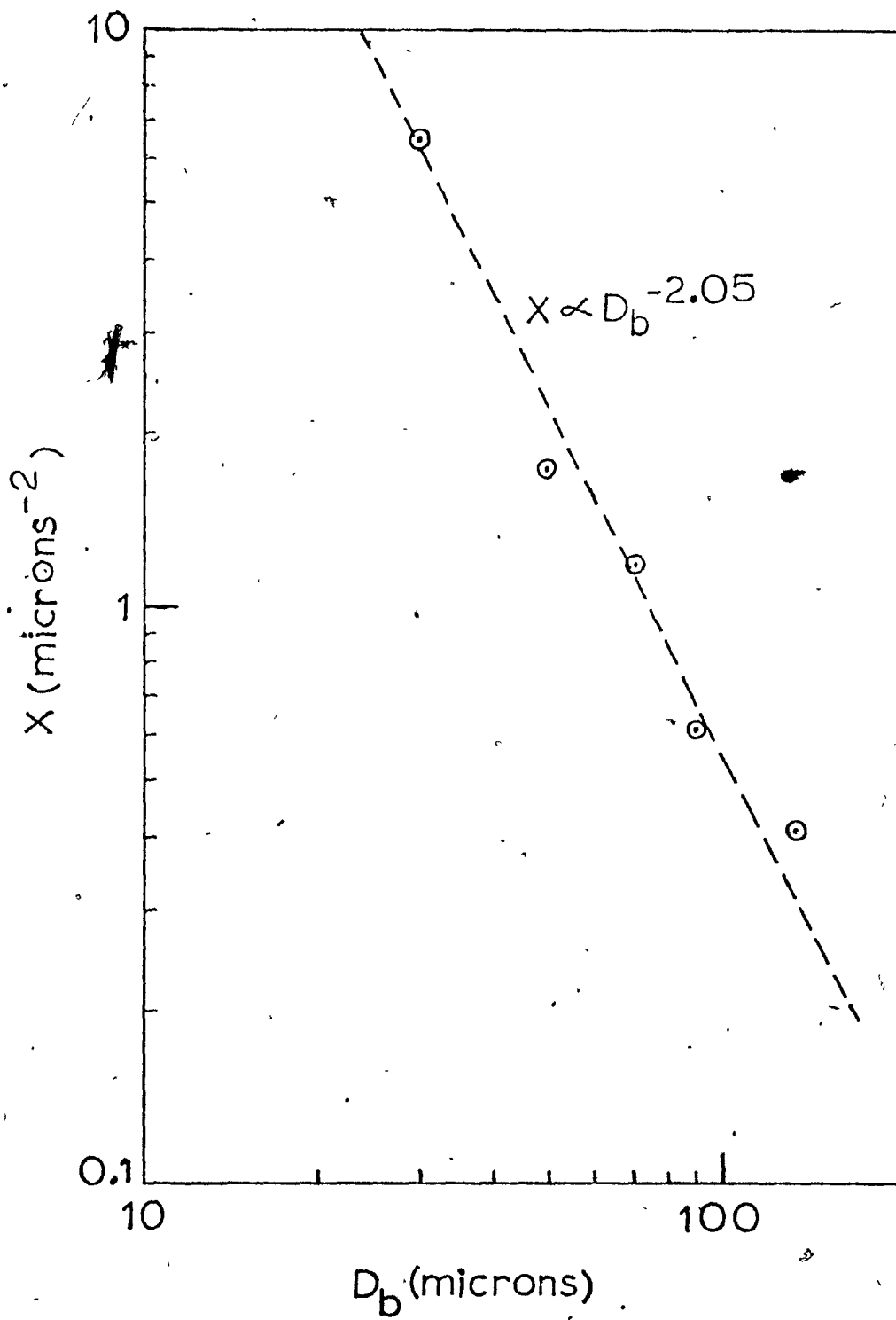
Average bubble diameter (microns):

Sequence	$\overline{D_b}$	$\sqrt{\overline{D_b^2}}$
A1	46	49
A2	62	69
A1 A2	56	61

In calculating X for each bubble size range, the value of  $D_b$  at the mid-point of the range has been used, except where noted.

Figure 6.3

X VERSUS  $d_p$



the data quite well.

Table 6.2 presents size distributions of collected particles (A sequences) and particles in suspension (B sequences). For B1 and B2 the field of view of the microscope travelled from the meniscus to the tip of the bottom electrode, whereas for B3 and B4 it travelled from the meniscus to the bottom of the bare portion of the bottom electrode. It is apparent that due to sedimentation the bubbles from the bottom of the electrode saw not only more particles but also a higher proportion of larger particles than those from the tip. Bubble generation appeared to be uniformly distributed along the electrode. The reasonably good agreement between B1 and B2, and again between B3 and B4, confirms that our suspensions were fairly reproducible. Table 6.3 shows that there was comparatively little agglomeration of particles in the suspension. This was important since there was no way of deciding whether collected particles had come from singlets or agglomerates.

Comparing the A and B sequences it is obvious that the larger particles are collected preferentially. The function  $Y = p_c / p_s$  is a measure of the probability of collection of particles in a given size fraction and is proportional to the collection efficiency  $E$ . According to the collision theory of Section 5.2, it should be proportional to  $d_p^{2.05}$  for particles of density 2.5 gm./ml. Figure 6.4 is a log-log plot of  $Y$  versus  $d_p$ . A straight line of slope 2.05 fits the data well up to a particle diameter of 15 microns (just over a quarter of the average bubble diameter), suggesting that our theory is valid in this region. At larger particle diameters the increase in collection efficiency with increasing  $d_p$  is much

TABLE 6.2

Particle diameter d <sub>p</sub> (microns)	Number of particles in focus (p)								
	Sequence		Σ P <sub>c</sub>	Sequence				Σ P <sub>s</sub>	Y = $\frac{\sum P_c}{\sum P_s}$
	A1	A2		B1	B2	B3	B4		
2-4	0	0	0	2	3	1	3	9	0
5-7	0	0	0	7	6	5	7	25	0
8-10	1	2	3	7	10	8	5	30	0.100
11-13	5	10	15	17	19	15	16	67	0.224
14-16	18	23	41	26	20	39	44	129	0.318
17-19	11	17	28	5	5	11	12	33	0.849
20-22	10	10	20	2	2	3	1	8	2.500
Total	45	62	107	66	65	82	88	301	

TABLE 6.3

Sequence	B1	B2	B3	B4
Singlets	62	61	77	86
Doublets	2	2	1	1
Triplets	0	0	1	0
Total Particles	66	65	82	88

Figure 6.4  
Y VERSUS  $d_p$  (LOG-LOG)

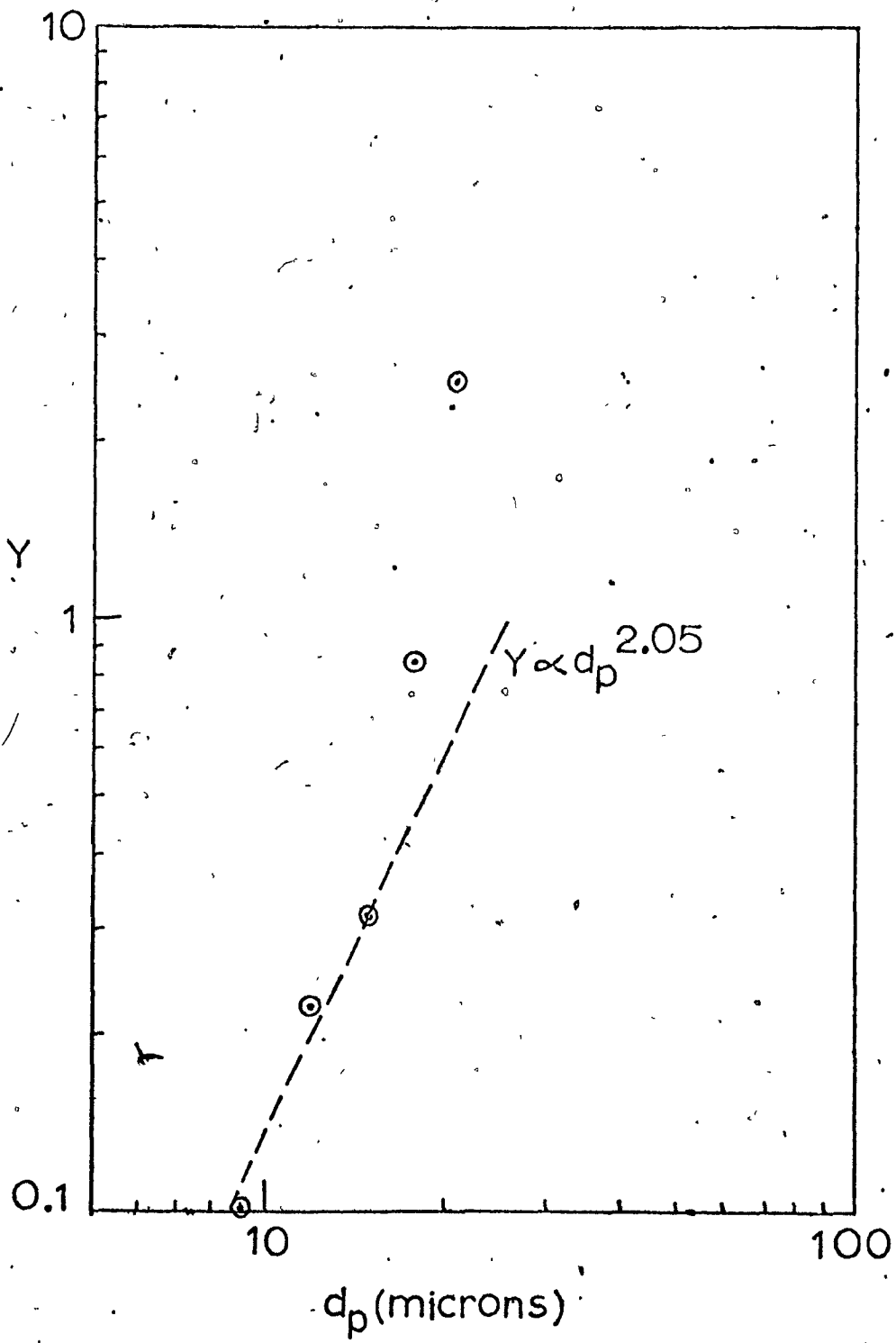
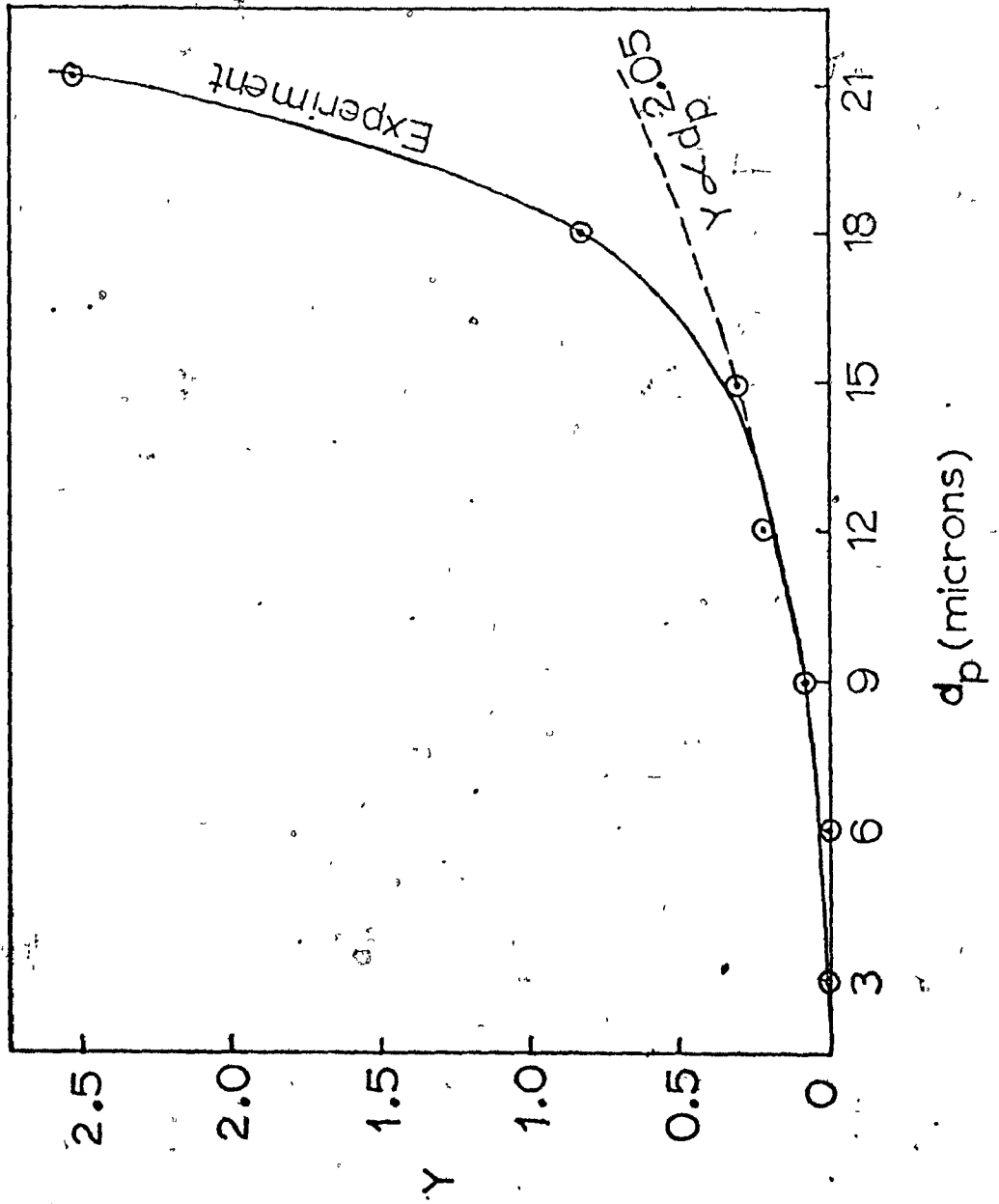


Figure 6.5  
Y VERSUS  $d_p$  (LINEAR)



greater than predicted. This is shown dramatically on a linear plot (Figure 6.5). The following are some possible explanations.

- (a) The statistical precision of the results is too low. If a lot more particles and bubbles had been observed perhaps a better fit to the model might have been obtained.
- (b) Perhaps the collision analysis is oversimplified and for  $d_p/D_b > 0.25$  it is not realistic to ignore the effect of the particle on the flow field round the bubble. This will be considered further in Chapter 8.
- (c) Perhaps when filming the A sequences there were more of the larger particles in suspension than when filming the B sequences despite allowing the same time after shaking the cell. This could occur if the thin stream of bubbles in the A sequences retarded settling appreciably.
- (d) Perhaps the attachment efficiency becomes strongly dependent on  $d_p$  above  $d_p^* = 15$  microns.

It was observed that collected particles were always held at the rear stagnation point of bubbles arriving at the meniscus (Fig.6.6). When a bubble carried more than one particle they were always grouped in a spherical cap around the rear stagnation point (Fig.6.7). When the bubble's motion became horizontal as it began to roll along the meniscus, the particles readily rolled around to the new rear stagnation point but remained firmly attached to the bubble. Just below the meniscus one collision resulting in stable

Figure 6.6 and Figure 6.7

6.6 BUBBLE CARRYING ONE PARTICLE

6.7 BUBBLE CARRYING TWO PARTICLES

FIG. 6.6

Direction  
of motion

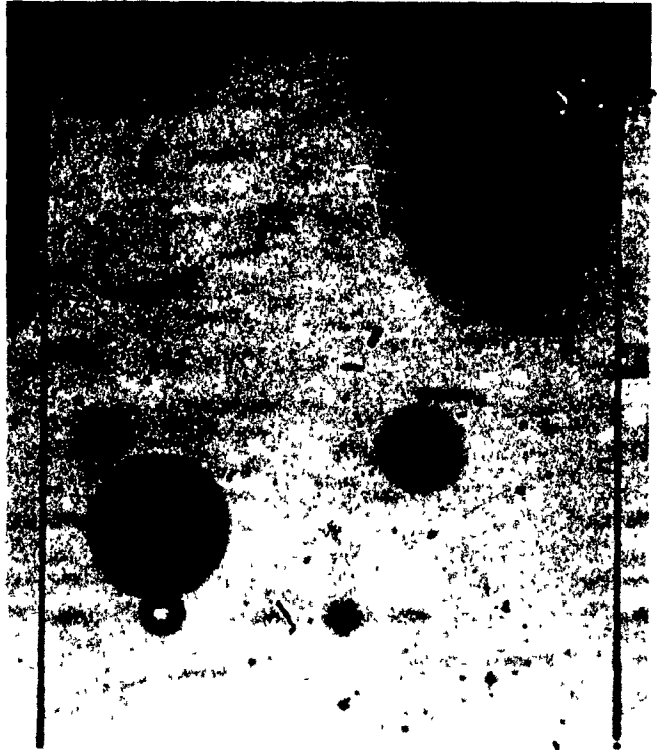
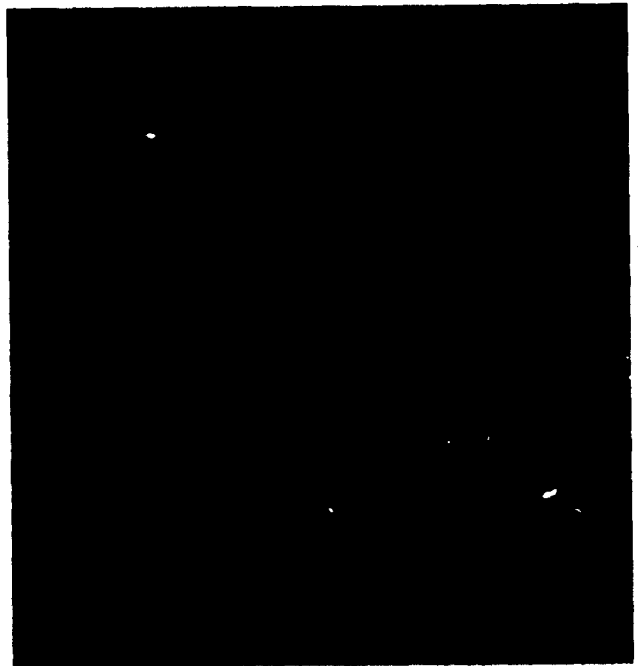


FIG. 6.7

Direction  
of motion



attachment was observed with sufficient clarity for it to be obvious that the collected particle was swept to the rear stagnation point while the bubble rose through one bubble diameter. This implies that in a taller cell or a more concentrated suspension, the collection efficiency of a bubble should remain constant until it has collected sufficient particles to cover completely the back half of its surface.

The angle of contact between bubbles and particles is too small to be measurable, yet once attachment had occurred it seemed to be very stable. A possible explanation is suggested in Chapter 8, Section 8.4.

#### 6.4 Closure

The experiments described in this chapter show that the flotation rate of glass beads increases strongly with increasing particle size and decreasing bubble size. The preliminary model developed in Chapter 5 gives fair agreement with experiment, but the data are too sparse and too uncertain to be decisive.

With the arrival of the Celloscope particle counter it became possible to observe flotation on a macroscopic rather than a microscopic scale, thereby obtaining results which are much more significant from a statistical viewpoint. These experiments are described in the next chapter.

## 7. THE BATCH CELL EXPERIMENTS

### 7.1 Introduction

The experiments described in the previous chapter confirmed that particle size and bubble size have large effects on collection efficiency. To estimate the magnitude of these effects with some precision it is essential that measurements be made over much larger numbers of particles and bubbles than was possible with the cinéphotomicrography equipment. This was done by carrying out batch flotation runs in cells containing 400 ml. of liquid and many millions of particles and bubbles. Samples were withdrawn at regular intervals and analysed for particle concentration and size distribution. This enabled the fall in concentration of particles of various sizes to be measured simultaneously and individual rate constants to be calculated for each size fraction. The bubbles were generated by forcing nitrogen through a porous glass frit in the base of the cell. By carrying out runs with frits of different pore sizes the bubble size could be varied and an estimate obtained of the effect of bubble size on the rate of removal of the various particle sizes. The following sections describe in detail the equipment, materials, preliminary tests, experimental procedure and final results.

### 7.2 Equipment

Exhibit 7.1 lists the principal equipment used. Fig.7-1 depicts the gas supply system.

EXHIBIT 7-1

Equipment

Flotation Rig

600 ml. Pyrex Buchner funnel with fritted disc:

- (a) fine frit            4 - 5.5  $\mu$  pores
- (b) medium frit        10 - 15  $\mu$  pores
- (c) coarse frit        40 - 60  $\mu$  pores

Foam suction plate (see Fig. 7.2)

Rotameter - Brooks model 1-15-6

Flow controller - Moore model 63BUL

Mercury manometer

Stirrer - Eberhard "Labstir", variable speed (see Fig. 7.2)

Stroboscope - General Radio "Strobotac" Type 1531-AB

Sampling

8 x 10 ml. pipettes

8 x 50 ml. conical flasks

8 x 13 ml. test tubes

Analysis

Celloscope model 111LS particle counter with 24 $\mu$ , 76 $\mu$  and 300 $\mu$  orifices and 16 $\mu$ l, 320 $\mu$ l and 5ml volumetric sections.

Nuclear Data model ND-110 pulse height analyzer.

Telequipment model S51B oscilloscope.

Dohrmann model SY-850 strip chart recorder.

Acoustica AS200 ultrasonic bath.

Geotec model 349-1838 planimeter.

Figure 7.1

BATCH CELL FLOTATION RIG; FLOWSHEET

Nitrogen  
cylinder

Glass wool  
filter

Manometer

Rotameter

Flow  
controller

Flotation cell

To aspirator

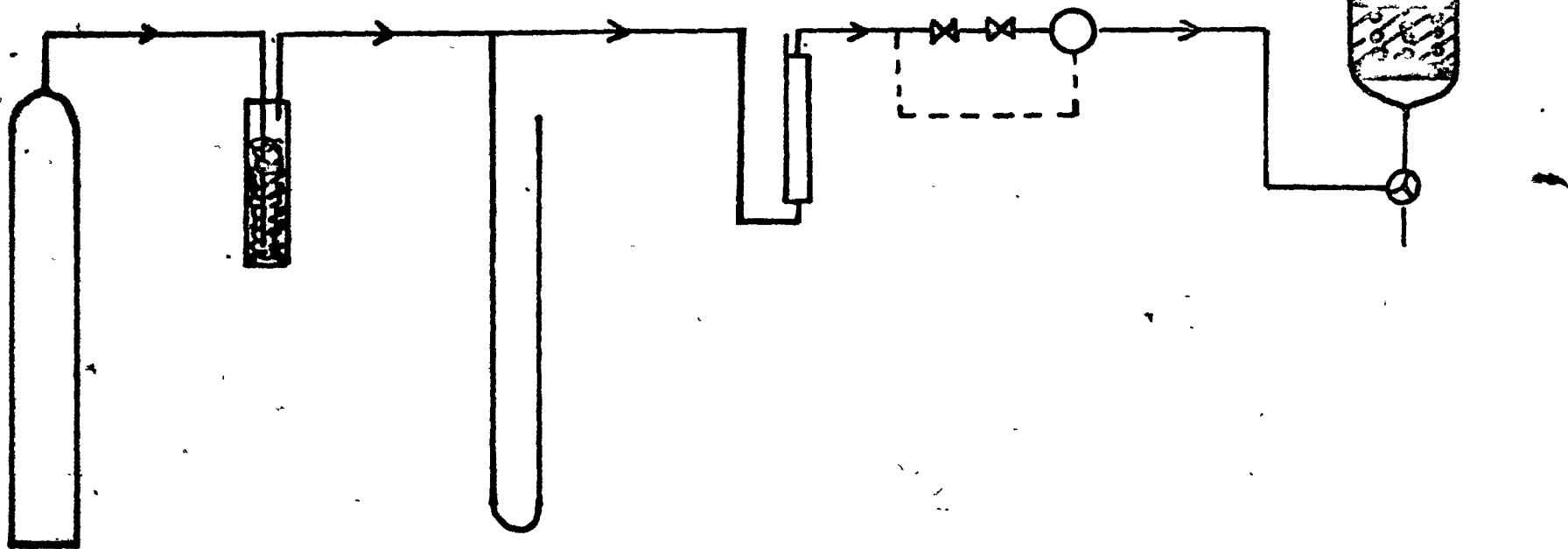
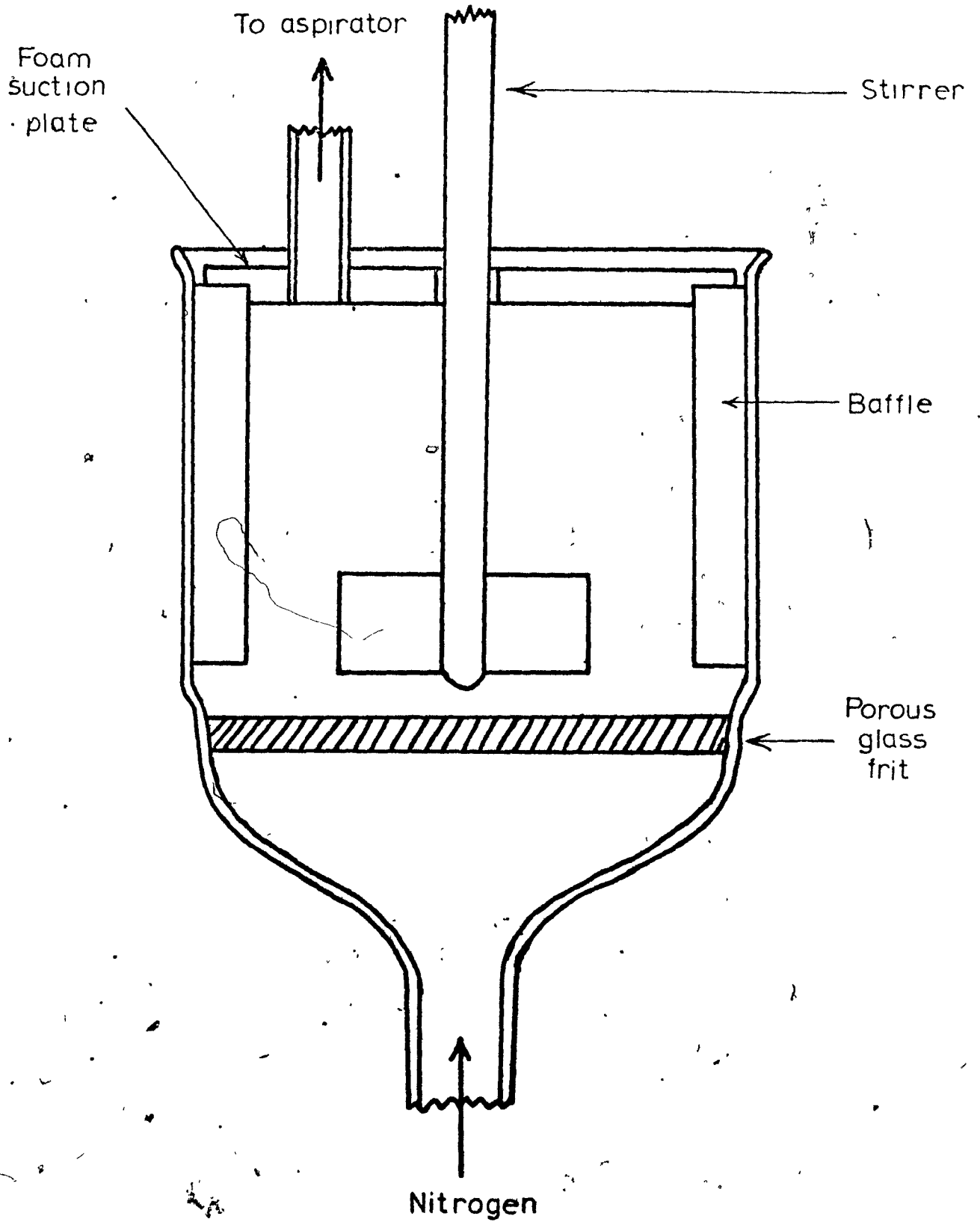


Figure 7.2

(A) BATCH CELL; SIDE VIEW (ACTUAL SIZE)

(B) BATCH CELL; TOP VIEW (ACTUAL SIZE)

7.2(a)



7.2(b)

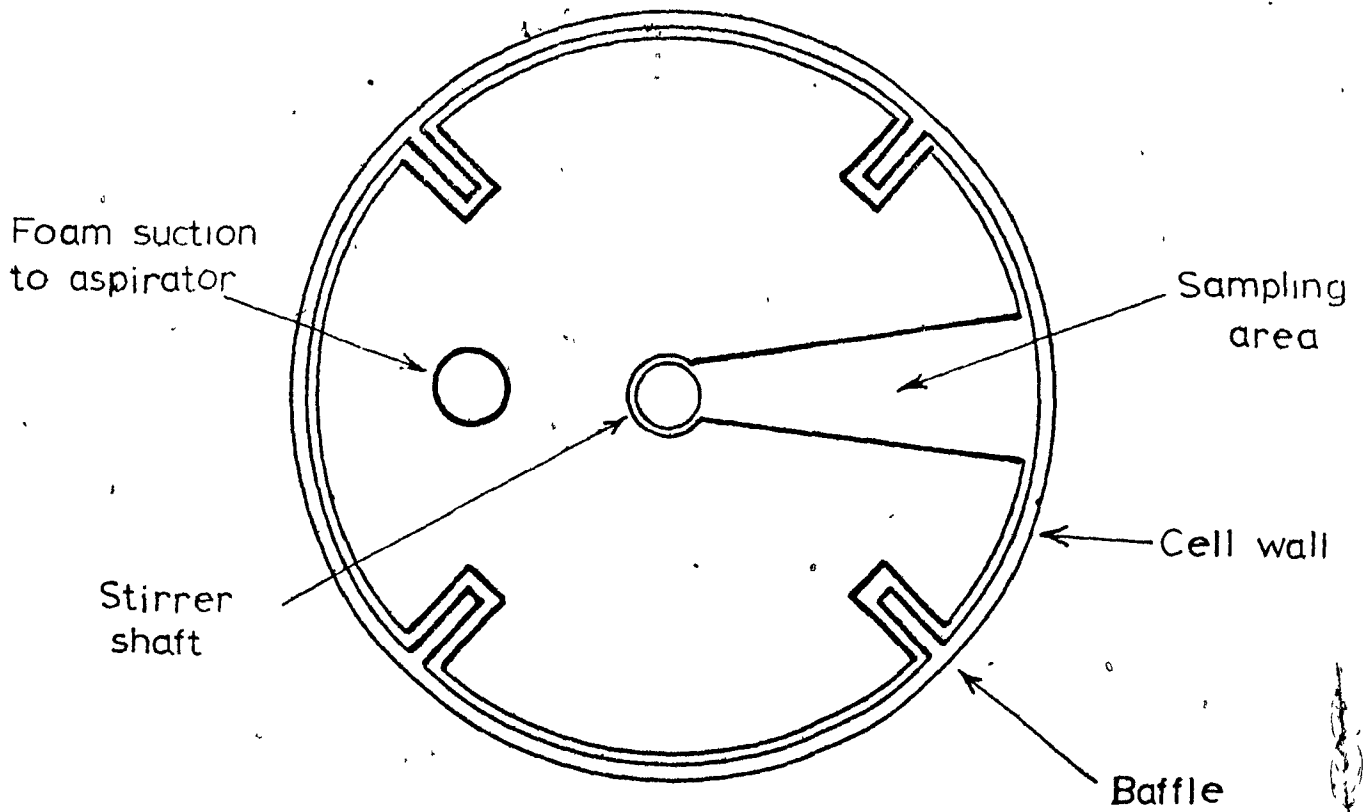
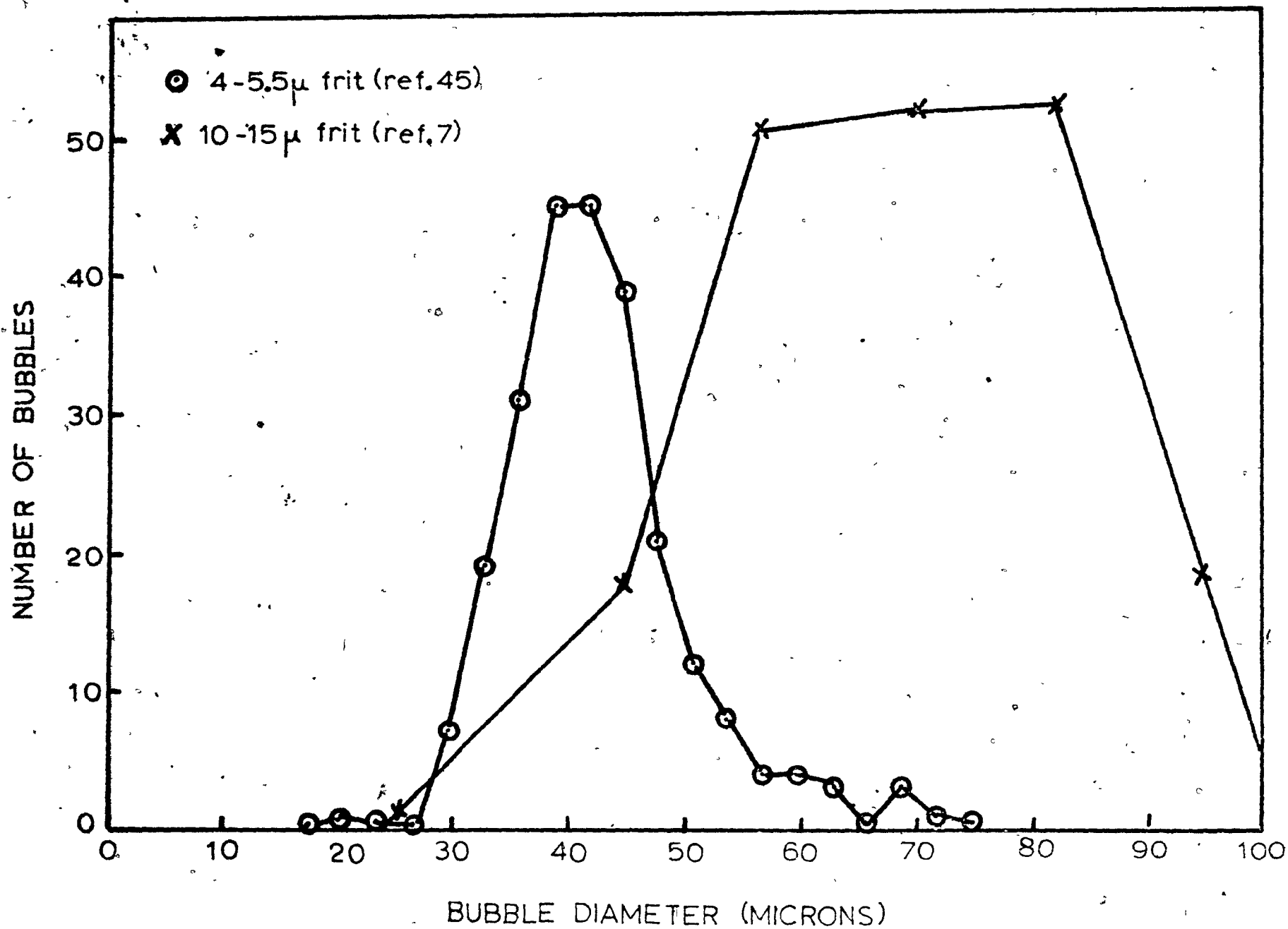


Figure 7.3

BATCH CELLS; BUBBLE SIZE DISTRIBUTIONS (TAKEN FROM  
KALMAN (7) AND KAUFMAN (45))



The 600 ml. Pyrex Buchner funnels used as flotation cells are available commercially in the three frit sizes listed. The only modification made to them was to glue four vertical Plexiglas baffles to the side walls as shown in Fig. 7.2 in order to prevent vortex formation when the stirrer was used. This type of flotation cell was selected because it had been shown in the past to give very reproducible bubble size distributions in the range desired when 0.1 to 0.5 vol.% of alcohol was added to the water in the cell (7,55). Also, the bubble size could be varied easily by using frits with different pore sizes. Generating the bubbles electrolytically at a grid of platinum wires was considered and rejected. On the basis of experience with the small cell used in the cinéphotomicrography experiments it was expected that in such a cell ageing of the electrodes would lead to poor reproducibility of bubble size distribution. Also, variation of the bubble size and measurement of the gas rate would be difficult.

Except for the baffles the cells used were identical to those employed by Kaufman (55) and Kalman (7). Using a photographic technique for bubble size measurement and employing similar gas flow rates to those used in the present experiments Kaufman found that the fine frit generated bubbles of average diameter 42 microns when the cell liquid was water containing in excess of 0.1 vol.% of a low molecular weight alcohol. As the alcohol concentration was increased to 0.5 vol.% the bubble size distribution became narrower but the mean did not change significantly. The mean was also not changed significantly by adding surfactant in concentrations up to

50 ppm or by varying the gas flow rate within the limits used in the present experiments. Under similar conditions Kalman found an average bubble diameter of 71 microns with the medium frit. Typical bubble size distributions obtained by Kaufman and Kalman are shown in Fig.7.3. Tests described later in this chapter indicate that the bubble size distributions were not affected significantly by the presence or absence of stirring in the cell.

The chief problem with the flotation rig was control of the gas flow rate. The control system used often gave very good, steady control but on other occasions the gas flow rate could be very unsteady, possibly due to particles of dirt sticking in a needle valve. With the fine and medium frits it was found essential before beginning a run to wash them with the surfactant solution to be used in the run, otherwise there was a jump of 10 to 15 per cent in the gas flow rate when surfactant was injected into the cell liquid.

Samples were taken with 10 ml. graduated pipettes rather than syringes because it was found that when samples were ejected from syringes a significant proportion of the particles stuck in the neck of the syringe and were lost.

The particle counter and ancillary equipment used for analysing the samples are described fully in Appendix A.

### 7.3 Materials

The principal materials used are listed in Exhibit 7-2.

The glass beads and styrene divinylbenzene (SDB) latex both consisted of perfectly spherical particles so there was no

EXHIBIT 7-2

Materials

Glass beads - Class IV, No.4000, type A glass microbeads, Cataphote Corporation, Jackson, Mississippi. Nominally 1 - 30 microns, density 2.5 gm./ml. Sieved in Allen-Bradley Sonic Sifter fitted with 20 microns electroformed sieve to remove +20 micron fraction (hole size actually 18 - 22 microns). Exhibit 7-3 shows a typical size distribution.

Latex - Styrene divinylbenzene copolymer, average diameter  $5.7\mu$ , density 1.05 gm./ml. Diagnostic Products Division, Dow Chemical Co., Indianapolis, Indiana (supplied as suspension containing 10% latex by wt.). Exhibit 7-4 shows a typical size distribution.

• Ethylhexdecyldimethylammonium bromide (EHDA-Br) -

Practical grade, Matheson, Coleman and Bell, Inc.

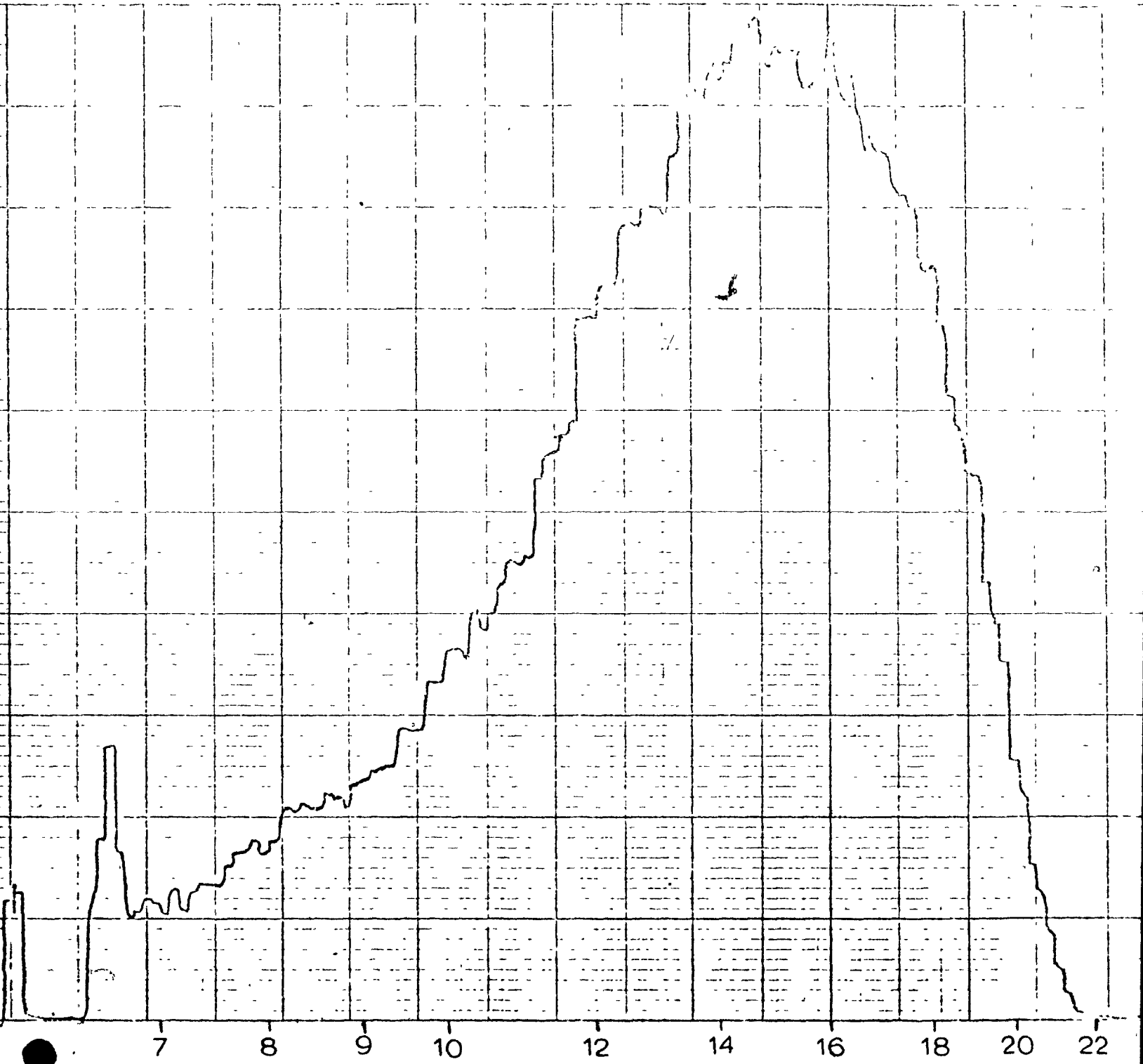
Isopropanol (IPA) -

A&C American Chemicals, Ville St-Laurent, Quebec.

Exhibit 7.3

GLASS BEAD SIZE DISTRIBUTION

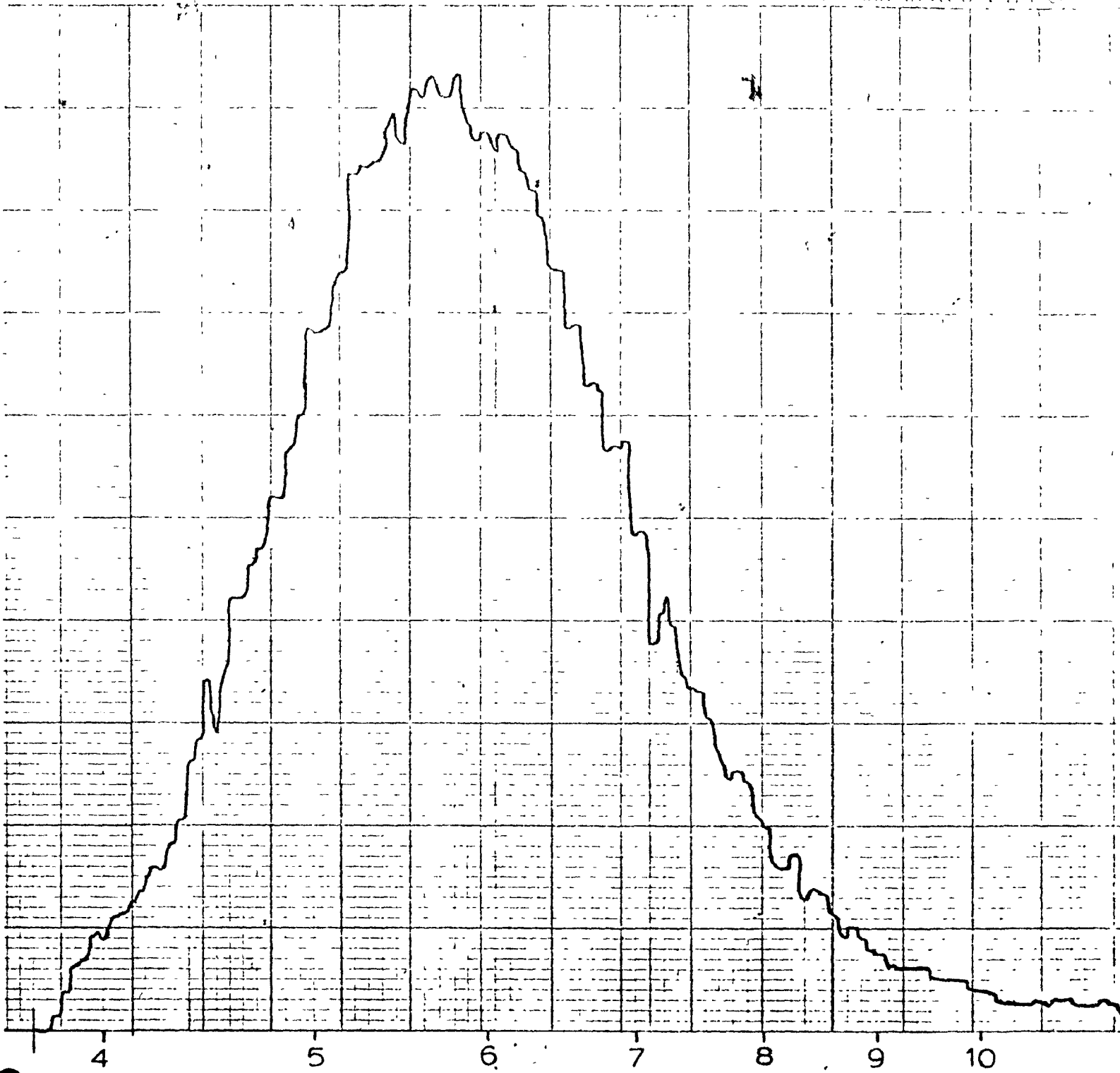
CP DIVISION LOHRMANN INSTRUMENTS CO



PARTICLE DIAMETER (MICRONS)

Exhibit 7.4

STYRENE DIVINYLBENZENE LATEX SIZE DISTRIBUTION



PARTICLE DIAMETER (MICRONS)

ambiguity about the definition of particle size. Furthermore, the fact that the particles were spherical reduced their tendency to coagulate in suspension. The initial concentration of glass beads in flotation runs was 1000 mg./ℓ., made up by suspending 0.4g. of beads in 400 ml. of distilled water. This gave an initial particle count of roughly 140,000 particles per ml., representing an average particle to particle separation of about 14 particle diameters. The latex was supplied as a suspension containing 10 wt.% solids. For flotation runs 20 drops of this were mixed with 400 ml. of water to give a solids concentration of about 130 mg./ℓ. (approximately  $1.3 \times 10^6$  particles per ml. or an average particle separation of about 16 particle diameters). Both types of particle had a negative charge in distilled water at pH 6.0 (the working pH for flotation runs). The zeta potential of the latex particles, measured by observing the motion of thirty particles in a Zeiss cytospherometer, was -7.5 mV. The zeta potential of the glass beads was very difficult to measure due to the rapid settling of the particles, but appeared to be in the region of -20 mV to -30 mV.

The same cationic surfactant, ethylhexadecyldimethylammonium bromide (EHDA-Br), was used in all flotation runs. The critical micelle concentration of this surfactant is about  $5 \times 10^{-4}$  M (56). The concentrations used in this work ranged from  $0.25 \times 10^{-4}$  M to  $10^{-4}$  M. At the lower end of this range the froth had to be stabilized by adding a few drops of a solution containing 1 part Dowfroth 350 to 1000 parts water. The EHDA-Br and the isopropanol (IPA) were made up into a stock solution (henceforth referred to as SF solution)

containing 50 vol.% IPA and  $10^{-2}$  M EHDA-Br. This solution could be stored indefinitely without micelle formation. Diluting 1 part of SF solution with 100 parts of water gave  $10^{-4}$  M EHDA-Br + 0.5 vol.% IPA. The latex particles had a zeta potential of +19.3 mV in  $10^{-4}$  M EHDA-Br and +10.6mV in  $0.5 \times 10^{-4}$  M EHDA-Br. The glass beads had a very small positive zeta potential in  $10^{-4}$  M EHDA-Br.

The starting suspensions for all flotation runs were made up using ordinary distilled water produced in a Corning AG-3 still and adjusting its pH to 6.0 by adding a drop or two of standard NaOH or HCl solution. Tests with the particle counter showed that this water was virtually free of particles larger than 3 microns.

Initially an attempt was made to be super-hygienic by filtering all distilled water through Millipore MF filters of pore size 0.22 microns. However, the results obtained showed no reproducibility whatever, flotation rates obtained under apparently identical conditions differing by two orders of magnitude. It was subsequently revealed by a Millipore salesman that MF filters are impregnated with a powerful wetting agent which is leached out into the filtrate. This is not mentioned in any of Millipore's promotional literature. Undoubtedly the wide variation in observed flotation rates could be ascribed to whether our distilled water had been filtered through a fresh or an old filter. Reproducibility of flotation rates was good when suspensions were made up in distilled water which had not been filtered.

Filtered water had one use. It was found that the wetting agent leached out from the filters prevented coagulation of particles

in samples more effectively than any other wetting agent tried. Therefore, all samples were diluted with filtered water as soon as they were taken, the dilution water having been prepared by filtering 300 ml. of water per filter. It was subsequently discovered that the wetting agent involved is Triton X100.

#### 7.4 Preliminary Tests

##### 7.4.1 Settling of glass beads

It was apparent immediately that at the low gas rates used the updraught provided by the rising gas bubbles was not sufficient to prevent substantial settling of the glass beads during a flotation run. Therefore, a stirrer was necessary. The stirrer is sketched in Fig.7.3. In turn this necessitated the fitting of vertical baffles to the sides of the cell (shown in Fig.7.2) to prevent the formation of a vortex which would suck froth back into the liquid. The stirrer speed was measured by a stroboscope. The maximum permissible stirrer speed was found to be 185 rpm, since above that speed interfacial turbulence began to cause re-entrainment of froth into the liquid. To allow some safety margin the stirrer speed was set at 165 rpm for all flotation runs involving glass beads. The stirrer was positioned centrally in the cell with the bottom edge of its blade 5/16" above the distributor. A check was now carried out to determine whether any settling of glass beads was taking place under these conditions.

400 ml. of water was placed in a cell and the stirrer allowed to warm up until its speed was steady at 165 rpm. Then

0.4g. of glass beads was dropped into the cell. There was no gas flow or addition of surfactant or alcohol. One minute was allowed for dispersion of the beads and then 3 ml. samples were taken every minute for the next five minutes. The particle concentrations found in the samples are listed in Table 7.1.

TABLE 7.1

<u>Time (mins.)</u>	<u>Particles per ml.</u>
1	136,000
2	149,000
3	131,000
4	137,000
5(1)	134,000
5(2)	139,000

The two 5-minute samples were taken simultaneously, sample 5(1) being from  $\frac{1}{4}$ " above the distributor and sample 5(2) from  $1\frac{1}{2}$ " above the distributor. It was concluded that no settling or stratification of particles was occurring in the cell. Since the test was carried out with no gas flow, obviously the same conclusions will hold when additional mixing is provided by gas bubbles.

#### 7.4.2 Coagulation During Flotation

Since particles are made floatable by adsorption of surfactant ions of charge opposite to that on the particles it is clear that their zeta potential must be reduced and conditions in the

flotation cell could be conducive to particle coagulation. If substantial agglomeration was occurring during the few minutes of a flotation run it would be revealed by the appearance in the samples of particles apparently larger than the largest particles in the starting material. No such particles were observed. It was concluded that there was no significant coagulation of particles during flotation runs.

#### 7.4.3 Coagulation of Samples

Sample analysis took up to fifteen minutes per sample. Usually eight samples were taken during a flotation run, so the last samples to be analysed could have been standing for up to two hours. It was found initially that signs of coagulation began to appear after half an hour's standing and this got progressively worse as time went on. This was prevented effectively by the following measures:

- (a) using filtered water for sample dilution instead of ordinary distilled water (see Section 7.3);
- (b) giving each sample five minutes in an ultrasonic bath immediately before analysis.

Neither of these measures by themselves was sufficient, but when used together they ensured that when analysed the particles were not coagulated. (Note: for the tests described in Sections 7.4.2 and 7.4.5 the samples were analysed as soon as they were taken; they were diluted with unfiltered water and were not subjected to ultrasonic treatment.)

#### 7.4.4 Coagulation During Analysis

The samples were stirred vigorously during analysis. It was expected that this would prevent settling of glass beads and particle coagulation during analysis. Repeat analyses on the same sample fifteen minutes apart showed no change in size distribution, indicating that the assumption was valid. However, with the glass beads it was found that if the samples contained no surfactant there was a reduction in particle count due to deposition of particles on the sides and bottom of the analysis beaker. Small particles were deposited just as readily as large ones so it was not a gravitational effect. It was prevented by adjusting all diluted samples to a surfactant concentration of  $10^{-4}$  M prior to analysis. Cationic and anionic surfactants were equally effective in preventing this phenomenon.

#### 7.4.5 Coagulation of Latex Prior to Flotation

For the flotation runs with SDB latex the latex suspension was made up and SF solution added to it 15 minutes before placing it in the flotation cell in order to allow plenty of time for surfactant adsorption. The suspension was not stirred. Samples taken at the beginning and end of this period showed no evidence of coagulation during it.

#### 7.4.6 Gas Hold-up in Liquid

The gas hold-up in the cell liquid was estimated crudely by withdrawing a sample with a graduated pipette, noting its apparent

volume, discharging it to a 10 ml. measuring cylinder, allowing all bubbles to rise to the surface and noting the final volume of the liquid. The percentage reduction in volume was taken to be the gas hold-up in the liquid. The cells were not stirred and the cell liquid contained  $10^{-4}$  M EHDA-Br and 0.5 vol.% IPA. Results were as follows:

TABLE 7.2

<u>Frit</u>	<u>Gas Rate (ml./min.)</u>	<u>% Gas Hold-up</u>
4-5.5 $\mu$	19	6
10-15 $\mu$	44	2
40-60 $\mu$	41	0

Happel and Pfeffer's analysis of bubble or particle assemblages suggests that at these concentrations the drag on the bubbles is unlikely to be much different from that on isolated bubbles (57).

With the 4-5.5  $\mu$  frit at gas rates above 40 ml./min. the froth-liquid interface was difficult to distinguish and gas hold-up in the liquid was greater than 20%. Under such conditions the carry-over of liquid into the foam phase must be so great that the value of flotation as a separation process becomes doubtful. No flotation runs were carried out under those conditions.

#### 7.4.7 Variation of Liquid Height with Time

The height of liquid in the cell decreased linearly with time as liquid was carried up into the froth. If  $h$  is the liquid

height in cm., G the gas flow rate in ml./min. and t the time in minutes, the following correlations were obtained:

fine frit:  $h = 6.1 - 0.0067 Gt$   
medium frit:  $h = 5.6 - 0.0055 Gt$

In the flotation runs to be described the gas rates were low enough and the run times short enough to make corrections for reduction in liquid height unnecessary.

7.4.8 Loss of Surfactant with Time

It was recognized that the surfactant concentration in the cell would fall with time due to preferential adsorption of surfactant on the bubbles. A test was carried out in which 400 ml. of water containing initially  $10^{-4}$  M EHDA-Br and 0.5 vol.% IPA was placed in the cell with the medium frit, nitrogen was bubbled through at 44 ml./min. and no particles were present. Samples were taken at five-minute intervals and their absorbance measured at  $218m\mu$  in a Beckmann UV spectrophotometer. EHDA-Br had been found to obey Beer's Law at this wavelength with no interference from the IPA. The results were as follows:

<u>Time (mins.)</u>	<u>EHDA-Br conc.</u>
0	$10^{-4}$ M
5	$0.81 \times 10^{-4}$ M
10	$0.62 \times 10^{-4}$ M
15	$0.53 \times 10^{-4}$ M

Most of the particle flotation runs were carried out at half this air rate and lasted for seven minutes. No falling off in flotation rate with time was observed, which suggested that flotation rate was not sensitive to minor reductions in surfactant concentration.

#### 7.4.9 Mixing

A dose of dye was injected into a cell under operating conditions. It dispersed immediately to give a completely uniform colour within 10 seconds.

#### 7.4.10 Effect of Stirring on Bubble Size

Fine and medium porosity frits were to be used both with and without stirring. Bubble size measurements were reported by Kaufman (55) for a fine frit with stirring and by Kalman (7) for a medium frit without stirring, both under operating conditions similar to ours. Therefore, it was necessary to check whether stirring altered the bubble size.

The comparison between bubble sizes with and without stirring was made using the particle counter fitted with a 300-micron orifice tube and a 5 ml. volumetric section. To the counter bubbles are indistinguishable from particles since they have zero electrical conductivity. The orifice was placed in the flotation cell and connected to the counter by a length of plastic tubing. The outer electrode was also placed in the cell and was connected to the counter terminals by a flexible lead. 0.1% NaCl solution was used in the

cell instead of distilled water in order to give the liquid sufficient conductivity for the counter to function. Otherwise, conditions were exactly as in flotation runs (except for the absence of particles). It was realized that the NaCl would depress the bubble size somewhat but Zieminski's data (58) show that at 0.1% concentration the reduction in bubble diameter should not be more than 2 or 3 per cent.

An absolute measurement of bubble size could not be made since the concentration of bubbles was so high that coincident appearance of several bubbles in the orifice at once was inevitable. However, a reduction in bubble size should lead to a reduction in the relative particle diameter at which the peak of the apparent size distribution occurs. The log 6 output mode was used throughout.

Table 7.3 lists the results. Kaufman and Kalman had shown previously that varying surfactant and alcohol concentrations within the limits used here has no significant effect on the bubble size. These data show that stirring has no effect either, at least not with our stirrer at 165 rpm. It seems that increasing the gas rate may increase the bubble size slightly with the fine frit, but otherwise it appears that the data of Kaufman and Kalman can be used for both stirred and unstirred situations.

With the coarse frit gas distribution was very poor since only a few sites were generating bubbles at the low gas rates which had to be used with our equipment. To obtain a rough estimate of the size of the bubbles a cathetometer was focussed on the bottom layer of bubbles in the froth and the hair-lines moved across the

TABLE 7.3

Run number	1	2	3	4	5	6	7
Frit size	10-15	10-15	10-15	10-15	4-5.5	4-5.5	4-5.5
Gas rate (ml./min.)	44	44	23	23	23	23	44
Stirrer speed (rpm)	0	165	0	165	0	165	0
EHDA-Br molarity	$0.5 \times 10^{-4}$	$10^{-4}$	$0.5 \times 10^{-4}$	$10^{-4}$	$0.5 \times 10^{-4}$	$10^{-4}$	$0.5 \times 10^{-4}$
Vol.% IPA	0.25	0.5	0.25	0.5	0.25	0.5	0.25
Counter settings:							
G	$4\frac{1}{2}$	$4\frac{1}{2}$	$4\frac{1}{2}$	$4\frac{1}{2}$	$8\frac{1}{2}$	$8\frac{1}{2}$	6
I	1/16	1/16	1/16	1/16	1/16	1/16	1/16
Relative peak diameter	100	101	98	100	71	73	79

bubbles. Both with and without stirring the average bubble diameter was of the order of 0.6 mm. with the range extending from 0.4 mm. to 1.0 mm.

## 7.5 Experimental Procedure for Flotation Runs

### 7.5.1 Glass Beads

The pH of 400 ml. of distilled water was adjusted to 6.0 by adding a few drops of standard NaOH or HCl solution. The water was split into two equal portions of 200 ml. One portion was placed in the cell, after which the gas flow and stirrer were started. The gas flow was adjusted to the desired rate and the stirrer speed adjusted to 165 rpm. Meanwhile, 0.4 gm. of glass beads was weighed out and added to the other 200 ml., stirring with a magnetic stirrer to keep the beads in suspension. When the gas rate and stirrer speed were steady at the desired settings the water containing the glass beads was added to the water in the cell. Thirty seconds was allowed for mixing, then the first sample was taken. Four ml. of SF solution were added to give a concentration of  $10^{-4}$  M EHDA-Br + 0.5 vol.% IPA; this was taken as zero time. Thereafter samples were taken every half minute with the fine frit, every minute with the medium frit and every two minutes with the coarse frit.

The sample dilution procedure took one of two forms depending on the frit size in use. With the medium and coarse frits the samples (volume V ml.) were ejected straight from the pipettes into 50 ml. flasks already containing (40-V) ml. of filtered water. This immediate dilution of samples helped to minimize coagulation prior to analysis.

The fine frit presented a problem in that the samples taken when it was in use contained a substantial proportion of very fine bubbles. These inflated the apparent sample volume and would also have a large number of particles attached to them which would distort the results if allowed to remain in the samples, since it was the residual particle concentration in the liquid which we wanted to measure. Therefore, each sample was ejected from its pipette into a test-tube and allowed to stand for a few minutes until all bubbles had risen to form a froth on the surface. This froth was then sucked off with a dropper and discarded. The underlying liquid was poured into a 10 ml. measuring cylinder, its volume  $V$  ml. noted, and then it was transferred to an empty 50 ml. flask. The test tube and measuring cylinder were then washed with  $(40-V)$  ml. of filtered water and the washings added to the sample in the flask. It was very difficult to suck off the froth without taking any of the underlying liquid; it is quite possible that a few of the larger particles which had been floated first did, in fact, remain in the samples.

Each diluted sample was given five minutes in the ultrasonic bath to break up any agglomerates which may have formed while it was waiting its turn to be analysed. 40 ml. of 1% NaCl solution were then added to it, followed by sufficient SF solution to restore the EHDA-Br concentration to  $10^{-4}$  M. The sample was now analysed on the particle counter for particle concentration and size distribution. A 76 micron orifice and 320 microlitre volumetric section were used. The current and amplifier settings were  $\frac{1}{4}$  and  $6\frac{1}{4}$  respectively and the output mode was Log 6. With the pulse height analyzer output

on  $10^3$  counts full scale the build-up of the size distribution curve was followed on the oscilloscope until the peak almost reached full scale. This could take up to 15 minutes depending on the particle concentration. While the curve was building up five replicate counts were taken with the trigger set at a level high enough to screen out noise. These counts gave the total particle concentration above the trigger level.

When the size distribution curve had been built up it was plotted out on the strip chart recorder. Each curve was divided into seven sections, each corresponding to a narrow size fraction. The area of each section was measured twice with a planimeter and the average taken. If this area is  $A_i$ , the total area under the curve  $\sum A_i$  and the total particle concentration  $\sum P_i$  then the concentration  $P_i$  of particles in size range  $i$  is  $\frac{A_i}{\sum A_i} \times \sum P_i$ . Hence, the fall in particle concentration with time for any size fraction could be followed.

At the particle concentrations used the background count and coincidence of two or more particles in the orifice were negligible.

#### 7.5.2 SDB Latex

The stirrer was not used (except for run L5) since these particles had virtually the same density as water. Again 400 ml. of distilled water was adjusted to pH 6.0. 2 ml. of SF solution was added to give  $0.5 \times 10^{-4}$  M EHDA-Br + 0.25 vol.% IPA, together with 10 ml. of a solution of 1 part Dowfroth 350 in 1000 parts water. The latter was added to ensure froth stability at this lower surfactant

concentration. Twenty drops of the 10% SDB latex suspension were then added and the mixture stirred momentarily to disperse the particles. It was then allowed to stand for 15 minutes to allow adequate time for surfactant adsorption. Meanwhile, the gas rate to the flotation cell was adjusted to the desired value. After 15 minutes standing the first sample was taken and the suspension poured into the cell. This was taken as time zero.

Thereafter, the procedure was the same as for glass beads except that the particle counter settings were current = 1/8, amplifier = 3, output = log 6; a 24 micron orifice and a 16 ml. volumetric section were used.

#### 7.6 Results

The detailed output and calculations for one run are given in Appendix B. In this section we present for each run:

- (a) curves of  $\log (P/P_0)$  versus time for each size fraction, where  $P_0$  is the initial particle concentration and  $P$  is the concentration at time  $t$ ;
- (b) a log-log curve of first order rate constant  $k$  versus particle diameter  $d_p$ .

Table 7-4 lists the runs performed, the operating conditions and the Figures on which the curves of  $\log (P/P_0)$  versus time and  $\log k$  versus  $\log d_p$  may be found. With each material two runs were performed with the medium frit and two with the fine frit. With the latex particles one run was performed with stirring (L5) in order to assess the effect of stirring. One run was performed with each

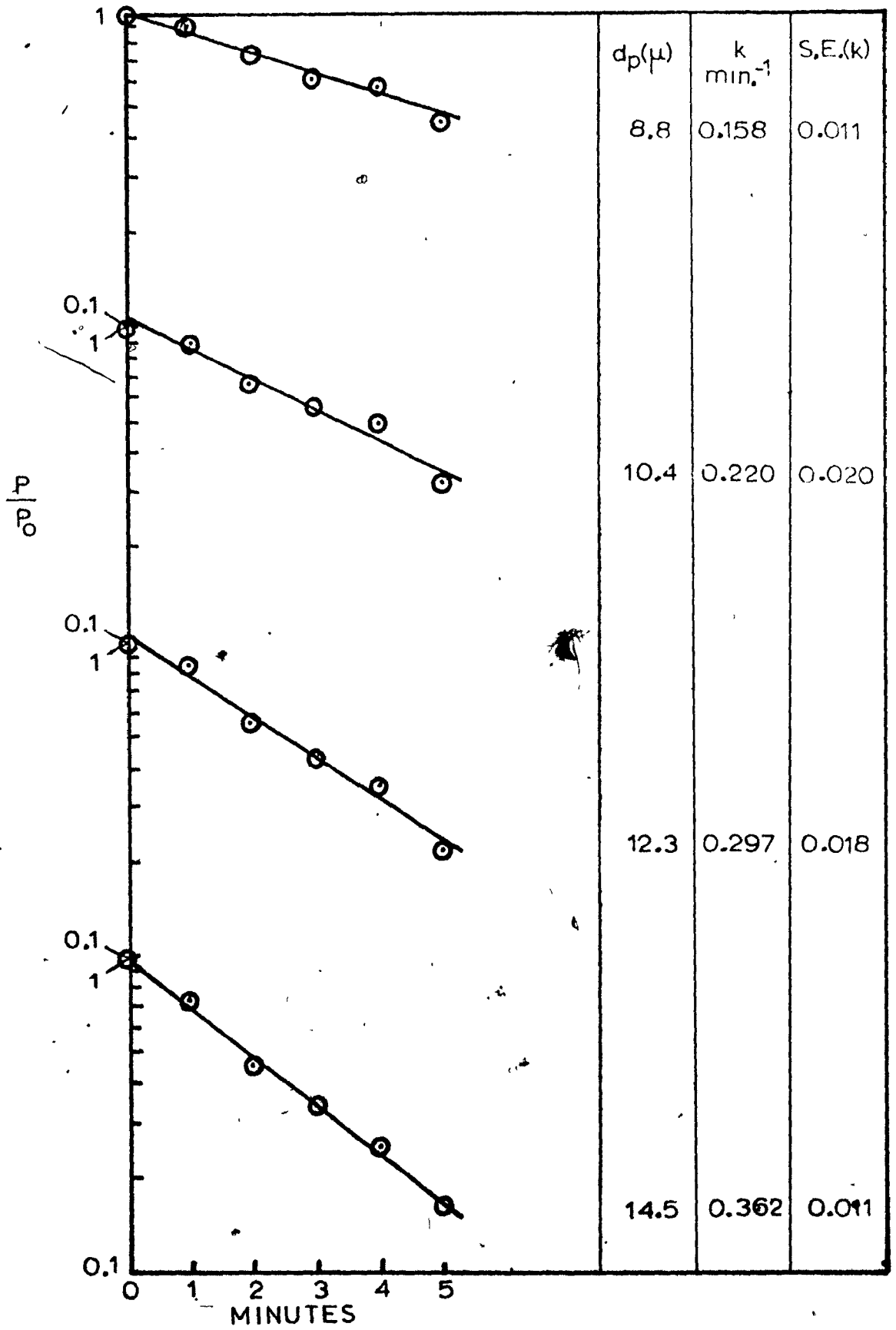
TABLE 7-4

Run No.	Material	Frit Size	EHDA-Br conc.	IPA vol. %	Gas Rate (ml./min.)	Stirrer Speed (rpm)	Fig. for $\log(P/P_0)$ v.t	Fig. for $\log k v. \log d_p$
G1	Glass beads	10-15	$10^{-4} M$	0.5	24	165	7.4	7.14
G2	"	10-15	"	"	24	"	7.5	"
G3	"	4-5.5	"	"	24	"	7.6	"
G4	"	4-5.5	"	"	25	"	7.7	"
G5	"	40-60	"	"	43	"	7.8	"
L1	SDB latex	10-15	$0.5 \times 10^{-4} M$	0.25	44	0	7.9	7.15
L2	"	10-15	"	"	46	"	7.10	"
L3	"	4-5.5	"	"	43	"	7.11	"
L4	"	4-5.5	"	"	25	"	7.12	"*
L5	"	10-15	"	"	44	165	7.13	"

\* k values multiplied by  $\frac{43}{25}$ .

Figure 7.4

RUN G1; LOG P/P<sub>o</sub> VERSUS TIME



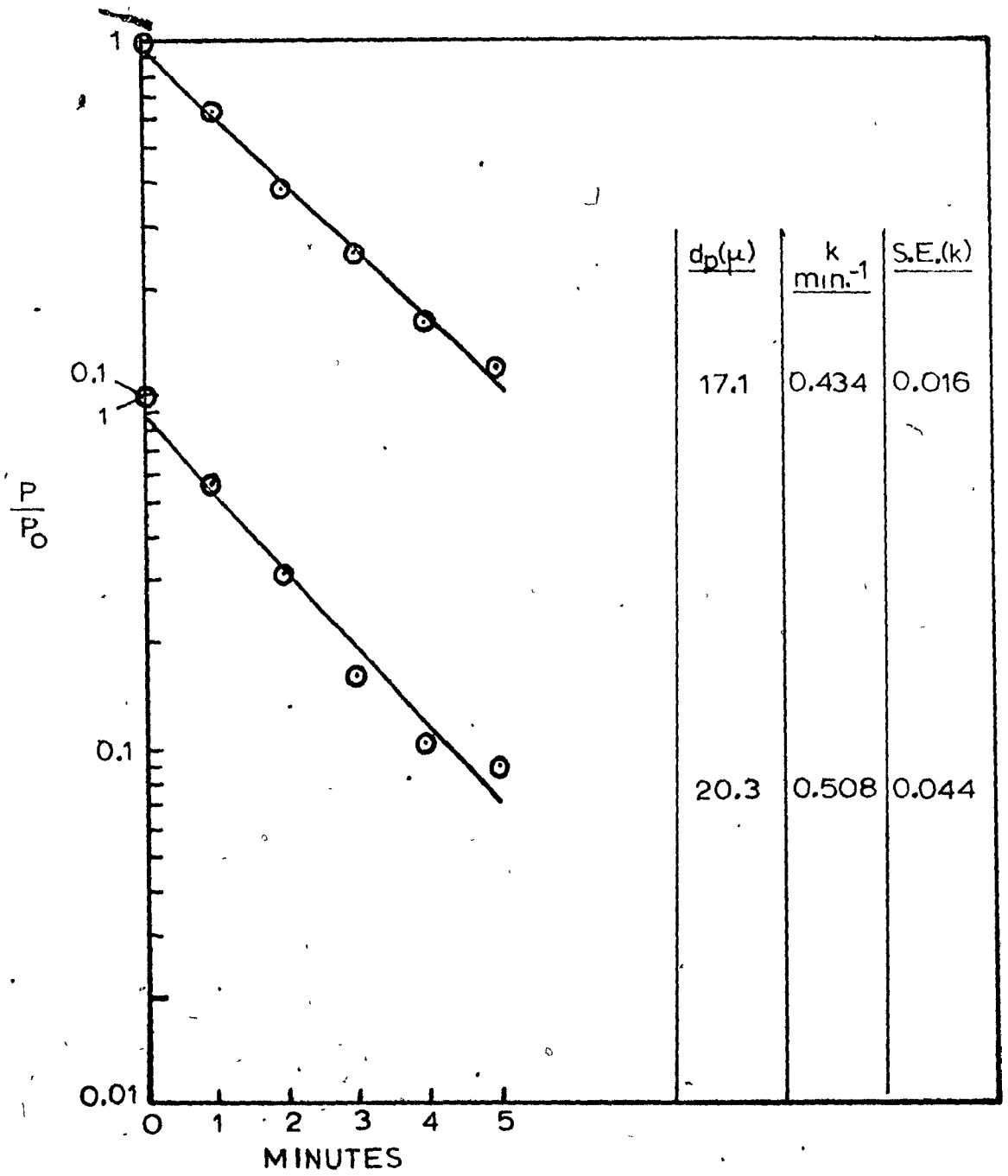
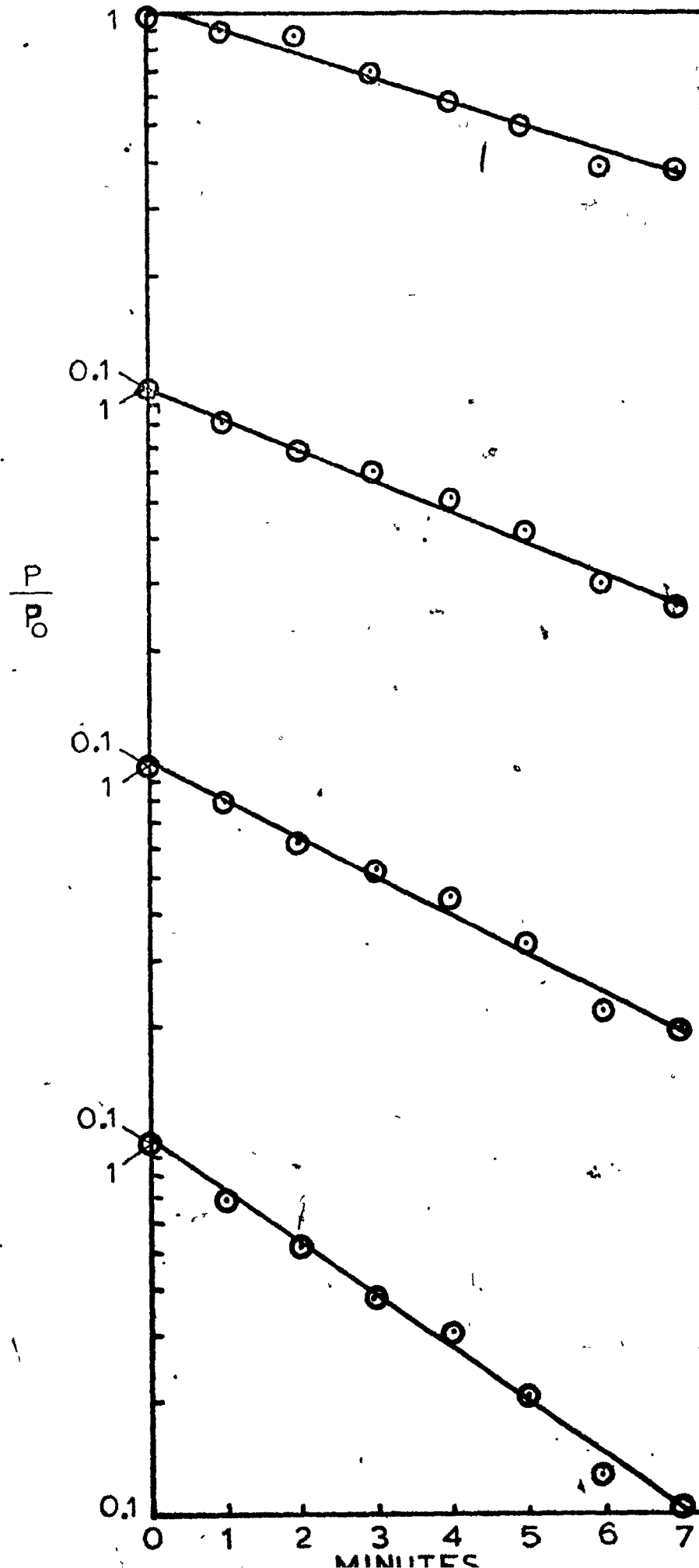
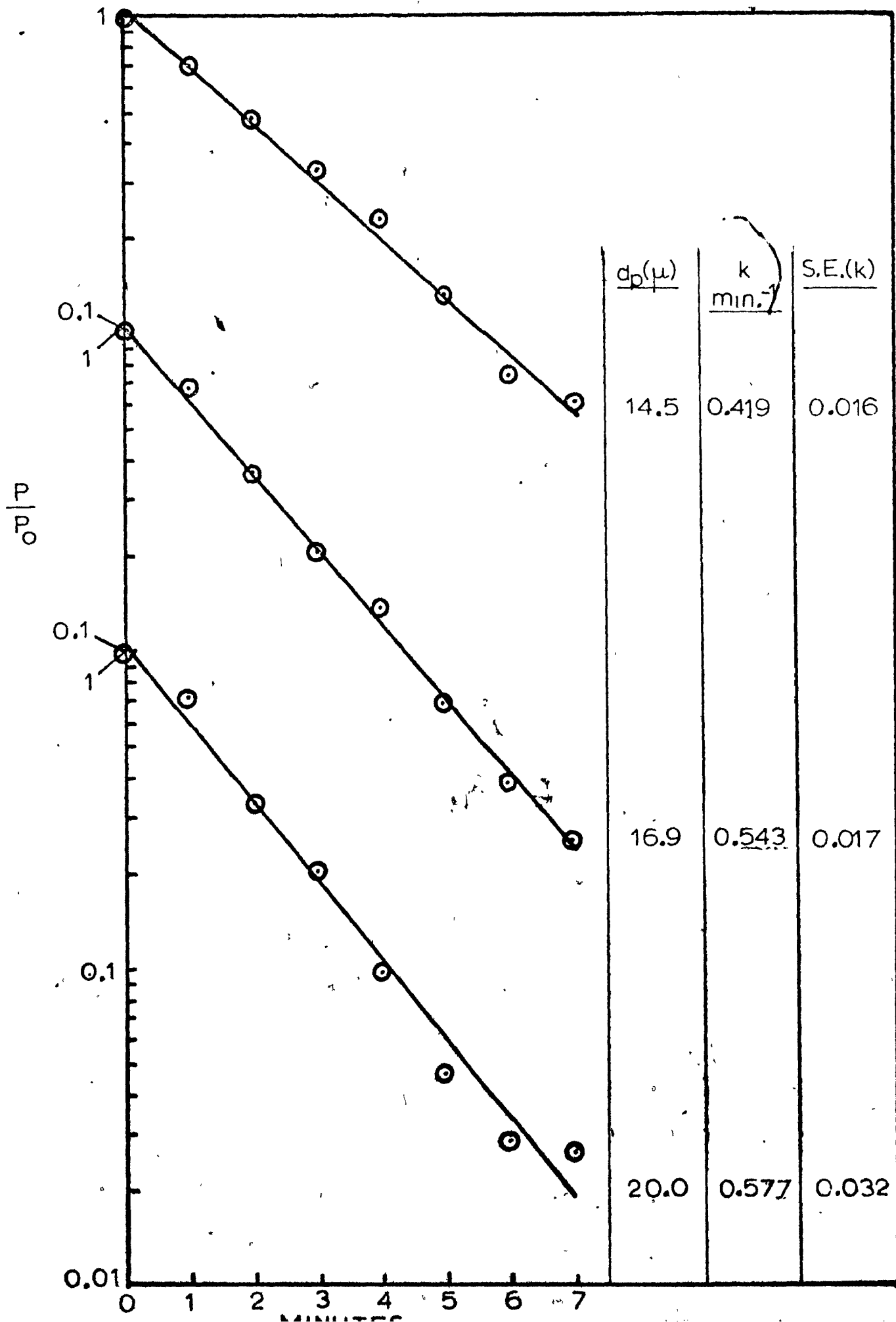


Figure 7.5

RUN G2; LOG P/P<sub>o</sub> VERSUS TIME

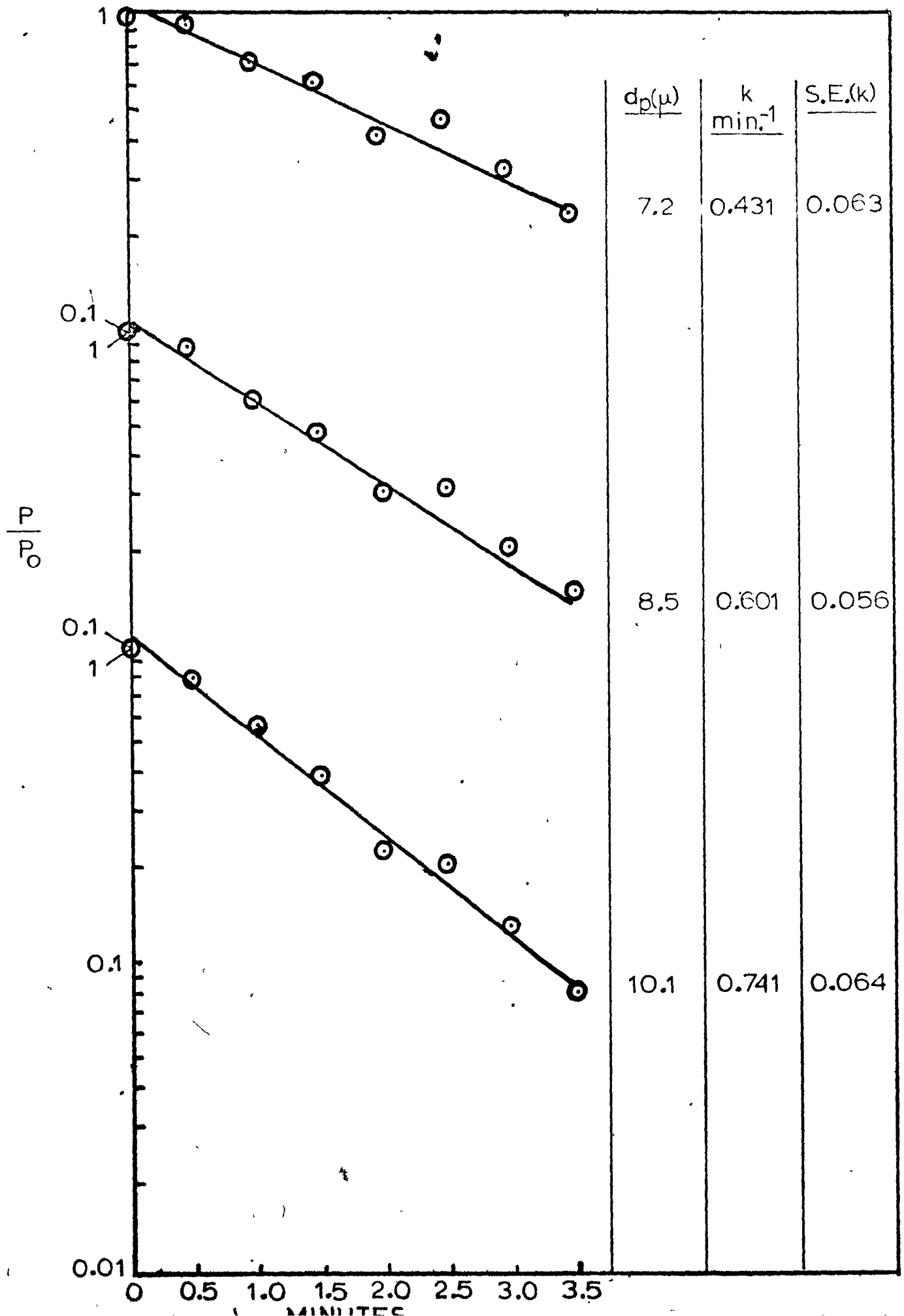


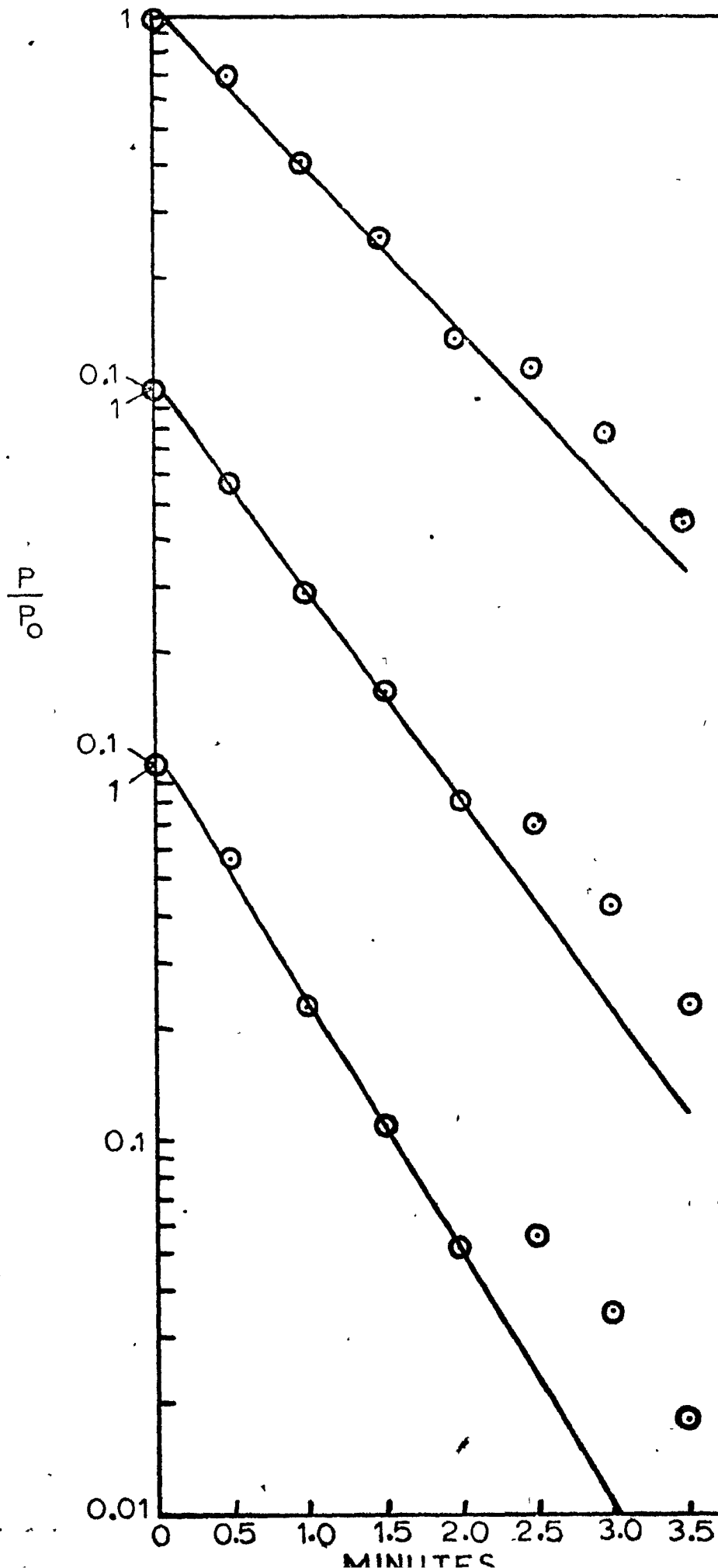
$d_p(\mu)$	$k$ min. <sup>-1</sup>	S.E.(k)
7.3	0.152	0.011
8.7	0.187	0.008
10.2	0.236	0.012
12.1	0.326	0.011



$d_p(\mu)$	$k$ <u>min.<sup>-1</sup></u>	S.E.(k)
14.5	0.419	0.016
16.9	0.543	0.017
20.0	0.577	0.032

Figure 7.6  
RUN G3; LOG P/P<sub>o</sub> VERSUS TIME





$d_p(\mu)$	$k$ <u>min.<sup>-1</sup></u>	<u>S.E.(k)</u>
11.9	0.995	0.051
14.0	1.272	0.020
16.6	1.511	0.050

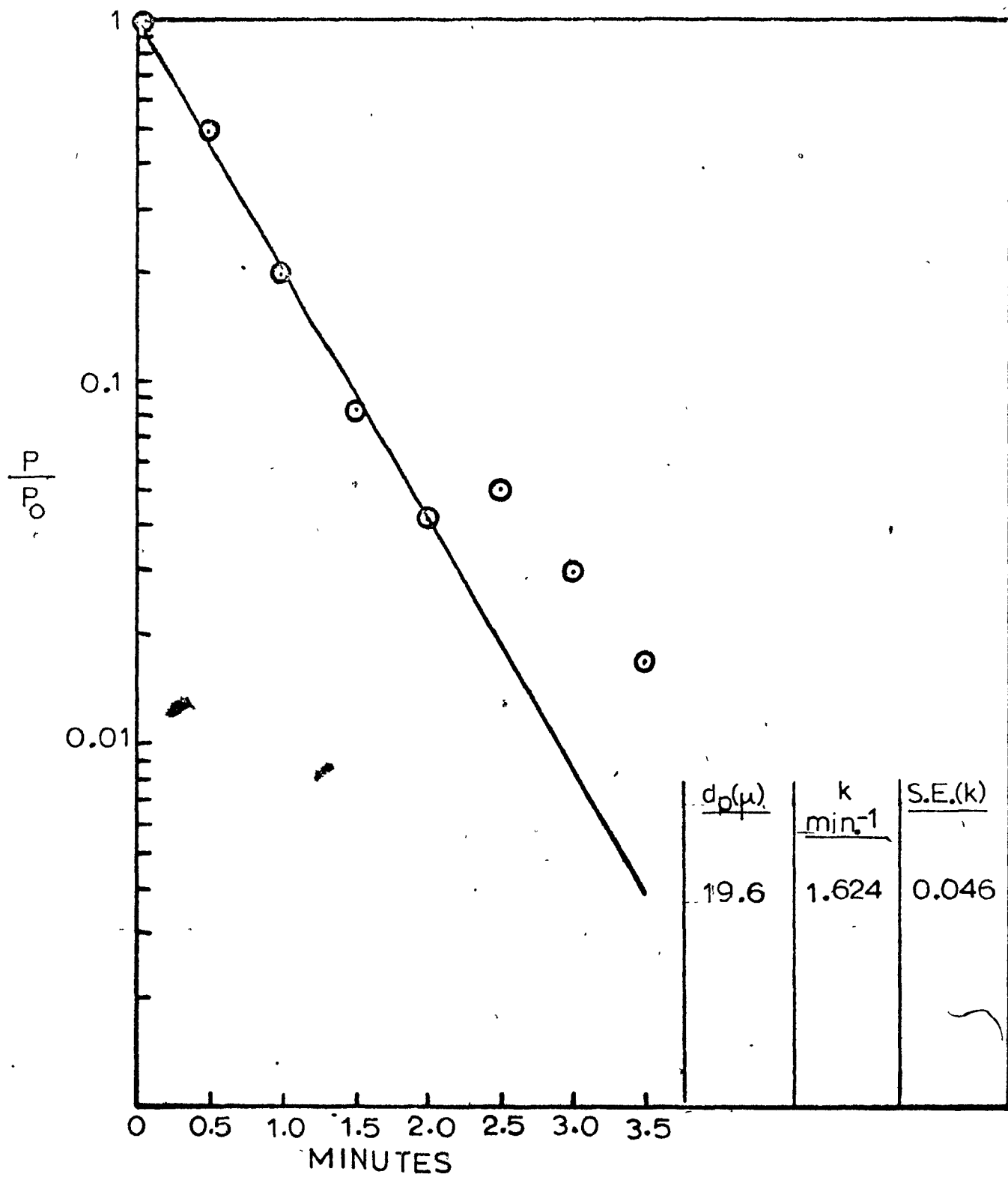
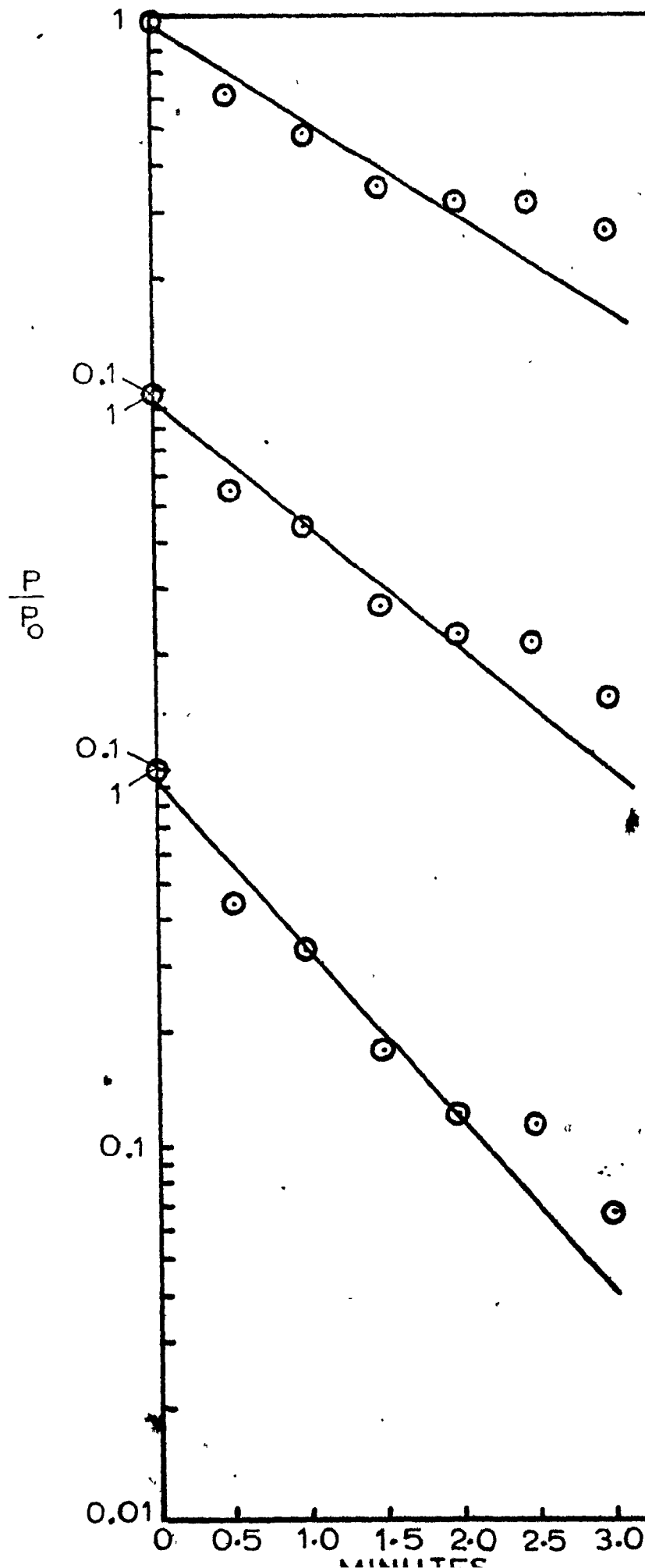
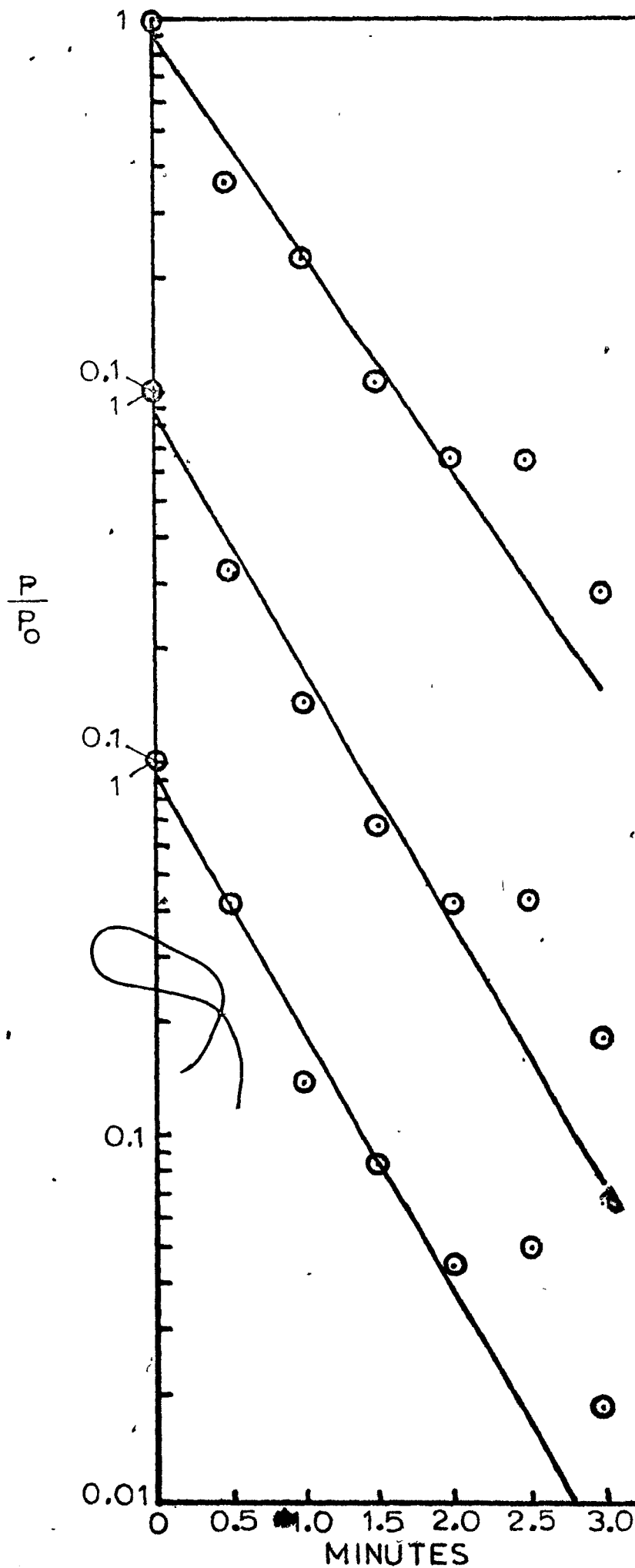


Figure 7.7

RUN G4; LOG P/P<sub>0</sub> VERSUS TIME .

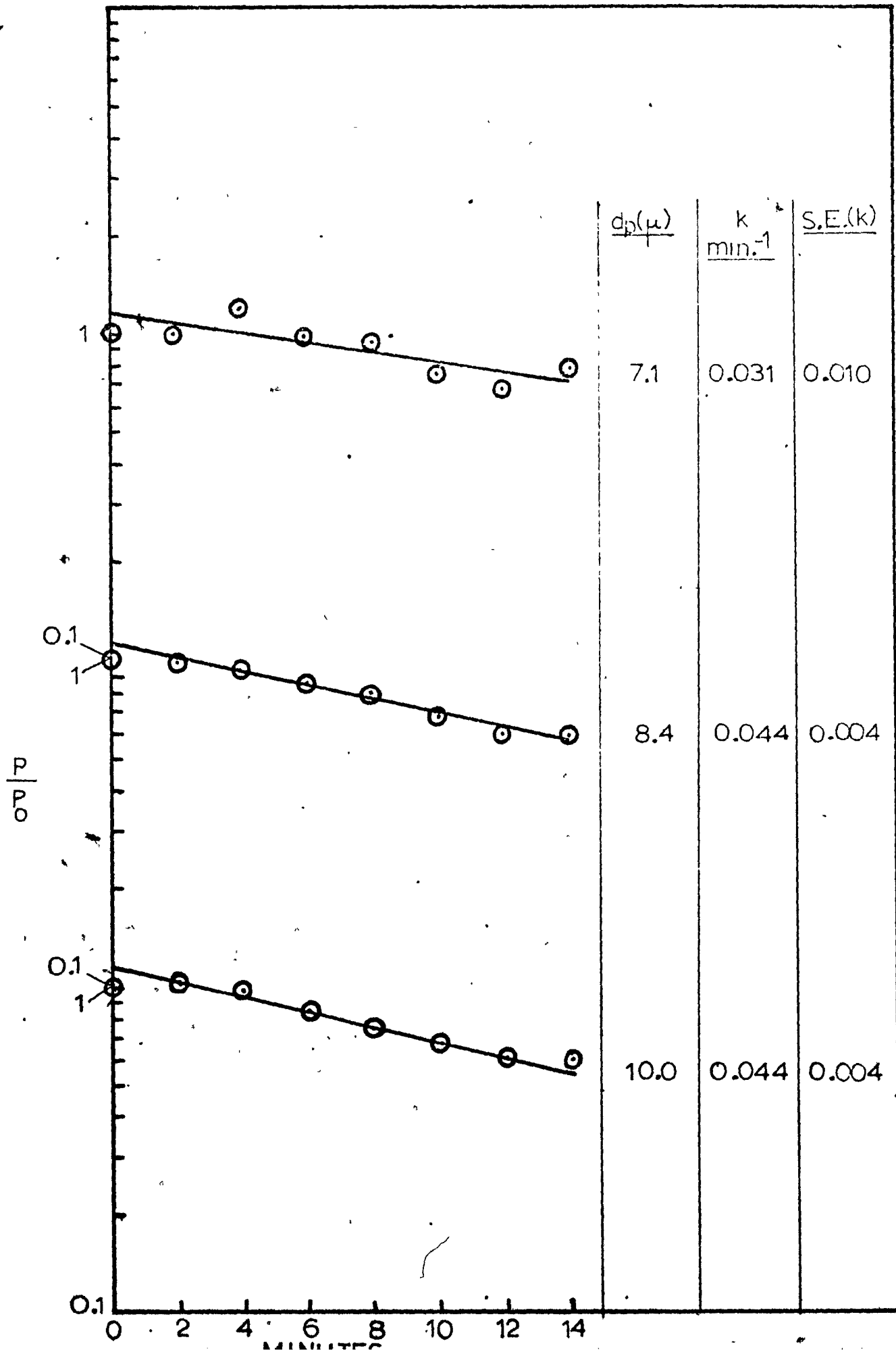


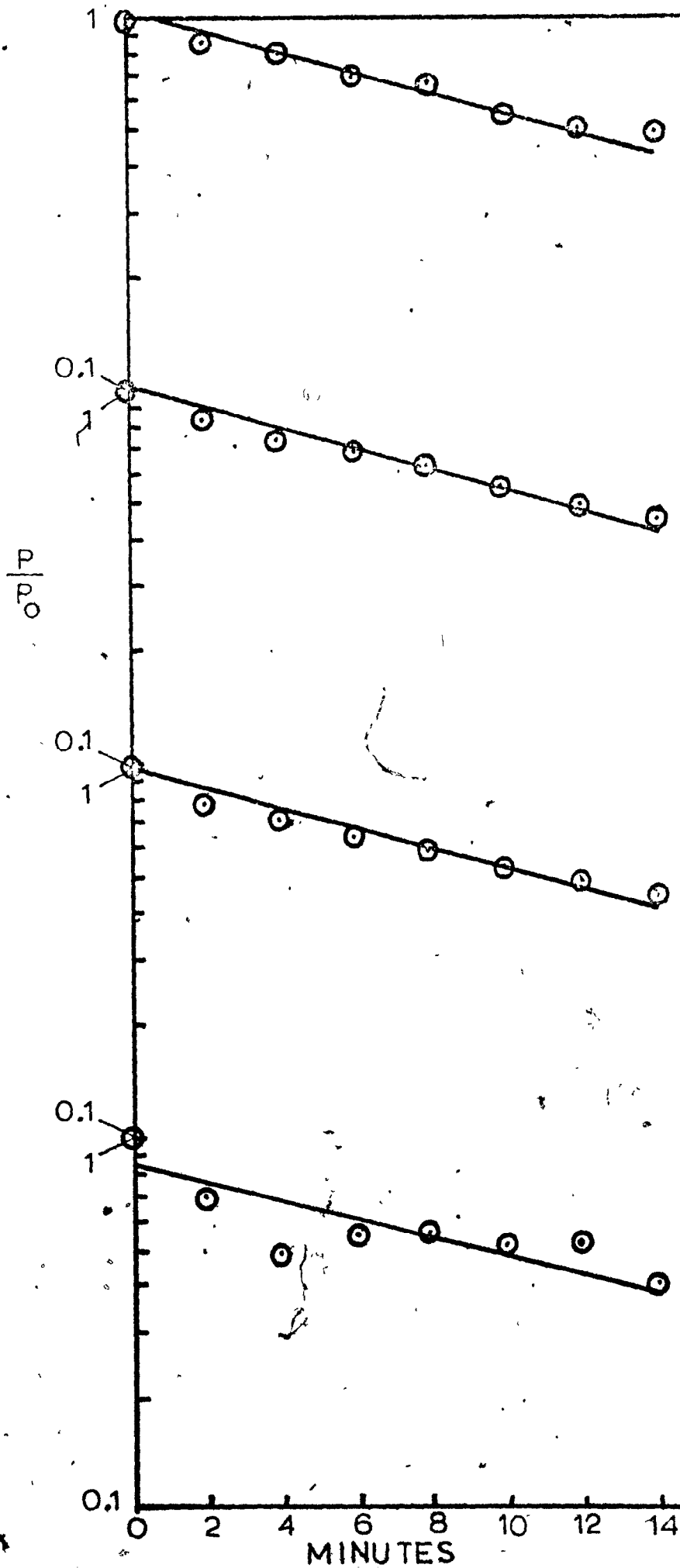
$d_p(\omega)$	$k$ <u>min.<sup>-1</sup></u>	<u>S.E.(k)</u>
7.7	0.589	0.063
9.2	0.759	0.058
11.1	1.052	0.051



$d_p(\mu)$	$k$ $\text{min.}^{-1}$	S.E.(k)
13.4	1.394	0.070
16.1	1.643	0.127
19.3	1.611	0.163

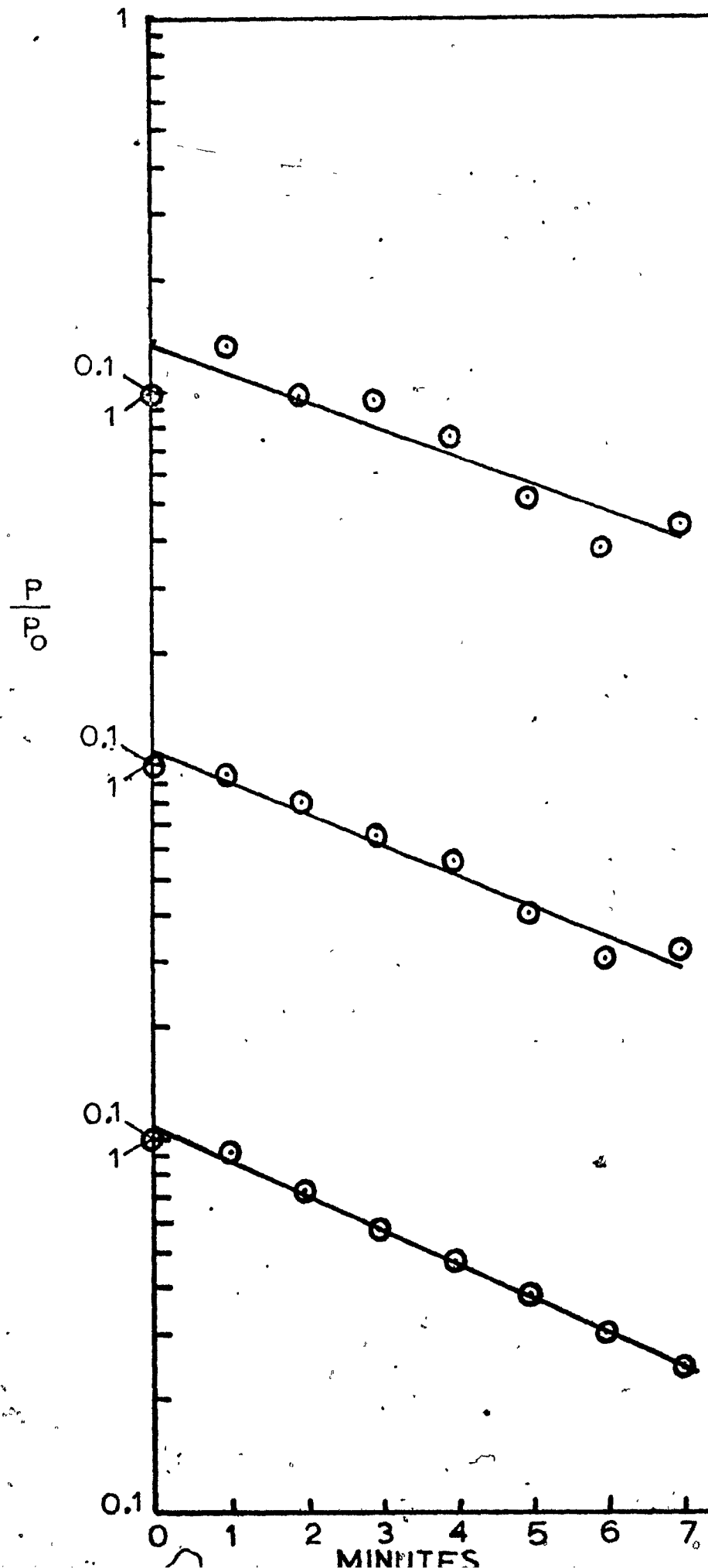
Figure 7.8  
RUN G5; LOG P/P<sub>0</sub> VERSUS TIME





$d_p(\mu)$	$k$ min. <sup>-1</sup>	S.E.(k)
11.8	0.053	0.003
13.9	0.054	0.002
16.4	0.054	0.004
19.5	0.045	0.013

Figure 7.9  
RUN L1; LOG P/P<sub>0</sub> VERSUS TIME



$d_p(\mu)$	$k$ $\text{min.}^{-1}$	S.E.(k)
3.9	0.170	0.030
4.6	0.191	0.015
5.4	0.209	0.006

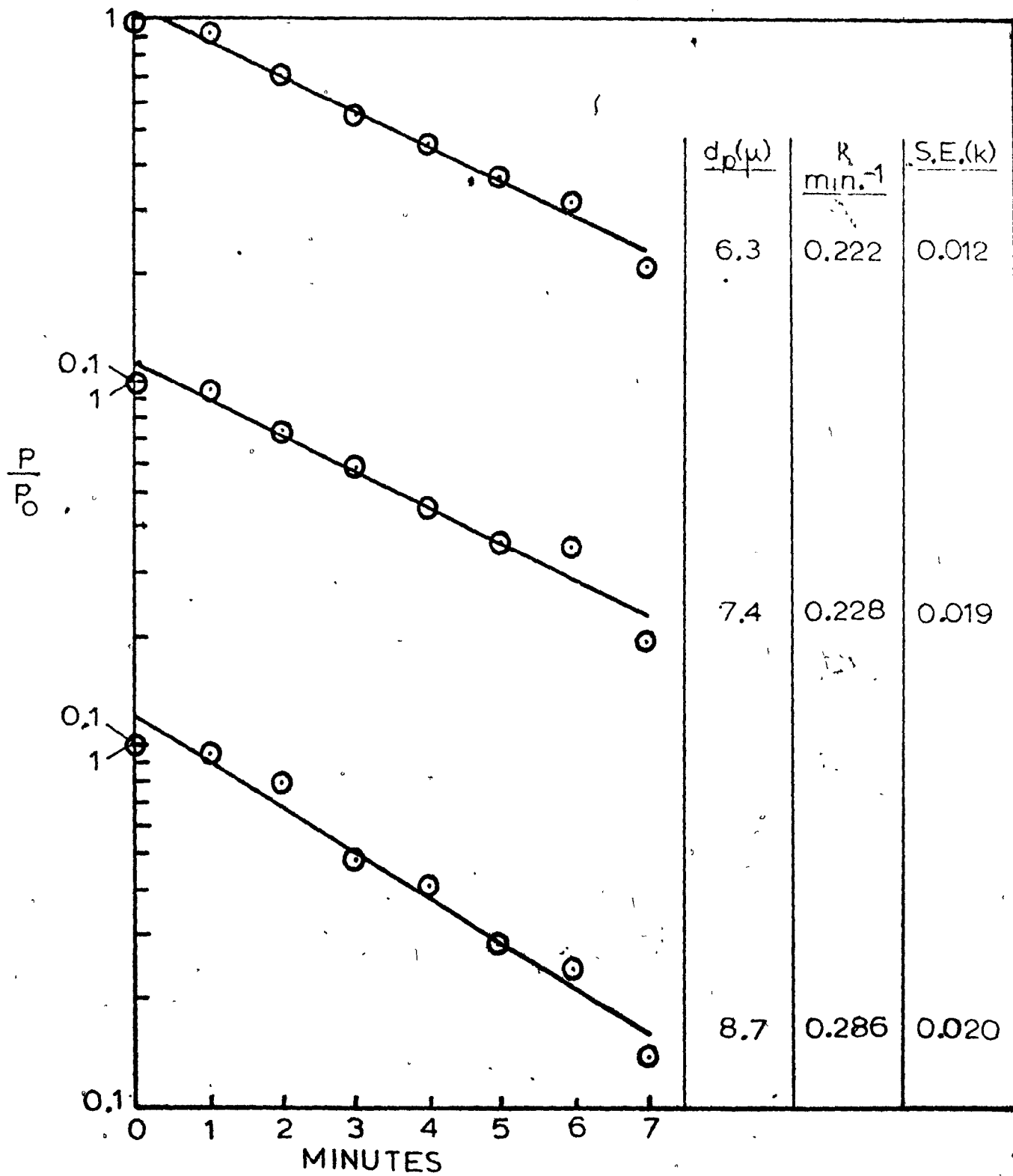
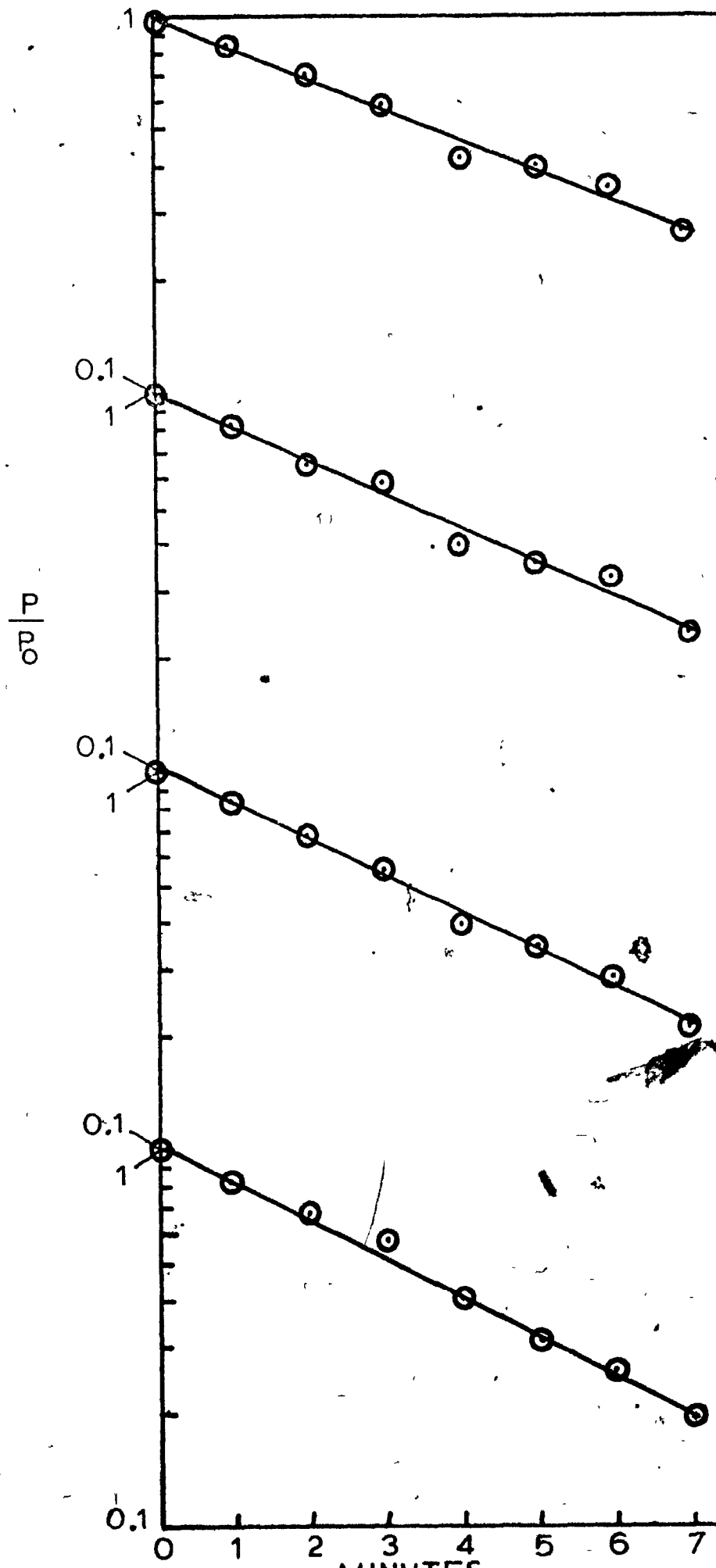


Figure 7.10

RUN L2; LOG P/P<sub>o</sub> VERSUS TIME



$d_p$ ( $\mu$ )	$k$ ( $\text{min}^{-1}$ )	S.E.(k)
3.9	0.186	0.010
4.6	0.205	0.011
5.4	0.220	0.007
6.3	0.237	0.008

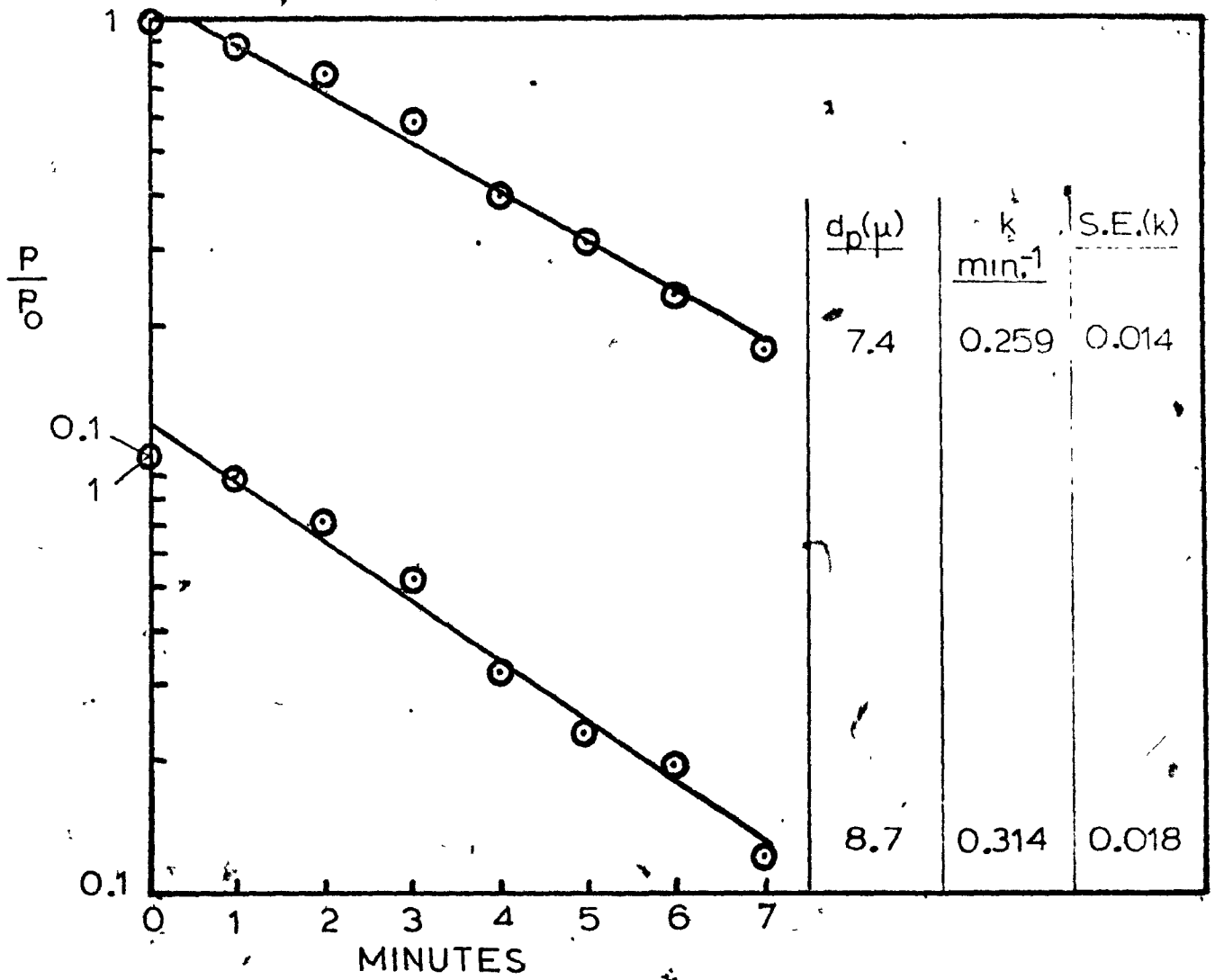
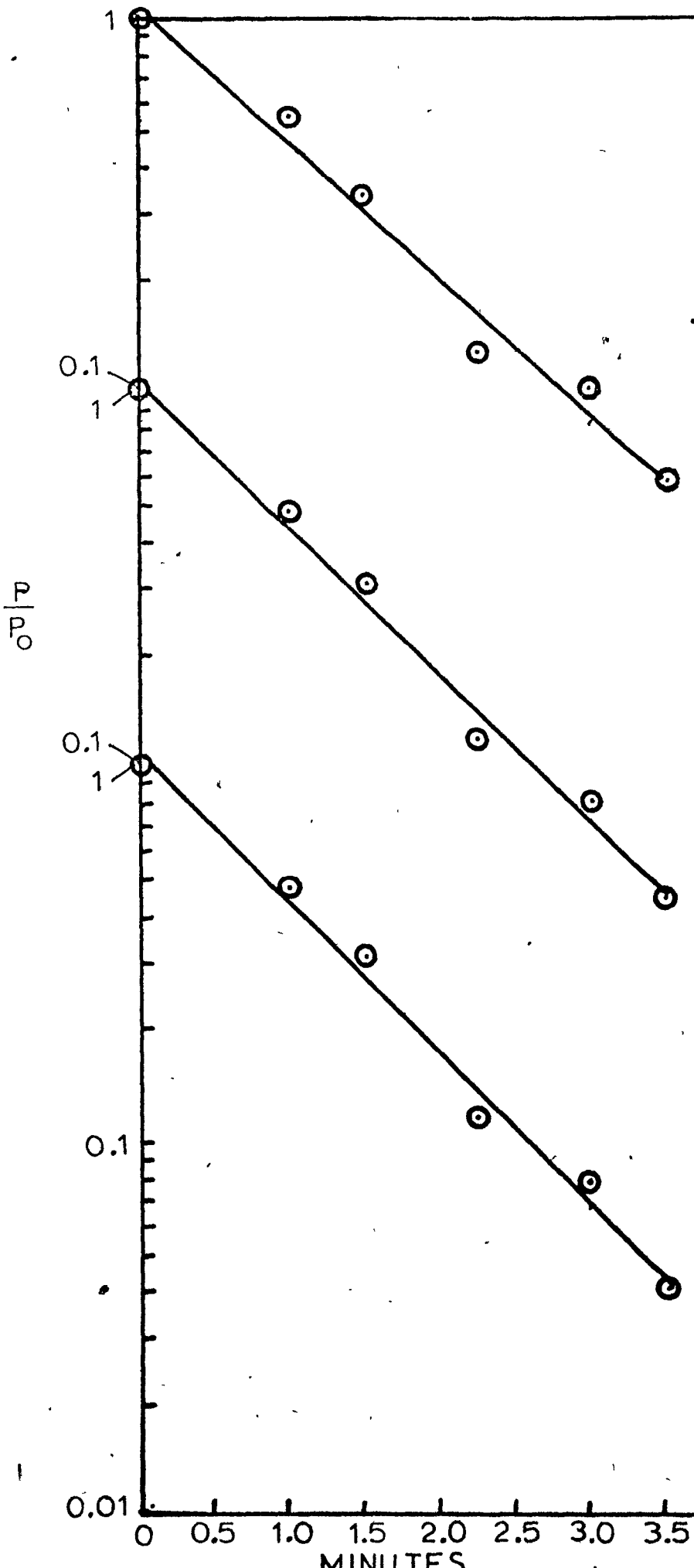
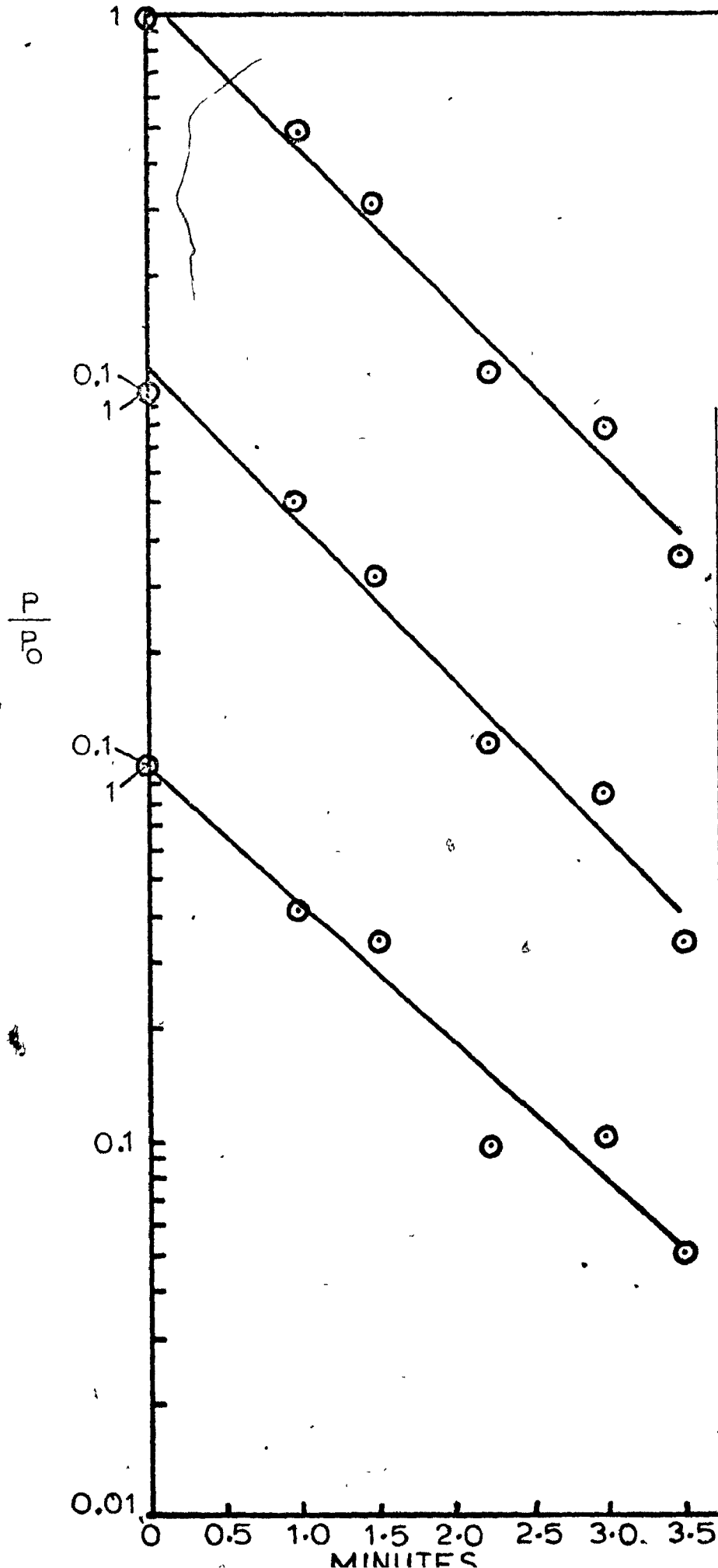


Figure 7.11  
RUN L3; LOG P/P<sub>o</sub> VERSUS TIME



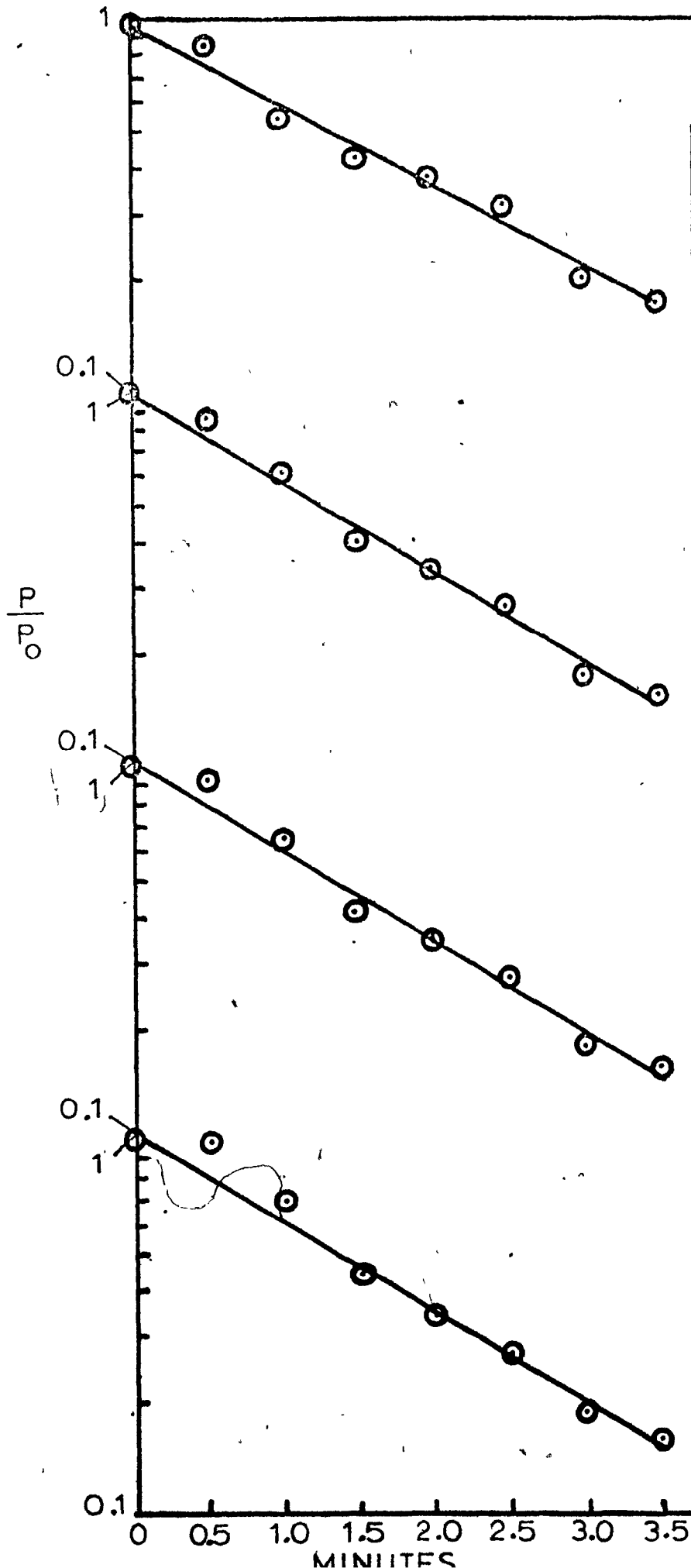
$d_p(\mu)$	$k$ $\text{min.}^{-1}$	<u>S.E.(k)</u>
3.9	0.835	0.061
4.6	0.900	0.043
5.4	0.926	0.048



$d_p(\mu)$	$k$ $\text{min}^{-1}$	$S.E.(k)$
6.3	0.946	0.064
7.4	0.954	0.074
8.7	0.838	0.092

Figure 7.12

RUN L4; LOG P/P<sub>o</sub> VERSUS TIME



$d_p(\mu)$	$k$ min. <sup>-1</sup>	S.E.(k)
3.9	0.490	0.030
4.6	0.548	0.025
5.4	0.547	0.025
6.3	0.550	0.027

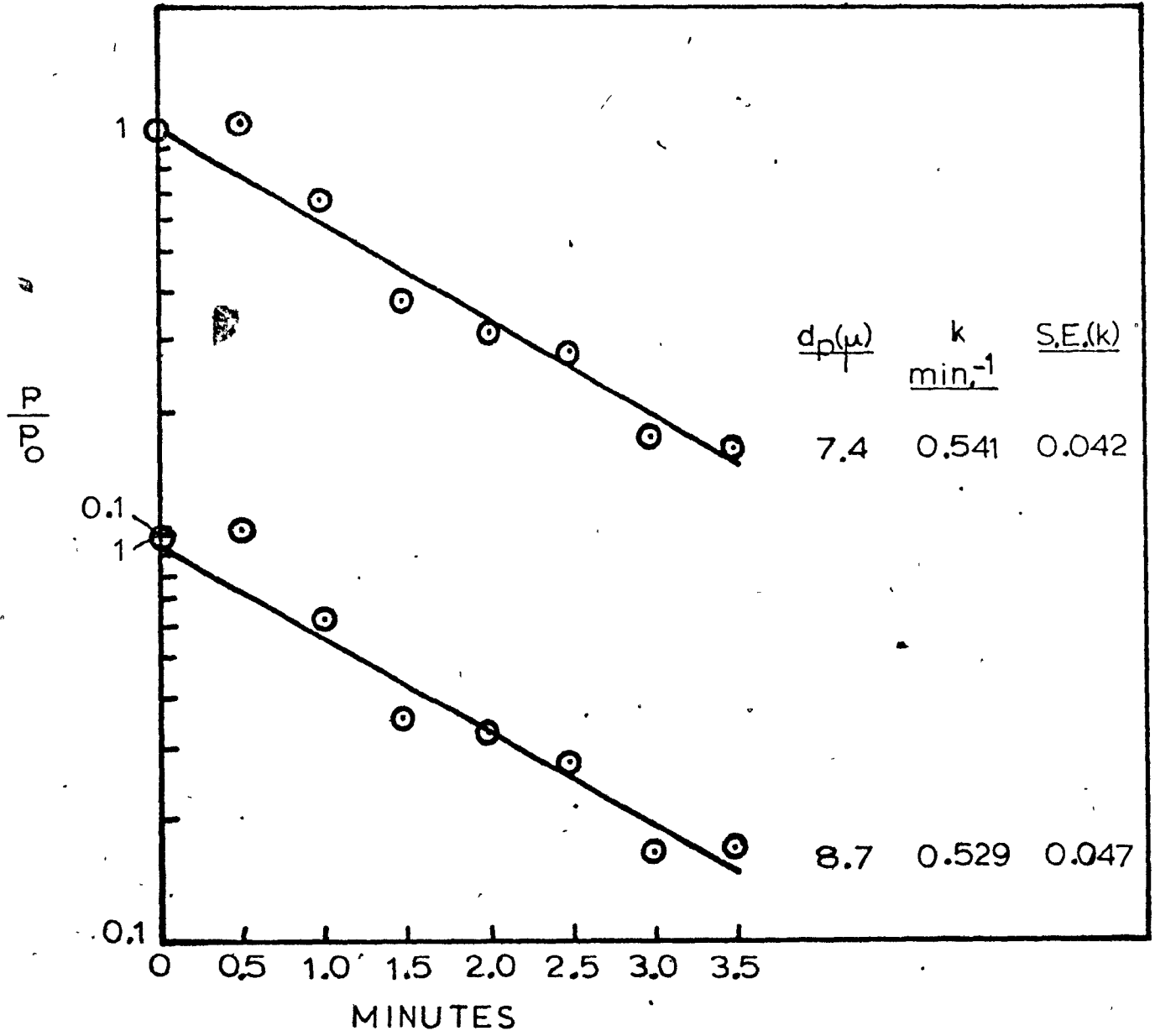
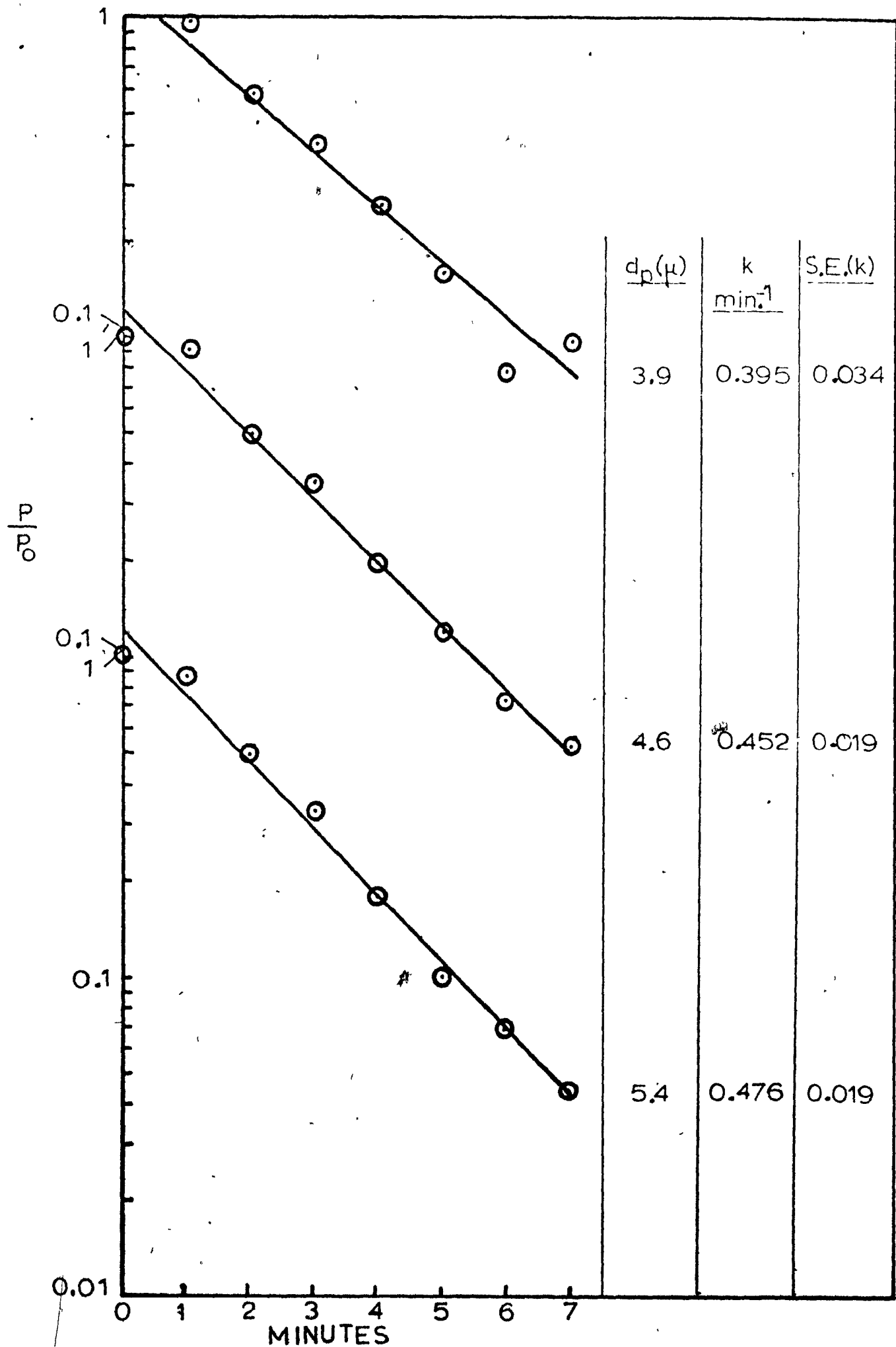


Figure 7.13

RUN L5; LOG P/P<sub>o</sub> VERSUS TIME



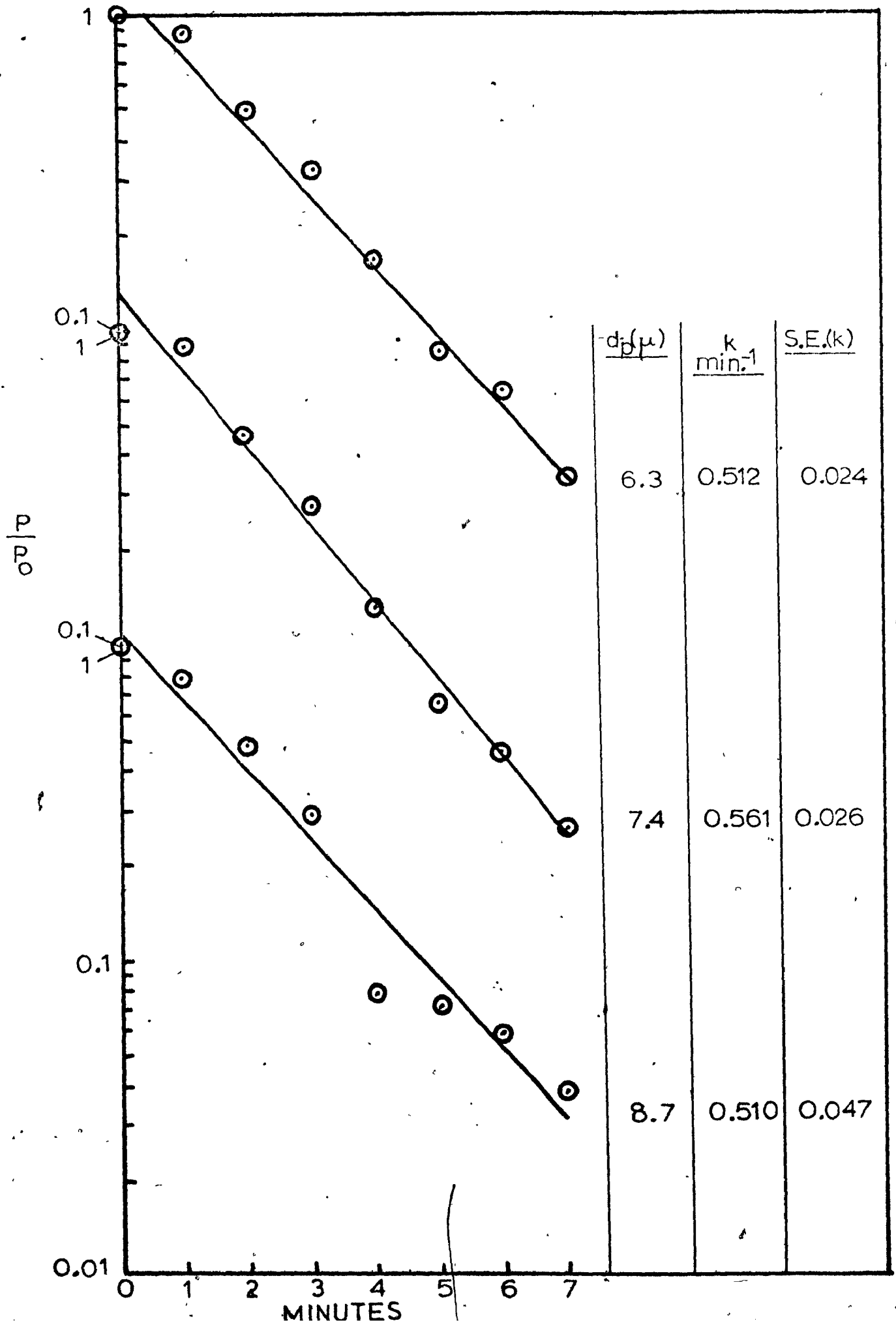


Figure 7.14

GLASS BEAD RUNS; LOG  $k$  VERSUS LOG  $d_p$

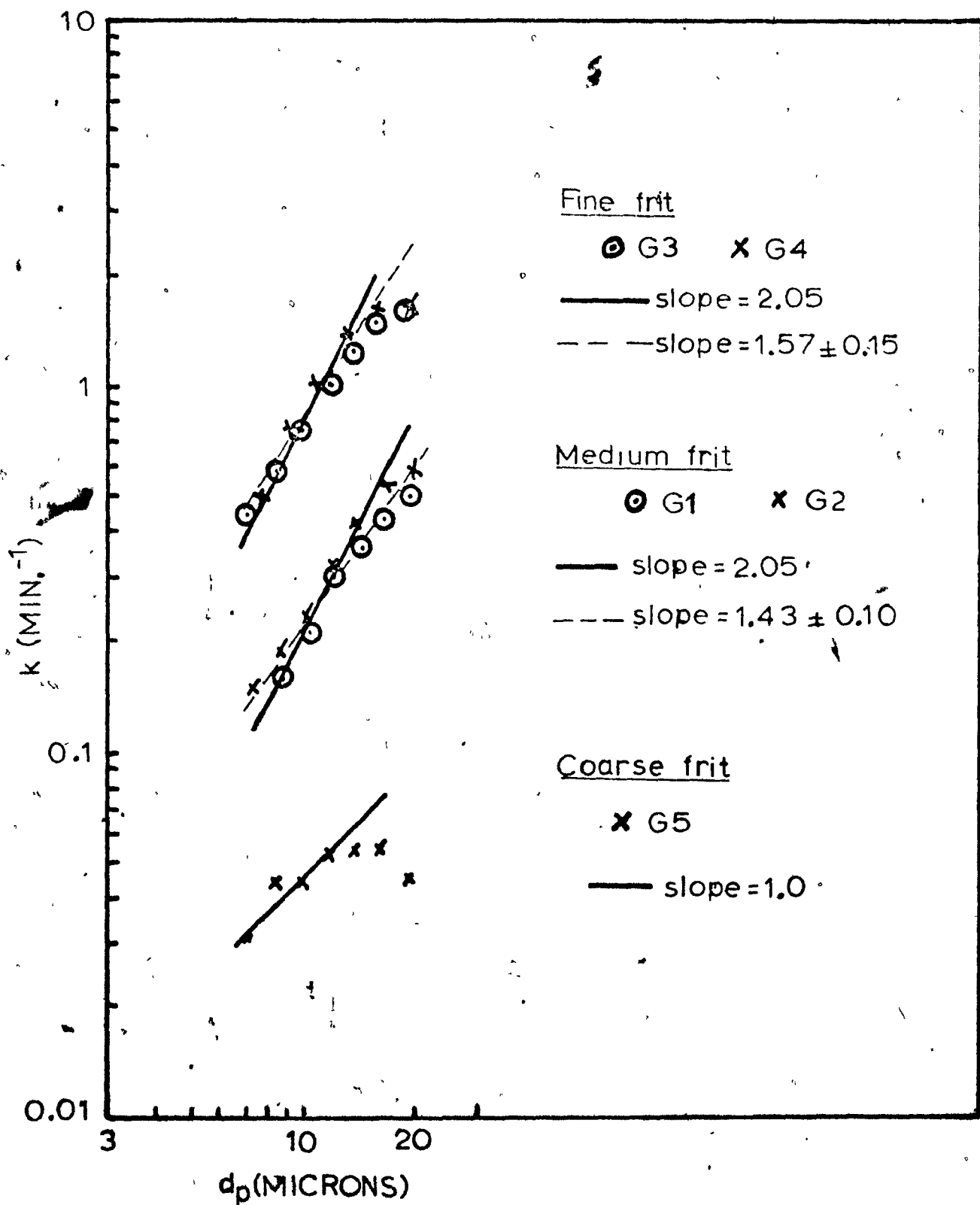
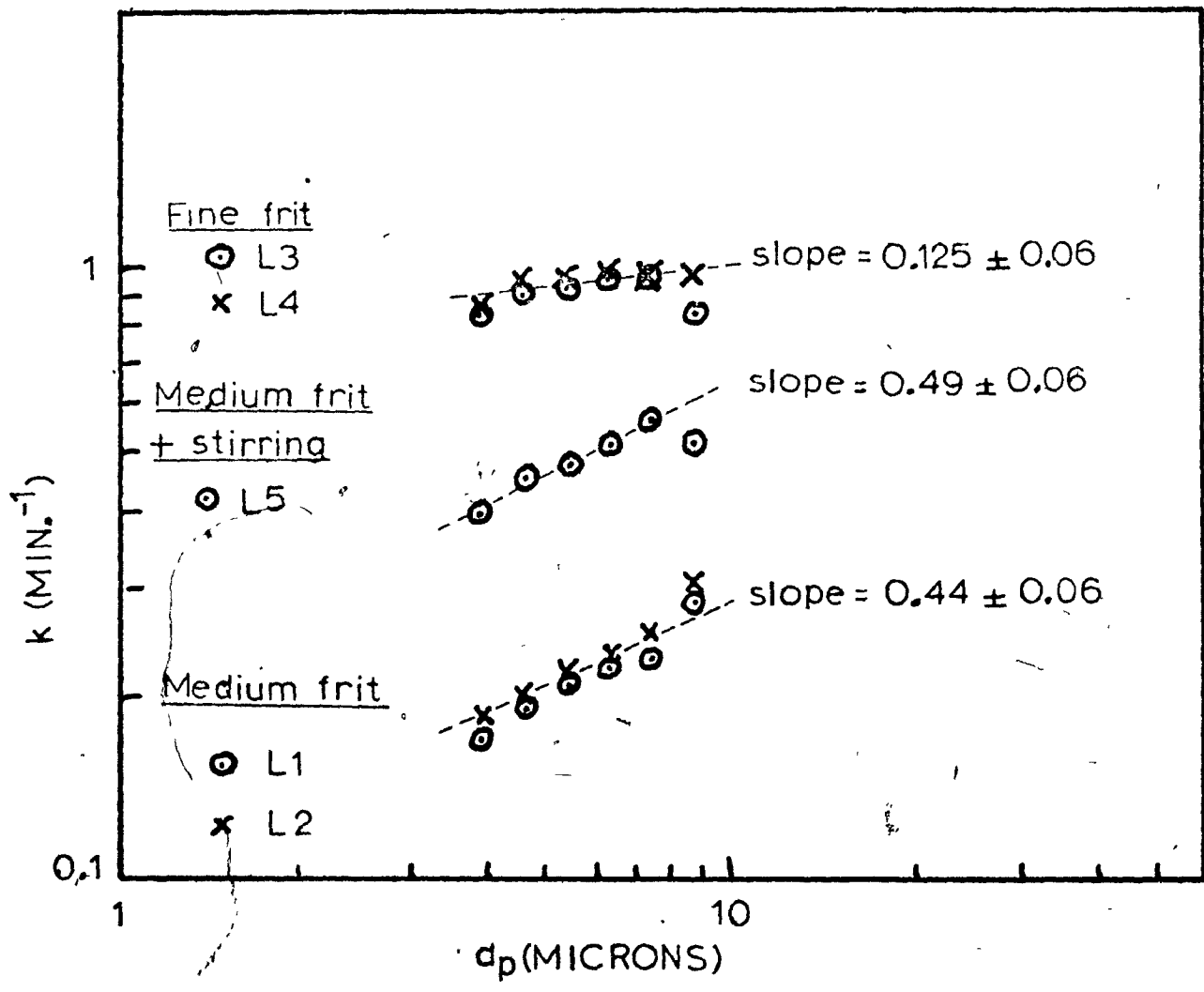


Figure 7.15

SDB LATEX RUNS; LOG k VERSUS LOG  $d_p$



material with the coarse frit but no results are presented for latex because no flotation was observed.

In all cases first order kinetics were observed. The first order rate constants quoted in Figs. 7.4-13 were obtained by least squares regression on the data points. In each case a standard error is quoted with the estimated rate constant.

In Figs. 7.14 and 7.15, where  $\log k$  is plotted against  $\log d_p$ , reproducibility between runs carried out under the same conditions is seen to be reasonable. The  $k$  values for L4 have been multiplied by  $43/25$  to correct for the difference in gas rate between L3 and L4. Good agreement between the L3  $k$ 's and the corrected L4  $k$ 's confirms that flotation rate is proportional to gas rate.

In Fig. 7.14 the solid lines are straight lines of slope 2.05 which have been forced to coincide with the glass bead experimental data at  $d_p = 11$  microns. These lines represent the predictions of the preliminary model developed in Chapter 5, Section 5.2 assuming Stokes flow round the front of the bubble. It is apparent that for glass beads this model slightly overestimates the dependence of flotation rate on  $d_p$ .

Best straight lines were fitted to the curves in Figs. 7.14 and 7.15 by least squares regression with each data point being weighted inversely by the variance of the line from which it was derived. For the glass bead runs with bubbles of average diameter 71 microns (G1 and G2) a straight line of slope 1.43 fits the data best, indicating a relation of the form  $k \propto d_p^{1.43}$ . This is close to the slope of 1.33 predicted for these particles by assuming

Hadamard-Rybczynski flow round the front half of the bubble. With the smaller bubbles of average diameter 42 microns (G3, G4) a straight line could reasonably be fitted only to those data points up to 15 microns. This line has a slope of 1.57, a little closer to the slope of 2.05 predicted by assuming Stokes flow round the front half of the bubble. The data points at 20 microns fall below the line. A possible explanation for this lies in the experimental procedure which had to be adopted with samples taken when the fine frit was in use. It was mentioned in Section 7.5 that it was difficult to suck off all the froth without taking any of the underlying liquid and it was likely that some particles which should have been discarded with the froth did remain in the samples. Since the froth would be richer than the liquid in large particles this would mean that the apparent rate of flotation of large particles would be less than the true value.

With regard to the effect of bubble size on flotation rate, assume that collection efficiency  $E$  is proportional to  $(1/D_b)^n$ . Stokes flow predicts  $n = 2.05$  for our glass beads and Hadamard-Rybczynski flow predicts  $n = 1.33$ . All the runs G1 to G4 were carried out with the same gas rate. At a given gas rate the volume swept out by the bubbles is inversely proportional to bubble diameter  $D_b$ . Flotation rate equals the product of collection efficiency and swept volume. Hence, if  $E \propto (1/D_b)^n$  we have  $k \propto (1/D_b)^{n+1}$ . By comparing flotation rates for a given particle size in the G1/G2 and G3/G4 runs we can estimate  $n$  for that particle size. The results are shown in Table 7.5.

TABLE 7.5

$d_p$ (microns),	$\frac{k(G3, G4)}{k(G1, G2)}$	$n$
7	3.56	1.4
10	3.76	1.5
13	3.90	1.6
16	3.72(4.10)	1.5(1.7)
19	3.00(4.21)	1.1(1.7)

The numbers in brackets for  $d_p = 16$  and 19 microns are the values obtained by following the straight line extension on the G3/G4 plot. Of course, since for each particle size we are comparing only two points we cannot prove that the relation is of the form  $E \propto (1/D_b)^n$  as predicted in Chapter 5. However, we can say that the results are not inconsistent with that relation with  $n$  taking values intermediate between those predicted for Stokes and Hadamard-Rybczinski flows.

The run performed with the coarse frit (G5) gave no obvious  $\log k$  versus  $\log d_p$  relationship. A relation of the form  $E \propto d_p$  proposed in Chapter 5 for potential flow around the front of the bubble looks as though it could be valid up to  $d_p = 12$  microns, but at larger particle sizes it is not supported by the data. It is noteworthy that when corrected to equal gas rates the flotation rate with the medium frit is very roughly ten times that with the coarse frit, which is not far from the inverse ratio of the average bubble diameters (600/71).

The  $\log k$  versus  $\log d_p$  curves for SDB latex (Fig.7.15) are completely different from those for glass beads. With the 42 micron bubbles (L3,L4) there is virtually no effect of particle size on flotation rate. With the 71 micron bubbles (L1,L2) there is a small effect (slope = 0.44). These results are completely at variance with the predictions of Chapter 5 for the neutral buoyancy case (predicted slope = 1.9). The effect of stirring is to double the flotation rate without altering significantly the slope of the  $\log k$  versus  $\log d_p$  curve. Possibly the increase in flotation rate comes about because the tangential velocity imparted to the bubbles by the stirrer increases their residence time in the liquid.

The rate constants in the two cases (L1,L2) and (L3,L4) may be compared, as for the glass bead runs to obtain an estimate of the exponent  $n$  in the relation  $E \propto (1/D_b)^n$ . The values of  $n$  obtained with SDB latex are 2.0 at  $d_p = 4$  microns and 1.6 at  $d_p = 8$  microns.

When correction is made for the difference in gas rates the flotation rates of SDB latex and glass beads are roughly the same in the overlap region of 7 to 8 microns with both the 71 micron and the 42 micron bubbles.

### 7.7 Discussion of Results

It is tempting to conclude from the glass bead results that the preliminary model developed in Chapter 5 is substantially correct except that the flow pattern at the front of the bubble is closer to Hadamard-Rybczynski flow than to Stokes flow. This implies that a substantial portion of the front half of the bubble surface is mobile and does not carry any excess surfactant. Unfortunately,

this picture conflicts with the evidence presented in Chapter 2, Section 2.5 that even at surfactant concentrations well below those employed here the surface of bubbles of diameter less than 100 microns will be covered completely by a stagnant layer of surfactant. The latter picture has sound experimental and theoretical backing, so the mobile surface hypothesis cannot be accepted. Of course, another reason for not accepting it is that it fails to explain the results obtained with SDB latex.

### 7.8 Miscellaneous Flotation Runs

A few runs were performed with SDB latex in which only the reduction in total particle concentration was measured. Their objective was a rapid screening of the effect of surfactant and frother concentration on flotation rate. In all of them the medium frit was used with a gas rate of 43 ml./min. and there was no stirring. The surfactant concentrations for the runs without frother were:

<u>Run</u>	<u>EHDA-Br</u>	<u>IPA</u>
L6	$10^{-4}M$	0.5 vol.%
L7	$0.5 \times 10^{-4}M$	0.25 "
L8	$0.25 \times 10^{-4}M$	0.125 "

The results are shown in Fig. 7.16. Also shown is the total particle concentration curve for L1 which was identical to L7 except that 10 ml. of a solution of 1 part Dowfroth 350 to 1000 parts water was added.

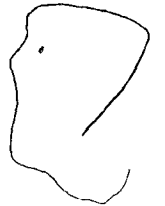
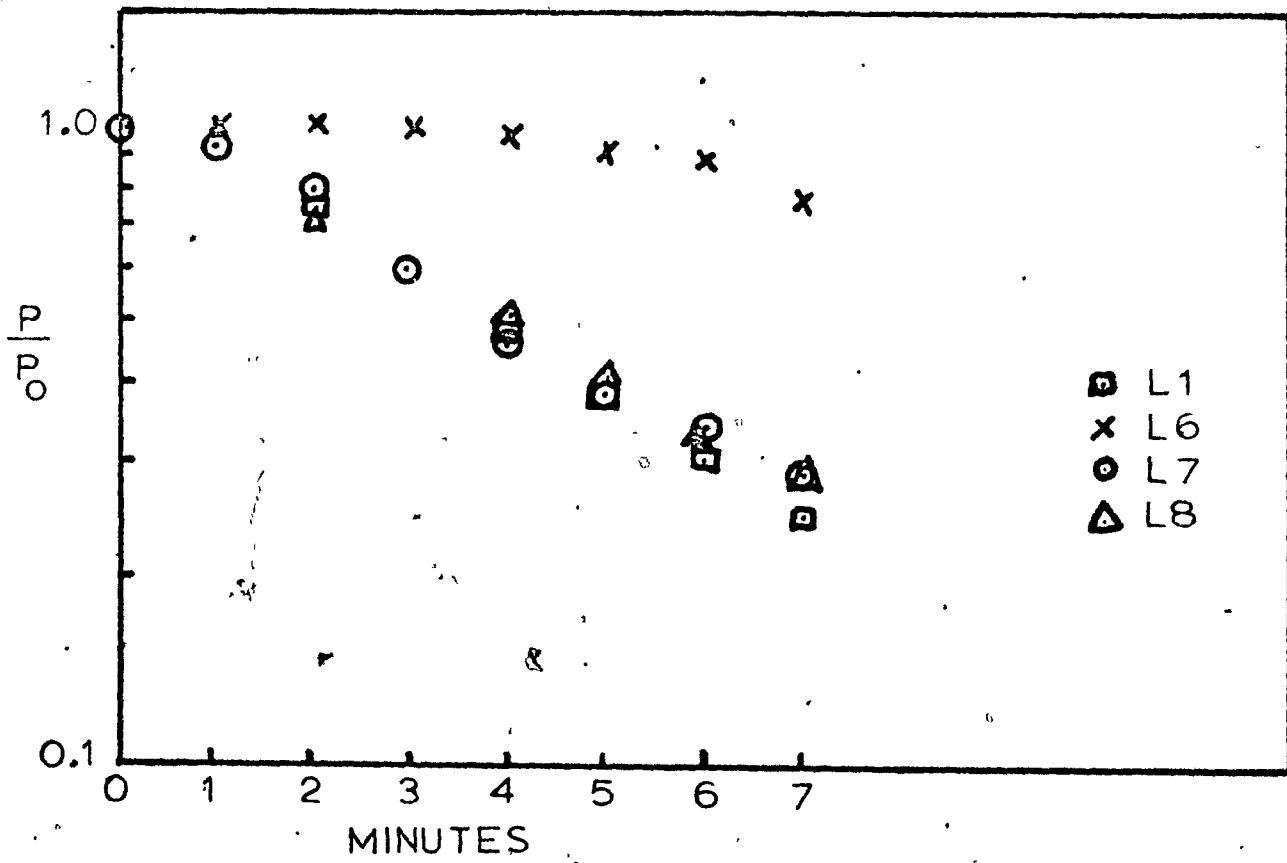


Figure 7.16

EFFECTS OF SURFACTANT AND FROTHER CONCENTRATIONS ON  
FLOTATION RATE



The curves for L7 and L8 are almost identical, showing that a modest reduction in surfactant concentration below  $0.5 \times 10^{-4} M$  has no noticeable effect on flotation rate. This was important, because it was known that the surfactant concentration decreased by 20 to 30 per cent during a flotation run (see Section 7.4.8).

The froth appeared a little unstable at surfactant concentrations below  $10^{-4} M$ , which was why Dowfroth was added for most of the SDB latex runs. It was suspected that if Dowfroth was not used some particles would fall back into the liquid. This was confirmed by comparing the curve for L1 with those for L7 and L8. Otherwise, the addition of Dowfroth did not appear to make any difference to the flotation rate.

Almost no flotation was observed at  $10^{-4} M$  (L6). In the light of Connor and Ottewill's adsorption data (discussed in Chapter 2, Section 2.4) a possible explanation is that at  $10^{-4} M$  the surface of the particles is saturated with surfactant ions, the close-packed ions are aligned vertically with their polar groups outward and the surface is hydrophilic. At lower surfactant concentrations the ions are less tightly packed on the surface, their orientation is between vertical and horizontal and the surface has some hydrophobic character.

### 7.9 Closure

In this chapter batch flotation experiments with glass beads and latex particles have been described. The results show that the preliminary model of Chapter 5 slightly overestimates the effects of particle size and bubble size on the rate of flotation of glass

beads. With latex particles the effect of bubble size is again over-estimated slightly but the effect of particle size is overestimated grossly. In the next chapter correction will be made for two of the weaker-looking assumptions of the preliminary model in an attempt to improve agreement with the experimental data.

## 8. THE VISCOUS INTERACTION MODEL

### 8.1 Introduction

Two of the weakest assumptions in the preliminary model developed in Chapter 5 were the following:

- (a) that the motion of the bubble is not affected by the presence of the particle;
- (b) that the fluid velocity to be used in computing the drag on a particle is the velocity which would exist at the point occupied by the centre of the particle if the particle were absent.

These assumptions are strictly valid only at  $r_p/R_b = 0$ . Since, for the purpose of calculating its trajectory, the particle is effectively replaced by a point mass located at its centre, theories based on these assumptions may be termed "point replacement" theories. The Flint-Howarth collision model is another example of this type. Such theories neglect the fact that when the bubble and particle are close together viscous forces retard thinning of the film of liquid between their surfaces and deflect the particle from its point replacement trajectory. This effect may be important when the particle surface is within one particle radius of the bubble surface.

In the present chapter we construct a speculative model of bubble-particle interactions which takes this effect into account. Whereas the preliminary model of Chapter 5 was based on Stokes flow round a single sphere this model is based on solutions which have been obtained to the problem of Stokes flow round two spheres. This sort of approach has been

used by Hocking and Jonas (63) to simulate collisions between raindrops. It is assumed that the surface of the bubble is rigid but the bubble is free to rotate.

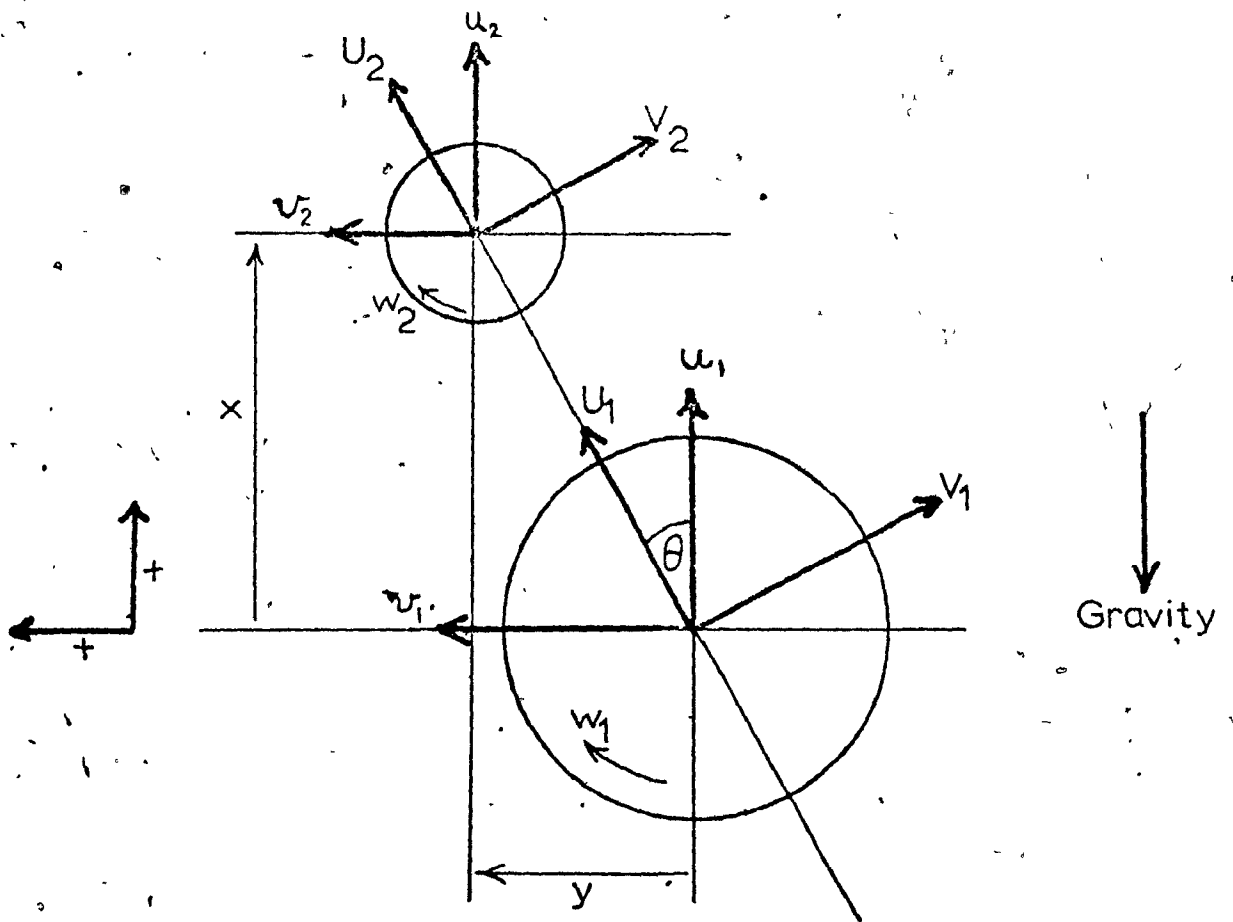
When applied to the flotation of glass beads and compared with the experimental data the predictions of this model are slightly better than those of the point replacement model as regards the effect of particle size but are worse as regards the effect of bubble size. When applied to the flotation of latex particles the model predicts an unexpected effect; it appears that if a particle gets close enough to the bubble surface at certain values of the bubble/particle radius ratio the particle can be pulled round to the back of the bubble and held at the rear stagnation point by purely hydrodynamic forces.

## 8.2 Development of the Model

Consider two rigid spheres of radii  $R_1$  and  $R_2$  moving through a fluid of viscosity  $\mu$  as shown in Fig. 8.1. At any instant their line of centres is at an angle  $\theta$  to the vertical, the vertical components of their velocities are  $u_1$  and  $u_2$  and the horizontal components are  $v_1$  and  $v_2$ . Resolved along the line of centres their velocities have components  $U_1$  and  $U_2$  and perpendicular to the line of centres  $V_1$  and  $V_2$ . The spheres have clockwise angular velocities  $w_1 = W_1/R_1$  and  $w_2 = W_2/R_2$  about axes perpendicular to the plane of motion. The coordinate system is centred at the centre of sphere 1; the centre of sphere 2 has vertical coordinate  $x$  and horizontal coordinate  $y$ . The positive directions are upwards and to the left and gravity acts downwards. Sphere 1 is the bubble and sphere 2 is the particle.

Figure 8.1

VISCOUS INTERACTION MODEL



1 = bubble

2 = particle

L

All velocities are dimensionless, with the reference velocity being the Stokes terminal rising velocity  $U_{1T}$  of the bubble in isolation, i.e.

$$6\pi\mu R_1 U_{1T} = -\frac{4}{3}\pi R_1^3 (\rho_1 - \rho_f) g$$

$$\text{or } U_{1T} = -\frac{2(\rho_1 - \rho_f) R_1^2 g}{9\mu}$$

Coordinates  $x$  and  $y$  are dimensionless with  $R_1$  the reference length.

With the Stokes approximation (omission of the non-linear fluid inertia terms) the Navier-Stokes equation becomes linear with respect to fluid velocity. A consequence of this is that drag forces can be resolved into directional components.

$$\text{Let drag on sphere 1 along line of centres} = 6\pi\mu R_1 f_1.$$

$$\text{Let drag on sphere 2 along line of centres} = 6\pi\mu R_2 f_2.$$

$$\text{Let drag on sphere 1 perp. to line of centres} = 6\pi\mu R_1 g_1.$$

$$\text{Let drag on sphere 2 perp. to line of centres} = 6\pi\mu R_2 g_2.$$

$$\text{Let torque on sphere 1} = 8\pi\mu R_1^2 h_1.$$

$$\text{Let torque on sphere 2} = 8\pi\mu R_2^2 h_2.$$

$f_1, f_2, g_1, g_2, h_1$  and  $h_2$  are dimensionless velocities.

Let the ratio of Stokes terminal velocities  $\frac{U_{2T}}{U_{1T}} = b$ .

For  $\rho_2 > \rho_f > \rho_1$ ,  $b$  will be negative.

$$\text{Gravitational force on sphere 1 along line of centres} = 6\pi\mu R_1 \cos \theta.$$

$$\text{Gravitational force on sphere 2 along line of centres} = 6\pi\mu R_2 b \cos \theta.$$

$$\text{Gravitational force on sphere 1 perp. to line of centres} = 6\pi\mu R_1 \sin \theta.$$

$$\text{Gravitational force on sphere 2 perp. to line of centres} = 6\pi\mu R_2 b \sin \theta.$$

We make a similar quasi-equilibrium assumption to that made for the

preliminary model, i.e. we assume that the inertias of the particle and the bubble are so small that, when a change occurs in the flow field surrounding them, their velocities adjust almost instantaneously to the new equilibrium values. It was pointed out in Chapter 5 that the Stokes number  $St$  is the ratio of the particle relaxation time to the characteristic time for changes in the flow field round the bubble, and we are concerned here with Stokes numbers ranging from  $10^{-6}$  to  $10^{-2}$ . Of course, the velocities are never exactly at their equilibrium values since the flow field is changing constantly, but we assume that at any instant the deviation from equilibrium is so small that it can be neglected. Hence, for each sphere the net force acting on it at any time is approximately zero.

Force balance on sphere 1:

(a) along line of centres:

$$6\pi\mu R_1 (f_1 + \cos \theta) = 0$$

$$\therefore F_1 = - \cos \theta.$$

(b) perpendicular to line of centres:

$$6\pi\mu R_1 (g_1 + \sin \theta) = 0$$

$$\therefore g_1 = - \sin \theta.$$

(c) torque:

$$8\pi\mu R_1^2 h_1 = 0$$

$$\therefore h_1 = 0.$$

Similarly, a force balance on sphere 2 gives:

$$f_2 = - b \cos \theta$$

$$g_2 = - b \sin \theta$$

$$h_2 = 0.$$

The velocities  $f_1$  and  $f_2$  can be expressed as:

$$f_1 = k_1 U_1 + k_2 U_2 = -\cos \theta \quad (8.1)$$

$$f_2 = k_3 U_1 + k_4 U_2 = -b \cos \theta \quad (8.2)$$

The coefficients  $k_1$  to  $k_4$  can be found from the results of Pshenay-Severin (64) and are functions of  $R_1/R_2$  and the distance between the spheres.

Pshenay-Severin's expressions for the coefficients are rather cumbersome infinite series which fortunately converge quickly. To facilitate computation the coefficients were evaluated for  $R_1/R_2 = 2, 3, 4, 5$  and 10 and  $S/R_2 = 10, 1, 10^{-1}, 10^{-2}$  and  $10^{-3}$  where  $S$  is the surface to surface separation, and for each value of  $R_1/R_2$  polynomial approximations were obtained in the form:

$$\ln(Zk_n) = A + B \ln X + C(\ln X)^2 + D(\ln X)^3 + E(\ln X)^4.$$

Where  $X = \frac{S}{R_2}$ ,  $Z = 1$  for  $n = 1$  and 4,  $Z = -1$  for  $n = 2$  and 3.

Details are given in Appendix C.

The velocities  $G_1, g_2, h_1$  and  $h_2$  can be expressed as:

$$g_1 = k_5 V_1 + k_6 V_2 + k_7 W_1 + k_8 W_2 = -\sin \theta \quad (8.3)$$

$$g_2 = k_9 V_1 + k_{10} V_2 + k_{11} W_1 + k_{12} W_2 = -b \sin \theta \quad (8.4)$$

$$h_1 = k_{13} V_1 + k_{14} V_2 + k_{15} W_1 + k_{16} W_2 = 0 \quad (8.5)$$

$$h_2 = k_{17} V_1 + k_{18} V_2 + k_{19} W_1 + k_{20} W_2 = 0 \quad (8.6)$$

Numerical values of  $k_5$  to  $k_{20}$  are given by Davis (65) for  $R_1/R_2 = 2, 5$  and 10 at  $S/R_2 = 10, 1, 10^{-1}, 10^{-2}$  and  $10^{-3}$  and by O'Neill and Majumdar for  $R_1/R_2 = 4$  at the same values of  $S/R_2$ . Values for  $R_1/R_2 = 3$  were found by interpolation. For computation at intermediate values of  $S/R_2$  cubic approximations were derived of the form:

$$k_n = A + B \log_{10} X + C(\log_{10} X)^2 + D(\log_{10} X)^3$$

where  $X = S/R_2$ . Details are given in Appendix C.

Given  $R_1$ ,  $R_2$ ,  $S$ ,  $\theta$  and  $b$  equations 8.1 and 8.2 can be solved for  $U_1$  and  $U_2$  and equations 8.3 to 8.6 can be solved for  $V_1$  and  $V_2$  using Cramer's rule. ( $W_1$  and  $W_2$  are not needed for calculating the trajectory of sphere 2 relative to sphere 1.)

Resolving velocities:

$$u_1 = U_1 \cos \theta + V_1 \sin \theta$$

$$u_2 = U_2 \cos \theta + V_2 \sin \theta$$

$$v_1 = U_1 \sin \theta - V_1 \cos \theta$$

$$v_2 = U_2 \sin \theta - V_2 \cos \theta$$

The rates of change of coordinates of sphere 2 relative to sphere 1 are:

$$\frac{dx}{dt} = u_2 - u_1 = (U_2 - U_1) \cos \theta + (V_2 - V_1) \sin \theta \quad (8.7)$$

$$\frac{dy}{dt} = v_2 - v_1 = (U_2 - U_1) \sin \theta - (V_2 - V_1) \cos \theta \quad (8.8)$$

( $t$  is dimensionless with the reference time being  $R_1/U_{1T}$ .) Hence, given an initial position the trajectory of sphere 2 relative to sphere 1 can be calculated.

The most convenient procedure is to start with the spheres in the collision position and work backwards along the trajectory until the particle's motion is almost vertical. This gives the grazing trajectory, and hence the collision efficiency, directly. (This would not have been possible without the quasi-equilibrium assumption. The velocity at the collision point would not have been known, so the trajectory would have had to be calculated forwards and the grazing trajectory found by a search procedure.)

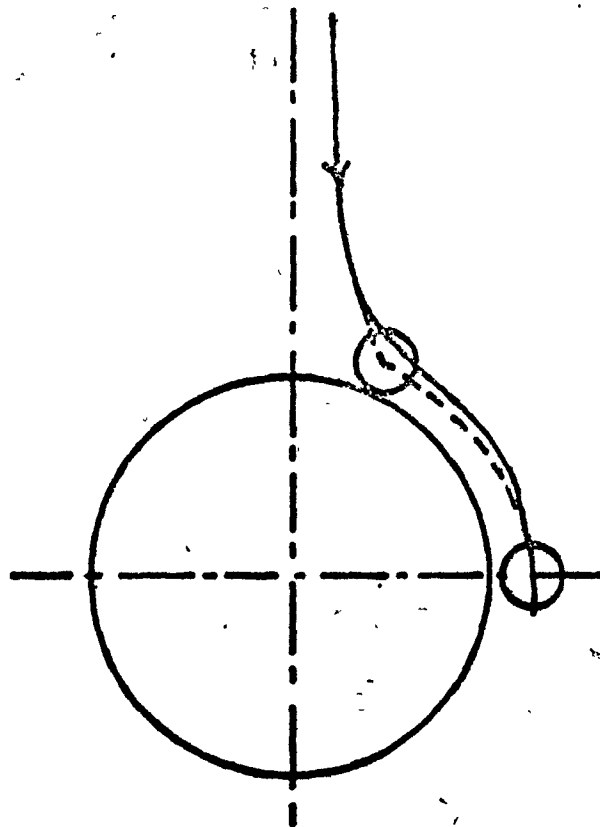
Since the spheres can never touch, an assumption must be made regarding the surface to surface separation corresponding to a "collision".

A clue is provided by the experiments of Evans (67). He observed the thinning of the water film between an air bubble and a rotating hydrophobic silica surface under which the bubble was trapped. The film ruptured at a thickness of about 0.3 microns. Presumably, some form of momentary instability provided a point rupture and since the surface was hydrophobic the rupture spread. Collision separations  $S_0$  of this order of magnitude would seem to be appropriate.

The actual starting point was defined by  $S = S_0$  and  $y/x = 0.001$  since computational problems were encountered if  $\cos \theta$  was initially zero. A Runge-Kutta-Merson numerical integration procedure was used. The Merson variation of the Runge-Kutta method is particularly convenient here since it automatically adjusts the step length to the largest possible value consistent with pre-set integration tolerances (89). Hence, the step length increased rapidly as the separation  $S$  increased and the flow field changed more slowly. The particle coordinates and the separation  $S$  (converted to microns) together with the time (in dimensionless units) were printed at frequent intervals. The integration was stopped when, over one doubling of  $y$ , the ratio  $\Delta x / \Delta y$  was less than  $10^{-6}$ . This usually occurred at twenty to thirty bubble diameters upstream. Exhibit D.2 is a sample computer output. The program is documented in Appendix D1. Fig. 8.2 shows a sample trajectory and compares it with a point replacement trajectory computed from the same starting point. They are very similar as long as the surfaces are more than about 5 microns apart, but when they are closer viscous resistance to thinning of the film causes considerable deviation from the point replacement trajectory.

Figure 8.2

VISCOUS INTERACTION MODEL; PARTICLE TRAJECTORY RELATIVE  
TO BUBBLE



———— Viscous interaction trajectory

----- Point replacement trajectory

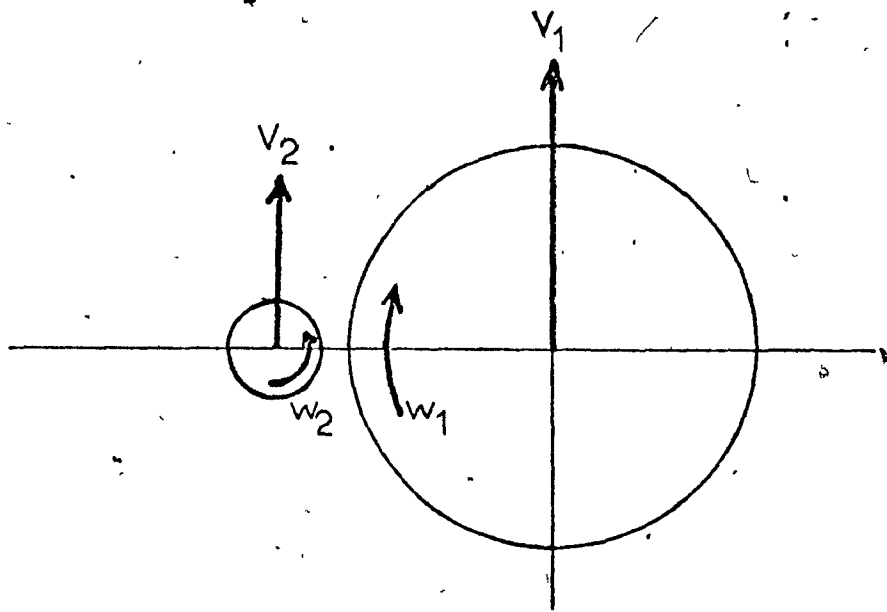
$R_1 = 25$  microns

$R_2 = 5$  microns

$\rho_2 = 2.5$  gm./ml.

Figure 8.3

VISCOUS INTERACTION MODEL; ROTATION OF PARTICLE AND BUBBLE



A hand calculation was carried out with  $R_1/R_2 = 5$ ,  $S/R_2 = 0.01$ ,  $\theta = 90^\circ$  and  $\rho_p = 2.5$  gm./ml. This represents a glass bead crossing the bubble's equatorial plane on what might be a grazing trajectory. The following velocities were found:

$$V_1 = 0.984$$

$$V_2 = 0.799$$

$$W_1 = 0.0336$$

$$W_2 = \sqrt{-0.113}$$

These velocities are dimensionless with reference velocity the bubble's terminal rising velocity.  $V_2$  is positive because the upward drift of fluid caused by the bubble's motion exceeds the particle's terminal falling velocity. The directions of rotation will be those sketched in Fig. 8.3. The rotational velocity of the bubble is negligible but that of the particle is significant.

### 8.3 Application to Glass Bead Flotation

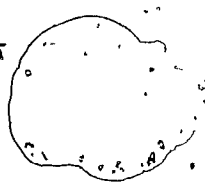
Runs were performed with  $\rho_p = 2.5$  gm./ml., bubble diameters 42 and 71 microns (the average bubble diameters generated by the fine and medium frits),  $R_1/R_2 = 2, 3, 4, 5$  and 10 and  $S_o = 0.75, 0.5$  and 0.25 microns. For  $S_o = 0.5$  microns runs were also performed with bubble diameters 30, 60, 90 and 130 microns in order to cover the bubble size range encountered in the cinephotomicrography experiments. From the results curves were constructed of collision efficiency  $E$  versus  $d_p/D_b$ . These are shown in Fig. 8.4.

It is obvious that the relation between  $E$  and  $d_p$  depends strongly on  $S_o$  and  $D_b$ . For  $S_o = 0.75$  microns the slope of the  $E$  versus  $d_p$  curves approach the value of 2.05 predicted from the point replacement model. In general, the point replacement slope is approached more closely for smaller than for larger bubbles. At first sight this seems surprising, but it may

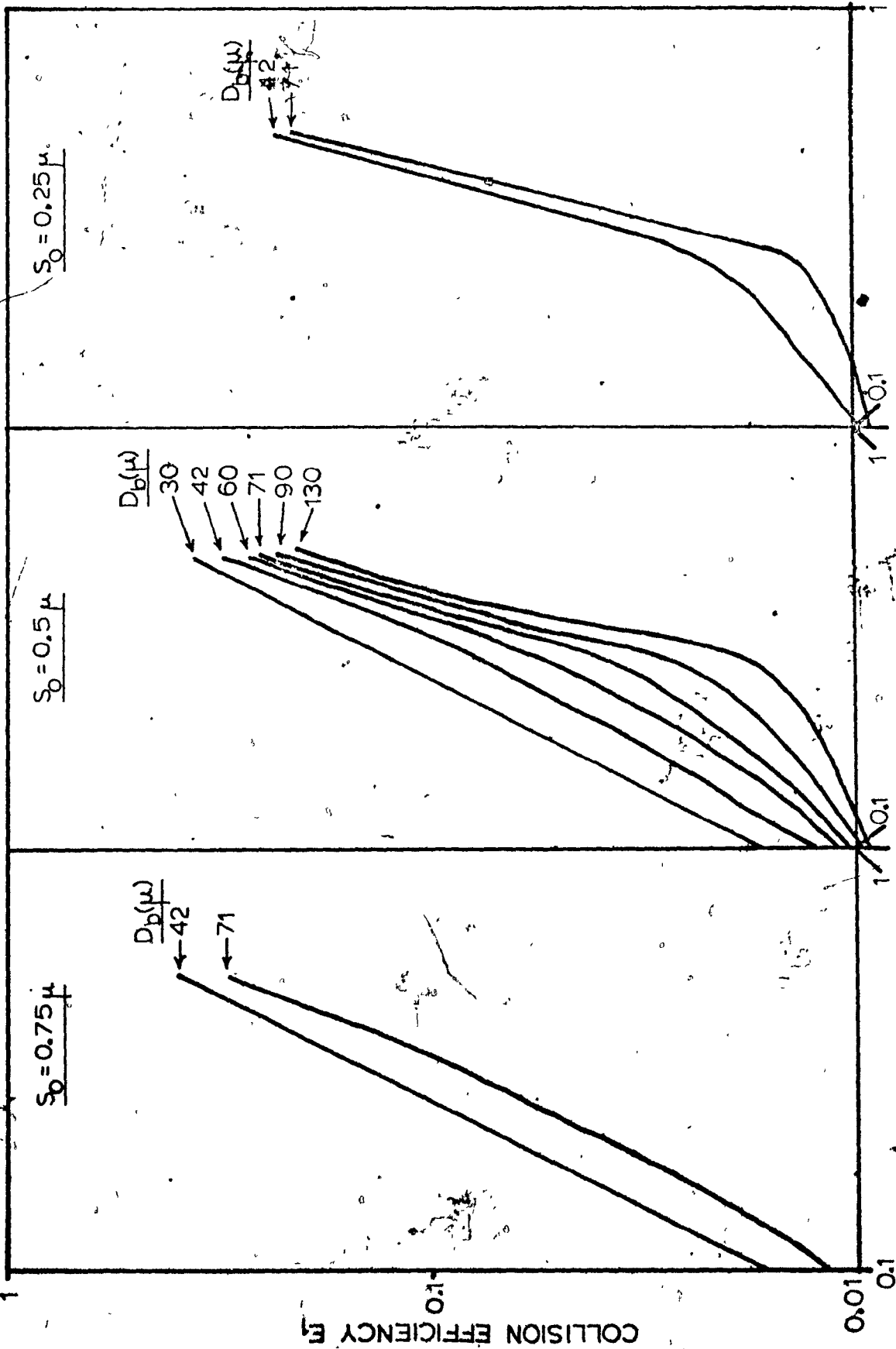
Figure 8.4

VISCOUS INTERACTION MODEL; COLLISION EFFICIENCY VERSUS  $d_p/d_b$

FOR  $\rho_p/\rho_f = 2.5$



$\rho_2 = 2.5 \text{ gm./ml.}$



$d_b / D_b (= R_2 / R_1)$

be because with smaller bubbles  $S_o$  is a larger fraction of the bubble radius, so on a dimensionless basis the particle is further out from the bubble surface.

$S_o = 0.5$  microns gives the best fit to the experimental data. Fig. 8.5 compares the predictions of this model (henceforth referred to as the viscous interaction model) at  $S_o = 0.5$  microns with those of the point replacement model and with the experimental data obtained in the batch cells. The predictions of both models are made to coincide with the data at particle diameter 11 microns. As regards the effect of particle size on collection efficiency, the present model's predictions are slightly closer to the data than those of the point replacement model, but there is little to choose between them.

Let us now compare the predictions of the two models with regard to the effect of bubble size on collection efficiency. With the same gas rate and two bubble diameters  $D_A$  and  $D_B$  the ratio of flotation rates is

$$\frac{k_A}{k_B} = \frac{E_A}{E_B} \times \frac{D_B}{D_A} \text{ where the } E\text{'s are collection efficiencies. For bubble}$$

diameters  $D_A = 42$  microns and  $D_B = 71$  microns the point replacement model predicts  $\frac{k_A}{k_B} = \left(\frac{71}{42}\right)^2 \times \frac{71}{42} = 4.8$ . With the viscous interaction model  $k_A/k_B$

will depend on  $d_p$  and  $S_o$ . Taking  $d_p = 14$  microns (the median diameter of the particle size distribution) and  $S_o = 0.5$  microns we obtain

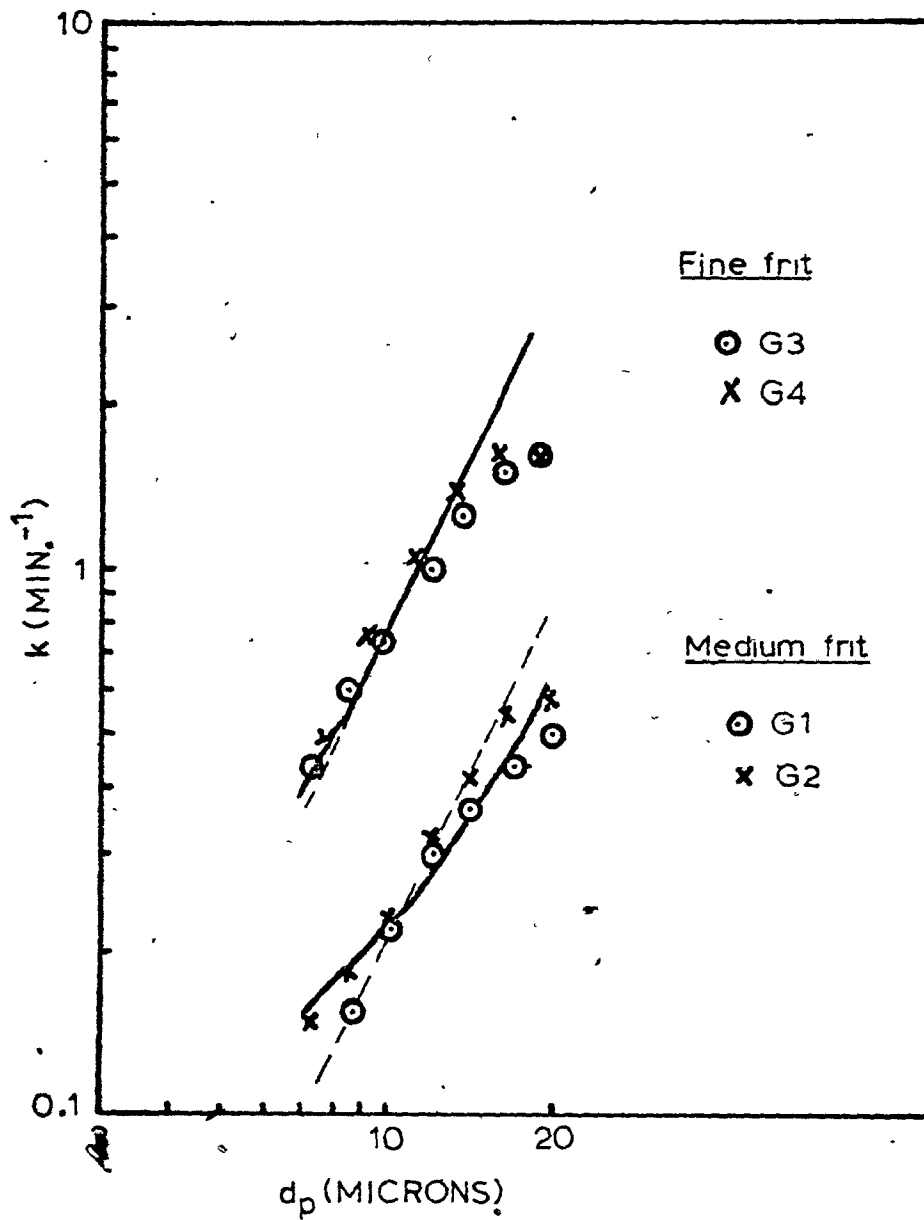
$$\frac{k_A}{k_B} = \frac{0.167}{0.0218} \times \frac{71}{42} = 13. \text{ From the experimental data } \frac{k_A}{k_B} = \frac{1.50}{0.39} = 3.8. \text{ Hence,}$$

the point replacement model is much closer to the experimental data than the viscous interaction model.

If, for some reason, the collision separation  $S_o$  were to be proportional to bubble diameter,  $S_o = 0.25$  microns would be a more appropriate

Figure 8.5

VISCOUS INTERACTION MODEL; COMPARISON OF PREDICTIONS WITH  
BATCH CELL GLASS BEAD RESULTS



----- Preliminary model (slope = 2.05)

———— Viscous interaction model

curve for the 42 micron diameter bubbles. We would have then

$$\frac{k_A}{k_B} = \frac{0.054}{0.0218} \times \frac{71}{42} = 4.2, \text{ which is close to the experimental value. However,}$$

we have no physical or chemical basis for such an assumption and  $S_o = 0.25$  microns gives a poorer fit to the  $\log k$  versus  $\log d_p$  data for the smaller bubbles.

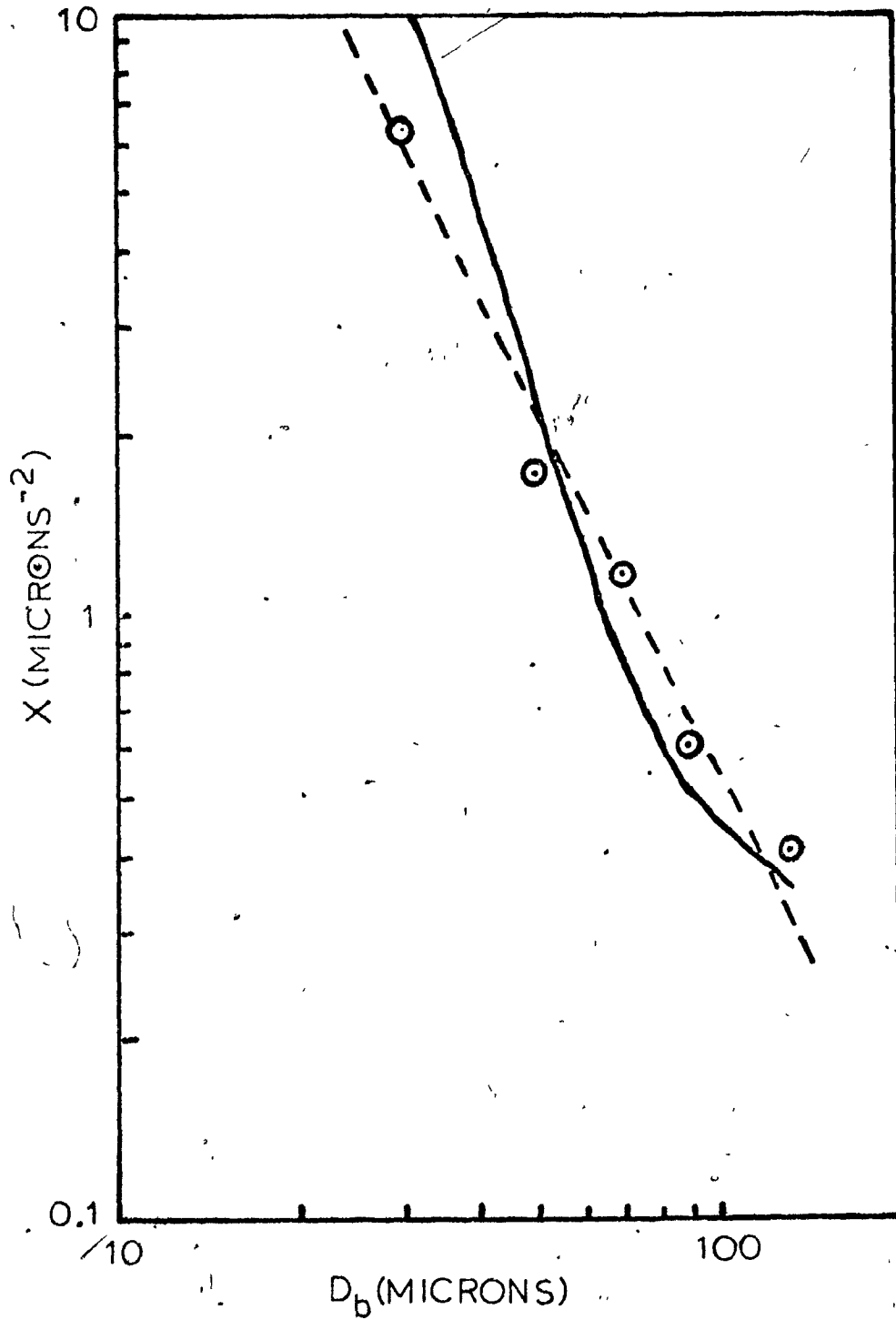
Figures 8.6 and 8.7 compare the predictions of the two models with the cinéphotomicrography data. With the viscous interaction model  $d_p = 14$  microns has been assumed in Fig. 8.6 and  $D_b = 60$  microns (the average bubble diameter in the cinéphotomicrography experiments) in Fig. 8.7. The curves have been positioned to coincide with the data at these points. Again, the viscous interaction model does not predict the effect of bubble size on collection efficiency as well as the point replacement model. With regard to the effect of particle size it gives a better prediction at the higher particle sizes but a poorer one at the lower end. However, the poorer fit at the lower end may be misleading because the experimental point at  $d_p = 9$  microns was obtained on the basis of only three captured particles. If a fourth had been observed it would have brought the experimental curve up to exactly the point predicted by the viscous interaction model.

#### 8.4 Application to SBD Latex Flotation

When applied to the flotation of SDB latex of density 1.05 gm./ml. the viscous interaction computer program worked satisfactorily for  $R_1/R_2 = 2$  and 10, insofar as it generated collision efficiencies which looked reasonable. It also worked for 42 micron diameter bubbles with a collision gap width  $S_o = 0.75$  microns and  $R_1/R_2 = 4$  and 5, so for this value of  $S_o$  it was possible to cover the experimental range of runs L3 and L4. The result is

Figure 8.6

VISCOUS INTERACTION MODEL; COMPARISON OF PREDICTED COLLISION  
EFFICIENCY VERSUS BUBBLE SIZE CURVE WITH CINEPHOTOMICROGRAPHY  
RESULTS

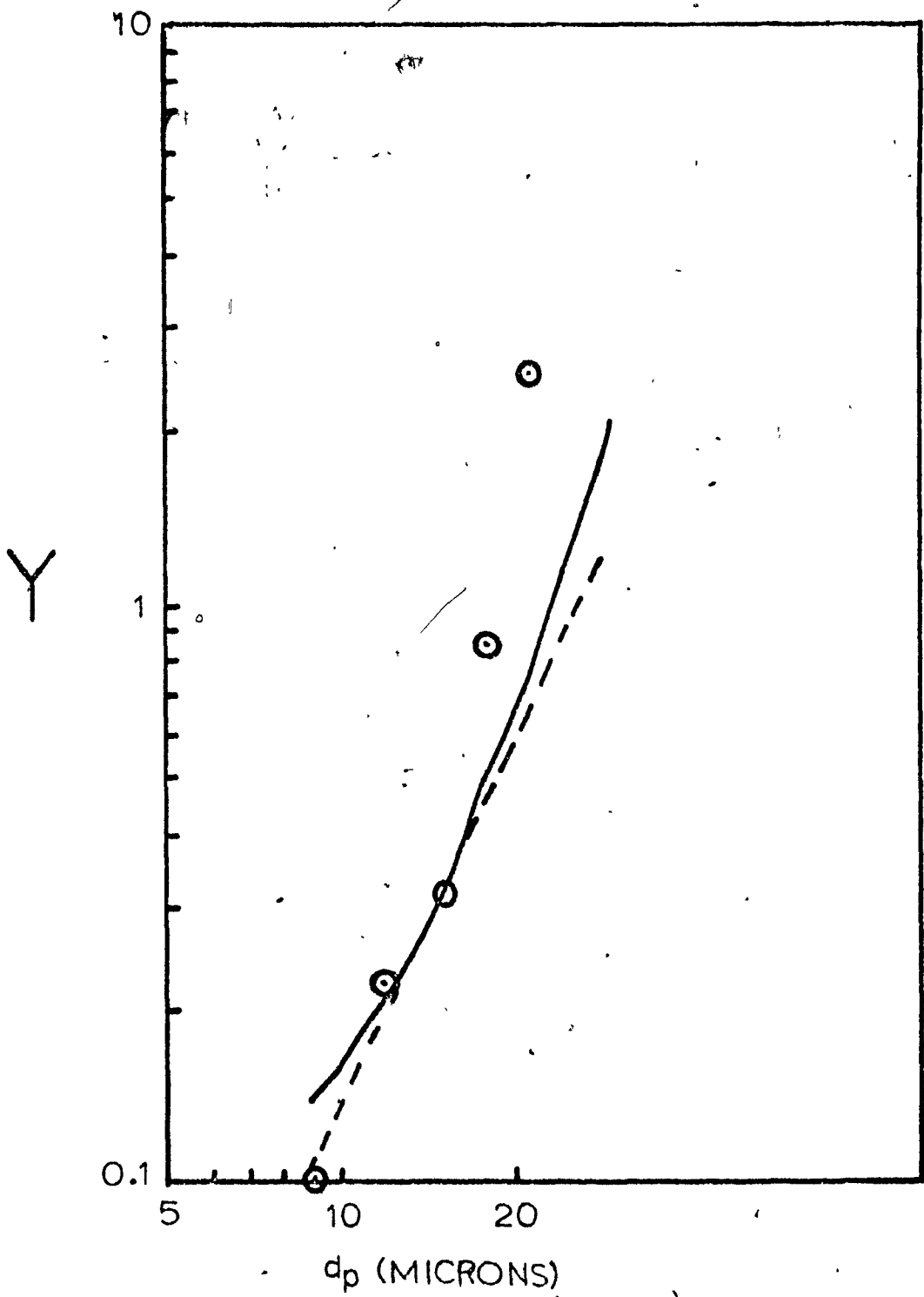


--- Preliminary model (slope = -2.05)

— Viscous interaction model

Figure 8.7

VISCOUS INTERACTION MODEL; COMPARISON OF PREDICTED COLLISION  
EFFICIENCY VERSUS PARTICLE SIZE CURVE WITH CINEPHOTOMICROGRAPHY  
RESULTS



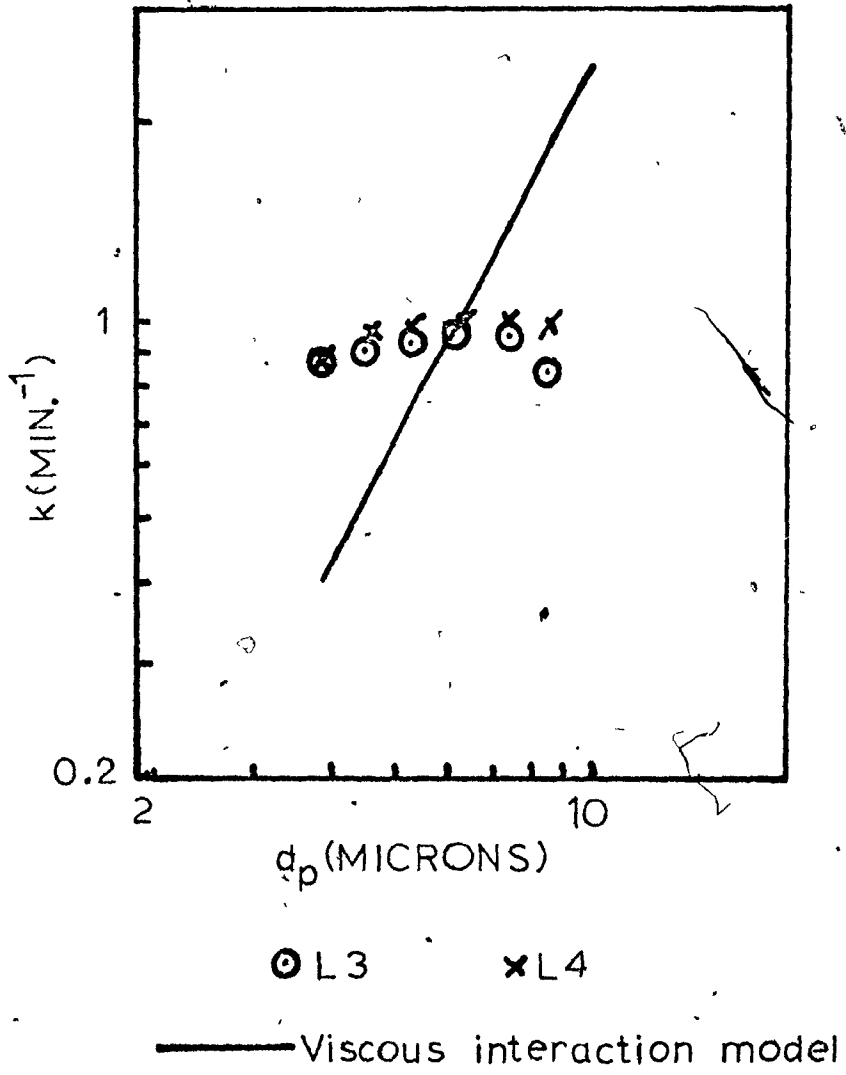
--- Preliminary model (slope = 2.05)

— Viscous interaction model

Figure 8.8

VISCOUS INTERACTION MODEL; COMPARISON OF PREDICTIONS WITH  
BATCH CELL SDB LATEX RESULTS

---



shown in Fig. 8.8. The line through the points has a slope of 1.9, which was the prediction of the preliminary model, whereas the experimental results of L3 and L4 had a slope of almost zero. (Fig. 7.15.)

By analogy with the glass bead trajectories the slope of the  $E_1$  versus  $r_p/R_b$  curves in the experimental range  $r_p/R_b (= R_2/R_1) = 0.1$  to 0.25 would be expected to decrease as  $S_0$  is decreased. However, at  $S_0$  values of 0.5 and 0.25 microns the particle refused to retreat to infinity. Instead, it crept round to the front stagnation point with  $S$  actually decreasing as it did so. The same occurred at all three collision gap widths  $S_0 = 0.75, 0.50$  and 0.25 microns with a bubble diameter of 71 microns and intermediate radius ratios  $R_1/R_2 = 3, 4$  and 5. Hence, collision efficiencies could not be obtained for these situations so a full test of the model was not possible.

This apparently anomalous behaviour at intermediate radius ratios was explored further by slightly altering the program to permit forward integration along the trajectory. (Details are given in Appendix D1) Integration was started with the particle twenty bubble diameters upstream and was terminated when the particle was either twenty bubble diameters downstream or within 0.05 microns of the bubble's vertical axis. Table 8.1 presents the results of several runs.  $y$  is the horizontal coordinate of the centre of the particle (distance from the bubble's vertical axis).

The purpose of the first run in Table 8.1 was to check the revised program by simulating a grazing trajectory which had already been obtained with  $\rho_2 = 2.5$  gm./ml. starting from  $S_0 = 0.5$  microns. Agreement was satisfactory. The second run had the same starting point but a density of 1.05 gm./ml. With less help from gravity it could not thin the film so much and only achieved  $S = 1.13$  microns at  $\theta = 90^\circ$ . The downstream trajectory was

TABLE 8.1

$R_1/R_2$	$R_1$	$R_2$	$\rho_2$	Initial y	S at $\theta = 90^\circ$	Final y	Final S
5	36	7.2	2.5	5.3	0.50	5.3	1397
	36	7.2	1.05	5.3	1.13	5.3	1397
	36	7.2	1.05	10.0	2.54	10.0	1397
	36	7.2	1.05	3.0	0.90	3.0	1397
	36	7.2	1.05	1.0	0.80	0.9	1397
	36	7.2	1.05	0.5	0.79	0.35	1397
	36	7.2	1.05	0.1	0.78	< 0.05	0.375
	22	4.4	1.05	1.0	0.50	0.94	814
	22	4.4	1.05	0.5	0.485	0.42	814
22	4.4	1.05	0.1	0.48	< 0.05	0.23	
4	22	5.5	1.05	1.0	0.61	0.78	813
	22	5.5	1.05	0.5	0.61	< 0.05	0.18
	22	5.5	1.05	0.1	0.61	< 0.05	0.18
3	22	7.33	1.05	1.0	0.62	0.70	811
	22	7.33	1.05	0.5	0.62	< 0.05	0.21
	22	7.33	1.05	0.1	0.62	< 0.05	0.21

$R_1, R_2, y$  and  $S$  in microns.

$\rho_2$  in gm./ml.

still a mirror image of the upstream trajectory. If the starting distance from the axis was reduced to  $y = 1$  micron as in the fifth run this was no longer completely true since the particle was being pulled slightly closer to the axis downstream than upstream. As the initial  $y$  was reduced below 1 micron the trajectories crowded together very closely at the  $90^\circ$  point; there appeared to be a limit to how close the particle could get to the bubble at this point, the limit being about  $S = 0.78$  microns. At the same time the particle was being pulled further in towards the axis on the downstream side. Eventually, at an initial  $y$  of 0.1 microns, the particle was pulled right in to the rear stagnation point with  $S$  decreasing continually. At smaller radius ratios this phenomenon occurred earlier, at an initial  $y$  of 0.5 microns.

Now all the equations governing the particle's trajectory are linear, so the downstream portion of the trajectory should be the mirror image of the upstream portion. The fact that in some cases it is not indicates some error or inaccuracy in the simulation. It is tentatively suggested that the lack of symmetry is due to approximations being used instead of absolute values for the force coefficients  $k_1$  to  $k_{20}$ .

From both forward and backward trajectories it is apparent that an approaching latex particle cannot get closer to the bubble than a critical gap width which depends on the sizes of the particle and the bubble. In the cases investigated the critical gap width is of the order of 0.5 to 0.8 microns. It seems from the simulations performed with backwards integration that trajectories closer to the bubble surface than the critical gap all have their origin at the forward stagnation point (and presumably terminate at the rear stagnation point to preserve symmetry).

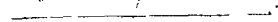
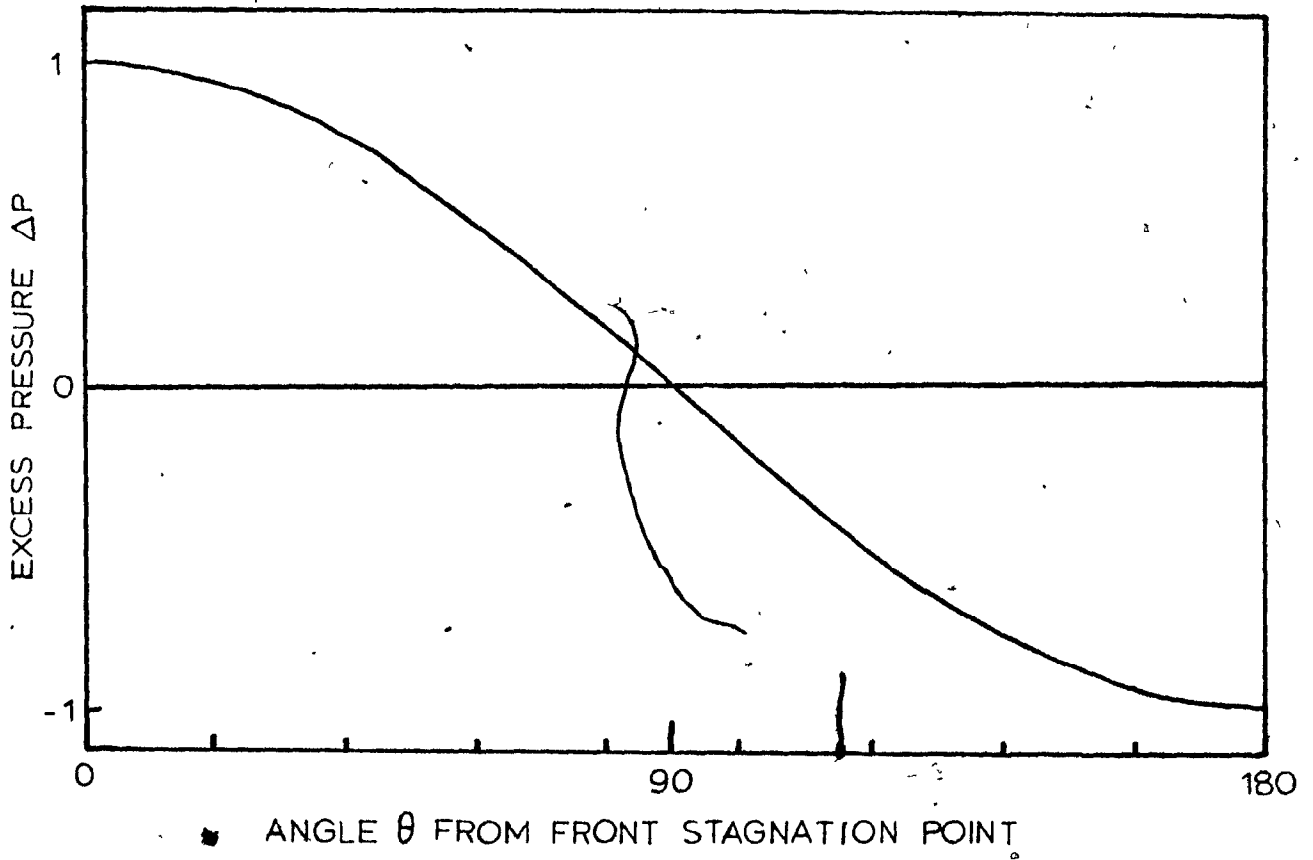


Figure 8.9

EXCESS PRESSURE ON SPHERE SURFACE IN STOKES FLOW



$$\Delta P = \frac{(P - P_{\infty}) d_p}{3\mu U}$$

particle trajectories cannot get as close to the bubble as the glass bead trajectories. Over the back half of the bubble there is a negative excess pressure at the surface so the pressure will increase with radial distance out from the surface. This pressure gradient will tend to push the particle towards the bubble. Fig. 8.10 shows the directions of the various forces acting on a particle upstream and downstream of the bubble. The closer the particle is to the bubble the stronger will be the pressure gradient, so if the particle is close enough on the downstream side and the downward pull of gravity is weak enough the particle will be sucked in toward the bubble. Another way of looking at it is that upstream there is viscous resistance to film thinning and downstream there is viscous resistance to film thickening.

A glass bead of density 2.5 gm./ml. will have to be much closer to the bubble surface than a latex particle of density 1.05 gm./ml. for hydrodynamic capture to occur, which is presumably why it was never observed with glass bead grazing trajectories at collision gap widths down to 0.25 microns. However, if the trajectory lies well inside the grazing trajectory the gap width could be very much less than this at the equator and it might be small enough for capture to occur despite the downward pull of gravity. To an observer it would appear as if the particle was rolling round the bubble with their surfaces touching. This is put forward as a possible explanation for the infinitesimally small contact angles observed in the cinephotomicrography experiments. (Refer back to the photographs in Chapter 6.)

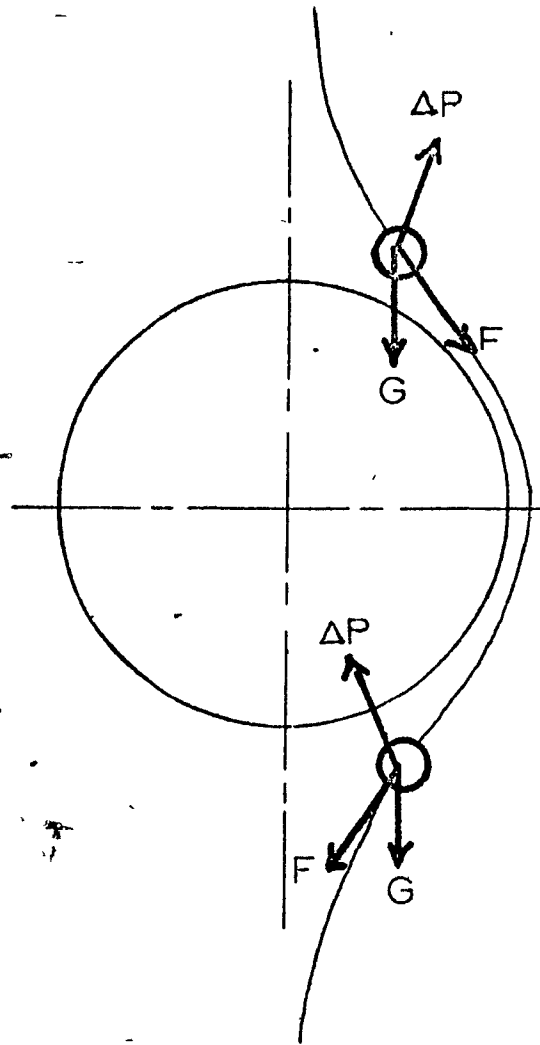
Conversely, hydrodynamic capture should be facilitated if the density of the particle is less than that of the medium - for example, if the particle is an oil drop. In the latter case, and possibly also in the neutral buoyancy case, there should be an observable increase in flotation



Figure 8.10

FORCES ACTING ON PARTICLE UPSTREAM AND DOWNSTREAM OF BUBBLE





F = viscous drag  
G = gravity  
 $\Delta P$  = pressure gradient

rate at radius ratios favouring hydrodynamic capture. It may even be possible to achieve appreciable flotation rates when chemical conditions are unfavourable. Experiments along these lines are included in our suggestions for further research. When chemical conditions are favourable for "chemical" capture the process should be assisted by hydrodynamic capture providing greatly increased contact times during which film rupture can take place.

It would be an interesting exercise to obtain for a set of bubble sizes, particle sizes and particle densities the critical trajectories for the onset of hydrodynamic capture. If, at an infinite distance upstream from the bubble this trajectory is a distance  $y_c$  from the bubble's vertical axis, collision efficiency could be defined as  $(y_c/R_b)^2$ . The variation with bubble size, particle size and particle density of a collision efficiency defined in this way could be determined and compared with our experimental data.

### 8.5 Closure

In this chapter it has been shown that correcting the preliminary model to take into account viscous resistance to film thinning and also the effect of the particle on the flow field round the bubble does not improve the agreement with experimental data. However, it does predict a phenomenon which we have called "hydrodynamic capture" whereby in some circumstances the particle can roll round to the rear stagnation point of the bubble and be held there by purely hydrodynamic forces. This could be an explanation of the apparently zero contact angle observed with glass beads in the cinematomicrography experiments.

In the next chapter the effect of correcting the preliminary model to take into account interactions between neighbouring bubbles is explored.

## 9. THE BUBBLE SWARM MODEL

Another assumption of the simple model which seems weak is that the bubble can be treated as though it were in isolation and interaction with other bubbles can be ignored. At 6% gas hold-up the bubbles generated by the fine frit will have on average a surface-to-surface separation of 1.5 bubble diameters. At 2% gas hold-up those from the medium frit will have on average a surface-to-surface separation of 2.7 bubble diameters. (This estimate agrees well with Kalman's photographs (7).) In this chapter we explore the effect of removing the isolated-bubble assumption.

We apply Happel's "free surface model" of flow past an assemblage of spherical particles (57,68) to flow past an assemblage of bubbles with rigid surfaces. Happel models a random assemblage of particles by a set of identical cells, each consisting of a particle surrounded by a spherical fluid envelope having a frictionless or "free" outer surface. The ratio of fluid volume to particle volume in a cell is set equal to the void fraction  $\epsilon$  of the whole assemblage. (In our system the "void fraction" is the ratio of liquid volume to total volume.) If  $R_p$  is the particle radius,  $b$  is the free surface radius, a spherical coordinate system  $(r, \theta)$  is centered at the centre of the particle and the particle moves through the fluid envelope with a constant velocity  $U$ , then the solution to the Navier-Stokes equation with the inertial terms removed is given in terms of the stream function as

$$\psi = \frac{U r^2 \sin^2 \theta}{2W} \left[ (2 + 3\gamma^5) - (3 + 2\gamma^5) \left(\frac{R_b}{r}\right) + \left(\frac{R_b}{r}\right)^3 - \gamma^5 \left(\frac{R_b}{r}\right)^2 \right]$$

where  $\gamma = \frac{R_b}{b} = 3\sqrt{1-\epsilon}$  and  $W = 2 - 3\gamma + 3\gamma^5 - 2\gamma^6$

We have  $\epsilon = 0.98$  for the medium frit and  $0.94$  for the fine frit, so we can neglect terms containing  $\gamma^5$  and  $\gamma^6$ . This leaves

$$\psi' = \frac{U r^2 \sin^2 \theta}{2 - 3\gamma} \left[ 1 - \frac{3}{2} \left(\frac{R_b}{r}\right) + \frac{1}{2} \left(\frac{R_b}{r}\right)^3 \right]$$

Therefore, if the Stokes stream function is  $\psi'_{st}$  we have

$$\psi = \frac{2}{2 - 3\gamma} \cdot \psi'_{st}$$

and  $u_{fr} = \frac{2}{2 - 3\gamma} \cdot (u_{fr})'_{st} = \frac{U \cos \theta}{1 - \frac{3}{2}\gamma} \left[ 1 - \frac{3}{2} \left(\frac{R_b}{r}\right) + \frac{1}{2} \left(\frac{R_b}{r}\right)^3 \right]$

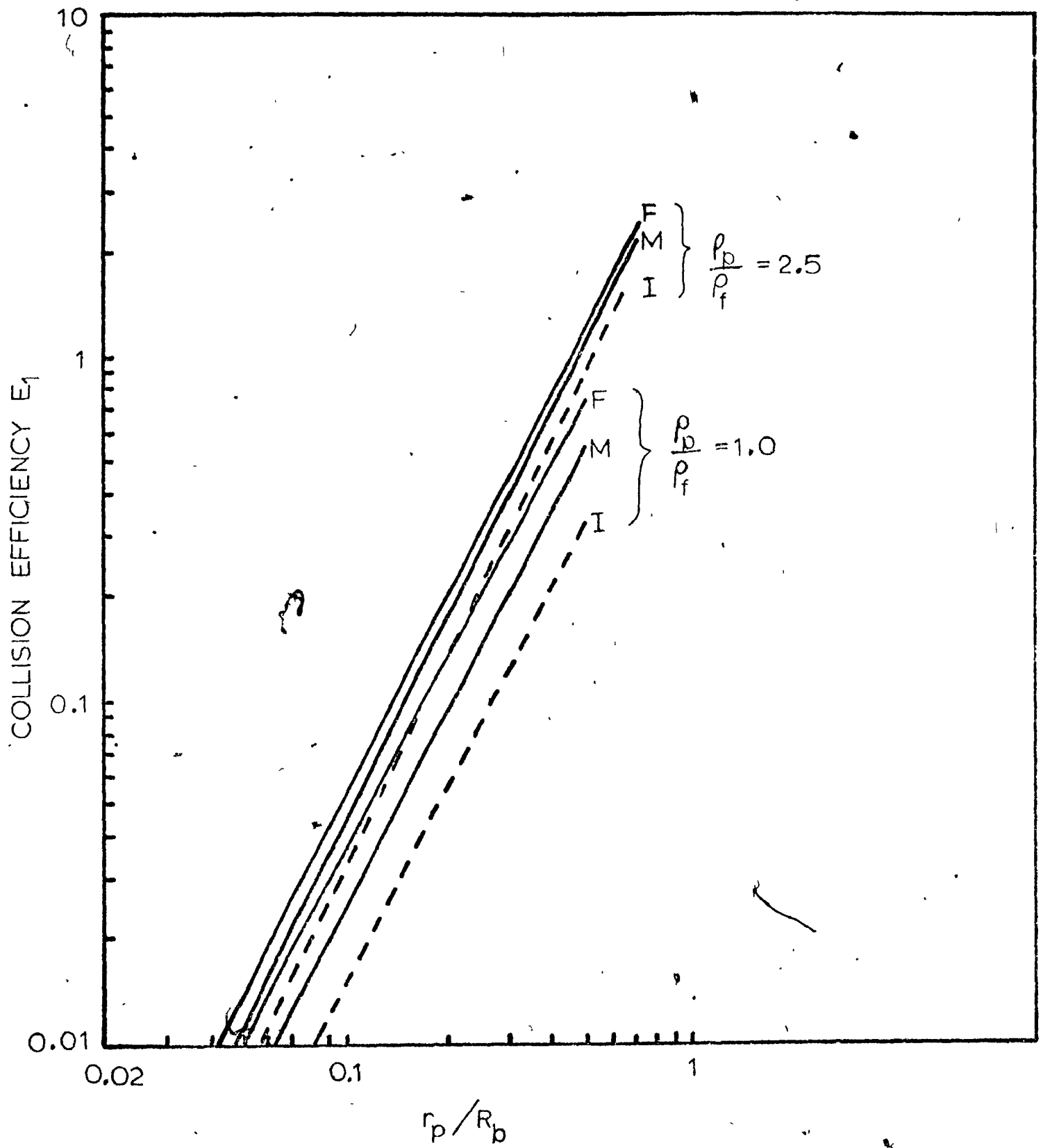
Following the procedure of section 5.2 we obtain the collision efficiency  $E_1 = \frac{K^2}{1 + u_{pt}^*} \left[ u_{pt}^* + \left(1 - \frac{3}{2}\gamma\right) \left(1 - \frac{3}{2}K + \frac{1}{2K^3}\right) \right]$

where  $K = 1 + \frac{r_p}{R_b}$ . This expression for  $E$  is the same as equation (5.7) except for the appearance of the term  $\left(1 - \frac{3}{2}\gamma\right)$ .

For the fine grit  $\gamma = (0.06)^{1/3} = 0.39$  and for the medium frit  $\gamma = (0.02)^{1/3} = 0.27$ . Figure 9.1 is a log-log plot of  $E_1$  versus  $\frac{r_p}{R_b}$  for both frits and for particle densities  $\rho_p = 2.5$  and  $1.0$  gm./ml. For comparison the corresponding lines for the isolated sphere case are shown (broken lines). The lines for this model are almost exactly parallel to those of the isolated sphere case so there will be no

Figure 9.1

BUBBLE SWARM MODEL;  $E_1$  VERSUS  $r_p/R_b$



F= fine frit  
M=medium frit  
I=isolated bubble

change in goodness of fit to experimental data on flotation rate versus particle size. As expected, the collision efficiency is a little higher for this model due to the streamlines being pushed in towards the bubble surface, the effect being higher for the fine frit where the bubbles are closer together. Because  $E_1$  is higher for the fine frit the rate of change of  $E_1$  with bubble diameter predicted by this model is slightly higher than that predicted by the simple model. As the simple model already overestimates the influence of bubble diameter on flotation rate we conclude that the bubble swarm model offers no improvement.

#### Closure

All the aspects of the preliminary model which looked weak from a hydrodynamic viewpoint have been corrected. Agreement with the experimental data has not been improved. In particular, we still have no explanation for the very small effect of particle size on the flotation rate of SDB latex.

In the next chapter a speculative attempt is made to correct the model to take into account possible electrical interaction between a particle and a bubble.

## 10. THE ELECTRICAL ATTRACTION HYPOTHESIS

In the previous two chapters all those assumptions in the preliminary model which looked weak from a hydrodynamic viewpoint have been corrected and we are still no closer to explaining the anomalous experimental results obtained with SDB latex. In this chapter we attempt to correct for the only remaining arbitrary assumption, that of no electrical interaction between particles and bubbles. The approach used is necessarily very speculative since very little is known about the electrical properties of bubbles.

The SDB latex particles had a zeta potential of +10.6 mV at the working surfactant concentration. The glass beads had a very small positive zeta potential, much less than +10 mV, which could not be measured because the glass beads settled rapidly. Pure water has a surface potential of -100 to -200 mV relative to air (81), so we might expect bubbles rising in pure water to have zeta potentials of this order. However, surface-active cations such as  $\text{EHDA}^+$  will adsorb at the interface and, if sufficient numbers are adsorbed, will reverse the sign of the charge on the bubbles. If EHDA-Br was the only surface-active solute this charge reversal would probably occur and the bubbles would tend to repel the particles. But in the batch cell experiments we also had isopropanol (IPA) present at about 700 times the molar concentration of EHDA-Br. Even though  $\text{EHDA}^+$  is much more surface-active than IPA it is likely that there were still many more IPA molecules than  $\text{EHDA}^+$  ions adsorbed on the bubble surface. These molecules would orient themselves with

their slightly negative -OH groups on the water side of the interface. If there was a sufficient excess of IPA at the interface it is possible that the bubbles still had a residual negative charge which would attract the positively charged particles. The latex particles would be attracted more strongly than the glass beads because of their higher charge.

Analysis of the interaction between electrical double layers of unlike species is a formidable problem which has been reviewed recently by Usuf (98). However, an estimate of the maximum possible magnitude of the attractive force can be obtained quite simply by assuming that the water between the hydrodynamic shear planes of the particle and the bubble contains no ions. In other words, the reduction in electrical potential due to an excess concentration of counter-ions outside the shear planes is neglected. The problem then becomes one of calculating the attractive force between two spheres immersed in a dielectric.

Let a particle and a bubble of radii  $r_p$  and  $R_b$  have zeta potentials  $Z_p$  and  $Z_b$  respectively. Then particle charge  $Q_p = 4\pi\epsilon_0\beta Z_p r_p$  and bubble charge  $Q_b = 4\pi\epsilon_0\beta Z_b R_b$  where  $\epsilon_0$  = permittivity of free space and  $\beta$  = dielectric constant of water. The repulsive force  $\underline{F}$  between particle and bubble when their centres are a distance  $r$  apart is given by

$$\underline{F} = \frac{1}{4\pi\epsilon_0\beta} \cdot \frac{Q_p Q_b}{r^2} \cdot \underline{i} \quad \text{where } \underline{i} = \text{unit vector along line of centres}$$

$$= 4\pi\epsilon_0\beta Z_p Z_b \cdot \frac{r_p R_b}{r^2} \cdot \underline{i}$$

We now add  $\underline{F}$  to the right hand side of the equation of motion of the particle (equation 5.1 in Chapter 5).

$$\frac{4}{3} \pi r_p^3 \rho_p \frac{du_p}{dt} = -6 \pi \mu_f r_p (u_p - u_f - \frac{u_{pt}}{r_p}) + \underline{F}$$

Dividing both sides by  $6 \pi \mu_f r_p U_b$  to make the equation dimensionless we obtain:

$$\text{St} \frac{du_p^*}{dt^*} = - \left( u_p^* - u_f^* - \frac{u_{pt}^*}{r_p^*} \right) + \frac{2 \epsilon_0 \beta Z_p Z_b R_b}{3 \mu_f U_b r^2} \cdot \frac{1}{r^*}$$

Neglecting the left hand term as in Chapter 5 and multiplying by  $U_b$  gives, in place of equation 5.3, the following equation:

$$u_p = u_f + \frac{u_{pt}}{r_p} + \underline{X} \left( \frac{R_b}{r} \right)^2$$

where 
$$\underline{X} = \frac{2 \epsilon_0 \beta Z_p Z_b}{3 \mu_f R_b} \cdot \frac{1}{R_b}$$

$\underline{X}$  will be directed along the line joining the centres of the particle and the bubble, so in place of equation 5.4 we have:

$$u_{pr} = u_{fr} + u_{pt} \cos \theta + \underline{X} \left( \frac{R_b}{r} \right)^2$$

Inserting the Stokes flow equation for  $u_{fr}$  yields:

$$u_{pr} = U_b \cos \theta \left[ 1 + \frac{u_{pt}^*}{U_b} - \frac{3}{2} \left( \frac{R_b}{r} \right) + \frac{1}{2} \left( \frac{R_b}{r} \right)^3 \right] + \underline{X} \left( \frac{R_b}{r} \right)^2$$

At  $r = r_p + R_b$  we have:

$$u_{pr} = U_b \cos \theta \left[ 1 + u_{pt}^* - \frac{3}{2K} + \frac{1}{2K^3} \right] + \frac{X}{K^2} \quad (10.1)$$

where  $K = \frac{r_p + R_b}{R_b}$ .

Following through the derivation of the collision efficiency  $E_1$  in Chapter 5 but using equation 10.1 for  $u_p$  gives:

$$\begin{aligned} E_1 &= \frac{K^2}{1 + u_{pt}^*} \left[ 1 + u_{pt}^* - \frac{3}{2K} + \frac{1}{2K^3} \right] - \frac{2X}{U_b (1 + u_{pt}^*)} \\ &= E_1' - \frac{2X}{U_b (1 + u_{pt}^*)} \end{aligned}$$

where  $E_1'$  is the collision efficiency calculated ignoring electrical interactions. Putting  $U_b$  equal to the Stokes terminal velocity

$\frac{2\rho_f R_b^2 g}{9\mu_f}$  we obtain:

$$\begin{aligned} E_1 &= E_1' - \frac{6\epsilon_0 \beta Z_p Z_b}{\rho_f g R_b^3} \cdot \frac{1}{(1 + u_{pt}^*)} \\ &= E_1' - E_1^{el} \end{aligned} \quad (10.2)$$

where  $E_1^{el}$  is the reduction in collision efficiency due to electrostatic repulsion. When  $Z_p$  and  $Z_b$  have opposite signs  $E_1^{el}$  will be negative and the collision efficiency will be increased.

Consider the neutral buoyancy case (SDB latex particles) for which  $u_{pt}^*$  is zero. In this case  $E_1^{el}$  is independent of  $r_p$ . If it can be shown to dominate  $E_1^i$  with  $Z_p \approx 10$  mV and reasonable values of  $Z_b$  then we have a possible explanation of the experimental results. In SI units:

$$\begin{aligned} \epsilon_0 &= 8.85 \times 10^{-12} \text{ coulombs/volt metre} \\ g &= 9.81 \text{ metres/sec.}^2 \\ \rho_f &= 10^{-3} \text{ kg./metre}^3 \\ \beta &= 81 \text{ for water.} \end{aligned}$$

If  $Z_p$  and  $Z_b$  are in millivolts and  $R_b$  is in microns then  $E_1^{el} = -440 \frac{Z_p Z_b}{R_b^3}$ . Consider  $R_b = 20$  microns (40 microns diameter).

Then  $E_1^{el} = -0.55 Z_b$ . For a particle diameter of 6 microns (the average diameter of the SDB latex particles) we have  $\frac{r_p}{R_b} = 0.15$  and, from Fig. 5.2,  $E_1^i = 0.034$ . A bubble surface potential  $Z_b = -0.6$  mV, which is not unreasonable, would be sufficient to make  $E_1^{el} = 10 E_1^i$ . This would result in the flotation rate being almost independent of particle diameter, which is what was observed with an average bubble diameter of 42 microns in runs L3 and L4 (Chapter 7).

As  $R_b$  increases  $E_1^{el}$  decreases more rapidly than  $E_1^i$  since it is proportional to  $\frac{1}{R_b^3}$  instead of  $\frac{1}{R_b^2}$ . Hence, at larger bubble sizes the electrical interactions should be less dominant and some increase of flotation rate with increasing particle size should be noticeable. This is what was observed in runs L1 and L2 (see Fig. 7.15).

In Table 10.1 total collision efficiencies have been calculated for latex particles of diameters 4, 6 and 8 microns and bubble diameters 40 and 70 microns, assuming in all cases a bubble zeta potential of  $-0.5\text{mV}$ . The results are compared with the experimental data in Fig.10.1 with the calculated efficiencies being forced to fit the experimental curve at  $d_p = 6$  microns. Agreement is much better than with any previous model.

The zeta potential of the glass beads is not known. However, we do know that it is much less than  $10\text{mV}$  but still positive. Therefore,  $E_1^{el}$  will be much smaller than with latex particles, especially when the term  $u_{pt}^*$  is taken into account. In contrast,  $E_1'$  will be much larger than with latex particles because of the larger particle size. As an example, suppose we take  $Z_p = +2\text{mV}$ ,  $Z_b = -0.5\text{mV}$ ,  $d_p = 14$  microns and  $D_b = 40$  microns. Then  $E_1' = 0.40$  and  $E_1^{el} = 0.04$ . In this case electrical attraction has very little influence, which explains why the preliminary model of Chapter 5 gave a much better fit to the glass bead data.

Of course, for given particle and bubble zeta potentials the above method of calculation probably over-estimates the attractive force considerably due to neglect of the counter-ions outside the shear plane. But suppose it is over-estimated by a factor of ten. The same conclusions could be reached by assigning to the bubble a zeta potential of  $-5\text{mV}$ , which is still not unreasonable. Clearly, some experimental data on bubble zeta potentials in surfactant solutions would be very welcome.

TABLE 10.1

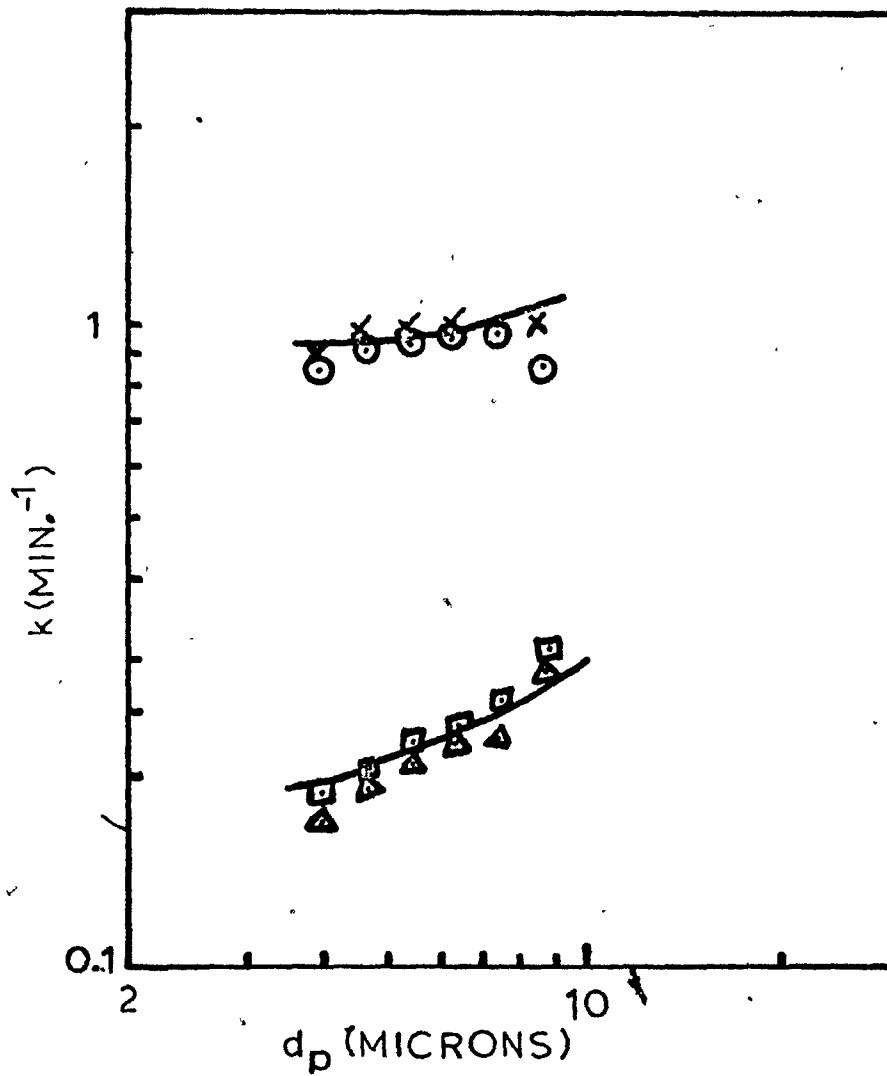
$$Z_p = + 10 \text{ mV}$$

$$Z_b = - 0.5 \text{ mV}$$

$D_b$ (microns)	$d_p$ (microns)	$E_1'$	$E_1^{e1}$	$E_1 (= E_1' - E_1^{e1})$
40	4	0.015	-0.225	0.240
40	6	0.034	-0.225	0.259
40	8	0.057	-0.225	0.282
70	4	0.005	-0.042	0.047
70	6	0.011	-0.042	0.053
70	8	0.019	-0.042	0.061

Figure 10.1

PRELIMINARY MODEL WITH ELECTRICAL ATTRACTION CORRECTION;  
COMPARISON OF PREDICTIONS WITH BATCH CELL SDB LATEX DATA



- ▲ L1
- ▣ L2
- ⊙ L3
- × L4

— Preliminary model corrected  
 for electrical attraction

In the case of latex particles the present model predicts a greater dependence of flotation rate on bubble size than does the preliminary model. With glass beads the predicted dependence is almost unchanged. Therefore, in this respect inclusion of electrical interactions does not improve matters because the preliminary model already slightly overestimates the effect of bubble size.

It would be interesting to reduce the zeta potential of the SDB latex particles to zero by adding electrolyte or a trace of an anionic surfactant and then to measure the variation of flotation rate with particle diameter. If the hypothesis of this chapter is correct a purely hydrodynamic model should apply in that situation and the slope of the  $\log k$  versus  $\log d_p$  curve should approach 1.9 (see Chapter 5).

Actually, we may have come close to doing this inadvertently. It was mentioned in Chapter 7, section 7.3 that the practice of filtering water through Millipore MF filters before making up the suspensions was stopped because unpredictable quantities of wetting agent leached out from the filters gave rise to unpredictable and irreproducible flotation results. The wetting agent is Triton X100 (octyl-phenoxy-polyethoxy-ethanol, manufactured by Rohm and Haas, Inc.). This material will compete strongly with the  $\text{EHDA}^+$  ions for space on the hydrocarbon surface of the latex particles. Any reduction in the number of  $\text{EHDA}^+$  ions adsorbed will result in a reduction of the positive charge on the particles. If the Triton X100 is adsorbed much more strongly than the  $\text{EHDA}^+$  ions and enough of it is present the charge on the particles could be reduced almost to

zero, with very little EHDA<sup>+</sup> being adsorbed other than that required to neutralise the original negative charge on the particles. With this picture in mind three features of the results obtained with filtered water can be explained on the basis of the electrical attraction hypothesis.

- (a) The unpredictability was only observed with SDB latex particles, never with glass beads. This is consistent with the glass beads being much larger and having a much smaller charge than latex particles so that electrical attraction plays only a very minor role.
- (b) The flotation rate of latex particles was usually much lower in filtered water than in unfiltered water.
- (c) The  $\log k$  versus  $\log d_p$  curves obtained with latex particles in filtered water and  $71\mu$  bubbles had slopes ranging from 0.7 to 1.4 (0.44 in unfiltered water).

These last two observations are consistent with electrical attraction playing a major role in latex flotation, the effect of the non-ionic wetting agent being to reduce the charge on the particles. Obviously, it would be desirable to repeat the experiments with a controlled reduction of the particles' zeta potential.

If the electrical attraction hypothesis is correct then in the absence of isopropanol the bubbles should be positively charged and should repel the latex particles quite strongly. It would be interesting to generate small bubbles electrolytically without the aid of isopropanol and see whether latex particles can still be floated.

Closure

In this chapter it has been proposed that if the preliminary model is corrected to allow for electrical attraction between particles and bubbles it will be possible to explain the main features of the flotation rate versus particle size curves obtained with both SDB latex and glass beads.

This concludes our attempts to find a model which fits the experimental data obtained using the batch cell. The next chapter returns to the question of the deviation of the drag on the particle from the steady state drag and its consequences for collision efficiency calculations.

11. A CRITERION FOR SAFE NEGLECT OF UNSTEADY STATE DRAG  
TERMS IN THE CALCULATION OF COLLISION EFFICIENCY

11.1 Introduction

This chapter refers to any particle collection system, not just the collection of small particles by small bubbles.

If the particle trajectory deviates from the fluid streamlines there is relative acceleration between the particle and the fluid as they approach the collector. If at any instant their relative velocity is  $\underline{u}_R$  the flow field around the particle, and hence the drag on the particle, is not the same as if the relative velocity was steady at  $\underline{u}_R$ . The drag can be regarded as the sum of the steady state drag force and an additional drag force arising from the relative acceleration (frequently called the unsteady state drag). Exact calculation of the latter is extremely difficult. When computing collision efficiencies the most common practice is to assume that it is small compared to the steady state drag and to insert only the steady state drag in the particle's equation of motion. The purpose of this chapter is to derive a criterion for assessing the merit of this approximation.

The criterion will be derived by estimating the relative magnitudes of the steady state and unsteady state drag terms, the basic assumption being that a large error in estimating the drag on the particle will lead to a large error in the collision efficiency. For simplicity a point replacement approach will be adopted and electrical interactions will be neglected.

11.2 Derivation of the Criterion

The velocity and acceleration of the particle relative to the fluid are not in the same direction, a situation which has not yet received satisfactory analysis in the theory of fluid-particle systems except for the special case of a particle moving in a circle (43). The best that can be done at present is to use Corrsin and Lumley's formulation of the Basset equation (88) with Odar's generalised coefficients (44). This formulation is a gross generalisation, representing a rather complicated field problem by a single integro-differential equation, but it has been justified a posteriori for rectilinear motion by the experiments of Clift, Adamji and Richards (94).

The total drag  $\underline{F}$  on the particle is the sum

$$\begin{aligned}
 \underline{F} = & \text{steady state drag } \underline{F}_{SS} \\
 & + \text{added mass drag } \underline{F}_{AM} \\
 & + \text{pressure gradient drag } \underline{F}_{PG} \\
 & + \text{history drag } \underline{F}_H \\
 = & -6\pi\mu_f r_p \underline{u}_R - \left[ c_A \cdot \frac{4\pi r_p^3}{3} \cdot \rho_f \frac{d\underline{u}_R}{dt} \right] \\
 & + \left[ \frac{4\pi r_p^3}{3} \cdot \rho_f \frac{d\underline{u}_f}{dt} \right] \\
 & - \left[ c_H \cdot r_p^2 \cdot (\pi\mu_f \rho_f)^{\frac{1}{2}} \int_0^t \left( \frac{d\underline{u}_R}{dt} \right)_{t-z} \frac{dz}{(t-z)^{\frac{3}{2}}} \right] \quad (11.1)
 \end{aligned}$$

- where
- $c_A$  = added mass coefficient,
  - $c_H$  = history coefficient,
  - $r_p$  = particle radius,
  - $\underline{u}_f$  = fluid velocity,

$\underline{u}_p$  = particle velocity,

$\underline{u}_R = \underline{u}_p - \underline{u}_f$ ,

$z$  = dummy variable (dimension = time)

$\rho_f$  = fluid density,

$\mu_f$  = fluid viscosity.

We have assumed that the particle Reynolds number  $Re_p = \frac{2 \rho_f |\underline{u}_R| r_p}{\mu_f}$  is small enough for  $\underline{F}_{SS}$  to be given by Stokes' Law. This is reasonable for most practical cases of collection of small particles. In most practical cases Stokes' Law will also apply at the particle's terminal falling velocity  $\underline{u}_{pt}$ . We can then write the particle's equation of motion as

$$\begin{aligned} \frac{4 \pi r_p^3 \rho_p}{3} \frac{d\underline{u}_p}{dt} &= \underline{F} + 6 \pi \mu_f r_p \underline{u}_{pt} \\ &= \underline{F}'_{SS} + \underline{F}_{AM} + \underline{F}_{PG} + \underline{F}_H \end{aligned} \quad (11.2)$$

where  $\rho_p$  = particle density

and  $\underline{F}'_{SS} = -6 \pi \mu_f r_p (\underline{u}_R - \underline{u}_{pt})$

and we have assumed gravity to be the only body force acting on the particle.

The physical significance of the added mass drag  $\underline{F}_{AM}$  is that the fluid surrounding the particle moves at a velocity between  $\underline{u}_p$  and  $\underline{u}_f$ . Therefore, when relative acceleration occurs the particle

must exert a force on this fluid to make it accelerate with the particle. The resulting reaction force gives an additional component of drag.

Since the velocity of the fluid varies around the collector, the fluid velocity  $u_f$  in the vicinity of the particle will change as the particle moves along its trajectory. Hence, there will be a pressure gradient in the fluid surrounding the particle and this will exert a force on the particle additional to that which would be exerted if  $u_f$  was constant along the trajectory. This is the origin of the pressure gradient drag.

The instantaneous drag is determined by the instantaneous flow field round the particle. If the fluid inertia is non-zero the flow takes a finite time to respond to changes in the particle's velocity. Hence, the instantaneous flow will be a function of the past history of the motion of the particle and will be influenced most strongly by the most recent history. This is the origin of the history drag term which includes the integral of past relative acceleration weighted by  $(t - z)^{-\frac{1}{2}}$ .

Let the reference velocity  $U$  be the velocity of the fluid relative to the collector at an infinite distance from the collector. Let the reference time be  $\frac{R_c}{U}$ , where  $R_c =$  collector radius. The dimensionless equation of motion is

$$\begin{aligned} \frac{du_p^*}{dt^*} = & - \frac{(u_R^* - u^*)}{St} - c_A \left(\frac{\rho_f}{\rho_p}\right) \frac{du_R^*}{dt^*} \\ & + \left(\frac{\rho_f}{\rho_p}\right) \frac{du_f^*}{dt^*} \\ & - c_H \cdot \left(\frac{1}{8\pi St}\right) \cdot \left(\frac{\rho_f}{\rho_p}\right)^{\frac{1}{2}} \int_0^{t^*} \left(\frac{du_R^*}{dt^*}\right) \frac{dz^*}{t^* - z^*} \quad (11.3) \end{aligned}$$

where  $\frac{u_R^*}{R_c} = \frac{u_R}{U}$ ,  $\frac{u_{pt}^*}{R_c} = \frac{u_{pt}}{U}$ ,  $\frac{u_f^*}{R_c} = \frac{u_f}{U}$ ,  $t^* = t U/R_c$ ,  $z^* = z U/R_c$

and  $St = \frac{2\rho_p U r^2}{9\mu_f R_c}$ . In the literature on particle collection St is referred to as the Stokes number, particle parameter or impaction parameter.

Since all the unsteady state terms are weighted by the density ratio  $\rho_f/\rho_p$  it is obvious that they will be much more important when the medium is water than when it is air. Also, inspection of equation 11.3 shows that relative to the steady state term they will be more important at high St than at low St.

Since  $\frac{u_f^*}{R_c} = \frac{u_R^*}{R_c} - \frac{u_{pt}^*}{R_c}$ , equation (11.3) may be rewritten:

$$\begin{aligned} \left(1 - \frac{\rho_f}{\rho_p}\right) \frac{du_{pt}^*}{dt^*} &= - \frac{(u_R^* - u_{pt}^*)}{St} \\ &- (c_A + 1) \left(\frac{\rho_f}{\rho_p}\right) \frac{du_R^*}{dt^*} \\ &- c_H \cdot \left(\frac{1}{8\pi St} \cdot \frac{\rho_f}{\rho_p}\right)^{\frac{1}{2}} \int_0^t \left(\frac{du_R^*}{dt^*}\right) \frac{dz^*}{t^* - z^* (t^* - z^*)^{\frac{1}{2}}} \end{aligned} \quad (11.4)$$

Most of the deviation from streamlines occurs within a distance  $R_c$  of the collector surface. Let  $t^* = 0$  when the particle enters this region. At this time  $\frac{u_R^*}{R_c} = 0$  ( $\frac{u_{pt}^*}{R_c}$ ). At time  $t^* = 0(1)$  the particle either collides with the collector or crosses the equatorial plane. Let  $\frac{u_R^*}{R_c} = \frac{u_R^*}{R_c}$  at this time. Let square brackets [ ] denote the average value over the interval  $t^* = 0$  to  $t^* = 1$  of the quantity inside the brackets. Since only orders of magnitude are being sought let equation 11.4 be rewritten in the following approximate form.

$$\begin{aligned}
 \left(1 - \frac{\rho_f}{\rho_p}\right) \left[\frac{du_p^*}{dt^*}\right] &= - \frac{[u_R^* - u_{pt}^*]}{St} \\
 &- (c_A + 1) \left(\frac{\rho_f}{\rho_p}\right) \left[\frac{du_R^*}{dt^*}\right] \\
 &- c_H \left(\frac{1}{8\pi St}\right) \cdot \left(\frac{\rho_f}{\rho_p}\right)^{\frac{1}{2}} [H]
 \end{aligned} \tag{11.5}$$

where 
$$\underline{H} = \int_0^{t^*} \left(\frac{du_R^*}{dt^*}\right)_{t^*=z^*} \cdot \frac{dz^*}{(t^*-z^*)^{\frac{1}{2}}}$$

Replacing the actual variation of  $u_R^*$  with  $t^*$  by a linear approximation in order to obtain orders of magnitude yields:

$$[u_R^* - u_{pt}^*] = 0 \left\{ \frac{1}{2}(u_R^{*1} - u_{pt}^*) \right\}$$

$$\left[\frac{du_R^*}{dt^*}\right] = 0 \cdot (u_R^{*1} - u_{pt}^*)$$

Ahmadi and Goldschmidt's theorem (40) states that the upper limit on the history integral H is given by:

$$\underline{H} \leq \frac{u_R^*(t^*) - u_R^*(0)}{\sqrt{t^*}}$$

$$[\underline{H}] \leq 0 \left\{ \frac{1}{2}(u_R^{*1} - u_{pt}^*) \right\}$$

Now we can compare the orders of magnitude of the three terms on the right hand side of equation 11.5. The first term represents the steady state drag. The second term can be neglected.

in comparison with it if  $2 \text{St}(c_A + 1) \left(\frac{\rho_f}{\rho_p}\right) \ll 1$  and the third term can be neglected if  $c_H \left(\frac{\text{St}}{8\pi} \frac{\rho_f}{\rho_p}\right)^{\frac{1}{2}} \ll 1$ . Clift, Adamji and Richards (94) show that when the particle's terminal Reynolds number is small, which is the case here, the appropriate values of  $c_A$  and  $c_H$  are the Bassett values  $c_A = 0.5$  and  $c_H = 6$ . Therefore, the second term can be neglected if  $\text{St} \left(\frac{\rho_f}{\rho_p}\right) \ll 0.33$  and the third term can be neglected if  $6 \left(\frac{\text{St}}{8\pi} \frac{\rho_f}{\rho_p}\right)^{\frac{1}{2}} \ll 1$  or  $\text{St} \left(\frac{\rho_f}{\rho_p}\right) \ll 0.70$ . Hence, both terms can be neglected if  $\text{St} \left(\frac{\rho_f}{\rho_p}\right) \ll 0.33$ , i.e. if  $\left(\frac{D}{R_c}\right)^2 \text{Re}_c \ll 9$  where the collector Reynolds number  $\text{Re}_c = \frac{\rho_f U_{R_c}}{\mu_f}$ .

The particle's equation of motion can then be written as:

$$\left(1 - \frac{\rho_f}{\rho_p}\right) \frac{du_p^*}{dt^*} = - \frac{(u_R^* - u_{pt}^*)}{\text{St}} \quad (11.6)$$

Only if  $\frac{\rho_f}{\rho_p} \ll 1$ , i.e. only if the medium is air, can the equation of motion be written in the conventional form:

$$\frac{du_p^*}{dt^*} = - \frac{(u_R^* - u_{pt}^*)}{\text{St}} \quad (11.7)$$

For the case of an aqueous medium let equation 11.6 be rewritten as:

$$\frac{u_p^*}{\rho_p} = \frac{u_f^*}{\rho_f} + \frac{u_{pt}^*}{\rho_p} - \text{St} \frac{du_p^*}{dt^*} \quad \text{St} \left(\frac{\rho_f}{\rho_p}\right) \frac{du_p^*}{dt^*} \quad (11.8)$$

At  $t^* = 0$ ,  $\frac{u_p^*}{\rho_p} \geq \frac{u_{pt}^*}{\rho_p}$ . At  $t^* = 1$ ,  $\frac{u_p^*}{\rho_p} \leq 1 + \frac{u_{pt}^*}{\rho_p}$ . Therefore,  $\left[\frac{du_p^*}{dt^*}\right] \leq 0(1)$ . In the vicinity of the collector the particle and fluid velocities will be a little less than the collector velocity (or

the free stream velocity if the collector is stationary) but will be of the same order of magnitude. Hence, as a rough approximation  $O(\underline{u}_p^*) = 1$  and  $O(\underline{u}_f^*) = 1$ . Hence if both  $St \ll 1$  and  $St(\frac{\rho_f}{\rho_p}) \ll 1$ ,  $\underline{u}_p^*$  can be obtained with negligible error from the quasi-equilibrium relationship:

$$\underline{u}_p^* = \underline{u}_f^* + \frac{u^*}{\tau_p t} \quad (11.9)$$

Usually, in an aqueous medium  $0.2 \leq \frac{\rho_f}{\rho_p} \leq 1.2$  (the upper limit corresponding to an oil drop), so both  $St \ll 1$  and  $St(\frac{\rho_f}{\rho_p}) \ll 1$  are satisfied if  $St(\frac{\rho_f}{\rho_p}) \ll 0.33$ .

To summarise, the criterion for safe neglect of the unsteady state drag terms is  $St(\frac{\rho_f}{\rho_p}) \ll 0.33$ . When the medium is air and the criterion is satisfied equation 11.7 can be used for the particle's equation of motion. When the medium is water and the criterion is satisfied the particle velocity can be obtained directly from equation 11.9. In the case of particles of diameter up to 20 microns colliding with bubbles of diameter up to 100 microns  $St$  is less than  $10^{-2}$  for reasonable values of  $\rho_p$ , so use of equation 11.9 is justified.

### 11.3 Computation of Collision Efficiency Including Unsteady State Drag Terms

The criterion was tested by writing a program to calculate collision efficiencies as a function of Stokes number both with and without the unsteady state drag terms. The collector was assumed to be an air bubble rising vertically.

The particle's equation of motion was written in the following form.

$$\begin{aligned}
 \frac{4\pi r_p^3 \rho_p}{3} \cdot \frac{du_p}{dt} &= 6\pi \mu_f r_p (u_p - u_f - u_{pt}) \\
 &- 0.5 \times \frac{4\pi r_p^3}{3} \cdot \rho_f \frac{d(u_p - u_f)}{dt} \\
 &+ \frac{4\pi r_p^3}{3} \rho_f \left( \frac{du_f}{dt} - \frac{\mu_f \nabla^2 u_f}{\rho_f} \right) \\
 &- 6r_p^3 (\pi \mu_f \rho_f)^{\frac{1}{2}} \int_0^t \left\{ \frac{d(u_p - u_f)}{dt} \right\}_{t=z} \frac{dz}{(t-z)^{\frac{1}{2}}}
 \end{aligned}
 \tag{11.10}$$

This is the same equation of motion as was used in the previous section except that:

- (a) the Bassett values 0.5 and 6 have been used for  $c_A$  and  $c_H$ ;
- (b) Corrsin and Lumley's correction to the pressure gradient term has been included (88).

Rearranging equation 11.10 and putting it in dimensionless form gives:

$$\begin{aligned}
 \frac{du_p^*}{dt^*} &= \left\{ - \frac{(u_p^* - u_f^* - u_{pt}^*)}{St} + 1.5 \cdot \left( \frac{\rho_f}{\rho_p} \right) \frac{du_f^*}{dt^*} \right. \\
 &- \frac{2(r_p/R_b)^2}{9 St} \cdot \nabla^2 u_f^* \\
 &\left. - 6 \left( \frac{1}{8\pi St} \cdot \left( \frac{\rho_f}{\rho_p} \right)^{\frac{1}{2}} \right) \frac{H}{\rho_p} \right\} / \left( 1 + 0.5 \left( \frac{\rho_f}{\rho_p} \right) \right)
 \end{aligned}
 \tag{11.11}$$

where 
$$\underline{H} = \int_0^{t^*} \left\{ \frac{d(u_p^* - u_f^*)}{dt^*} \right\}_{t^*=z^*} \cdot \frac{dz^*}{(t^*-z^*)^2}$$

Since the fluid flow round the bubble is steady  $\frac{du_f^*}{dt^*}$  is just the convective acceleration  $u_p^* \frac{du_f^*}{dl^*}$  moving with the particle, where  $l^*$  is dimensionless distance along the particle's trajectory (reference length is bubble radius  $R_b$ ).

Each of the terms in equation 11.11 is now resolved into vertical and horizontal components with dimensionless vertical and horizontal coordinates  $x$  and  $y$  (reference length  $R_b$ ) defining the particle's position relative to the centre of the bubble.

The vertical component is:

$$\begin{aligned} \frac{du_{px}^*}{dt^*} = & \left\{ - \frac{(u_{px}^* - u_{fx}^* - u_{pt}^*)}{St} + 1.5 \left( \frac{\rho_f}{\rho_p} \right) u_{px}^* \frac{du_{fx}^*}{dx} \right. \\ & - \frac{2(r_p/R_b)^2}{9 St} \left( \frac{\partial^2 u_{fx}^*}{\partial x^2} + \frac{\partial^2 u_{fx}^*}{\partial y^2} \right) \\ & \left. - 1.20 \left( \frac{\rho_f/\rho_p}{St} \right) H_x \right\} / \left( 1 + 0.5 \frac{\rho_f}{\rho_p} \right) \end{aligned} \quad (11.12)$$

where 
$$H_x = \int_0^{t^*} \left\{ \frac{d(u_{px}^* - u_{fx}^*)}{dt^*} \right\}_{t^*=z^*} \cdot \frac{dz^*}{(t^*-z^*)^2}$$

The horizontal component is similar except that  $u_{pt}^*$  does not exist in the horizontal direction.

$$\begin{aligned} \frac{du_{py}^*}{dt^*} = & \left\{ - \frac{(u_{py}^* - u_{fy}^*)}{St} + 1.5 \left( \frac{\rho_f}{\rho_p} \right) u_{py}^* \frac{du_{fy}^*}{dy} \right. \\ & - \frac{2(r_p/R_b)^2}{9 St} \left( \frac{\partial^2 u_{fy}^*}{\partial y^2} + \frac{\partial^2 u_{fy}^*}{\partial x^2} \right) \\ & \left. - 1.20 \left( \frac{\rho_f/\rho_p}{St} \right) H_y \right\} / \left( 1 + 0.5 \frac{\rho_f}{\rho_p} \right) \end{aligned} \quad (11.13)$$

where 
$$H_y = \int_0^{t^*} \left\{ \frac{d(u_{py}^* - u_{fy}^*)}{dt^*} \right\}_{t^*=z^*} \cdot \frac{dz^*}{(t^* - z^*)^2}$$

The rate of change of particle position is given by:

$$\frac{dx}{dt} = u_{px}^* \tag{11.14}$$

$$\frac{dy}{dt} = u_{py}^* \tag{11.15}$$

The particle trajectory was computed by integrating equations 11.12 to 11.15 numerically using the fourth order Runge-Kutta-Merson technique (89) and starting from  $x = 30$ , i.e. with the particle centre initially 30 bubble radii upstream of the bubble centre. Increasing the initial  $x$  to 50 made less than 1% difference to the computed collision efficiencies.

The contributions of the history integral components  $H_x$  and  $H_y$  were approximated by sub-dividing the interval  $30 \geq x \geq 0$  into a series of sections of variable length  $\Delta x$ . When the particle has traversed  $N$  such sections let the time be  $t_N^*$ . In its previous motion suppose it completed the  $n$ th section ( $n \leq N$ ) at time  $t_n^*$  ( $t_n^* \leq t_N^*$ ). Then for the interval  $t^* = 0$  to  $t^* = t_N^*$  the integral in the  $x$  direction is approximated by the summation:

$$H_x = \sum_{z^*=0}^{t^*} \left\{ \left[ \frac{\Delta(u_{px}^* - u_{fx}^*)}{\Delta t^*} \right]_{t^*=z^*} \cdot \left[ \frac{\Delta z^*}{(t^* - z^*)^2} \right] \right\}$$

$$\begin{aligned}
 &= \sum_{n=2}^N \left\{ \left[ \frac{(u_{px}^* - u_{fx}^*)_n - (u_{px}^* - u_{fx}^*)_{n-1}}{t_n^* - t_{n-1}^*} \right] \left[ \frac{t_n^* + t_{n-1}^*}{(t_N^* - (t_n^* + t_{n-1}^*)/2)^{1/2}} \right] \right\} \\
 &= \sqrt{2} \sum_{n=2}^N \frac{(u_{Rx}^*)_n - (u_{Rx}^*)_{n-1}}{T_n} \quad (11.16)
 \end{aligned}$$

where  $(u_{Rx}^*)_n = (u_{px}^* - u_{fx}^*)$  at the end of the nth section

and  $T_n = (2 t_N^* - t_n^* - t_{n-1}^*)^{1/2}$ .

The value of  $H_x$  calculated using equation 11.16 at the end of the Nth section is then used as a constant throughout the (N+1)th section.

$H_y$  is calculated and used similarly.

The mechanics of the computation are simple. Four arrays are set up to hold values of  $(u_{Rx}^*)_n$ ,  $(u_{Ry}^*)_n$ ,  $t_n^*$  and  $T_n$ . At the end of a section the latest values of  $(u_{Rx}^*)_n$ ,  $(u_{Ry}^*)_n$  and  $t_n^*$  are placed in the nth position of their arrays; previous values occupy positions 1 to (n-1). This latest value of  $t_n^*$  is  $t_N^*$ . The entire  $T_n$  array is then recalculated using the new  $t_N^*$ , after which  $H_x$  and  $H_y$  are calculated.

Obviously, the values obtained for  $H_x$  and  $H_y$  become more accurate as  $\Delta x$  is made smaller. The following sequence was found to be adequate.

- (a) For  $30 \gg x \gg 3$  set  $\Delta x = x/2$ . In this region the relative acceleration is small so the sections can be large.
- (b) For  $3 > x \gg 0.25$  set  $\Delta x = x/8$ . The relative acceleration is greater as the particle approaches the bubble and the streamlines curve more sharply, so the sections must be smaller.

- (c) For  $0.25 > x \geq 0.025$  set  $\Delta x = x/4$ . The sections are still small because  $x$  is now small.
- (d) For  $x < 0.025$  set  $\Delta x = x$ . This has to be done eventually if  $x$  is to reach zero.

Halving the section lengths in sections (a), (b) and (c) made less than 1% difference to the computed collision efficiency.

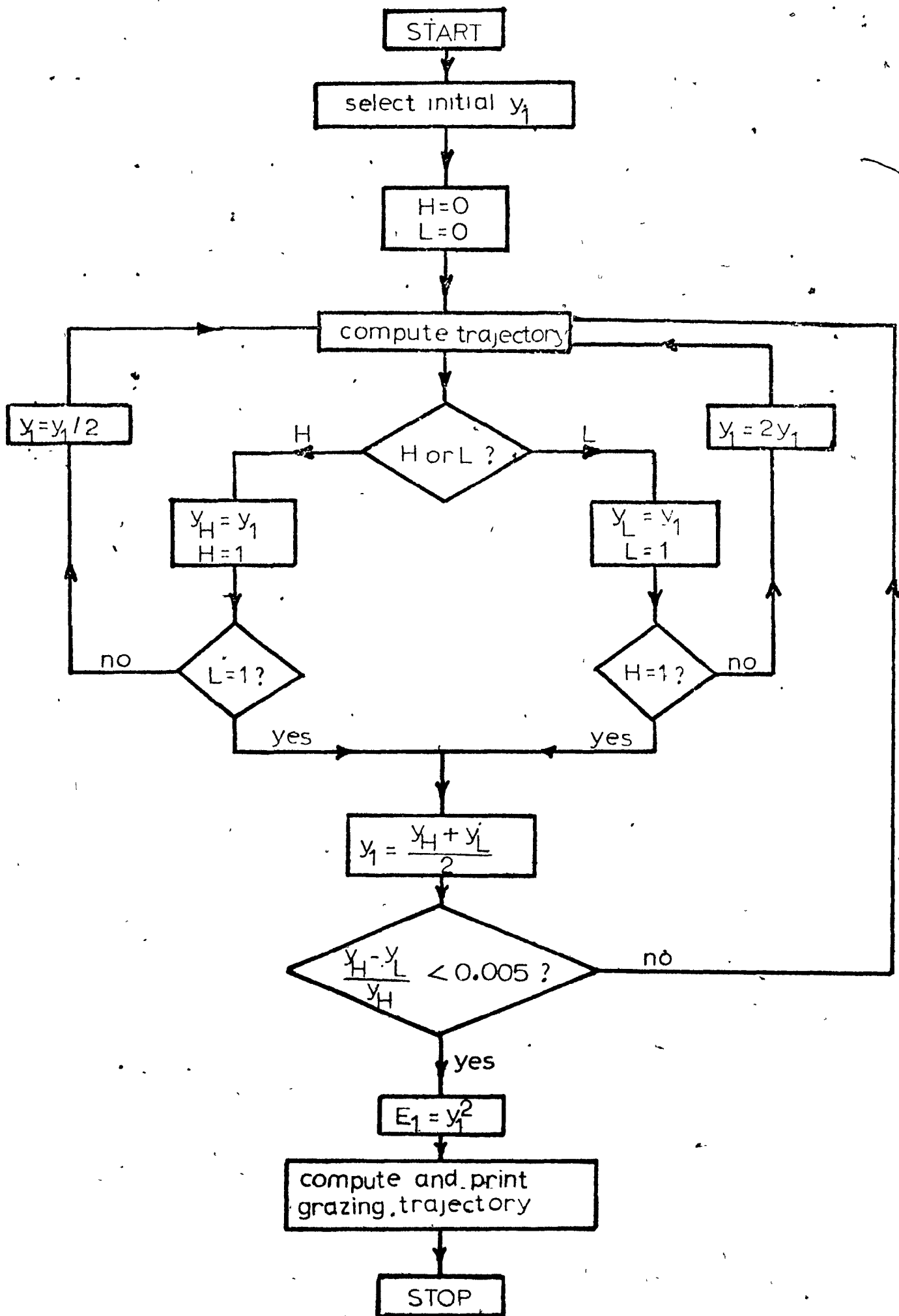
The initial value of the horizontal coordinate  $y$  (designated  $y_1$ ) was a guess for the first trajectory. The value  $y_{1G}$  giving a grazing trajectory was found by a dichotomous search technique. Then the collision efficiency  $E_1$  equals  $y_{1G}^2$ . The mechanics of the search technique are shown in Fig. 11.1.  $H$  denotes a trajectory whose  $y_1$  is too high, i.e. it reached  $x = 0$  (the equator) without the particle surface touching the bubble surface.  $L$  denotes a trajectory whose  $y_1$  is too low, i.e. the surfaces touched at  $x > 0$ . When the contents of the registers  $y_H$  and  $y_L$  differed by less than 0.5% their mean was taken to be  $y_{1G}$ . The collision efficiency had then been located with a precision of  $\pm 0.5\%$ . Usually, about ten trajectories had to be calculated before  $y_{1G}$  was found.

Expressions for the fluid velocities  $u_{fx}^*$  and  $u_{fy}^*$  for Stokes and potential flow together with their differentials are given in Appendix E. The complete program is documented in Appendix D2 together with a sample output.

The total computing time with the unsteady state drag terms included was very little greater than when they were omitted, so if the method outlined in this section is considered valid there seems to be little point in omitting them in future calculations.

Figure 11.1

SEARCH PROCEDURE FOR LOCATING GRAZING TRAJECTORY



#### 11.4 Testing of the Criterion

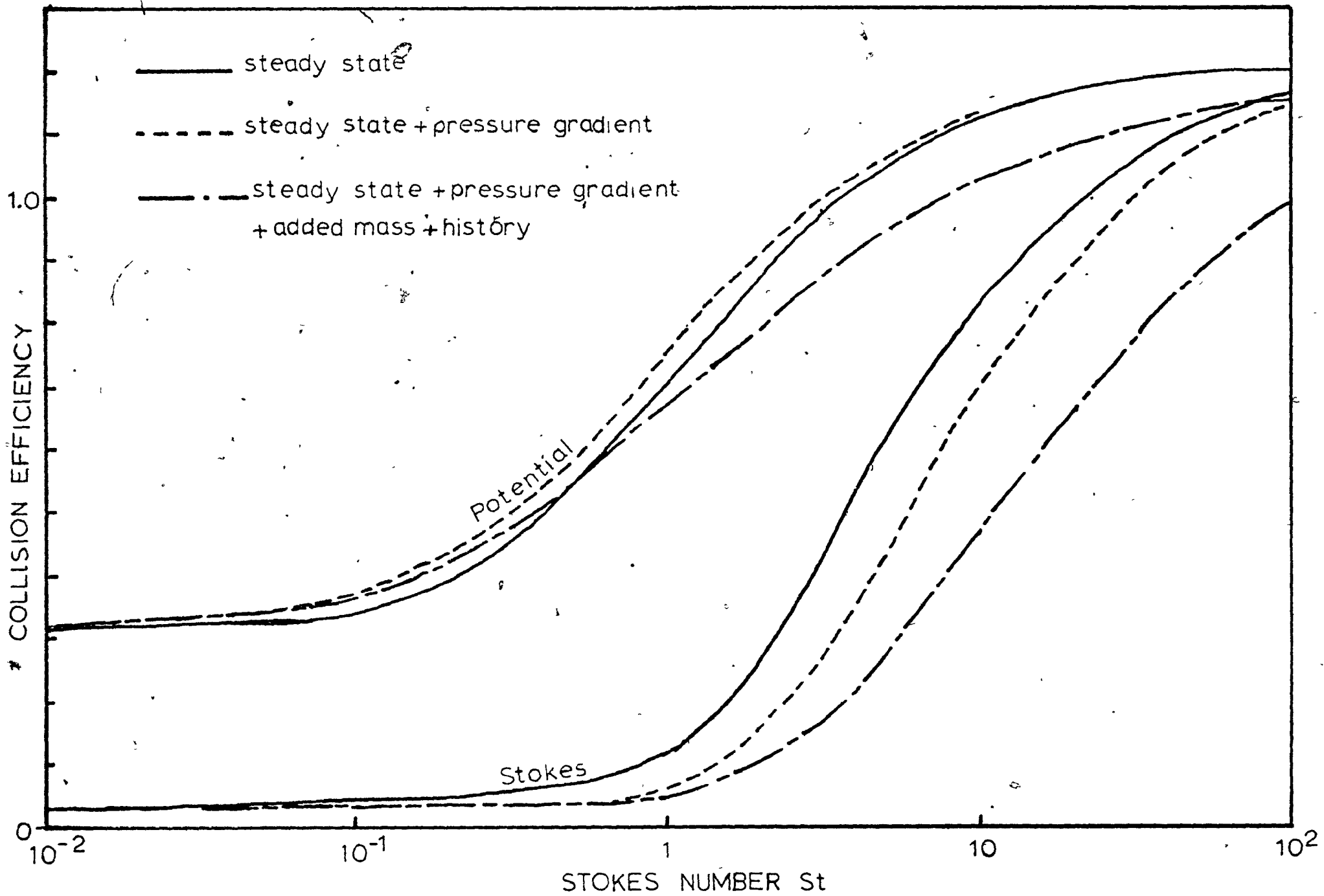
An option was provided in the program whereby the unsteady state drag terms could be either included or excluded. Collision efficiencies were calculated as a function of Stokes number  $St$  for both modes using a density ratio  $\rho_f/\rho_p$  of 0.4. This corresponds to glass beads or silica particles in water. For this density ratio the criterion  $St \left(\frac{\rho_f}{\rho_p}\right) \ll 0.33$  predicts that the unsteady state terms should be unimportant if  $St \ll 0.8$ . The radius ratio  $r_p/R_b$  was set arbitrarily at 0.1. Then with Stokes flow around the bubble  $u_{pt}^* = \left(\frac{\rho_p}{\rho_f} - 1\right) \left(\frac{r_p}{R_b}\right)^2 = 0.015$ . With potential flow  $u_{pt}^*$  was set arbitrarily at the same value.

Figure 11.2 shows the computed collision efficiencies for Stokes numbers from  $10^{-2}$  to  $10^2$ . With Stokes flow the unsteady state terms are seen to have a negligible effect below  $St = 0.1$ . Hence,  $St \ll 0.8$  is a valid criterion for their neglect. Above  $St = 0.8$  including the unsteady state terms reduces the computed collision efficiency by up to 60%. Below  $St = 0.1$  the collision efficiency is effectively constant at 0.033. This is the value obtained for  $r_p/R_b = 0.1$  and  $\rho_p/\rho_f = 2.5$  in Chapter 5 (Fig. 5.2) by neglecting particle inertia. Hence, the quasi-equilibrium assumption which is the basis of equations 5.3 and 11.9 is a good approximation when  $St \ll 0.1$ .

With potential flow the unsteady state terms have a much smaller effect than with Stokes flow. They never reduce the calculated collision efficiency by more than 10% and at low  $St$  they increase it slightly. Therefore, our criterion for their neglect is on the

Figure 11.2

COMPARISON OF COLLISION EFFICIENCIES WITH AND WITHOUT  
UNSTEADY STATE DRAG TERMS INCLUDED



conservative side. The reason for this is apparent if one examines the variation of excess pressure ( $P - P_\infty$ ) at the surface of a sphere with angle  $\theta$  from the nose of the sphere (Fig.11.3, taken from reference 60). In Stokes flow ( $P - P_\infty$ ) is always positive up to  $90^\circ$  so the pressure gradient always pushes the particle away from the sphere. In potential flow ( $P - P_\infty$ ) is negative for  $48^\circ < \theta < 90^\circ$ , so in the region which is most critical as far as the grazing trajectory is concerned the pressure gradient is pulling the particle in toward the bubble surface. Since the added mass and history terms always tend to reduce the collision efficiency by increasing the drag in the direction of fluid motion, this means that the pressure gradient term reinforces the latter two terms in Stokes flow but opposes them in potential flow. This is illustrated in Fig.11.2 where the ---- lines show collision efficiencies calculated with the pressure gradient term as the only unsteady state term.

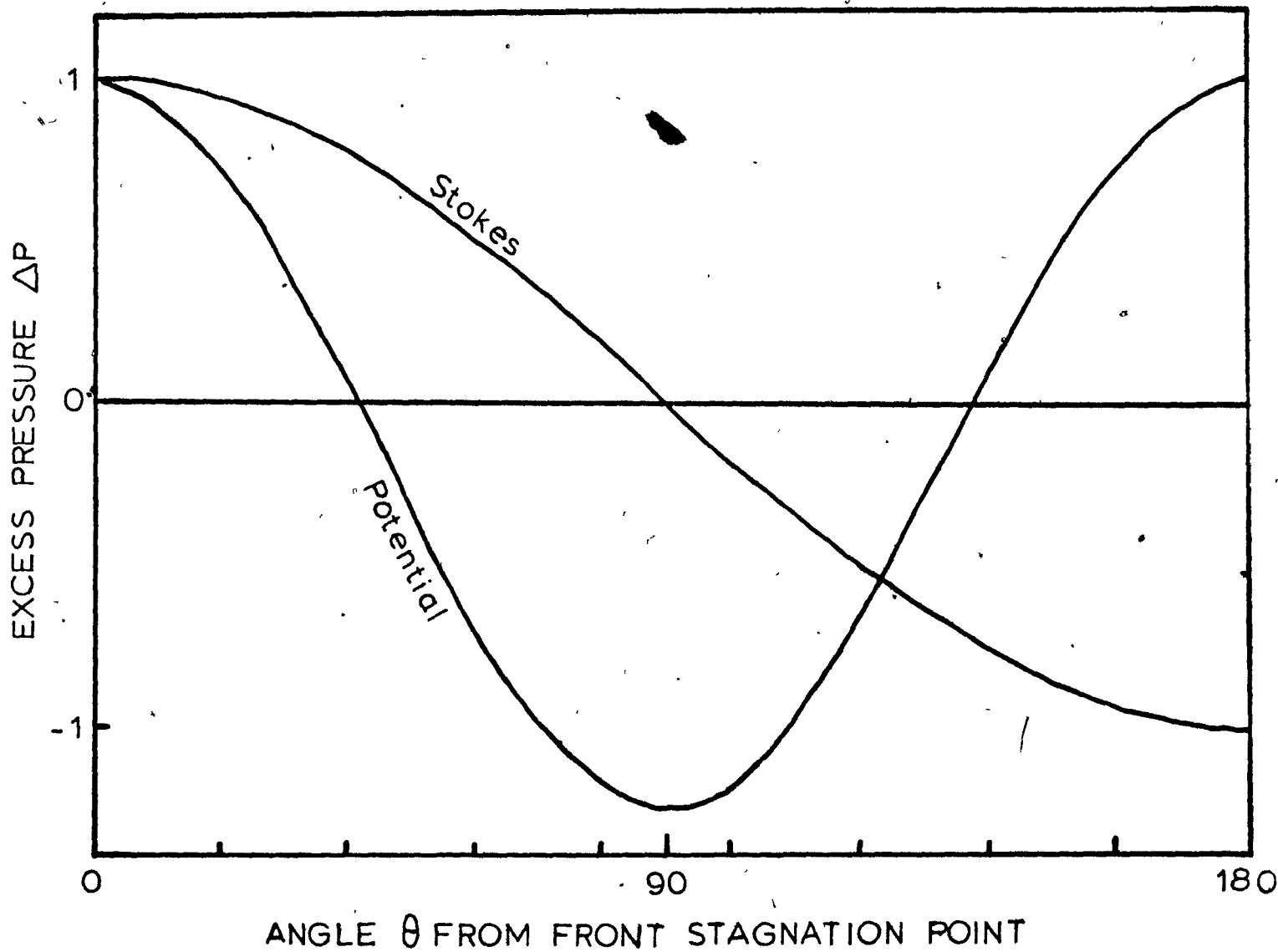
### 11.5 Closure

In this Chapter the criterion  $St(\rho_f/\rho_p) \ll 0.33$  has been developed for deciding under what circumstances unsteady state drag terms can be neglected when calculating collision efficiencies. Sample calculations for the case  $\rho_f/\rho_p = 0.4$  confirmed the validity of the criterion for Stokes flow round the collector but showed it to be conservative for potential flow. The quasi-equilibrium approximation was shown to be valid for  $St < 0.1$ .

The next chapter analyses the economics of removing fine particles from water by dispersed air flotation.

Figure 11.3

EXCESS PRESSURE AT THE SURFACE OF A SPHERE; COMPARISON  
OF STOKES AND POTENTIAL FLOW



Stokes flow:

$$\Delta P = \frac{P - P_{\infty}}{3\mu U}$$

Potential flow:

$$\Delta P = \frac{(P - P_{\infty}) d_p}{\frac{1}{2} \rho U^2}$$

## 12. ECONOMICS OF DISPERSED AIR FLOTATION

### 12.1 Introduction

This is not a detailed cost study. It is in the nature of a preliminary feasibility study such as would be performed early in a research project in order to select those areas in which effort should be concentrated. The cost data are very approximate at best and should only be taken as representing the order of magnitude of the costs involved. Conclusions will be based only on differences in orders of magnitude.

We begin by taking as a base case the well-established coagulation-sedimentation process for fine particle removal. The recently-commercialised Electroflotation process, in which small bubbles are generated electrolytically, is considered next. Finally, costs are estimated for flotation with bubbles generated at a porous distributor.

In all cases the design capacity of the unit is assumed to be one million U.S. gallons of effluent per day. This is the order of magnitude of the effluent from a small town or a medium-sized industrial unit (90). Other assumptions are:

- (a) construction in 1973;
- (b) annual capital charges are 15% of initial investment (7½% for capital recovery plus 7½% interest);
- (c) no profit required from a pollution control investment;
- (d) average throughput is 80% of design capacity;
- (e) fixed operating costs are the same for all cases.

## 12.2 Coagulation-sedimentation

The data source is Smith (91).

1967 capital cost = \$50,000.00. Assume 6% p.a. cost escalation between 1967 and 1973.

Then 1973 capital cost = \$70,000.00.

∴ Capital charges = \$10,500.00 p.a.

= 3.6 c/1000 USG.

The principal variable operating cost is the cost of the coagulating chemical, here assumed to be lime used at a dosage of 300 mg./l. and costing \$20/ton, i.e. 2.5 c/1000 USG of effluent.

Summary:	<u>c/1000 USG</u>
capital charges	3.6
chemicals	<u>2.5</u>
TOTAL:	6.1

Coagulation-sedimentation units usually only remove 85 to 90% of the incoming solids (90), so if greater purity is required a final polishing sand filter may be needed. This could add at least 50% to the capital charges. Coagulation-sedimentation works regardless of whether the particles are hydrophilic or hydrophobic.

## 12.3 Electroflotation

The data source is Kuhn (4,5). An example is quoted in which Electroflotation achieves 90 to 95% removal of solids and oil from steel rolling mill wastes. For a flow rate of 75 m<sup>3</sup>/hr. (475,000 USG/day) the cell volume is 25 m.<sup>3</sup> (6600 USG) and the power consumption

is 275 Wh per m.<sup>3</sup> treated (1.0 KWh per 1000 USG). Bubble diameters are said to be less than 100 microns (3).

Assume that cell volume required is proportional to volumetric feed rate. Then for 1 MG/day a cell of capacity 14,000 USG is needed. Since the cell operates at ambient pressure and temperature its cost (minus electrodes and skimmer) should be in the same region as that of a storage tank with the same capacity. Peters and Tarrerhaus (92) give a 1967 purchase cost of \$5000 for a 14,000 USG carbon steel storage tank. The recommended material of construction for Electroflotation cells is polyethylene or similar material. No cost data could be found for plastic tanks, but PVC piping is known to be about 20% more expensive than carbon steel piping (92). Applying the same differential to tanks and escalating to 1973 gives a cost of \$8400.

The electrodes corrode and foul and have to be replaced several times during the life of the plant so they are treated as a variable operating cost rather than a capital cost. The skimmer, which skins floated material off the top of the liquid, is a completely unknown quantity. As a pure guess its cost is put at 20% of the tank cost, giving a total equipment purchase cost of \$10,000. Instrumentation, piping, foundations, paint, power supply, construction expenses, engineering fees, contractor's profit, contingencies and working capital are accounted for by multiplying the purchase cost by a Lang factor of 5 (92) to give a total installed cost of \$50,000. The working capital allowance of 15% in the Lang factor can be taken in this case to apply to the initial pair of electrodes.

Hence, capital charges are \$7500 or 2.6 c/1000 USG, which is 40% less than for coagulation-sedimentation. If electricity is available at 1.5 c/KWh (92) the power cost is 1.5 c/1000 USG. Kuhn quotes an application involving the purification of paint-bearing water and states that the operating cost is "0.7 c/1000 gal., which includes the cost of chemical dosing agents and electrode replacement costs." In view of the stated power requirement Kuhn's operating cost must refer to a situation where the cost of electricity is abnormally low. It will be assumed here that the variable operating cost is 0.7 c/1000 USG plus the power cost, provided no surfactant is required. Since both oily iron dust particles and paint droplets are hydrophobic it is presumed that no surfactant is used in Kuhn's examples. The "chemical dosing agents" referred to are probably alkali to raise the conductivity of the water and possibly also a flocculant.

To summarise for situations where no surfactant is needed:

	<u>c/1000 USG</u>
capital charges	2.6
power	1.5
chemicals and electrodes	<u>0.7</u>
TOTAL:	4.8

Therefore, in these situations Electroflotation is at least competitive with coagulation-sedimentation and may be cheaper. It also offers the following benefits, which may often be important:

- (a) Greater % solids removal (90 to 95% versus 85 to 90%).
- (b) More compact.
- (c) No lime sludge.
- (d) Oxygenation of the waste stream by oxygen generated at one of the electrodes.

Unfortunately, the process becomes much too expensive if surfactant has to be added to make the particles stick to the bubbles. Almost all the laboratory studies on hydrophilic particles reported in Chapter 3 have used 20 to 40 ppm of surfactant to make the particles hydrophobic. Taking an average figure of 30 ppm (0.24 lb./1000 USG) and assuming a cationic surfactant costing typically 40 c/lb. the surfactant cost is 10 c/1000 USG. This triples the cost of the process and makes it much more expensive than coagulation-sedimentation.

It also creates a pollution problem since surfactants cause foaming on rivers and most authorities prohibit the discharge of waste streams containing more than 1 ppm of detergents (i.e. long-chain surfactants such as are used in flotation). Probably not more than one-third of the surfactant would be removed in the flotation cell (see Chapter 7, section 7.4.8), so the remaining 20 ppm would have to be removed by downstream processing. Removing it by foam fractionation or adsorption on activated carbon would at least double the cost of flotation (26). If the surfactant is biodegradable it could be removed by biological oxidation, but the 5-day B.O.D. of 20 ppm of surfactant is about 40 ppm and this could be a significant increment unless the effluent already has a very high B.O.D. A further drawback is that cationic surfactants are mild disinfectants and could have deleterious effects on the operation of biological

oxidation units.

The conclusion is that Electroflotation is only applicable when the particles stick to the bubbles without the aid of surfactants. Yet, one or two of the applications quoted by Kuhn refer to materials which one would expect to be hydrophilic, e.g. glass fibres and asbestos wastes.

#### 12.4 Flotation with Bubbles Generated at a Porous Distributor

The only way that commercially available porous frits can be used to generate bubbles as small as those generated in Electroflotation is to add 0.1 vol.% or more of ethanol or other short-chain alcohol to the water. This technique has been used by Rubin, Cassell, Pinfold, Sebba, Ratcliff and others (6,7,12-23,50,55,59) and was used in the batch cell experiments described in Chapter 7 of this thesis. However, while this technique may be very convenient in the laboratory it is a non-starter for large-scale applications. Ethanol costs about 30 c/USG, so at a 0.1 vol.% dosage the cost of generating small bubbles by this method would be 30 c/1000 USG. Furthermore, 1400 ppm would be added to the 5-day B.O.D.

Suppose that a fine (4-5.5 ) frit is used without either surfactant or alcohol. Our own visual observations in our batch cell suggest that at an air rate per unit frit area of about 0.3 ml. per min. per cm.<sup>2</sup> the bubble diameter is of the order of 0.5 mm. We now suppose that such a frit is installed in the Electroflotation cell of the previous section instead of the electrodes and we proceed

to estimate the air rate required to give the same performance as the bubbles which were generated electrolytically at the stated power consumption of 275 Wh/m.<sup>3</sup> (1.0 Kwh/1000 USC).

The power consumption of commercial water electrolysis units is about 150 kWh per 1000 SCF of H<sub>2</sub> (93). Assuming that hydrogen and oxygen are generated in the volumetric ratio 2:1 the rate of gas production is 1500 SCF per 150 kWh, i.e. 10 SCF per kWh. If the electrode efficiency of Electroflotation units is similar then their gas production is about 10 SCF per 1000 USG treated.

Suppose the size of the Electroflotation bubbles is of the same order as those in our batch cell runs G1 and G2 (average diameter 71 microns). Our electrolytically-generated bubbles in the cinéphotomicrography experiments were a little smaller (average diameter about 60 microns) but they came from a fine wire rather than a grid. Comparing our run G5 with runs G1 and G2 in Fig. 7.14 and correcting for the difference in air rates between runs we obtain for a constant air rate the ratio of flotation rate constants

$$\frac{k(0.5 \text{ mm.})}{k(71)} = \frac{0.05}{0.4} \times \frac{24}{43} = \frac{1}{14}$$

Hence, the air rate required to give the same performance is  $14 \times 10 = 140$  SCF/1000 USG. Given a cell height of 1 metre, which is what Kuhn recommends, the cell area is 25 m.<sup>2</sup> and the air rate per unit cell area is 0.4 ml. per min. per cm.<sup>2</sup>. This is similar to that used in our batch cell. A typical factory cost for filtered, dried 25 psig air is 10 c/1000 SCF (92), so the cost of generating bubbles in this

case is 1.4 c/1000 USG. This is similar to the cost of generating bubbles electrolytically for the same performance given a power cost of 1.5 c/kwh.

A likely reason for preferring the electrolytic method is that 0.5 mm. bubbles will arrive at the liquid surface with much more kinetic energy than the smaller electrolytic bubbles. In the absence of a stable froth this will cause much more re-dispersion of material which has been floated but not yet skimmed off.

The bubble diameter is reduced to 0.2 mm. in the presence of 38 ppm of the surfactant EHDA-Br (23) which would reduce the air consumption, but the arguments developed in the previous section against the use of surfactants at this sort of concentration apply here also.

### 12.5 Closure

In this chapter it has been shown that dispersed air flotation may be cheaper than coagulation-sedimentation if the particles are already hydrophobic. If the particles have to be made hydrophobic by adding 30 ppm of a surfactant the process becomes economically and environmentally undesirable.

In the next chapter a new process will be suggested which enables hydrophilic particles to be floated at surfactant concentrations below 1 ppm.

### 13. EFFERVESCENT FLOTATION

#### 13.1 Introduction

All laboratory studies to date on the removal of hydrophilic particles from water by dispersed air flotation have used surfactant concentrations of the order of 20 to 40 ppm. It was shown in the previous chapter that at these surfactant levels the process is more expensive than alternative particle removal processes and will probably require downstream processing to reduce the surfactant concentration to below 1 ppm before the waste stream can be discharged to the environment. And yet such a high concentration of surfactant is not necessary from an adsorption viewpoint. The data of Connor and Ottewill (56) on adsorption of cationic surfactants by polystyrene latex and of Jaycock and Ottewill (69) on adsorption of similar surfactants by silver bromide show that less than 1 ppm is enough to reduce the zeta potential of the particles to zero, at which point the particles would be hydrophobic enough to float. The real reason for using such high concentrations of surfactants is that they are essential if a stable froth is to be formed, and a stable froth is a very convenient way of collecting particles. In the experiments described in chapter 7 it was found that at an EHDA-Br concentration of  $0.25 \times 10^{-4}$  M ( $\approx 10$  ppm) the froth did not seem very stable. In the absence of isopropanol DeVivo and Karger (23) could not get a stable froth with EHDA-Br below  $10^{-4}$  M. Such high concentrations would not be needed if another way of collecting the floated particles could be devised.

Recent work in oceanography suggests a possible technique. Oceanographers have been interested for some time in the mechanism of formation of stable marine fogs. A favourite current theory is that when the sea is rough, waves crashing down on to the sea surface entrain millions of small air bubbles down to a depth of two or three feet. As they rise back up they pick up solid particles (dead plankton, mineral debris, etc.). The bubbles burst at the surface and eject these into the air where the wind catches them and evaporates the water. The atmosphere above the sea contains a lot of these particles and when conditions are ripe they act as nuclei for fog formation.

Wallace et al. (70) have shown that the low level of surfactant naturally present in sea water (much lower than 1 ppm) is sufficient to render floatable particles present in the water. (The surfactant comes from lysing of dead cells - in artificial sea water the particles didn't float.) We know from our cinéphotomicrography experiments (Chapter 6) that collected particles are swept round to the back of bubbles. MacIntyre (71) has shown by high-speed photography that when a bubble bursts at the surface of a liquid the liquid which was at the back of the drop is carried forward by its own momentum and is ejected into the air as a jet droplet. Because they come from the back of the bubble we would expect these droplets to be richer in particles than the underlying liquid. Blanchard and Syzdek (72) have measured the concentration of bacteria in jet drops and found it to be up to  $10^4$  times higher than the concentration in the bulk liquid. If a method can be devised for catching these drops

we have the particle collection technique we are looking for. We call it effervescent flotation.

### 13.2 Experiment

The batch cell with the medium frit was filled to  $\frac{1}{2}$  in. from the top with distilled water containing 70 mg./l. of SDB latex particles. Nitrogen was bubbled through at 41 ml./min. A piece of stiff absorbent paper was laid on top of the cell with a weight above it to keep it flat. 7 ml. samples were taken at eight-minute intervals and their total particle count measured on the Celloscope.

With no surfactant present there was no removal of particles. Particle removal began when 0.8 ppm of LHDA-Br was added. Figure 13.1 shows the rate of removal. 85% of the particles were removed in 53 minutes. The absorbent paper was changed at twenty minute intervals as by then it was very wet. The paper was blue, and after drying in an oven a white disc of collected latex particles was clearly visible. Figure 13.2 is a photograph of the first disc.

### 13.3 Discussion

85% removal in 53 minutes is as good a performance as most coagulation/sedimentation units achieve. The gas rate used was very low, and undoubtedly particle removal would be faster at higher gas rates. Compared to coagulation/sedimentation, effervescent flotation has the great advantage of giving aeration at the same time as particle removal. Compared to conventional dispersed air (froth) flotation the advantage of having less than 1 ppm of sur-

Figure 13.1

RATE OF REMOVAL OF SDB LATEX PARTICLES FROM WATER BY  
EFFERVESCENT FLOTATION

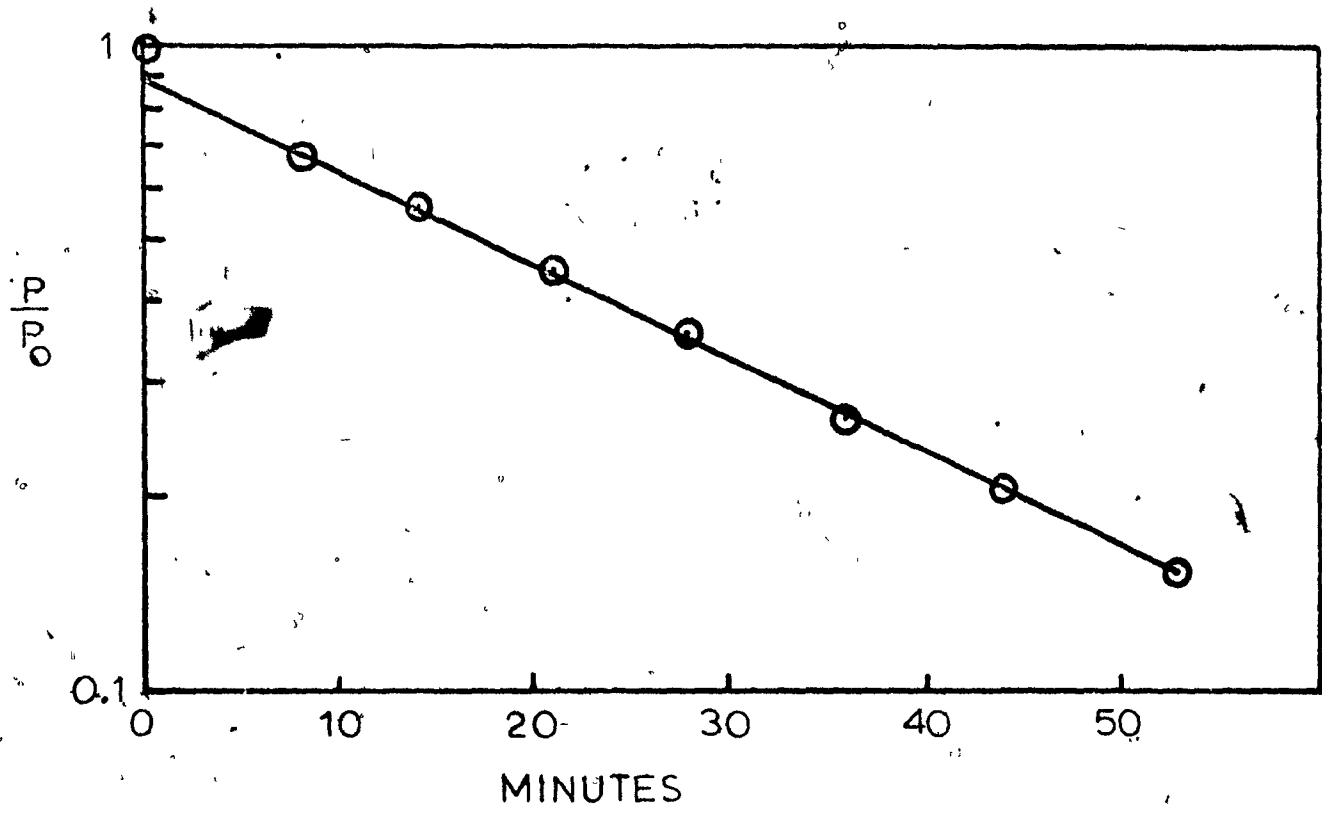


Figure 13.2

PARTICLES REMOVED BY EFFERVESCENT FLOTATION

- (A) NO SURFACTANT
- (B) 0.8 PPM OF EHDA-Br

a) No surfactant



b) 0.8ppm EHDA-Br



factant far outweighs any increased capital cost due to the longer residence time. At 0.8 ppm of a surfactant costing 40¢/lb., the chemical costs are 0.25¢/1000 USG, i.e. one-tenth those of coagulation-sedimentation.

Patents on the process have been applied for.

#### 13.4 Closure

In this chapter a novel process for removing fine hydrophilic particles from water has been described and shown to be feasible. It has several advantages over existing processes.

This concludes the description of work performed in this project. The next chapter collects together the main conclusions.

#### 14. CONCLUSIONS

When particles with diameters between 3 and 20 microns are floated by bubbles of diameter less than 100 microns the flotation rate always increases rapidly with decreasing bubble size. It may or may not increase rapidly with increasing particle size depending on the nature of the particles. The latter result cannot be explained by collision theories based purely on hydrodynamics which always predict a large dependence of flotation rate on particle size. It is speculated that when the particles are very small and possess an appreciable zeta potential electrical interactions between particles and bubbles become important and that this accounts for the observed variation in the effect of particle size.

Specifically, the main features of the experimental data on the flotation of glass beads and styrene divinylbenzene latex particles can be predicted by a collision model based on the following assumptions:

- (a) The bubble has a rigid surface and its motion is not affected either by the presence of the particle or by neighbouring bubbles. Consequently, the fluid flow round the bubble can be represented by Stokes flow.
- (b) Viscous resistance to thinning of the film of liquid between the surfaces of the particle and the bubble can be neglected.
- (c) As a consequence of (a) and (b), the particle can be regarded as a point mass when calculating its trajectory.

- (d) The inertia of the particle is negligible compared to the fluid drag force but the effect of gravity is not necessarily negligible.
- (e) The bubbles are negatively charged under the experimental conditions of the batch cell runs.
- (f) The attachment efficiency is independent of particle size and bubble size.

Models which ignore electrical effects but refine the hydrodynamic treatment by taking into account viscous resistance to film thinning, the effect of the particle on the flow field round the bubble and the effect of neighbouring bubbles on fluid streamlines are unable to explain the relatively small effect of particle size on flotation rate observed with styrene divinylbenzene latex particles. Experimental data on bubble zeta potentials is a pre-requisite to further progress in this area. An experimental study of the effect of particle zeta potential on the relation between flotation rate and particle size would also be very useful.

The criterion  $St(\rho_f/\rho_p) \ll 0.33$  appears to be valid for deciding whether unsteady state drag terms can be neglected without serious error when computing collision efficiencies. The effect of these terms is less for potential flow than for Stokes flow round

the collector because in the former case the pressure gradient opposes the other unsteady state terms whereas in the latter case they reinforce each other.

Dispersed air flotation may be a cheaper means of removing fine particles from water than coagulation-sedimentation if the particles in the feed are already hydrophobic. If 30 ppm of surfactant has to be added to the feed to make the particles hydrophobic and/or to provide a stable froth to retain them at the liquid surface the process is rendered undesirable on both economic and environmental grounds. With hydrophilic particles effervescent flotation, which requires less than one part per million of surfactant, appears to be much more attractive.

15. CLAIMS TO ORIGINAL WORK

1. Measurement of the effects of particle size and bubble size on the rate of flotation of fine particles by small bubbles with Reynolds numbers less than 0.5.
2. Development of a model which successfully predicts the main features of the experimental results.
3. Invention of the effervescent flotation process for removing fine hydrophilic particles from water by dispersed air flotation at a surfactant concentration below one part per million.
4. Development of a method for including the effect of unsteady state drag terms when computing collision efficiencies for Stokes or potential flow around the collector. Derivation of a simple criterion for predicting when such terms can be neglected without appreciable error.

16. SUGGESTIONS FOR FURTHER RESEARCH

1. Measurement of the rate of flotation of SDB latex particles as a function of particle size with the zeta potential of the particles reduced to zero by controlled addition of an electrolyte. If the slope of the  $\log k$  versus  $\log d_p$  curve approaches the predictions of a purely hydrodynamic model the electrical attraction hypothesis will be confirmed. This will be an important step forward in our understanding of fine particle flotation.
2. Development of a technique for measuring the zeta potentials of small bubbles in surfactant solutions. Experimental data in this area are a prerequisite to further progress in modelling the flotation of fine particles by small bubbles.
3. Development of the effervescent flotation process. The most immediate needs are:
  - (a) proving that it works on a variety of particulate materials;
  - (b) measuring the effect on process efficiency of collector height above the liquid surface; this will be related to bubble size and air rate;
  - (c) designing and testing a practical large-scale spray collection system.
4. Measurement of flotation rate as a function of particle size and bubble size for sub-micron particles. It may be found that in the model proposed in Chapter 5 the particle diffusivity calculated from the Stokes-Einstein formula will have to be modified to take electrical attraction into account.

can be floated purely by hydrodynamic capture; experimental studies aimed at discovering whether the flotation rate of hydrophobic particles is increased significantly given the physical conditions favouring hydrodynamic capture.

5. Measurement of flotation rate as a function of particle size and bubble size for sub-micron particles. It may be found that in the model proposed in Chapter 5 the particle diffusivity calculated from the Stokes-Einstein formula will have to be modified to take electrical attraction into account.

NOMENCLATURE

CHAPTER 2

D	diameter of sphere
Eo	Eotvos number
Re	Reynolds number
U	terminal velocity of sphere
$U_H$	terminal velocity according to Hadamard-Rybczinski equation
$U_{st}$	terminal velocity according to Stokes' Law
Y	$U/U_{st}$
$\gamma$	$M_1/\mu$
$\mu$	viscosity of medium
$M_1$	viscosity of drop
$\rho_1$	density of sphere
$\rho_2$	density of medium
$\Delta\rho$	$\rho_1 - \rho_2$
$\Delta\sigma$	difference in surface tension between front and rear stagnation points of a bubble
$\theta$	half angle subtended by mobile portion of bubble surface

CHAPTER 3

$d_p$	particle diameter
$D_b$	bubble diameter
G	volumetric gas flow rate
k	first order flotation rate constant
L	bubble path length

CHAPTER 4

A	Hamaker's constant
$D_b$	bubble diameter
E	collection efficiency
$E_1$	collision efficiency
$E_2$	attachment efficiency
m	particle mass
$r_p$	particle radius
$R_c$	collector radius
$r_p^*$	$r_p/R_c$
St	Stokes number
$t_c$	contact time
U	fluid velocity at infinity
$u_p^*$	dimensionless particle velocity (reference velocity U)
$u_f^*$	dimensionless fluid velocity (reference velocity U)
$u_{pt}^*$	dimensionless particle terminal velocity under gravity (reference velocity U)
$y_\infty$	distance of grazing trajectory from collector axis at infinity
$\gamma$	surface tension
$\delta$	double layer thickness
$\epsilon$	dielectric constant
$\lambda$	$1 + r_p^*$
$\mu$	fluid viscosity
$\rho_p$	particle density
$\theta$	angular coordinate
$\zeta$	particle zeta potential

## CHAPTER 5

$c_p$	number concentration of particles
$c_{ps}$	number concentration of unadsorbed particles in layer adjacent to bubble surface
$D$	particle diffusivity
$D_b$	bubble diameter
$E$	collection efficiency
$E_1$	collision efficiency
$E_2$	attachment efficiency
$f$	$(c_p - c_{ps})/c_p$
$g$	acceleration due to gravity
$k$	Boltzmann number
$k_p$	particle mass transfer coefficient
$K$	$1 + r_p/R_b$
$N$	flow of particles through volume swept out by bubble in unit time
$N'$	rate at which particles collide with the bubble
$N''$	net flow of particles to bubble surface in unit time
$Pe$	Peclet number
$r$	radial coordinate
$r_p$	particle radius
$r_p^*$	$r_p/R_b$
$R_b$	bubble radius
$Re_b$	bubble Reynolds number
$Sh$	Sherwood number
$St$	Stokes number
$t$	time

$t^*$	$U_b t / R_b$
$T$	absolute temperature
$u_p$	particle velocity relative to bubble
$u_f$	fluid velocity relative to bubble
$u_{pr}$	radial component of $u_p$
$u_{fr}$	radial component of $u_f$
$u_p^*$	$u_p / U_b$
$u_f^*$	$u_f / U_b$
$u_{pt}$	particle terminal falling velocity
$u_{pt}^*$	$u_{pt} / U_b$
$U_b$	bubble terminal rising velocity
$X$	$\mu_d / \mu_c$
$y_\infty$	distance of grazing trajectory from bubble axis at infinity
$\delta$	average thickness of concentration boundary layer
$\psi$	stream function
$\mu_c$	viscosity of continuous phase
$\mu_d$	viscosity of dispersed phase
$\mu_f$	fluid viscosity
$\rho_f$	fluid density
$\rho_p$	particle density
$\theta$	angular coordinate

CHAPTER 6

$b$	number of bubbles observed
$D_b$	bubble diameter
$E$	collection efficiency

$p_c$  number of particles collected  
 $p_s$  number of particles in suspension  
 $r_p$  particle radius  
 $X$  average number of particles per bubble per unit bubble cross-sectional area  
 $Y$   $p_c / p_s$

CHAPTER 7

$A_i$  area of section  $i$  under curve  
 $d_p$  particle diameter  
 $G$  (i) volumetric gas flow rate (section 7.4.7)  
(ii) amplifier gain (Table 7.3)  
 $h$  liquid height in cell  
 $I$  current  
 $k$  first order flotation rate constant  
 $n$  exponent in the relation  $E \propto 1/D_b^n$   
 $P$  particle concentration  
 $P_0$  initial particle concentration  
 $t$  time  
 $V$  sample volume

CHAPTER 8

Subscript 1 — larger sphere  
Subscript 2 — smaller sphere  
 $A_n$  parameter in approximation for  $k_n$   
 $b$   $U_{2T}/U_{1T}$

$B_n$	parameter in approximation for $k_n$
$C_n$	parameter in approximation for $k_n$
$d_p$	particle diameter
$D_b$	bubble diameter
$D_n$	parameter in approximation for $k_n$
$E_n$	parameter in approximation for $k_n$
$E_1$	collision efficiency
$f$	(drag component along line of centres) / $6\pi\mu R$
$g$	(drag component perpendicular to line of centres) / $6\pi\mu R$
$h$	(torque) / $8\pi\mu R^2$
$k_n$	$n$ th force coefficient ( $n = 1$ to $20$ )
$P$	pressure at surface of larger sphere
$P$	pressure at infinity
$R$	sphere radius
$R_b$	bubble radius
$S$	separation of sphere surfaces
$S_0$	value of $S$ at $\theta = \pi/2$
$t$	time
$u$	vertical velocity component
$U$	velocity component along line of centres
$U_T$	Stokes terminal velocity
$v$	horizontal velocity component
$V$	velocity component perpendicular to line of centres
$w$	angular velocity
$W$	$wR$
$x$	vertical coordinate of centre of sphere 2

$y$	horizontal coordinate of centre of sphere 2
$y_c$	horizontal distance from bubble axis at infinity of critical trajectory for hydrodynamic capture
$\mu$	fluid viscosity
$\rho$	density of sphere
$\rho_f$	fluid density
$\theta$	angular coordinate

CHAPTER 9

$b$	free surface radius
$E_1$	collision efficiency
$K$	$1 + r_p/R_b$
$r$	radial coordinate
$r_p$	particle radius
$R_b$	bubble radius
$U$	sphere velocity
$u_{fr}$	radial component of fluid velocity
$u_{pt}^*$	$u_{pt}/U$
$U_{pt}$	particle terminal velocity
$W$	$2 - 3\gamma + 3\gamma^5 - 2\gamma^6$
$\epsilon$	void fraction
$\gamma$	$\sqrt[3]{1 - \epsilon}$
$\rho_p$	particle density
$\theta$	angular coordinate
$\psi$	stream function
$\psi_{st}$	Stokes stream function for an isolated sphere

CHAPTER 10

$E_1$	collision efficiency
$E_1^{el}$	component of $E_1$ due to electrical interaction
$E_1'$	component of $E_1$ obtained by ignoring electrical interaction
$F$	repulsive force between particle and bubble
$Q_b$	charge on bubble
$Q_p$	charge on particle
$X$	$2 \epsilon_0 \beta Z_p Z_b / (3 \mu_f R_b)$
$Z_b$	bubble zeta potential
$Z_p$	particle zeta potential
$\beta$	dielectric constant
$\epsilon_0$	permittivity of free space.

Other symbols have the same meaning as in Chapter 5.

CHAPTER 11

	Subscript x — vertical component
	Subscript y — horizontal component
$c_A$	added mass coefficient
$c_H$	history coefficient
$F$	total drag on particle
$F_{ss}$	steady state drag
$F'_{ss}$	$F_{ss} + 6\pi\mu_f r_p u_{pt}$
$F_{AM}$	added mass drag
$F_H$	history drag
$F_{PG}$	pressure gradient drag
$H$	history integral

$n, N$	step numbers
$R_c$	collector radius
$t_n^*$	time at end of nth-step
$T_n$	$(2 \cdot t_n^* - t_n^* - t_{n-1}^*)^{\frac{1}{2}}$
$U$	fluid velocity at an infinite distance from the collector
$x$	vertical coordinate of particle centre
$y$	horizontal coordinate of particle centre
$y_1$	initial value of $y$
$y_{1G}$	value of $y_1$ giving a grazing trajectory
$z$	dummy variable (dimension time)
$z^*$	$z R_c / U$

Other symbols have the same meaning as in Chapter 5.

APPENDIX A

$a$	(i) area of slice through particle (section A.1) (ii) slope of calibration curve (section A.3)
$a'$	$a/3$ (section A.3)
$A$	orifice area
$b$	intercept of calibration curve
$b'$	$(b + \log(6/\pi))/3$
$C$	chart division
$C_L$	chart division corresponding to $V_L$
$C_S$	chart division corresponding to $V_S$
$d$	particle diameter
$D$	orifice diameter
$G$	amplifier gain
$G_r$	value of $G$ at which calibration was performed

I	current
$I_r$	value of I at which calibration was performed
k	$1 - \rho_o/\rho_p$
N	number of particles per ml.
$r_o$	orifice radius
$r_p$	particle radius
V	particle volume
$V_L$	volume of larger reference particle
$V_S$	volume of smaller reference particle.
x	distance of slice from centre of particle
$\alpha$	$r_p/r_o$
$\rho_o$	resistivity of electrolyte solution
$\rho_p$	resistivity of particle

APPENDIX B

Symbols have the same meaning as in Chapter 7.

APPENDIX C

$\Delta_n$	parameter in Pshenay-Severin equations,
$x_n$	parameter in Pshenay-Severin equations
$\alpha$	parameter in Pshenay-Severin equations
$\beta$	parameter in Pshenay-Severin equations

Other symbols have the same meaning as in Chapter 8.

APPENDIX E

Symbols have the same meaning as in Chapter 11.

REFERENCES

1. Beychuk, M.R., "Aqueous Wastes from Petroleum and Petrochemical Plants", John Wiley and Sons (1967)
2. Eckenfelder, W.W., "Industrial Water Pollution Control", McGraw-Hill (1966)
3. Fillooi, P., Chem. Eng. 75 (16), 82 (1968)
4. Kuhn, A.T., Chemistry and Industry, 21 August 1971, p. 946
5. Kuhn, A.T., in "Electrochemistry of a Cleaner Environment" ed. Lockris, J. O'M., Plenum Press (1972)
6. Kalpan, K.S. and Ratcliff, G.A., Can. J. Chem. Eng. 49, 626 (1971)
7. Kalpan, K.S., Ph.D. Thesis, Department of Chemical Engineering, McGill University, Montreal (1970)
8. Lemlich, R., "Adsorptive Bubble Separation Techniques", Academic Press (1971)
9. Karger, B.L. and De Vivo, D.G., Sep. Sci. 3 (5), 393 (1968)
10. Somasundaran, P., Sep. Purif. Methods 1, (1), 117 (1972)
11. Karger, B.L., Grieves, R.B., Lemlich, R., Rubin, A.J. and Sebba, F., Sep. Sci. 2, 401 (1967)
12. Rubin, A.J., J. Amer. Water Works Assoc. 60, 832 (1968)
13. Sebba, F., "Ion Flotation", Elsevier (1962)
14. Cassell, E.A., Matijevic, E., Mangravite, F.J. Jr., Buzzell, T.M. and Blabac, S.B., A.I.Ch.E.J. 17 (6), 1486 (1971)
15. Rubin, A.J., Cassell, E.A., Henderson, O., Johnson, J.D. and Lamb, J.C. III, Biotechnol Bioeng. 8, 135 (1966)
16. Rubin, A.J., Biotechnol Bioeng. 10, 89 (1968)
17. Rubin, A.J. and Lackey, S.C., J. Amer. Water Works Assoc. 60, 1156 (1968)
18. Mahne, E.J. and Pinfold, T.A., J. Appl. Chem. 18, 52 (1968)
19. Mahne, E.J. and Pinfold, T.A., J. Appl. Chem. 18, 140 (1968)
20. Sheiham, I. and Pinfold, T.A., J. Appl. Chem. 18, 217 (1968)

21. Mahne, E.J. and Pinfold, T.A., J. Appl. Chem. 19, 57 (1969)
22. Pinfold, T.A. and Mahne, E.J., J. Appl. Chem. 19, 188 (1969)
23. De Vivo, D.G. and Karger, B.L., Sep. Sci. 5, 145 (1970)
24. Bhattacharyya, D., Romans, J.D. and Grieves, R.B., A.I.Ch.E.J. 18 (5), 1024 (1972)
25. Bhattacharyya, D. and Grieves, R.B., A.I.Ch.E.J. 18 (1), 200 (1972)
26. Grieves, R.B. and Bewley, J.L., Can. J. Chem. Eng. 50, 261 (1972)
27. Grieves, R.B., Malone, D.F. and Bewley, J.L. Water Research 6, 145 (1972)
28. Bhattacharyya, D., Carlton, J.A. and Grieves, R.B., A.I.Ch.E.J. 17 (2), 419 (1971)
29. Grieves, R.B. and Lee, R.W., Ind. Eng. Chem. Proc. Des. and Dev. 10 (3), 390 (1971)
30. Grieves, R.B., Ogbu, I.U., Bhattacharyya, D. and Conger, W.L., Sep. Sci. 5 (5), 583 (1970)
31. Grieves, R.B., Conger, W.L. and Malone, D.P., J. Amer. Water Works Assoc. 62 (5), 304 (1970)
32. Gaudin, A.M., "Flotation", 2nd ed., McGraw-Hill (1957)
33. Morris, T.M., Trans. A.I.M.E., 193, 794 (1952)
34. Bushell, C.M.G., Trans A.I.M.E., 223, 266 (1962)
35. Tomlinson, H.S. and Fleming, M.G. in "Mineral Processing", ed. A. Roberts, Pergamon Press (1963)
36. Gaudin, A.M., Schuhmann, R. Jr. and Schlechten, A.W., J. Phys. Chem., 46, 902 (1942)
37. Suwanasing, P., M. Eng. Thesis, Dept. of Metallurgical Engineering, McGill University, Montreal (1970)
38. Klassen, V.I. and Mokrousov, V.A., "An Introduction to the Theory of Flotation", Butterworths, London (1963)
39. Goldsmith, H.L., 4th European Conf. on Microcirculation, Biblio. Pheca, Anat., 9, 259 (1967)
40. Ahmadi, G. and Goldschmidt, V.W., J. Appl. Mech, p. 561, June 1971.

41. Yag, K.-M., Habibian, M.T. and O'Melia, C.R., *Envir. Sci. Tech.*, 5, 1105 (1971)
42. Flint, L.R. and Howarth, W.J., *Chem. Eng. Sci.* 26, 1155 (1971)
43. Odar, F., *J. Appl. Mech. (ASME Ser. E)*, 90, 652 (1968)
44. Odar, F. and Hamilton, W.S., *J. Fluid Mech.* 18, 302 (1964)
45. Richardson, E.G., (editor), "Aerodynamic Capture of Particles", Pergamon Press (1960)
46. Friedlander, S.K., *J. Colloid Interf. Sci.*, 23, 157 (1967)
47. Michael, D.H. and Norey, P.W., *J. Fluid Mech.*, 37, 565 (1969)
48. Whelan, P.E. and Brown, D.J., *Trans. I.M.M.* 65, 181 (1956)
49. Levich, V.G., "Physicochemical Hydrodynamics", Prentice-Hall, (1962)
50. Fung, D.T.-F., M. Eng. Thesis, Dept. of Chemical Engineering, McGill University (1972)
51. Savic, P., National Research Council of Canada Report No. MF-22, July 1953
52. Davis, R.E. and Acrivos, A., *Chem. Eng. Sci.* 21, 681 (1966)
53. Wace, P.F. Alder, P.J. and Banfield, D.L., *Chem. Eng. Progr. Symp. Ser.*, 65, No. 91, 19 (1969).
54. Brodkey, R.S., "The Phenomena of Fluid Motions", Addison-Wesley (1967)
55. Kaufman, K.M., M. Eng. Thesis, Dept. of Civil Engineering, Clarkson College of Technology (1972)
56. Connor, P., and Ottewill, R.H., *J. Colloid Interf. Sci.* 37, 642 (1971)
57. Happel, J., *A.I.Ch.E.J.*, 4, 197 (1958)
58. Zieminski, S.A. and Whittemore, R.C., *Chem. Eng. Sci.* 26, 509 (1971)
59. Zieminski, S.A., Caron, M.M. and Blackmore, R.B., *Ind. Eng. Chem. Fund.*, 6, 233 (1967)
60. Clift, R., Grace, J.R. and Weber, M.E., "Bubbles, Drops and Particles", to be published by Academic Press (1974)

61. Bond, W.N. and Newton, D.A., Philosophical Magazine, Ser. 7, vol. 5, p. 794 (1928)
62. Schulman, J.H. and Rideal, E.K., Proc. Roy. Soc. (London) B122, 29, 46 (1937).
63. Hocking, L.M. and Jonas, P.R., Quart. J.R. Met. Soc. 96, 722 (1970)
64. Pshenay-Severin, S.V., Bull. (Izv.) Acad. Sci. U.S.S.R., Geophysics Ser. (English translation), 10, 724 (1958)
65. Davis, H.H., Chem. Eng. Sci., 24, 1769 (1969)
66. O'Neill, M.E. and Majumdar, S.R., ZAMP. 21, 164 (1970)
67. Evans, L.F., Ind. Eng. Chem., 46, 2420 (1954)
68. Pfeffer, R., Ind. Eng. Chem. Fund., 3 (4), 380 (1964)
69. Jaycock, M.J. and Ottewill, R.H., Trans. I.M.M., 72, 497 (1963)
70. Wallace, G.T. Jr., Loeb, G.I. and Wilson, D.F., J. Geophys. Res., 77, 5293 (1972)
71. MacIntyre, F., J. Geophys. Res., 77, 5211 (1972)
72. Blanchard, D.C. and Syzdek, L.D., J. Geophys. Res. 77, 5087 (1972)
73. Kruyt, H.R., "Colloid Science, vol. 1", Elsevier (1952)
74. Derjaguin, B. and Dukhin, S.S., Trans. I.M.M., 70, 221 (1960)
75. Herne, H., pp. 26-34 in "Aerodynamic Capture of Particles", ed. Richardson, E.G., Pergamon Press (1960)
76. Langmuir, I., J. Met. 5 (5), 175 (1948)
77. Philippoff, W., Trans. Amer. Inst. Min. (Metall.) Engrs., 193, 386 (1952)
78. Shafrir, V. and Gal-Chen, T., J. Atmos. Sci. 28, 741 (1971)
79. Zebel, G., J. Colloid Interf. Sci. 27, 294 (1968)
80. Pich, J., in "Aerosol Science", ed. Davies, C.N., Academic Press (1966)
81. Davies, J.T. and Rideal, E.K., "Interfacial Phenomena", 2nd ed., Academic Press (1963)
82. Ison, C.R. and Ives, K.J., Chem. Eng. Sci. 24, 717 (1969)

83. Spielman, L.A. and Goren, S.L., *Envir. Sci. Tech.* 4, 135 (1970).
85. Dorman, R.G. in "Aerosol Science", ed. Davies, C.N., Academic Press (1966).
86. Cockson, J.T., *Envir. Sci. Tech.* 4, 128 (1970).
87. Riddick, T.M. and Ravina, L.A., *Ind. Eng. Chem.* 62, (7), 70 (1970).
88. Corrsin, S. and Lurley, J.L., *Appl. Sci. Res.* 6A, 114 (1956).
89. Lance, G.N., "Numerical Methods for High-Speed Computers", p.56, Iliffe and Sons Ltd., London (1960).
90. McGahay, P.H., "Engineering Management of Water Quality", McGraw-Hill (1968).
91. Smith, R., *Journal WPCF*, 40, 1546 (1968).
92. Peters, M.S. and Timmerhaus, K.D., "Plant Design and Economics for Chemical Engineers", McGraw-Hill (2nd Ed., 1968).
93. Gregory, D.P., Ng, D.Y.C. and Long, G.M. in "Electrochemistry of Cleaner Environments", ed. Bockris, J. O'M., Plenum Press (1972).
94. Clift, R., Adamji, F.A. and Richards, W.D., *Int. Conf. on Particle Technology*, IIT Research Institute, Chicago (1973).
95. Batch, B.A., *J. Inst. Fuel*, p.455, October 1964.
96. Mattern, C.F.T., Brackett, F.S. and Olson, B.J., *J. Appl. Physiology* 10 (1), Jan. 1957.
97. Chatfield, C., "Statistics for Technology", Penguin (1970).
98. Usui, S., in "Progress in Surface and Membrane Science, Vol.5", ed. Danielli, J.F., Rosenberg, M.D. and Cadenhead, D.A., Academic Press (1972).

A. CELLOSCOPE PARTICLE COUNTER

The Celloscope Model IIIIS particle counter is made by Particle Data Inc., Elmhurst, Illinois.

A.1 The Basic Principle

Consider a cylindrical orifice of radius  $r_o$  and area  $A$  filled with electrolyte solution of resistivity  $\rho_o$  and containing a particle of radius  $r_p$  and resistivity  $\rho_p$  (Fig.A.1). Consider a slice of thickness  $dx$  perpendicular to the orifice axis and cutting the particle at a distance  $x$  from its centre. This element of the particle has an area  $a$  and a resistance in the direction of the

orifice equal to  $\frac{\rho_p dx}{\pi(r_p^2 - x^2)} = \frac{\rho_p dx}{a}$ . The resistance of the annulus

of electrolyte solution is  $\frac{\rho_o dx}{\pi[r_o^2 - (r_p^2 - x^2)]} = \frac{\rho_o dx}{A - a}$ . The total resistance across the element is:

$$dR = \frac{\rho_o \rho_p dx}{a \rho_o + \rho(A-a)}$$

$$= \frac{\rho_o dx}{A - a k} \text{ where } k = 1 - \rho_o / \rho_p.$$

The increase in the resistance of the element due to the particle

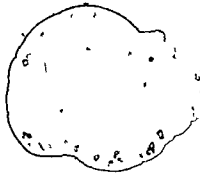
$$\text{is } d(\Delta R) = \frac{\rho_o dx}{A - a k} - \frac{\rho_o dx}{A}$$

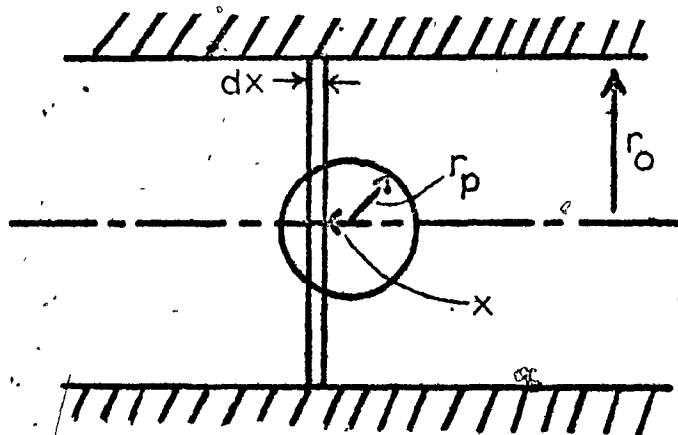
$$\frac{k \rho_o a dx}{A^2 (1 - ka/A)}$$

Integrating over the particle gives the total increase in resistance as:

Figure A.1

PARTICLE IN ORIFICE





$$\begin{aligned}
 \Delta R &= \frac{2k\rho_o}{A^2} \int_0^{r_p} \frac{\pi(r_p^2 - x^2) dx}{1 - k\pi(r_p^2 - x^2)/A} \\
 &= \frac{2k\rho_o}{A^2} \int_0^{r_p} \left[ \pi(r_p^2 - x^2) + \frac{k\pi^2}{A} (r_p^2 - x^2)^2 \dots \right] dx \\
 &= \frac{4k\pi r_p^3 \rho_o}{3A^2} \left[ 1 + \frac{4k\pi r_p^2}{5A} + \frac{24k^2\pi^3 r_p^4}{35A^2} \dots \right] \\
 &= \frac{k\rho_o v}{A^2} \left[ 1 + \frac{4}{5} k\alpha^2 + \frac{24}{35} k^2\alpha^4 \dots \right] \tag{A1}
 \end{aligned}$$

where  $v$  is the volume of the particle and  $\alpha$  is the ratio of particle radius  $r_p$  to orifice radius  $r_o$ . Hence, if  $\alpha$  is small the increase in resistance when a particle enters the orifice is proportional to the particle volume. Batch (95) has derived similar expressions for cylindrical and conical particles. In practice, the particles always behave as if they are non-conducting even if they are metallic, presumably because of a large interfacial resistance to electron transfer, so  $k$  is always unity. Therefore, the relation between  $R$  and  $v$  is linear to within 10% if  $\alpha < 0.35$ .

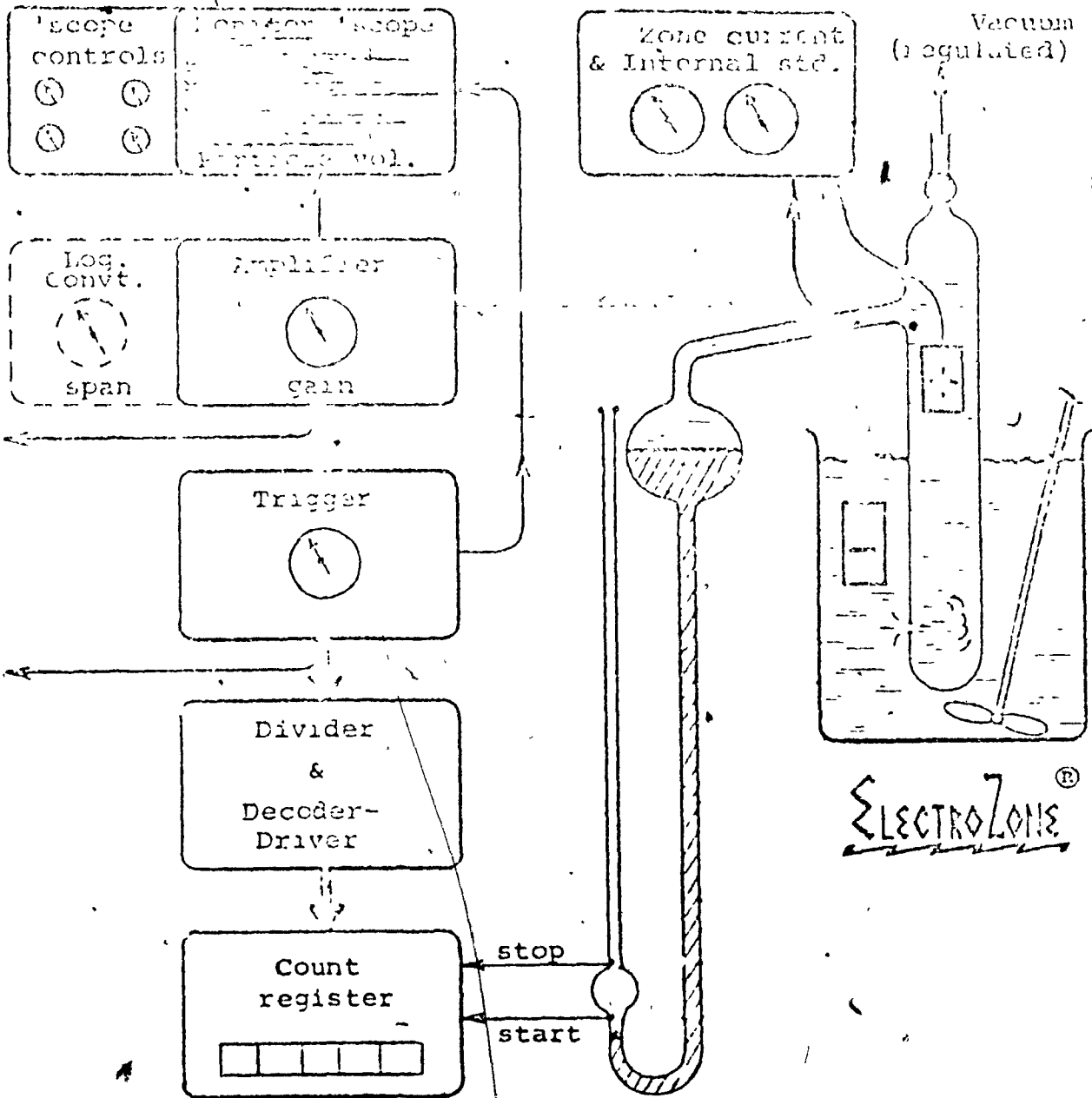
## A.2 The Instrument

Fig.A2 (adapted from the Particle Data instruction manual) is a basic schematic of the instrument. The heart of the instrument is a glass tube with a small jewel set in its wall. Through the jewel is drilled a tiny orifice of accurately controlled diameter. In the present work tubes with orifices of diameter 24, 76 and 300 microns were used. The tube is immersed in a beaker of electrolyte

Figure A.2  
CELLOSCOPE PARTICLE COUNTER; BASIC SCHEMATIC



BASIC SCHEMATIC



Functional sequence diagram of essentials of ElectroZone/Celoscope<sup>®</sup> general instrument, all models (see text on next page).

\* Outputs for multi-channel size distribution analyzers, particle data accumulation, computer processing, etc.

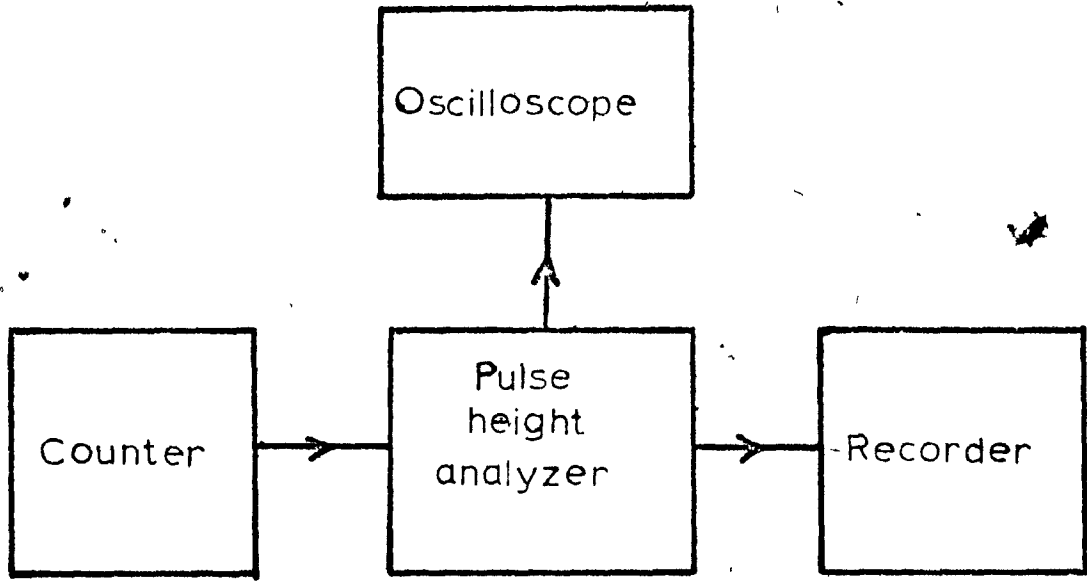
solution (0.5% sodium chloride solution in the present work) containing the particles in suspension. One electrode is located inside the tube and the other in the beaker. A vacuum pump sucks electrolyte solution through the orifice. When a particle passes through the orifice the resistance between the electrodes changes according to equation A1 and a voltage pulse proportional to the volume of the particle is generated. This pulse is amplified and sent either to an external pulse height analyzer or to a gate circuit. The pulses may be generated at the rate of several hundred per second depending on the concentration of the suspension.

Fig.A3 shows the counter in relation to the ancillary instruments. The pulse height analyzer is a Nuclear Data Model ND110 identical to those used in radiochemical work except that its input circuitry has been modified by Particle Data to handle the longer rise time of the signals produced by the counter. The ND-110 sorts the incoming signals into 128 channels according to pulse height (i.e. particle volume) so that in its memory a particle volume frequency distribution curve is built up. The build-up of the curve is followed on the X-Y oscilloscope (Telequipment Model S51B). When sufficient particles have been sized the curve is plotted by a Dohrmann SY-850 recorder. In the size distribution curves produced in the present work full scale represents 1000 particles per channel.

The orifice tube is connected to a U-tube containing mercury. When the vacuum is applied the mercury is in the position shown in Fig.A2. When the vacuum is shut off the mercury rises up the left leg of the U-tube. Suspension is still being sucked through the

Figure A.3

CELLOSCOPE PARTICLE COUNTER; ANCILLARY INSTRUMENTS



→ Data flow

orifice, the volume sucked through being equal to the volume swept out by the rising mercury meniscus. Meanwhile, amplified pulses have been entering the gate circuit where they are compared with a variable reference voltage whose magnitude is set by an external trigger dial. When the mercury meniscus reaches the start contact the count register starts counting all the pulses larger than the reference voltage. Counting stops when the meniscus reaches the stop contact. The accumulated count, displayed on electronic glow numerals, is the total number of particles larger than the size corresponding to the reference voltage which are contained in a volume of suspension equal to the volume between the start and stop contacts. This volume is known accurately. Hence, if the reference voltage is set at a level high enough to screen out noise but low enough for the smallest particles in the suspension to be counted the total concentration of particles in the suspension can be measured. Since we already have the size distribution curve the concentration of particles in any size range is readily obtained.

The left leg of the U-tube is called the volumetric section. These are available with various sizes of bulb between the start and stop contacts. To keep counting times reasonably short smaller bulbs are used in conjunction with smaller orifices. In the present work a 16 microlitre volumetric section was used with the 24 micron orifice, a 320 microlitre section with the 76 micron orifice and a 5 ml. section with the 300 micron orifice. Counting times were of the order of 15 to 20 seconds.

The two principal operating controls are the current  $I$  supplied to the electrodes (which are held at a p.d. of about 200 volts) and the gain  $G$  of the amplifier. The height of the output signal is proportional to the product  $IG$ .  $I$  can be varied over a 128:1 range and  $G$  over a 48:1 range. The larger values of  $IG$  are used with particles whose diameters are very small compared to the orifice diameter and which consequently give relatively weak signals. The manufacturer claims that particles with diameters as small as 2% of the orifice diameter can be detected, but in practice we found 5% to be the limit; the pulses from smaller particles could not be distinguished from background noise.

The output signal may be in the range 0 to 8 volts. Larger signals are truncated. The output signals may be observed as horizontal lines on a small monitor oscilloscope built into the instrument (see Fig.A2). The length of the line is proportional to the pulse height with the right hand side of the screen corresponding to 8 volts. The current  $I$  and gain  $G$  are adjusted until settings are found at which the pulses from the largest particles of interest are just inside the 8 volt cut-off. Fine tuning of the current is available.

There is an alternate output mode in which, after leaving the amplifier, the output signals are attenuated so as to be proportional to the logarithm of the particle volume instead of linearly related to the volume. This is extremely useful since most particle size distributions follow a log-normal rather than a normal distribution curve. The proportionality constant can be varied by means

of a selector switch in order to obtain 4, 6, 8, 10, 12 or 14 doublings of particle volume over the full 0 to 8 volts range. In practice the usefulness of the higher settings is undermined by a serious increase in the noise level. All work on the present project was carried out with the log selector switch at setting 6, i.e. 6 doublings of particle volume or a 4:1 diameter ratio over full scale.

Fig.A4, taken from the Particle Data instruction manual, shows an over-all view of the instrument.

### A.3 Calibration

Details will only be presented here for calibration with the logarithmic output mode since the linear mode was not used in the present work.

Two samples of fairly mono-disperse particles are required. Their sizes should be different but close enough together so that at a single GI value both peaks are below the 8 volts cut-off but above the noise level. Let the volume of the larger particles at the peak of their distribution curve be  $V_L$  and that of the smaller particles  $V_S$ .

With the recorder chart drive on High setting 8 volts corresponds to 84 chart divisions counting horizontally along the chart paper. Let the peak of the curve obtained with the larger particles be at chart division  $C_L$  and that of the smaller particles be at  $C_S$ . The relation between  $\log V$  and  $C$  is linear as shown in Fig.A5.

Figure A.4  
CELLOSCOPE PARTICLE COUNTER; EXTERNAL VIEW

# CELLOSCOPE®

Particle Data, Inc.  
Elmhurst, Illinois

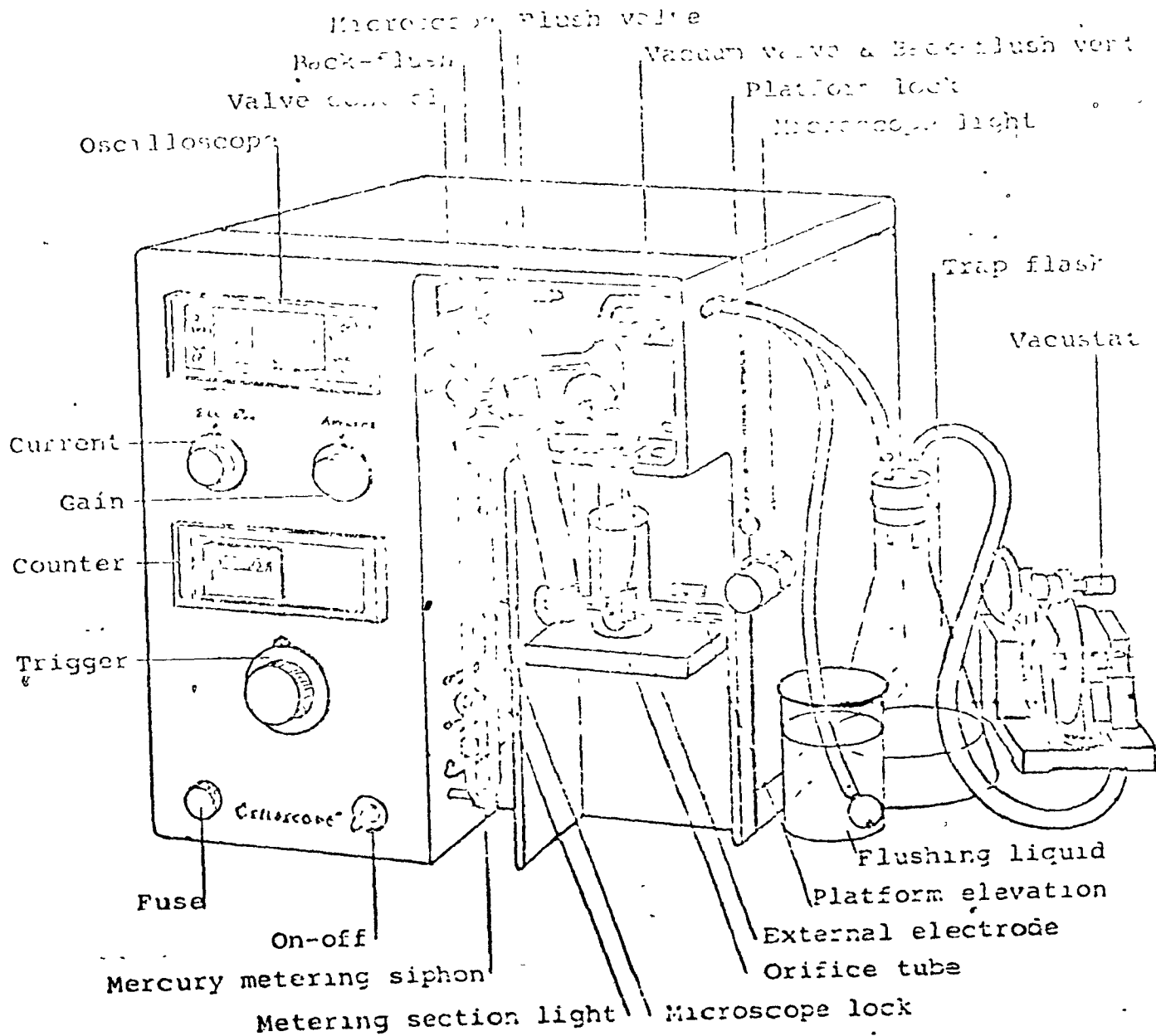


Figure A.5

CELLOSCOPE PARTICLE COUNTER; LOG V VERSUS C

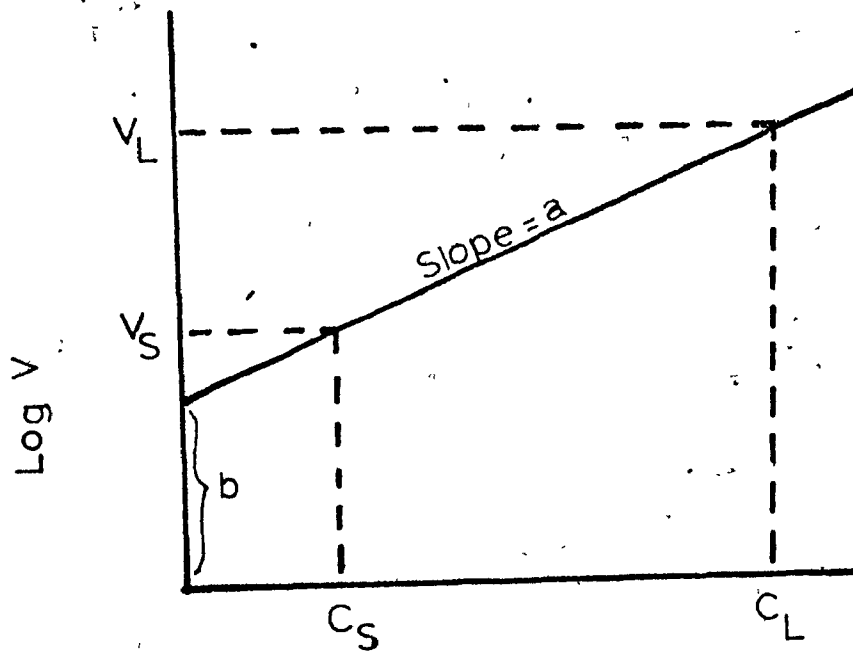


Chart division C

$$\log V = b + a C$$

or

$$\log d = b' + a' C$$

where  $d =$  particle diameter

$$a' = a/3$$

$$b' = (b + \log(6/\pi))/3.$$

The slope  $a$  is given by

$$a = \frac{\log V_L - \log V_S}{C_L - C_S} = \frac{\log(V_L/V_S)}{C_L - C_S}$$

and the intercept  $b$  is given by

$$b = \log V_L - a C_L.$$

Hence,  $a'$  and  $b'$  can be found.

Let  $G I_{r r}$  be the reference value of GI at which the calibration has been made. Suppose that at this setting a particle of volume  $V_r$  generates a pulse which, after amplification and attenuation shows up at position  $C$  on the recorder chart.

Then  $b + a C = \log V_r.$

Let the current and/or the gain be altered to give a new value of

GI. Position  $C$  will now be occupied by pulses coming from particles of volume  $V = V_r \times \frac{G I_{r r}}{G I}$ .

$$b + a C = \log\left(\frac{V \frac{GI}{r r}}{\frac{GI}{r r}}\right)$$

$$\text{or } V = \frac{\frac{GI}{r r}}{\frac{GI}{r r}} \text{ antilog } (b + a C)$$

$$\text{or } d = 3 \sqrt{\frac{\frac{GI}{r r}}{\frac{GI}{r r}}} \text{ antilog } (b' + a' C)$$

This is the calibration equation.

The particles used for calibrating the three orifices used in this work were as follows.

24  $\mu$  orifice:

- (a) polystyrene latex particles of mean diameter 1.01  $\mu$ .
- (b) Polystyrene latex particles of mean diameter 1.95  $\mu$ .

76  $\mu$  orifice:

- (a) paper mulberry pollen particles of mean diameter 16.0  $\mu$ ;
- (b) ragweed pollen particles of mean diameter 18.35  $\mu$ .

300  $\mu$  orifice:

- (a) pecan pollen particles of mean diameter 42.2  $\mu$ .
- (b) corn pollen particles of mean diameter 88.5  $\mu$ .

The latex particles were obtained from Dow Chemical Co., Diagnostic Products Division, Indianapolis. Their mean diameter had been measured by the manufacturer using an electron microscope. The pollen particles were obtained from Greer Chemical Co., Allergy Division, Lenoir, North Carolina. To obtain their mean diameters

samples were suspended in water containing  $10^{-4}$  M EHDA-Br and 0.5 vol.% IPA. A few drops were placed on a microscope slide and photographed through a microscope. About 300 particles of each pollen were photographed. A scale was also photographed. The particle diameters on the photographs were measured with calipers and converted to microns by comparison with the scale.

The calibration equations obtained were as follows.

24 $\mu$  orifice:

$$d = \sqrt[3]{\frac{48}{GI}} \text{ antilog } (0.00635 C - 0.114).$$

76 $\mu$  orifice:

$$d = \sqrt[3]{\frac{1.5}{GI}} \text{ antilog } (0.00727 C + 0.773)$$

300 $\mu$  orifice:

$$d = \sqrt[3]{\frac{1.06}{GI}} \text{ antilog } (0.0137 C + 1.414)$$

These calibrations all refer to the log 6 setting. The 24 $\mu$  and 76 $\mu$  calibrations were obtained using 0.5% sodium chloride solution as the electrolyte and the 300 $\mu$  calibration was obtained using 0.1% sodium chloride solution. They are valid only for the electrolyte strengths at which they were obtained.

The 24 $\mu$  calibration predicted the 5.7 $\mu$  peak of the styrene-divinylbenzene particles accurately and the 76 $\mu$  calibration predicted the 22 $\mu$  cut-off point of the glass beads accurately.

A.4 Particle Coincidence

If at any time the orifice contains more than one particle a spuriously high pulse will be generated. Simultaneously, if the count register is activated a spuriously low count will be accumulated. Obviously the probability of this occurring will be larger the larger the orifice and the higher the particle concentration. A measure of the seriousness of this effect is the per cent coincidence loss, defined as the percentage by which the actual count is below the true count due to coincident passage of particles through the orifice. Mattern et al. (96) showed that the arrival of particles at the orifice could be represented by a Poisson distribution and derived the formula:

$$\% \text{ coincidence loss} = 0.13 ND^3$$

where  $N$  = number of particles per ml.

and  $D$  = orifice diameter (mm.).

For the three orifices used in the present project the particle concentrations at which the coincidence loss reaches 1% are as follows.

24 $\mu$	560,000/ml.
76 $\mu$	17,500/ml.
300 $\mu$	286/ml.

In the batch cell runs described in Chapter 7 the maximum count obtained when using the 24 $\mu$  orifice was of the order of 1000 SDB latex particles per 16 microlitres, i.e. 62,500/ml., so distortion of the results due to particle coincidence was negligible. When using the 76 $\mu$  orifice the maximum count was of the order of 2000 per 320 microlitres, i.e. 6,250/ml., so again coincidence effects were negligible. However, when attempting to measure bubble sizes with the 300 $\mu$  orifice the counts obtained were of the order of 70,000 to 100,000 per 5 ml., so there must always have been several bubbles in the orifice simultaneously. Under such conditions measurement of the bubble size distributions was impossible and all that could be inferred was a crude indication of relative bubble sizes under various conditions.

#### A.5 Operating Precautions

The resistivity of common electrolyte solutions such as 0.5% sodium chloride in water changes by about 1% per  $^{\circ}$ F at room temperature. To preserve constant resistivity the instrument was located in a room whose temperature was maintained at 72 $^{\circ}$ F.

The particles are kept in suspension during analysis by means of a variable-speed stirrer. It was found important not to have the stirring too vigorous as air bubbles would then be precipitated out from the water and counted as particles. For the same reason, dilution of samples and pouring of diluted samples into the analysis beaker had to be done very gently.

The orifice had to be watched constantly through the microscope during the course of an analysis. If any debris or clumps of

particles were seen to block or partially cover the orifice the vacuum had to be shut off immediately and a back pressure applied by pushing in the back-flush plunger (Fig.A4). Usually, this was sufficient to clear the blockage. If it failed the next recourse was to gently scrape the orifice entrance with the tip of a plastic dropper. Metal or glass points could not be used as these might scratch the orifice. The last resort was to remove the orifice tube from the counter, fill it with water or acetone and force a small cork into the top entrance. Under no circumstances could the tube be immersed in an ultrasonic bath as this would fracture the tube at the point where the orifice was set into it.

Orifice blockages due to stray debris were minimised by keeping all flasks stoppered when not in use and all beakers covered with PVC film. The only particles which showed a tendency to form clumps were the paper mulberry pollen particles.

#### A.6 Repeatability of Counts

One hundred repeat counts were taken with a suspension of glass beads, the  $76\mu$  orifice and the 320 microlitre volumetric section. The standard deviation  $\sigma$  was 2.1% of the arithmetic mean  $\mu$ . The ratio of mean deviation to standard deviation was 0.79. The theoretical ratio for a normal distribution is 0.80, so it was concluded that the counts were distributed normally.

Let the above 100 counts be regarded as a population. Suppose a sample of  $n$  counts is taken and has mean  $\bar{x}$ . The standard deviation  $\sigma_m$  of the sample mean  $\bar{x}$  is expected to be  $(2.1/\sqrt{n})\%$  of

the true mean  $\mu$ . Specifically, if  $n = 5$ ,  $\sigma_m$  is expected to be 0.94% of  $\mu$ . Then we have 68% probability that the true mean  $\mu$  is within  $\pm 1\%$  of  $\bar{x}$  and 95% probability that  $\mu$  is within  $\pm 2\%$  of  $\bar{x}$ .

In the experiments described in Chapter 7 all particle concentration measurements were based on an average of five repeated counts.

#### A.7 Time Required for Analysis

A single count took 15 to 20 seconds.

When building up the size distribution curves the pulse height analyser was set so that for individual channels full scale was 1000 pulses. Therefore, when the peak of the curve was approaching the top of the oscilloscope screen almost 1000 pulses had been accumulated in the most highly populated channel. Given a total of 128 channels and the fairly spread-out nature of the glass bead and SDB latex size distributions this meant that something like 40,000 particles had been measured. Analysis was stopped just before the peak reached full scale. It took from two to fifteen minutes to reach this stage depending on the particle concentration in the sample. Samples from later in the flotation runs were larger than those taken earlier and were diluted less to ensure that curve build-up was not excessively slow.

B. SAMPLE RUN (G2)

10 - 15 $\mu$  frit.

Glass beads in 10<sup>-4</sup> M EHDA-Br + 0.5 vol.% IPA

pH = 6.0.

Stirrer speed = 165 rpm.

N<sub>2</sub> flow rate = 24 ml./min.

Eight samples of volume V ml. taken at one minute intervals, each diluted with 40 ml. of 1% NaCl and (40-V) ml. of water.

76 $\mu$  orifice, 320 $\mu^l$  volumetric section.

I =  $\frac{1}{4}$ , G<sub>2</sub> = 6 $\frac{1}{4}$ , output mode = log 6.

Trigger setting = 11.5% of full scale.

Background count C<sub>B</sub> = 15.

$$\text{Total particle concentration } P = \frac{(C - C_B)}{0.32} \times \frac{80}{V} = 250 \frac{(C - C_B)}{V}$$

where C = average count.

Table B1 presents the counts obtained on each sample, the calculated values of P and the ratio  $\frac{\sum P}{(\sum P)_0}$  of residual particle concentration to initial particle concentration.

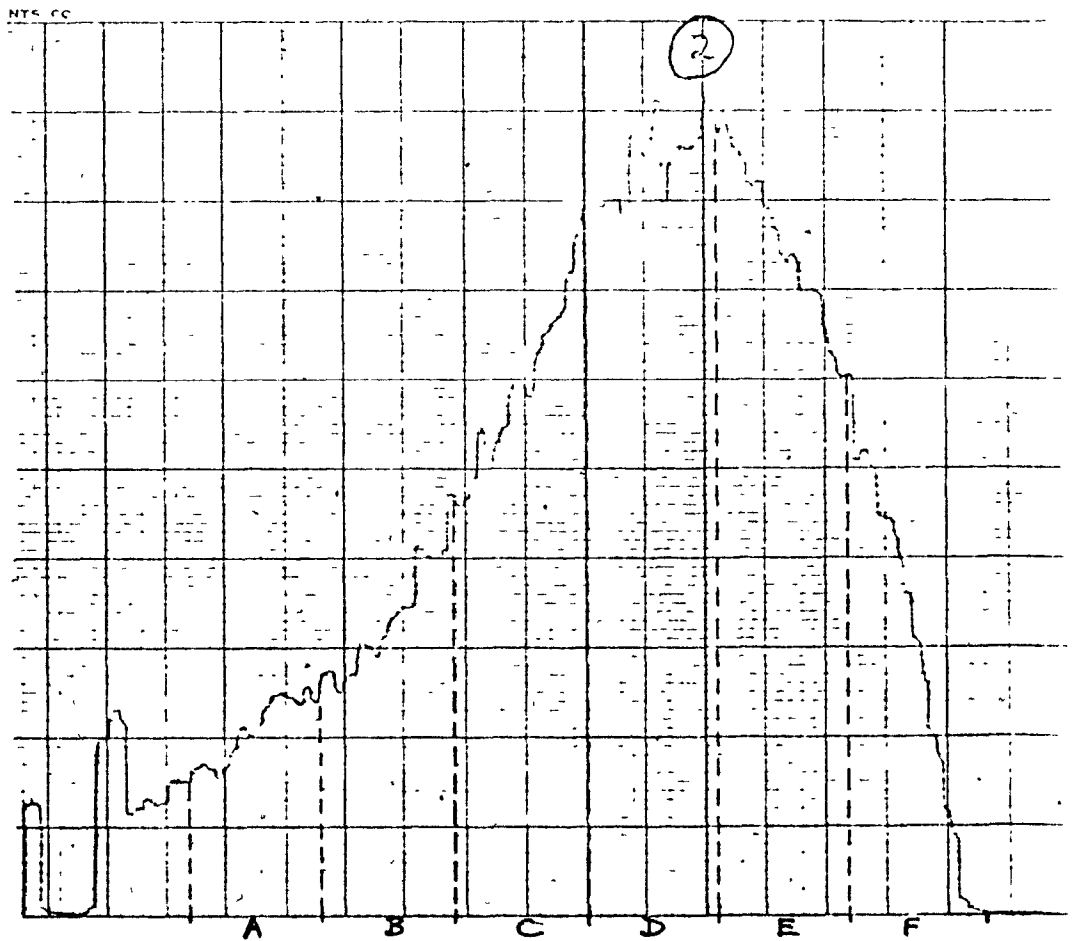
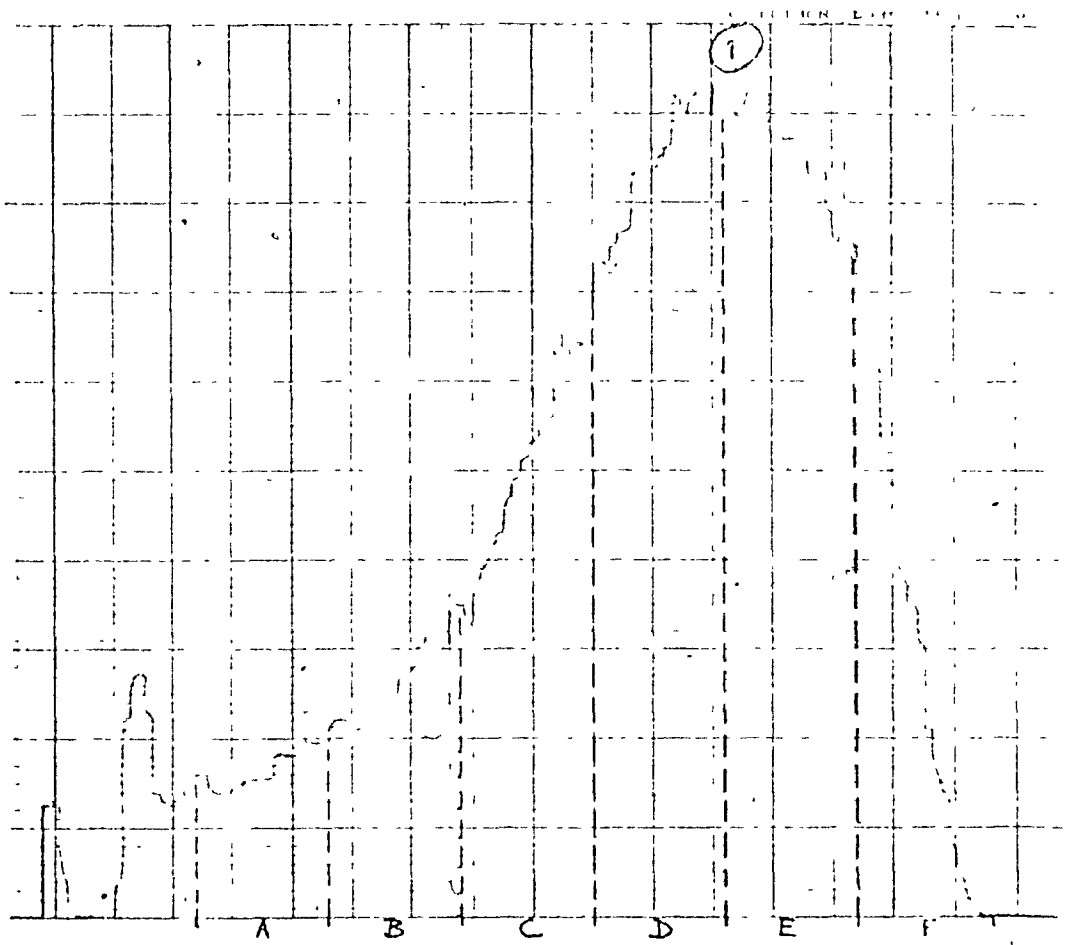
Exhibit B1 shows in reduced form the size distribution curves plotted by the recorder for each sample. Also shown are the sections into which the curves were divided for area measurement with the planimeter. The particle diameter at the mid-point of each section is as follows.

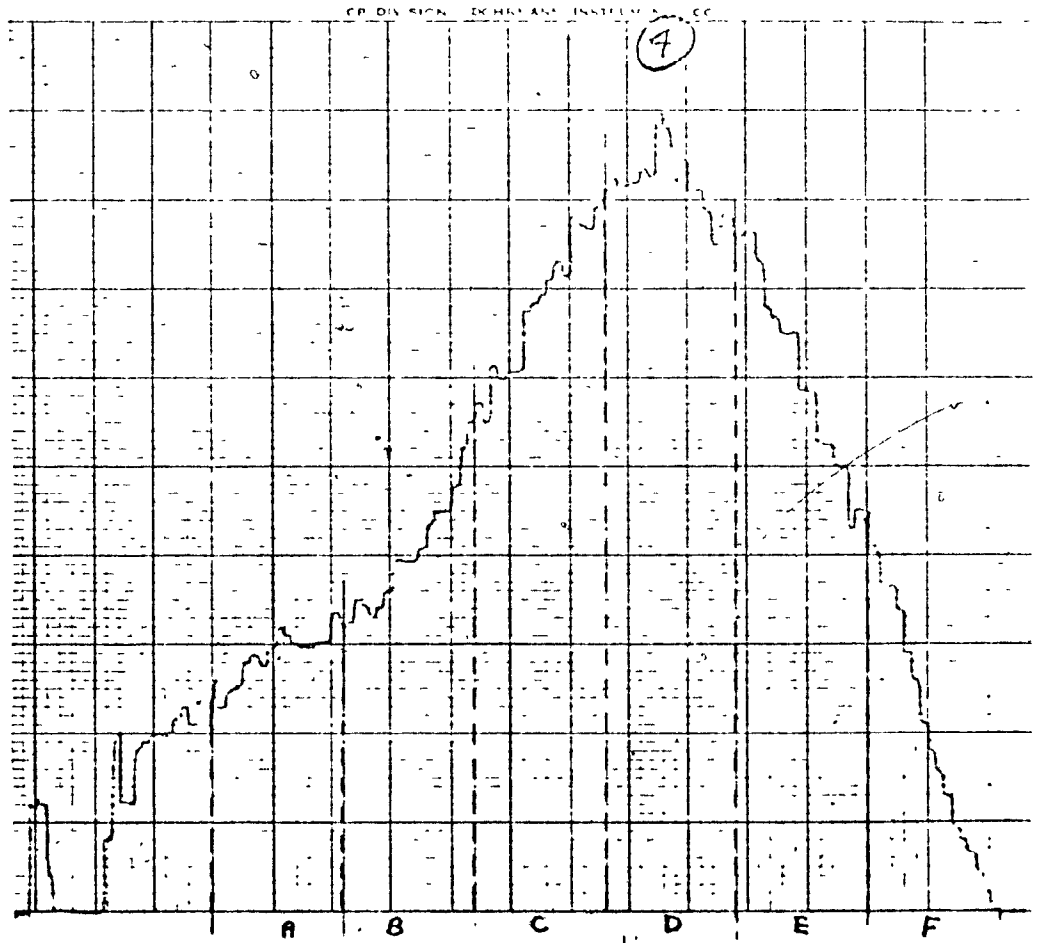
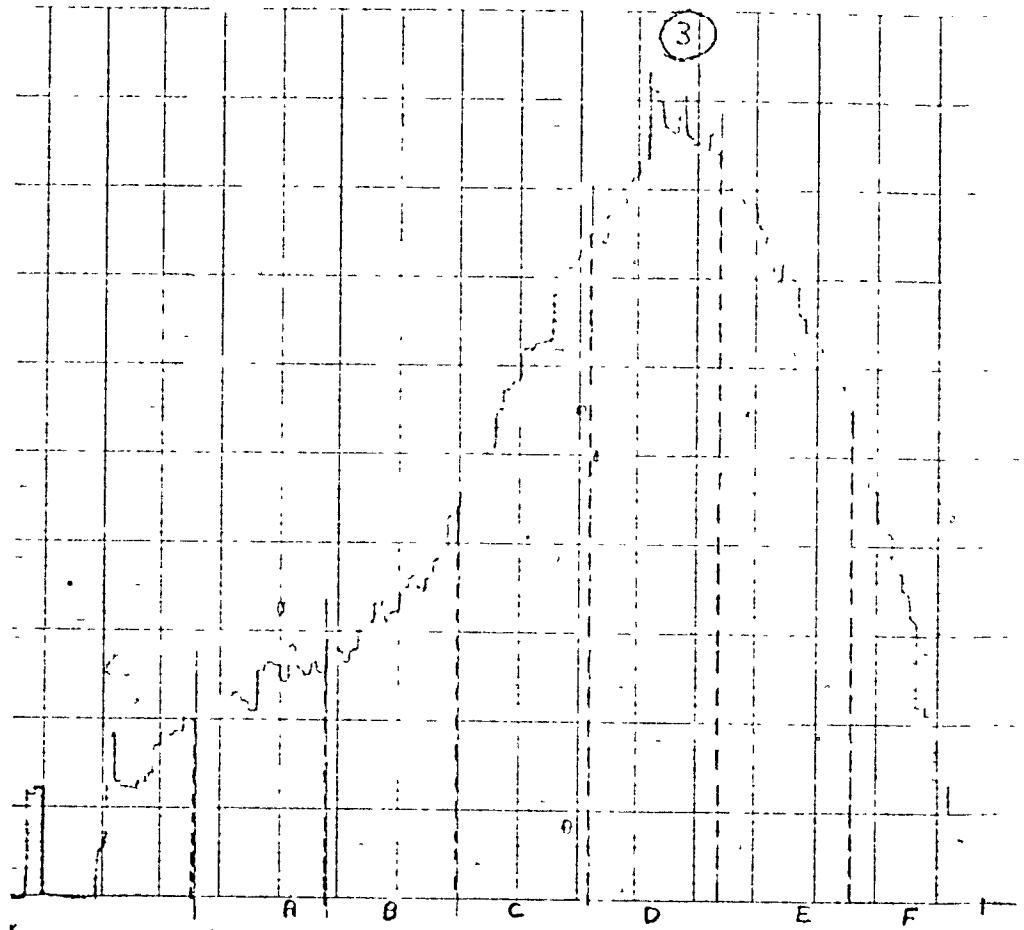
TABLE B1

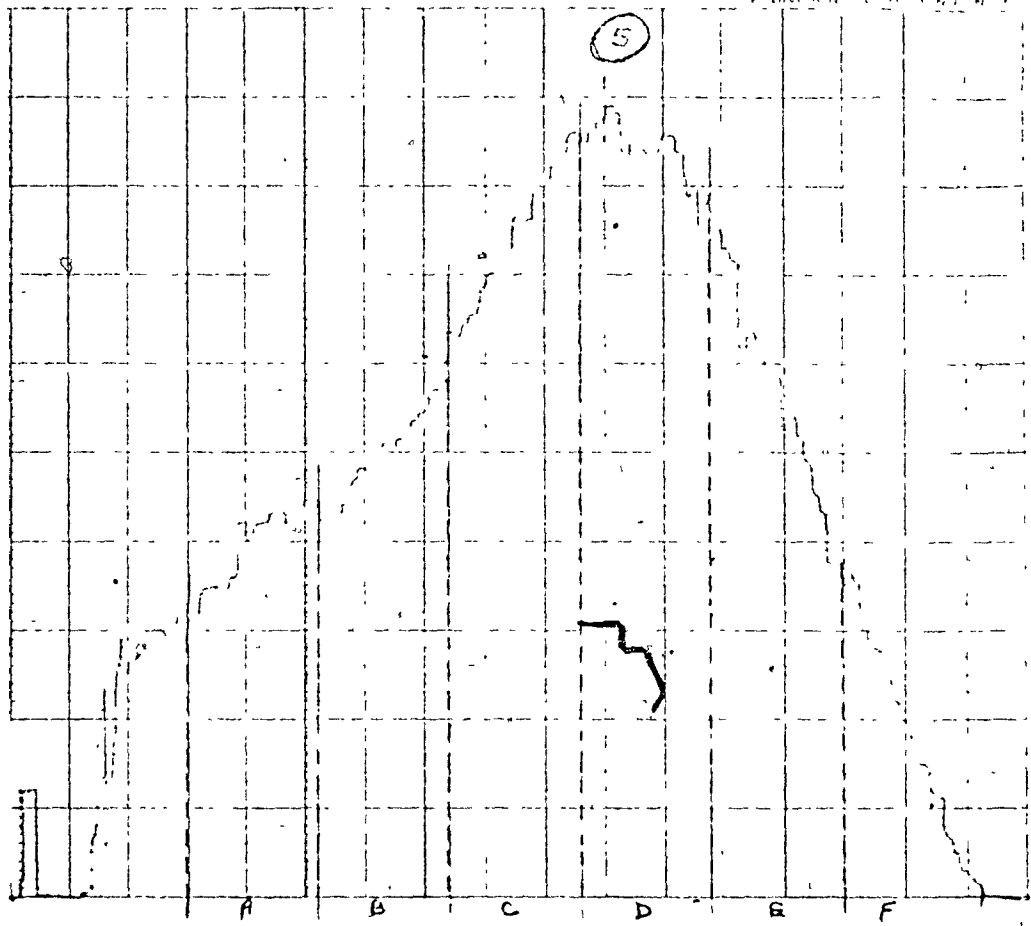
Sample No.	Time (mins.)	V (ml.)	Counts					C	$\Sigma P$	$\frac{\Sigma P}{(\Sigma P)_0}$
0	0	3.1	1444	1555	1515	1546	1585	1529	122,100	1.000
1	1	4.05	1402	1418	1428	1444	1476	1434	87,500	0.716
2	2	5.05	1253	1218	1230	1197	1156	1211	59,200	0.485
3	3	6.1	1049	1052	1090	1076	1036	1061	42,900	0.351
4	4	7.25	917	907	935	931	980	934	32,200	0.264
5	5	8.1	736	696	731	688	714	713	21,600	0.176
6	6	9.2	539	533	549	508	509	528	13,900	0.114
7	7	10.2	472	497	490	514	511	497	11,800	0.097

Exhibit B.1

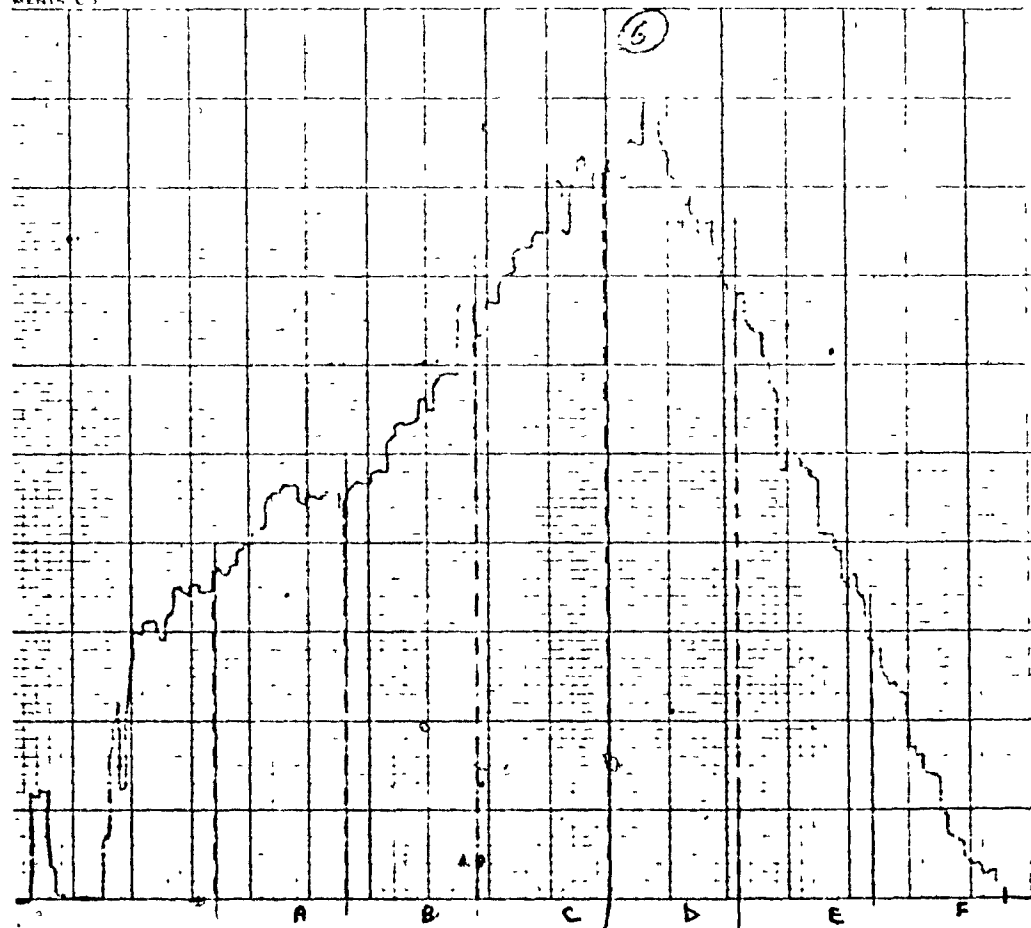
SAMPLE RUN; SIZE DISTRIBUTIONS OF SAMPLES



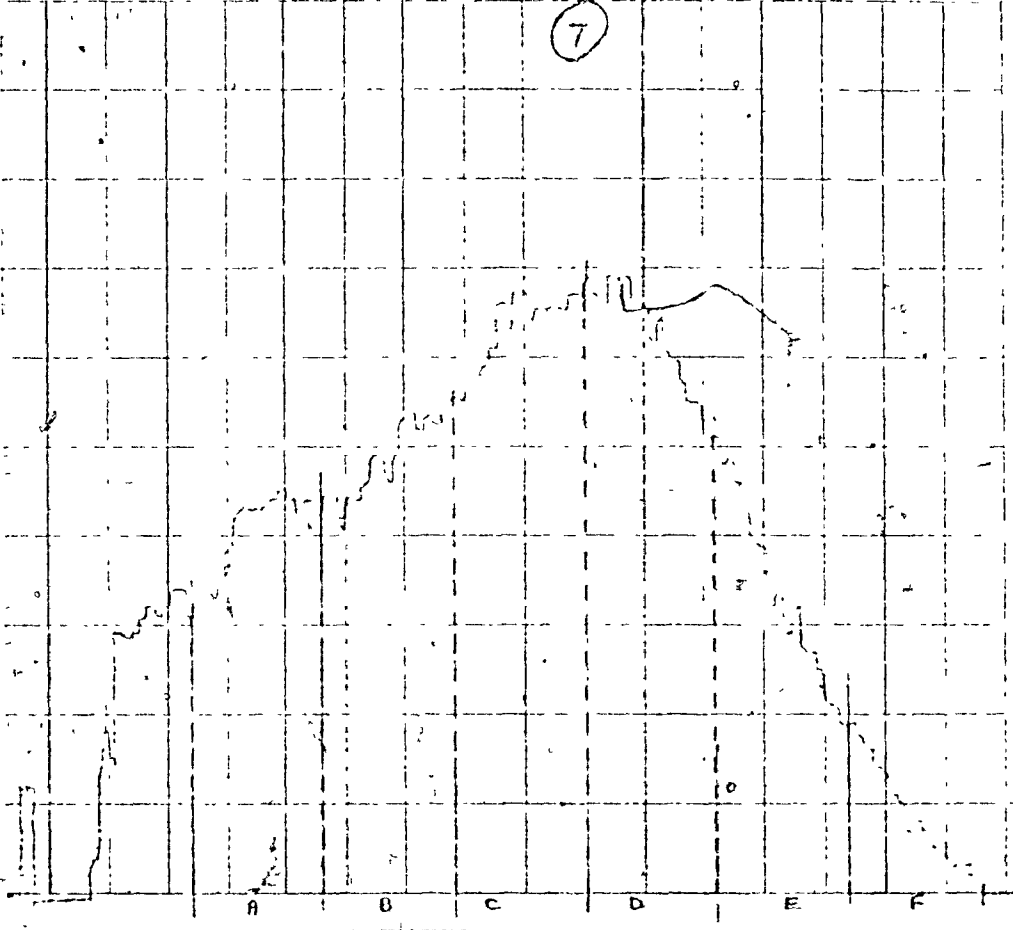




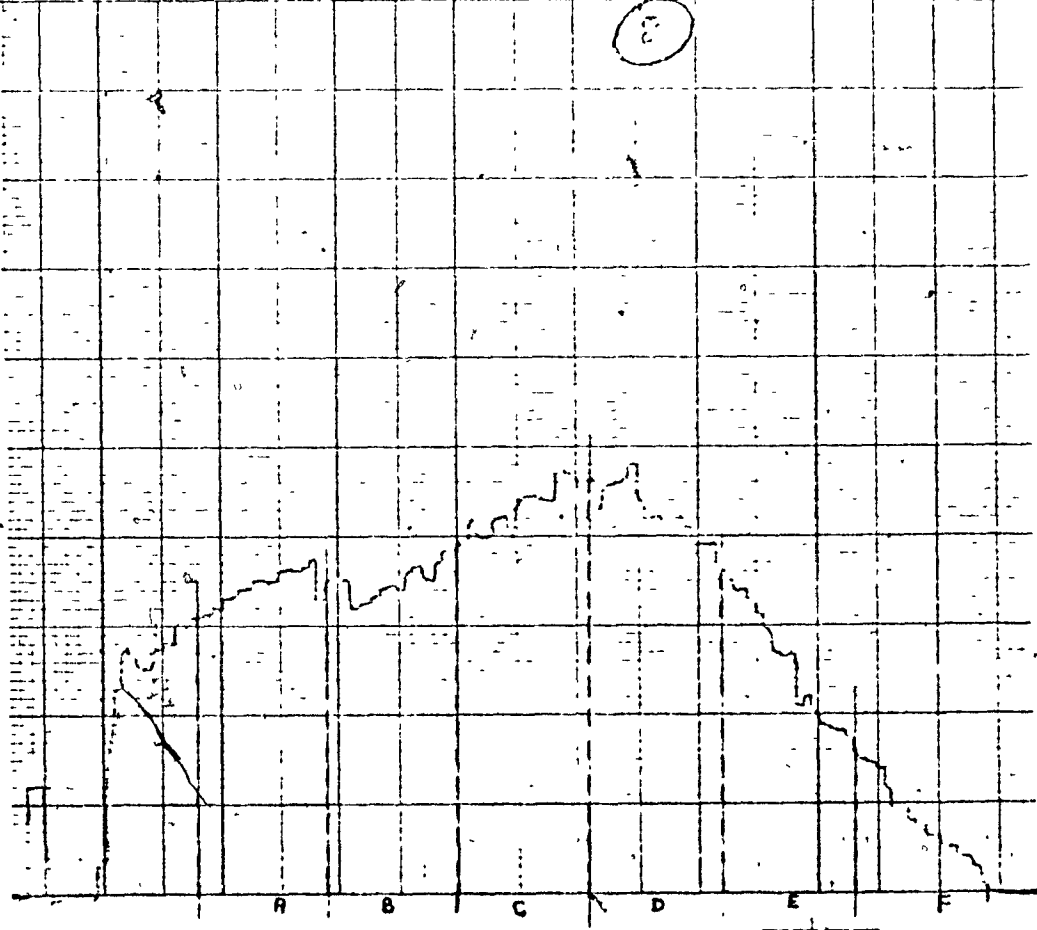
MENIS 2



7



8



<u>Section</u>	<u>Chart Divisions</u>	<u>Mid-point <math>d_p (\mu)</math></u>
A	7.5 - 17.5	7.3
B	17.5 - 27.5	8.6
C	27.5 - 37.5	10.2
D	37.5 - 47.5	12.1
E	47.5 - 57.5	14.3
F	57.5 - 67.5	16.9
G	67.5 - 77.5	20.0

For each sample  $i$  and section  $j$  the area  $A_{ij}$  under the curve was measured twice with a planimeter and the average taken. These data occupy the first three columns of Table B2. The fourth column shows the fraction  $F_{ij}$  of the total area under the curve accounted for by that section. Then for the particle size range represented by that section the ratio  $P/P_0$  of residual particle concentration to initial particle concentration is given by

$$\frac{P}{P_0} = \frac{F_{ij}}{F_{0j}} \times \frac{\sum P}{(\sum P)_0}$$

The last column contains the values of  $P/P_0$ . These are the values which were plotted in Fig.7.5.

TABLE B2

<u>Section</u>	<u>Areas</u>		<u>A<sub>ij</sub></u>	<u>F<sub>ij</sub></u>	$\frac{P}{P_o}$
OA	0.65	0.63	0.64	.038	1.000
OB	1.09	1.11	1.10	.066	1.000
OC	1.77	1.76	1.765	.106	1.000
OD	3.29	3.25	3.27	.197	1.000
OE	4.21	4.19	4.20	.252	1.000
OF	4.05	4.08	4.065	.244	1.000
OG	1.60	1.60	1.60	.096	1.000
1A	0.83	0.85	0.84	.048	.904
1B	1.29	1.31	1.30	.074	.803
1C	2.07	2.05	2.06	.118	.797
1D	3.29	3.34	3.315	.189	.687
1E	4.31	4.30	4.305	.246	.699
1F	3.99	4.00	4.005	.228	.669
1G	1.71	1.70	1.705	.097	.723
2A	1.22	1.21	1.215	.069	.881
2B	1.59	1.57	1.58	.090	.661
2C	2.35	2.39	2.37	.135	.618
2D	3.74	3.71	3.725	.212	.522
2E	4.32	4.35	4.335	.246	.473
2F	3.22	3.18	3.20	.182	.362
2G	1.16	1.18	1.17	.066	.333
3A	1.43	1.41	1.42	.076	.702
3B	2.08	2.10	2.09	.112	.596
3C	3.09	3.12	3.105	.167	.523
3D	3.99	4.01	4.00	.215	.383
3E	4.29	4.26	4.275	.230	.320
3F	2.64	2.69	2.665	.143	.206
3G	1.04	1.04	1.04	.056	.205

TABLE B2 (cont'd)

<u>Section</u>	<u>Areas</u>		<u>A<sub>ij</sub></u>	<u>F<sub>ij</sub></u>	<u><math>\frac{P}{P_o}</math></u>
4A	1.55	1.54	1.545	.085	.591
4B	2.34	2.31	2.325	.128	.500
4C	3.25	3.27	3.26	.179	.446
4D	4.17	4.15	4.16	.229	.307
4E	3.94	3.96	3.95	.217	.227
4F	2.32	2.33	2.325	.128	.138
4G	0.65	0.63	0.64	.035	.096
5A	1.52	1.54	1.53	.108	.500
5B	2.18	2.19	2.185	.155	.413
5C	2.83	2.87	2.85	.202	.335
5D	3.28	3.27	3.275	.232	.207
5E	2.60	2.57	2.585	.183	.128
5F	1.33	1.37	1.35	.096	.059
5G	0.36	0.36	0.36	.025	.046
6A	2.59	2.61	2.60	.130	.390
6B	3.54	3.51	3.525	.176	.304
6C	4.09	4.08	4.085	.204	.219
6D	4.46	4.41	4.435	.222	.128
6E	3.20	3.20	3.20	.160	.072
6F	1.66	1.70	1.68	.084	.039
6G	0.49	0.47	0.48	.024	.028
7A	2.97	2.98	2.975	.151	.385
7B	3.53	3.57	3.55	.180	.265
7C	4.26	4.26	4.26	.216	.198
7D	4.07	4.09	4.08	.207	.102
7E	3.03	3.00	3.015	.153	.059
7F	1.27	1.29	1.28	.065	.026
7G	0.53	0.50	0.515	.026	.026

C. FORCE COEFFICIENTS FOR VISCOUS INTERACTION MODEL

C.1 Motion Perpendicular to the Line of Centres

Consider two spheres of radii  $R_1$  and  $R_2$  moving perpendicular to their line of centres with translational velocities  $V_1$  and  $V_2$ . Let the spheres have angular velocities  $\omega_1 = V_1/R_1$  and  $\omega_2 = V_2/R_2$  about axes through their centres perpendicular to the plane of motion. Let the steady state drag on sphere 1 be expressed as  $6\pi\mu R_1 g_1$  and that on sphere 2 as  $6\pi\mu R_2 g_2$  where  $\mu$  is the fluid viscosity. Let the torque on sphere 1 be  $8\pi\mu R_1^2 h_1$  and that on sphere 2 be  $8\pi\mu R_2^2 h_2$ . Davis (65) and O'Neill and Majumdar (66) formulated the problem in spherical bipolar coordinates and showed that if the non-linear terms are neglected in the Navier-Stokes equation  $g_1, g_2, h_1$  and  $h_2$  take the following forms:

$$g_1 = k_5 V_1 + k_6 V_2 + k_7 W_1 + k_8 W_2$$

$$g_2 = k_9 V_1 + k_{10} V_2 + k_{11} W_1 + k_{12} W_2$$

$$h_1 = k_{13} V_1 + k_{14} V_2 + k_{15} W_1 + k_{16} W_2$$

$$h_2 = k_{17} V_1 + k_{18} V_2 + k_{19} W_1 + k_{20} W_2$$

The nomenclature of Chapter 8 has been preserved in the above equations. Table C1 shows the relation between our coefficients  $k_5$  to  $k_{20}$ , Davis' coefficients  $C_1$  to  $C_{16}$  and O'Neill and Majumdar's coefficients.

Let  $S$  be the distance between sphere surfaces. The coefficients are functions only of  $R_1/R_2$  and  $S/R_2$  (or  $S/R_1$ , depending on which radius is selected as the reference length; Davis uses  $S/R_2$ , while O'Neill and Majumdar use  $S/R_1$ ). Davis presents a convenient tabulation of numerical values of the coefficients for  $R_1/R_2 = 1, 2, 5$  and  $10$  at  $S/R_2 = 10, 1, 10^{-1}, 10^{-2}$  and  $10^{-3}$ . O'Neill and Majumdar present additional values for  $R_1/R_2 = 4$ . Values for  $R_1/R_2 = 3$  were found by interpolation.

For each coefficient a cubic regression (97) was performed on the tabulated values at a given radius ratio with  $\log_{10}(S/R_2)$  as the independent variable. The equation had the form:

$$k_n = A_n + B_n \log_{10} S/R_2 + C_n (\log_{10} S/R_2)^2 + D_n (\log_{10} S/R_2)^3 \dots (C.1)$$

For a given coefficient  $A_n, B_n, C_n$  and  $D_n$  were functions of  $R_1/R_2$ . Table C2 presents the values obtained for  $R_1/R_2 = 2, 3, 4, 5$  and  $10$ . Values of  $k_n$  calculated from equation C.1 agreed with the tabulated values of Davis and of O'Neill and Majumdar to within 1% in most cases and always to within 2%.

## C2. Motion Parallel to the Line of Centres

Suppose the two spheres are now moving parallel to their line of centres with velocities  $U_1$  and  $U_2$ . There is now no rotation of the spheres. Let the steady state drag on sphere 1 be expressed as  $6\pi\mu R_1 f_1$  and that on sphere 2 as  $6\pi\mu R_2 f_2$ . Pshenay-Severin (64) formulated the problem in spherical bipolar coordinates and showed that if the non-linear terms are neglected in the Navier-

Stokes equation  $f_1$  and  $f_2$  take the forms:

$$f_1 = k_1 U_1 + k_2 U_2$$

$$f_2 = k_3 U_1 + k_4 U_2$$

Unfortunately, he did not present tabulated numerical values of the coefficients  $k_1$  to  $k_4$ . Instead, they were presented as the following infinite series:

$$k_1 = \frac{\sinh \alpha}{3} \sum_{n=1}^{\infty} \frac{x_n}{\Delta n} \left\{ 2(2n-1)(2n+3) \left[ \exp(-[2n+1]\beta) - \exp(-[2n+1]\alpha) \right] \right.$$

$$-2(2n+1)(2n+3) \sinh \left[ (n+3/2)(\alpha-\beta) \right] \exp \left[ -(n-1/2)(\alpha+\beta) \right]$$

$$\left. -2(2n+1)(2n-1) \sinh \left[ (n-1/2)(\alpha-\beta) \right] \exp \left[ -(n+3/2)(\alpha+\beta) \right] \right\}.$$

$$k_2 = \frac{\sinh \alpha}{3} \sum_{n=1}^{\infty} \frac{x_n}{\Delta n} \left\{ 16 \exp \left[ -(n+1/2)(\alpha-\beta) \right] \sinh \left[ (n+1/2)(\alpha-\beta) \right] \right.$$

$$+ (2n+1)^2 \sinh(\alpha-\beta) \left[ (2n+3) \exp(\alpha-\beta) + (2n-1) \exp(\beta-\alpha) \right]$$

$$\left. + (2n-1)(2n+1)(2n+3) \left[ \sinh 2\beta - \sinh 2\alpha \right] \right\}$$

$$k_3 = -(\sinh \beta / \sinh \alpha) k_2.$$

$$k_4 = -\frac{\sinh \beta}{3} \sum_{n=1}^{\infty} \frac{x_n}{\Delta n} \left\{ 2(2n-1)(2n+3) \left[ \exp([2n+1]\alpha) - \exp([2n+1]\beta) \right] \right.$$

$$-2(2n+1)(2n+3) \sinh \left[ (n+3/2)(\alpha-\beta) \right] \exp \left[ (n-1/2)(\alpha+\beta) \right]$$

$$\left. -2(2n+1)(2n-1) \sinh \left[ (n-1/2)(\alpha-\beta) \right] \exp \left[ (n+3/2)(\alpha+\beta) \right] \right\}.$$

$$x_n = \frac{n(n+1)}{(2n+3)(2n-1)}$$

$$\Delta n = 4 \sinh^2[(n+1/2)(\alpha-\beta)] - (2n+1)^2 \sinh^2(\alpha-\beta).$$

$\alpha$  and  $\beta$  are functions of the coordinates of the sphere centres. They are obtained most simply by the following sequence of equations adapted from those presented by Davis (65):

$$C/R_2 = S/R_2 + R_1/R_2 + 1$$

$$D_1/R_2 = [(C/R_2)^2 + (R_1/R_2)^2 - 1] / (2C/R_2)$$

$$D_2/R_2 = [(C/R_2)^2 + 1 - (R_1/R_2)^2] / (2C/R_2)$$

$$B/R_2 = [(D_1/R_2)^2 - (R_1/R_2)^2]^{1/2}$$

$$\xi_1 = \ln[(D_1/R_2) + (B/R_2)] - \ln(R_1/R_2) = \alpha.$$

$$\xi_2 = \ln[(D_2/R_2) + (B/R_2)] = -\beta.$$

Hence,  $\alpha$  and  $\beta$  are functions only of  $S/R_2$  and  $R_1/R_2$ . This implies that  $k_1$  to  $k_4$  are also functions only of  $S/R_2$  and  $R_1/R_2$ .

It would have been very cumbersome to evaluate the above infinite series at every step in a collision efficiency calculation. Instead, they were evaluated only at  $S/R_2 = 10, 1, 10^{-1}, 10^{-2}$  and  $10^{-3}$  using  $R_1/R_2 = 2, 3, 4, 5$  and  $10$ , i.e. the same conditions for which the perpendicular coefficients had been tabulated. Convergence was rapid. For each coefficient the numerical values obtained at a

given radius ratio were subjected to a quartic regression (97) with  $\ln(S/R_2)$  as the independent variable. Best results were obtained with  $\ln k_n$  as the dependent variable for  $n = 1$  and 4 and  $\ln(-k_n)$  for  $n = 2$  and 3. The quartic equations are:

$n = 1$  and 4:

$$\begin{aligned} \ln k_n = & A_n - B_n \ln S/R_2 + C_n (\ln S/R_2)^2 + D_n (\ln S/R_2)^3 \\ & + E_n (\ln S/R_2)^4 \end{aligned} \quad (C.2)$$

$n = 2$  and 3:

$$\begin{aligned} \ln(-k_n) = & A_n + B_n \ln S/R_2 + C_n (\ln S/R_2)^2 \\ & + D_n (\ln S/R_2)^3 + E_n (\ln S/R_2)^4 \end{aligned} \quad (C.3)$$

For a given coefficient  $A_n$ ,  $B_n$ ,  $C_n$ ,  $D_n$  and  $E_n$  are functions of  $R_1/R_2$ . Table C3 presents values for  $R_1/R_2 = 2, 3, 4, 5$  and 10. Values of  $k_n$  calculated from these equations agree with those obtained from the Pshenay-Severin formulae to within 1% in most cases and always to within 2%.

TABLE CI

Equivalence of Coefficients

<u>Our</u> <u>Coefficients</u>	<u>Lewis</u> <u>Coefficients</u>	<u>O'Neill and Majumdar</u> <u>Coefficients</u>
$k_5$	$C_1$	$-f_{21}(k, \epsilon)$
$k_6$	$C_5$	$-f_{22}(k^{-1}, \epsilon k^{-1})$
$k_7$	$C_9 / (R_1 / R_2)$	$-f_{11}(k, \epsilon)$
$k_8$	$C_{13}$	$f_{12}(k^{-1}, \epsilon k^{-1}) \times (R_1 / R_2)$
$k_9$	$C_2$	$-f_{22}(k, \epsilon)$
$k_{10}$	$C_6$	$-f_{21}(k^{-1}, \epsilon k^{-1})$
$k_{11}$	$C_{10} / (R_1 / R_2)$	$-f_{12}(k, \epsilon) / (R_1 / R_2)$
$k_{12}$	$C_{14}$	$f_{11}(k^{-1}, \epsilon k^{-1})$
$k_{13}$	$C_3$	$-g_{21}(k, \epsilon)$
$k_{14}$	$C_7$	$-g_{22}(k^{-1}, \epsilon k^{-1})$
$k_{15}$	$C_{11} / (R_1 / R_2)$	$-g_{11}(k, \epsilon)$
$k_{16}$	$C_{15}$	$g_{12}(k^{-1}, \epsilon k^{-1}) \times (R_1 / R_2)$
$k_{17}$	$C_4$	$g_{22}(k, \epsilon)$
$k_{18}$	$C_8$	$g_{21}(k^{-1}, \epsilon k^{-1})$
$k_{19}$	$C_{12} / (R_1 / R_2)$	$g_{12}(k, \epsilon) / (R_1 / R_2)$
$k_{20}$	$C_{16}$	$-g_{11}(k^{-1}, \epsilon k^{-1})$

$R_1$  = radius of larger sphere

$R_2$  = radius of smaller sphere

TABLE C2

Perpendicular Force Coefficients (Equation C.1)

λ

$R_1/R_2$	n	$A_n$	$B_n$	$C_n$	$D_n$
2	5	-1.11178	0.17740	-0.06022	-0.01115
	6	0.24115	-0.22140	0.03230	0.00598
	7	0.06935	-0.15879	0.07727	0.01283
	8	0.07188	-0.10764	0.03705	0.00478
	9	0.48231	-0.44280	0.06458	0.01196
	10	-1.14410	0.29691	-0.13556	-0.02302
	11	0.29834	0.40762	-0.11218	-0.01928
	12	-0.03697	0.14668	-0.09898	-0.01235
	13	0.05201	-0.11910	0.05796	0.00963
	14	-0.11187	0.15286	-0.04208	-0.00723
	15	-1.03815	0.12984	-0.07983	-0.01192
	16	-0.01945	0.03715	-0.01589	-0.00220
	17	0.10783	-0.16147	0.05558	0.00717
	18	-0.02773	0.11001	-0.07423	-0.00926
	19	-0.03889	0.07430	-0.03178	-0.00490
	20	-1.01366	0.17403	-0.14738	-0.01566

TABLE C2 (cont'd)

$R_1/R_2$	n	$A_n$	$B_n$	$C_n$	$D_n$	
3	5	-1.11148	0.15566	-0.04295	-0.00901	
	6	0.20026	-0.17490	0.02585	0.00511	
	7	0.08369	-0.14553	0.05065	0.00319	
	8	0.04592	-0.06313	0.01823	0.00105	
	9	0.60204	-0.53186	0.08329	0.01715	
	10	-1.19816	0.35395	-0.14356	-0.02048	
	11	-0.42228	0.53369	-0.13762	-0.02945	
	12	-0.04868	0.13171	-0.07995	-0.00394	
	13	0.06300	-0.11303	0.04299	0.00789	
	14	-0.10870	0.13505	-0.03251	-0.00650	
	15	-1.05377	0.11892	-0.05133	-0.00771	
	16	-0.01579	0.02626	-0.00995	-0.00095	
	17	0.10770	-0.14833	0.04709	0.00334	
	18	-0.03646	0.09881	-0.05999	-0.00297	
	19	-0.04668	0.07711	-0.02920	-0.00209	
	20	-1.04555	0.19124	-0.12209	-0.00067	
	4	5	-1.10620	0.13766	-0.03375	-0.00736
		6	0.17328	-0.14728	0.02317	-0.00466
		7	0.08734	-0.13640	0.04044	0.00753
		8	0.03346	-0.04437	0.01414	0.00045
9		0.69308	-0.58913	0.09271	0.01863	
10		-1.22727	0.40995	-0.14479	-0.01879	
11		-0.53454	0.61524	-0.13385	-0.02789	
12		-0.04821	0.12690	-0.06470	0.00052	
13		0.06546	-0.10232	0.03035	0.00566	
14		-0.10023	0.11538	-0.02511	-0.00524	
15		-1.05878	0.10584	-0.03614	-0.00547	
16		-0.01190	0.01965	-0.00722	-0.00037	
17		0.09998	-0.13330	0.04299	0.00165	
18		-0.03614	0.09517	-0.04852	0.00039	
19		-0.04786	0.07833	-0.02881	-0.00141	
20		-1.05563	0.20169	-0.11912	0.00495	

TABLE C2 (cont'd)

$R_1/R_2$	n	$A_n$	$B_n$	$C_n$	$D_n$	
5	5	-1.10270	0.17989	-0.02441	-0.00435	
	6	0.15514	-0.12545	0.01683	0.00255	
	7	0.08587	-0.12005	0.03276	0.00570	
	8	0.02376	-0.03314	0.01261	0.00103	
	9	0.77573	-0.62727	0.08414	0.01275	
	10	-1.22300	0.43484	-0.19248	-0.03150	
	11	-0.63802	0.66452	-0.10803	-0.01673	
	12	-0.02769	0.12152	-0.08704	-0.00921	
	13	0.06439	-0.09005	0.02458	0.00429	
	14	-0.09571	0.09968	-0.01620	-0.00251	
	15	-1.05618	0.09249	-0.03198	-0.00538	
	16	-0.00897	0.01545	-0.00667	-0.00057	
	17	0.08909	-0.12425	0.04729	0.00387	
	18	-0.02077	0.09114	-0.06528	-0.00690	
	19	-0.04487	0.07727	-0.03337	-0.00283	
	20	-1.01853	0.21551	-0.18145	-0.01883	
	10	5	-1.07760	0.07468	-0.01050	-0.00168
		6	0.09905	-0.07061	0.00990	0.00090
		7	0.07083	-0.07709	0.01293	0.00226
		8	0.00893	-0.01084	0.00488	-0.00066
9		0.98721	-0.71288	0.10509	0.01379	
10		-1.28088	0.52183	-0.22455	-0.03577	
11		-0.89546	0.77373	-0.09877	-0.01204	
12		-0.01806	0.10099	-0.07828	-0.00731	
13		0.05312	-0.05781	0.00969	0.00169	
14		-0.06748	0.05736	-0.00681	-0.00044	
15		-1.04910	0.05943	-0.01210	-0.00223	
16		-0.00400	0.00594	-0.00290	-0.00041	
17		0.06130	-0.09311	0.04724	0.00331	
18		-0.01355	0.07574	-0.05871	-0.00548	
19		-0.03554	0.06877	-0.03745	-0.00248	
20	-1.02177	0.23481	-0.19643	-0.02017		

TABLE C3

Parallel Force Coefficients (Equations C.2 and C.3)

$R_1/R_2$	n	$A_n$	$B_n$	$C_n$	$D_n$	$E_n$
2	1	0.30935	-0.26287	0.07706	-0.00418	-0.00073
	2	-0.61273	-0.66304	0.02056	-0.00684	-0.00074
	3	0.08042	-0.66304	0.02056	-0.00684	-0.00074
	4	0.47084	-0.37598	0.08739	-0.00238	-0.00080
3	1	0.27666	-0.23459	0.07441	-0.00469	-0.00071
	2	-0.79292	-0.63234	0.02868	-0.00753	-0.00090
	3	0.30568	-0.63233	0.02868	-0.00753	-0.00090
	4	0.55323	-0.41709	0.08879	-0.00168	-0.00077
4	1	0.24015	-0.20793	0.07241	-0.00516	-0.00071
	2	-0.95327	-0.60674	0.03522	-0.00802	-0.00103
	3	0.43305	-0.60676	0.03521	-0.00802	-0.00103
	4	0.60321	-0.44001	0.08925	-0.00128	-0.00076
5	1	0.20846	-0.18544	0.07036	-0.00553	-0.00069
	2	-1.09449	-0.58621	0.04044	-0.00835	-0.00112
	3	0.51494	-0.58621	0.04045	-0.00835	-0.00112
	4	0.63705	-0.45445	0.08933	-0.00103	-0.00074
10	1	0.11103	-0.11456	0.06013	-0.00629	-0.00055
	2	-1.61309	-0.52983	0.05642	-0.00866	-0.00133
	3	0.68959	-0.52985	0.05639	-0.00866	-0.00133
	4	0.71578	-0.48474	0.08913	-0.00051	-0.00071

D. COMPUTER PROGRAMS

D.1 Viscous Interaction Model (Chapter 8)

D.1.1 Backwards Integration

The program is designed so that several trajectories at various size ratios can be computed in a single run. The trajectories are grouped according to radius ratio; i.e. all trajectories at a given radius ratio ( $R_1/R_2$ ) are computed before moving on to the next ratio.

The input data deck is in the following order.

Card 1:

- (a) NO = no. of radius ratios in this group of runs.
- (b) LRN = previous run number (required for titles),

Cards 2 to 21:

Force coefficients for the first radius ratio; each card contains A, B, C, D and E for a given coefficient (see Appendix C).

E = 0 for perpendicular coefficients  $k_5$  to  $k_{20}$ .

Card 22:

M = no. of runs at first size ratio.

Cards 23 to (22 + M):

Each card refers to one run and gives the following data:

- (a) R1 = bubble radius (microns).
- (b) R2 = particle radius (microns).
- (c) E = separation  $S_0$  of surfaces at  $\theta = 90^\circ$  (microns)
- (d) RH02 = particle density (gm./ml.)

Additional Cards:

The above sequence (except Card 1) is repeated for each radius ratio.

Exhibit D1 is a program listing and Exhibit D2 is a typical output: "Limiting  $LY(2)/DY(1)$ " is the ratio  $\Delta y/\Delta x$  at which integration was stopped. TOLNM is the accuracy required for evaluation of the dependent variables in the numerical integration subroutine (MERSON).

D.1.2 Forwards Integration

The input data deck is identical to that for backwards integration except that cards 23 to  $(22 + M)$  have two extra fields giving the initial vertical and horizontal coordinates  $Y(1)$  and  $Y(2)$  of the centre of the particle. The third field on these cards ( $S_0$ ) may be left blank.

Exhibit D3 is a program listing and Exhibit D4 is a typical output.

D2. Calculation of Collision Efficiency Including Unsteady State Drag Terms (Chapter 11).

The input data deck is in the following order.

Card 1:

- (a) H, or whatever single alphanumeric character is desired to indicate on the output a trajectory whose starting value of  $y$  was too high.

- (b) L, or whatever is desired to indicate a low trajectory.
- (c) MO = number of runs in this deck.
- (d) MO1 = sequence number of first run (required for titles).

Cards 2 to (1 + M):

Each card refers to one run and gives the following data:

- (a) G = dimensionless terminal velocity  $u_{pt}^*$  of the particle.
- (b) K = Stokes number St.
- (c) RHOPF = fluid to particle density ratio ( $\rho_f/\rho_p$ ).
- (d) RPS = ratio of particle radius to bubble radius.
- (e) YIN = initial value of y, the horizontal coordinate of the centre of the particle.
- (f) FLOW = flow parameter (1 for Stokes, anything for potential).
- (g) NSS = drag term parameter (1 if only steady state term is to be included; 2 if pressure gradient term is to be included; 3 if all unsteady state terms are to be included.)

Exhibit D5 is a program listing and Exhibit D6 is a typical output.

Exhibit D.1

VISCOUS INTERACTION MODEL; COMPUTER PROGRAM  
FOR BACKWARDS INTEGRATION

```

1      DIMENSION Y(10),DY(10)
2      COMMON /DFP/Y/GRAD/DY/ACC/TOLKM(10)
3      COMMON K(25,5),R1,R2,S,B,RATIO,TOL
4      REAL K
5      READ(5,299)MO,LRN
6-    999  FORMAT(11,15)
7      DO 303 LA=1,MO
8      DO 1 I=1,20
9      READ(5,2)(K(I,J),J=1,5)
10     2  FORMAT(5F15,9)
11     1  CONTINUE
12      READ(5,298)M
13     998  FORMAT(12)
14      DO 100 L=1,M
15      L=L+LRN
16      L=L+M*(LA-1)
17      WRITE(6,253)L
18     253  FORMAT('1',////,60X,'RUN NUMBFR',I4)
19      L=L-M*(LA-1)
20      L=L-LRN
21      WRITE(6,274)
22     274  FORMAT(59X,'-----')
23      READ(5,210)R1,R2,E,RHO2
24     210  FORMAT(4F10,5)
25      RAT=R1/R2
26      TOL=-.000001
27      FAC1=.01
28      FAC=.001
29      WRITE(6,211)R1,R2,RAT,RHO2
30     211  FORMAT(///,20X,'R1=',F6,2,' MICRONS',//,20X,'R2=',F6,2,' MICRONS',
31           ;//,20X,'R1/R2 =',F5,2,/,20X,'DENSITY OF PARTICLE =',F6,2,' GMS/ML
32           **)
33      WRITE(6,212)E,TOL,FAC1,FAC
34     212  FORMAT(//,20X,'INITIAL SEPARATION =',F5,3,' MICRONS',//,20X,'LIMITI
35           NG DY(2)/DY(1) =',E9,2,/,20X,'TOLKM =',F6,4,/,R1,/,20X,'INITIAL
36           + Y(1)/Y(2) =',F6,4)
37      WRITE(6,101)
38     101  FORMAT(////,20X,'VERTICAL DISTANCE',10X,'HORIZONTAL DISTANCE',10X
39           X,'SEPARATION',16X,'TIME')
40      RHO1=.0012928
41     C
42     C      DENSITY OF AIR.
43     C
44     C      RHO1=1.00
45     C
46     C      DENSITY OF FLUID.
47     C
48     C      UF=0.01
49     C
50     C      VISCOSITY OF FLUID.
51     C
52      Y(2)=(R1+R2+E)/R1
53      Y(1)=FAC*Y(2)
54      UIT=-2*(RHO1-RHO2)*R1*R1*281)/(9*UF*10**8.)
55      B=(R2*R2*(RHO1-RHO2))/(R1*R1*(RHO1-RHO2))
56      X=0.0
57      TOLKM(1)=FAC1/R1
58      TOLKM(2)=FAC1/R1

```

```

59      N=2
60      DX=Y(1)
61      J=1
62 15   DXMIN=Y(1)/20000
63      IF(Y(1).GT.0.25) GO TO 16
64      DELX=0.25
65      GO TO 13
66 16   DELX=Y(1)
67 13   Y01=Y(1)
68 C
69 C      AT THIS POINT WE HAVE DEFINED ALL THE QUANTITIES THAT ARE NECESSARY
70 C      FOR THE INTEGRATION OF THE DEPENDENT VARIABLES Y(1) TO Y(2), WITH
71 C      RESPECT TO X THE INDEPENDENT VARIABLE. OVER THE RANGE X TO X+DELX.
72 C      ACCORDINGLY THE CURRENT VALUES OF Y(1),Y(2) ARE HANDED OVER TO
73 C      MERSON WHICH THEN RETURNS THE VALUES OF Y(1),Y(2) AT X+DELX.
74 C
75      CALL MERSON(X,DELX,DX,DXMIN,IFAIL,ITS,N,L1,L2,L3,L4)
76      IF(J.EQ.1) GO TO 54
77      DIV1=Y(1)/Y01
78      IF(DIV1.LT.1.010) GO TO 50
79 54   J=J+1
80      CONTINUE.
81      IF(L4.EQ.40) GO TO 40
82      IF(L1.EQ.10) GO TO 10
83      IF(L2.EQ.20) GO TO 20
84      IF(L3.EQ.30) GO TO 30
85 C
86 C      L1=10  INDICATES INTEGRATION HAS BEEN SUCCESSFUL IN THE RANGE X TO
87 C            X+DELX.
88 C      L2=20  OCCURS WHEN MERSON FAILS TO INTEGRATE Y(1) AND/OR Y(2) FROM X
89 C            TO X+DELX. THIS IS DUE EITHER TO A LARGE DXMIN OR A SMALL TOLKM
90 C            WHICH IS USED.
91 C      L3=30  OCCURS WHEN THE LIMITING RATIO OF DY(2)/DY(1) HAS BEEN REACHED.
92 C            THIS INDICATES THAT A FURTHER INCREASE IN THE VERTICAL DISTANCE
93 C            LEADS TO NO SIGNIFICANT CHANGE IN THE HORIZONTAL DISTANCE. THAT
94 C            FOR ALL INTENTS AND PURPOSES, THIS POINT CAN BE CONSIDERED AS A
95 C            POINT AT INFINITY FROM WHICH THE PARTICLE IS STARTING ITS
96 C            JOURNEY.
97 C      L4=40  INDICATES THAT THE SEPARATION HAS BECOME NEGATIVE. ANY FURTHER
98 C            CALCULATIONS WILL LEAD TO ERRORS AND EXPENSIVE STOPPAGES. MOST
99 C            PROBABLE CAUSE FOR SEPARATION BECOMING NEGATIVE IS THE LOW VALUE
100 C           OF THE INITIAL SEPARATION WHICH WAS SPECIFIED. THE TRAJECTORY
101 C           IS UNSTABLE AT LOW SEPARATIONS AND RESULTS IN A NEGATIVE
102 C           SEPARATION.
103 C
104 10   STEP=DX*UIT/R1
105      Y(1)=Y(1)*R1
106      Y(2)=Y(2)*R1
107      S=S*R2
108      WRITE(6,12)Y(1),Y(2),S,X
109 12   FORMAT(//.23X,F9.3,19X,F8.3,15X,F9.3,16X,F8.3)
110      Y(1)=Y(1)/R1
111      Y(2)=Y(2)/R1
112      S=S/R2
113      GO TO 15
114 C
115 C      WE RETURN TO 15 AS THE WHOLE TRAJECTORY IS NOT YET COMPLETED.
116 C

```

```

117 20 WRITE(6,21)
118 21 FORMAT(//,5X,'SMALLER DXMIN OR LARGER TOLKM REQUIRED FOR SUCCESSFU
119    L INTFRGATION')
120    Y(1)=Y(1)*R1
121    Y(2)=Y(2)*R1
122    S=S*R2
123    WRITE(6,22)Y(1),Y(2),S,IFAIL
124 22  FURMAT(///,10X,'Y CO-ORDINATE =',F8.5,10X,'X CO-ORDINATE =',F8.5,/
125    %/,10X,'SEPARATION =',F8.5,10X,'THE VARIABLE WHICH FAILS=',I3)
126    GO TO 100
127  C
128  C     SINCE THE INTEGRATION HERE HAS FAILED( AND RECTIFICATION MEASURES ARE
129  C     REQUIRED )WE SIMPLY MOVE ON TO THE NEXT RUN.
130  C
131 30  WRITE(6,31)
132 31  FORMAT('1',//////////,20X,'*****')
133    *****')
134    COLLE=Y(2)*Y(2)
135    Y(1)=Y(1)*R1
136    Y(2)=Y(2)*R1
137    E=S*R2
138    WRITE(6,444)
139 444  FURMAT(20X,'*',78X,'*',/,20X,'*',78X,'*')
140    WRITE(6,440)
141 440  FORMAT(20X,'*',31X,'ULTIMATE VALUES',32X,'*')
142    WRITE(6,445)
143 445  FURMAT(20X,'*',78X,'*',/,20X,'*',78X,'*')
144    WRITE(6,441)Y(1),Y(2)
145 441  EOPMAT(20X,'*',7X,'VERTICAL DISTANCE=',F9.3,10X,'HORIZONTAL DISTAN
146    CE=',F),3.5X,'*')
147    WRITE(6,446)
148 446  FURMAT(20X,'*',78X,'*',/,20X,'*',78X,'*')
149    WRITE(6,442)F,X
150 442  FURMAT(20X,'*',7X,'SEPARATION=',F9.3,17X,'TIME=',F9.3,20X,'*')
151    WRITE(6,447)
152 447  FURMAT(20X,'*',78X,'*',/,20X,'*',78X,'*')
153    WRITE(6,500)COLLE
154 500  FURMAT(20X,'*',24X,'COLLISION EFFICIENCY=',E9.3,24X,'*')
155    WRITE(6,401)
156 401  FURMAT(20X,'*',78X,'*',/,20X,'*',78X,'*')
157    WRITE(6,443)
158 443  FURMAT(20X,'*****')
159    ?*****')
160    WRITE(6,448)
161 448  FURMAT(////////,20X,'NOTE:',8X,'DISTANCES AND SEPARATION ARE IN MICR
162    SONS')
163    WRITE(6,449)
164 449  FURMAT(17X,'-----',7X,'TIME IS DIMENSIONLESS (REFERENCE TIME=8U
165    BBLE RADIUS/BUBBLE TERMINAL VELOCITY )')
166    GO TO 100
167  C
168  C     AS THE FULL TRAJECTORY HAS NOW BEEN CHARTED, WE CAN MOVE ON TO THE NEXT
169  C     RUN.
170  C
171 40  WRITE(6,41)
172 41  FURMAT(///,40X,'RUN TERMINATED AS SEPARATION BECOMES NEGATIVE')
173    WRITE(6,42)
174 42  FURMAT(39X,'-----')

```

```

175      Y(1)=Y(1)*R1
176      Y(2)=Y(2)*R1
177      S=S*R2
178      WRITE(6,43)Y(1),Y(2),S
179 43    FORMAT(///,20X,'VERTICAL DISTANCE =',F8.3,10X,'HORIZONTAL DISTANCE
180      ?',F8.3,///,30X,'SEPARATION =',F8.3)
181      WRITE(6,44)
182 44    FORMAT(///,20X,'NOTE ::,10X,'ABOVE DISTANCES ARE IN MICRONS',/,19X,
183      a'-----')
184      GO TO 100
185  C
186  C      AGAIN RECTIFICATION IS REQUIRED, AS THE SEPARATION HAS BECOME NEGATIVE.
187  C      AND WE CONTINUE ON TO THE NEXT SET OF DATA.
188 50    Y(1)=Y(1)*R1
189      Y(2)=Y(2)*R1
190      S=S*R2
191      WRITE(6,52)Y(1),Y(2),S
192 52    FORMAT(///,40X,'LESS THAN 1% CHANGE IN VERTICAL DISTANCE ',/,20X
193      , 'VERTICAL DISTANCE =',F8.3,///,20X,'HORIZONTAL DISTANCE =',F8.3,///
194      ,20X,'SEPARATION =',F8.3,///,20X,'NOTE ::,10X,'ABOVE DISTANCES ARE
195      & IN MICRONS',/,19X,'-----')
196 100   CONTINUE
197 303   CONTINUE
198      STOP
199      END
200      SUBROUTINE MERSON(X,DELX,DX,DXMIN,IFAIL,ITS,N,L1,L2,L3,L4)
201  C      INTEGRATES FROM X TO (X+DELX)                                MERSN002
202  C      DX IS ESTIMATE FOR INTEGRATION STEP NECESSARY                MERSN003
203  C      DXMIN IS MINIMUM STEP LENGTH TO BE PERMITTED                 MERSN004
204  C      TOLKM IS REQUIRED ACCURACY                                     MERSN005
205  C      N IS NUMBER OF DEPENDENT VARIABLES                           MERSN006
206  C      CONTROL TRANSFERRED TO FIRST LABEL IF INTEGRATION FAILS: X AND Y(I) MERSN007
207  C      1 THEN CONTAIN NEW VALUES                                    MERSN008
208  C      CONTROL TRANSFERRED TO SECOND LABEL IF INTEGRATION FAILS: X AND MERSN009
209  C      2 Y(1) THEN CONTAIN MOST RECENT CORRECT VALUES              MERSN010
210  C      IN EITHER CASE, DX CONTAINS CURRENT STEP LENGTH              MERSN011
211      DIMENSION Y(10),YOLD(10),FK(5,10),DY(10),ERR(10)
212      COMMON /DEP/Y/GRAD/DY/ACC/TOLKM(10)
213      COMMON K(25,5),R1,R2,S,B,RATIO,TUL
214      REAL K
215      TOL1=80.
216      ITS=0
217      FINTS=DELX/DX+0.5                                                MERSN016
218      INTS=IFIX(FINTS)                                                MERSN017
219      IF(INTS.LT.1)INTS=1                                             MERSN018
220      DX=DELX/INTS                                                    MERSN019
221      FMULT=DX/3.                                                     MERSN020
222      GO TO 4                                                         MERSN021
223  C      ERROR CHECK                                                 MERSN022
224  I      DO 172 I=1,2
225      IF(ERR(I).GT.(TOLKM(I)*5.0)) GO TO 20
226 172   CONTINUE
227      DO 173 I=1,2
228      IF(ERR(I).GT.(TOLKM(I)/32.)) GO TO 174
229 173   CONTINUE
230      GO TO 21
231 174   CONTINUE
232  C      INTEGRATION SATISFACTORY: CALCULATE NEW POINTS              MERSN025

```



```

291 C   MAIN INTEGRATION PROCESS STARTS HERE ****           MERSN063
292 C   ADVANCE X BY DX           MERSN064
293 9   CALL DERIVS(X,N,L4)
294   IF(L4.EQ.40) RETURN 4
295   DO 18 IS=1,5
296   GO TO (31,30,32,33,30),IS           MERSN066
297   31 X=X+FMULT           MERSN067
298   GO TO 30           MERSN068
299   32 X=X+0.5*FMULT           MERSN069
300   GO TO 30           MERSN071
301   33 X=XOLD+DX           MERSN072
302 C   UPDATE Y(I)           MERSN073
303   DO 10 I=1,N           MERSN074
304   FK(IS,I)=FMULT*DY(I)           MERSN075
305   GO TO (11,12,13,14,10),IS           MERSN076
306 C   PREDICTOR AT (X+DX/3.)           MERSN077
307   11 Y(I)=YOLD(I)+FK(1,I)           MERSN078
308   GO TO 10           MERSN079
309 C   CORRECTOR FOR (X+DX/3.)           MERSN080
310   12 Y(I)=YOLD(I)+0.5*(FK(1,I)+FK(2,I))           MERSN081
311   GO TO 10           MERSN082
312 C   ADVANCE TO (X+DX/2.)           MERSN083
313   13 Y(I)=YOLD(I)+0.375*FK(1,I)+1.125*FK(3,I)           MERSN084
314   GO TO 10           MERSN085
315 C   ADVANCE TO (X+DX)           MERSN086
316   14 Y(I)=YOLD(I)+1.5*FK(1,I)-4.5*FK(3,I)+6.0*FK(4,I)           MERSN087
317   10 CONTINUE           MERSN088
318   IF(IS.EQ.5) GO TO 16           MERSN089
319 C   EVALUATE DERIVATIVES           MERSN090
320   CALL DERIVS(X,N,L4)
321   IF(L4.EQ.40) RETURN 5
322   GO TO 18           MERSN092
323 C   ON LAST INTEGRATION, EVALUATE ERROR           MERSN093
324 16   DO 17 I=1,2
325 17   ERR(I)=ABS(FK(1,I)-4.5*FK(3,I)+4.0*FK(4,I)-0.5*FK(5,I))
326   18 CONTINUE           MERSN099
327   GO TO 1           MERSN100
328           MERSN101
329 C
330 C   DERIVS IS THE SUBPROGRAM WHICH CALCULATES THE DIFFERENTIALS DY(I)'S
331 C   GIVEN Y(I)'S AND X.
332 C
333   SUBROUTINE DERIVS(X,N,L4)
334   DIMENSION Y(10),DY(10),T(30)
335   COMMON /DEP/Y/GRAD/DY/ACC/TOLKM(10)
336   COMMON K(25,5),R1,R2,S,B,RATIO,TOL
337   REAL K
338   R=SQRT((Y(1)*Y(1)+Y(2)*Y(2)))
339   COST=Y(1)/R
340   SINT=Y(2)/R
341   S=R*R1/R2-R1/R2-1.
342   IF(S.LE.0.0) GO TO 10
343   SLOG=ALOG10(S)
344   SLO=ALOG(S)
345   DO 1 I=1,4
346   T(I)=K(I,1)+K(I,2)*SLO+K(I,3)*SLO**2+K(I,4)*SLO**3+K(I,5)*SLO**4
347   T(I)=EXP(T(I))
348   IF(I.EQ.1) GO TO 3

```

```

349 IF(I.F0.4) GO TO 3
350 GO TO 1
351 3 T(1)=-T(1)
352 1 CONTINUE
353 DO 2 I=5,20
354 T(1)=K(I,1)+K(I,2)*SLOG+K(I,3)*SLOG**2+K(I,4)*SLOG**3
355 2 CONTINUE
356 P=((T(3)+T(4)-B*(T(1)+T(2)))/(T(1)*T(4)-T(2)*T(3)))*COST
357 Q=((T(15)*T(20)-T(19)*T(16))*(T(9)+T(10)-(T(5)+T(6))*B)
358 ? +(T(7)*B-T(11))*(T(20)*(T(13)+T(14))-T(16)*(T(17)+T(18)))
359 ? +(T(8)*B-T(12))*(-T(19)*(T(13)+T(14))+T(15)*(T(17)+T(18))))*SINT
360 ? /((T(15)*T(20)-T(19)*T(16))*(T(5)*T(10)-T(9)*T(6))
361 ? +(T(11)*T(20)-T(19)*T(12))*(T(13)*T(6)-T(5)*T(14))
362 ? +(T(11)*T(16)-T(15)*T(12))*(T(5)*T(18)-T(17)*T(6))
363 ? +(T(7)*T(20)-T(19)*T(8))*(T(7)*T(14)-T(13)*T(10))
364 ? +(T(7)*T(16)-T(15)*T(8))*(T(17)*T(10)-T(9)*T(18))
365 ? +(T(7)*T(12)-T(11)*T(8))*(T(13)*T(18)-T(17)*T(14)))
366 DY(1)=-P*COST-Q*SINT
367 DY(2)=-P*SINT+Q*COST
368 RATIO=DY(2)/DY(1)
369 L4=0
370 RETURN I
371 10 L4=40
372 C
373 C L4=40 INDICATES THAT SEPARATION HAS BECOME NEGATIVE, AND RETURNS
374 C TO SUBROUTINE MERSON.
375 C
376 RETURN 2
377 END

```

Exhibit D.2

VISCOUS INTERACTION MODEL; SAMPLE OUTPUT WITH  
BACKWARDS INTEGRATION

RUN NUMBER 253

R1= 36.00 MICRONS

R2= 7.20 MICRONS

R1/R2 = 5.00

DENSITY OF PARTICLE = 2.50 GMS/ML

INITIAL SEPARATION = 0.500 MICRONS

LIMITING DY(2)/DY(1) = -0.10E-05

TOLKM = 0.0100/R1

INITIAL Y(1)/Y(2) = 0.0010

VERTICAL DISTANCE	HORIZONTAL DISTANCE	SEPARATION	TIME
2.089	43.651	0.501	0.250
4.125	43.508	0.503	0.500
6.147	43.273	0.508	0.750
8.145	42.948	0.514	1.000
10.113	42.536	0.522	1.250
12.280	41.973	0.533	1.531
14.838	41.157	0.550	1.872
17.800	39.993	0.576	2.284
21.144	38.375	0.615	2.779
24.791	36.200	0.675	3.366

Vertical Distance Horizontal Distance Separation Time

Weight - Unadjusted, Horizontal, Feet

28.597	33.402	0.772	4.055
32.377	29.997	0.937	4.849
35.978	26.106	1.250	5.748
39.456	21.961	1.950	6.748
43.499	17.894	3.826	7.844
50.379	14.344	9.205	9.052
64.662	11.613	22.500	10.451
93.363	9.578	50.653	12.248
148.858	7.989	105.870	14.841
256.303	6.730	213.190	18.976
470.611	5.809	427.444	26.095
926.253	5.340	883.065	39.168



Exhibit D.3

VISCOUS INTERACTION MODEL; COMPUTER PROGRAM  
FOR FORWARD INTEGRATION

```

1     DIMENSION Y(10),DY(10)
2     COMMON /DEP/Y/GRAD/DY/ACC/TOLKM(10)
3     COMMON K(25,5),R1,R2,S,H,RATIO,TOL,Y2MIN,YIN
4     REAL K
5     READ(5,999)MO,LRN
6     999 FORMAT(11,15)
7     DO 303 LA=1,40
8     DO 1 I=1,20
9     READ(5,2)(K(I,J),J=1,5)
10    2   FORMAT(5F15.9)
11    1   CONTINUE
12     READ(5,998)M
13     998 FOPMAT(12)
14     DO 100 L=1,M
15     L=L+LRN
16     L=L+M*(LA-1)
17     WRITE(6,253)L
18     253 FOPMAT('1',////////.60X,'RUN NUMBER',14)
19     L=L-M*(LA-1)
20     L=L-LRN
21     WRITE(6,274)
22     274 FOPMAT(59X,'-----')
23     READ(5,210)R1,R2,E,RHO2,Y(1),Y(2)
24     210 FOPMAT(6F10.5)
25     RAT=R1/R2
26     TOL=-.000001
27     FAC1=.01
28     FAC=.001
29     WRITE(6,211)R1,R2,RAT,RHO2
30     211 FOPMAT(///.20X,'R1=',F6.2,' MICRONS',///.20X,'R2=',F6.2,' MICRONS',
31     ;///.20X,'R1/R2 =',F5.2,///.20X,'DENSITY OF PARTICLE =',F6.2,' GMS/ML
32     **)
33     WRITE(6,212)Y(1),Y(2)
34     212 FOPMAT(/2JX,'INITIAL Y(1) =',F9.3,' MICRONS'//
35     ?   20X,'INITIAL Y(2) =',F6.3,' MICRONS')
36     WRITE(6,101)
37     101 FOPMAT(////////.20X,'VERTICAL DISTANCE',10X,'HORIZONTAL DISTANCE',10X
38     X,'SEPARATION',16X,'TIME')
39     RHO1=.0012928
40    C
41    C   DENSITY OF AIR.
42    C
43    C   RHO1=1.30
44    C
45    C   DENSITY OF FLUID.
46    C
47    C   UF=0.01
48    C
49    C   VISCOSITY OF FLUID.
50    C
51     Y(2)=Y(2)/R1
52     Y2MIN=0.05/R1
53     Y(1)=Y(1)/R1
54     YIN=-Y(1)
55     UIT=-((2*(RHO1-RHOF)*R1*R1*981)/(9*UF*10**E))
56     B=(R2*R2*(RHO1-RHO2))/(R1*R1*(RHO1-RHOF))
57     X=C*0
58     TOLKM(1)=FAC1/R1

```

1968-1969 University Microfilms

```

59     TOLKM(2)=FAC1/R1
60     N=2
61     DX=Y(1)/10
62     J=1
63     15 AY=ABS(Y(1))
64     DXMIN=AY/20000
65     IF(AY.GT,0.1) GO TO 16
66     DELX=2*AY
67     GO TO 13
68     16 DELX=AY/2
69     13 YD1=Y(1)
70     C
71     C     AT THIS POINT WE HAVE DEFINED ALL THE QUANTITIES THAT ARE NECESSARY
72     C     FOR THE INTEGRATION OF THE DEPENDENT VARIABLES Y(1) TO Y(2), WITH
73     C     RESPECT TO X THE INDEPENDENT VARIABLE OVER THE RANGE X TO X+DELX.
74     C     ACCORDINGLY THE CURRENT VALUES OF Y(1), Y(2) ARE HANDED OVER TO
75     C     MERSON WHICH THEN RETURNS THE VALUES OF Y(1), Y(2) AT X+DELX.
76     C
77     CALL MERSON(X,DELX,LX,DXMIN,IFAIL,ITS,N,L1,L2,L3,L4)
78     YTEST=Y(1)*R1
79     IF(YTEST.GE,0.01) GO TO 54
80     IF(YTEST.LE,-0.01) GO TO 54
81     Y(1)=-0.01
82     54 CONTINUE
83     IF(L4.EQ,40) GO TO 40
84     IF(L1.EQ,10) GO TO 10
85     IF(L2.EQ,20) GO TO 20
86     IF(L3.EQ,30) GO TO 30
87     10 STEP=DX*0.1/R1
88     Y(1)=Y(1)*R1
89     Y(2)=Y(2)*R1
90     S=S*R2
91     WRITE(6,12)Y(1),Y(2),S,X
92     12 FORMAT(///,27X,F9.3,19X,F8.3,15X,F9.3,16X,F8.3)
93     Y(1)=Y(1)/R1
94     Y(2)=Y(2)/R1
95     S=S/R2
96     GO TO 15
97     C
98     C     WE RETURN TO 15 AS THE WHOLE TRAJECTORY IS NOT YET COMPLETED.
99     C
100    30 WRITE(6,21)
101    21 FORMAT(///,5X,'SMALLER DXMIN OR LARGER TOLKM REQUIRED FOR SUCCESSFUL
102    21 INTEGRATION')
103    Y(1)=Y(1)*R1
104    Y(2)=Y(2)*R1
105    S=S*R2
106    WRITE(6,22)Y(1),Y(2),S,IFAIL
107    22 FORMAT(///,10X,'Y CO-ORDINATE =',F8.5,10X,'X CO-ORDINATE =',F8.5,10X,
108    22 'SEPARATION =',F8.5,10X,'THE VARIABLE WHICH FAILS=',I3)
109    GO TO 100
110    C
111    C     SINCE THE INTEGRATION HERE HAS FAILED( AND RECTIFICATION MEASURES ARE
112    C     REQUIRED )WE SIMPLY MOVE ON TO THE NEXT RUN.
113    C
114    30 WRITE(6,311)
115    311 FORMAT(///,40X,'TRAJECTORY COMPLETED')
116    GO TO 100

```

```

117 31  FORMAT('1',//////////,20X,'*****')
118      $*****')
119      COLLE=Y(2)*Y(2)
120      Y(1)=Y(1)*P1
121      Y(2)=Y(2)*P1
122      E=S*R2
123      WRITE(6,444)
124 444  FORMAT(20X,'*',78X,'*',/,20X,'*',78X,'*')
125      WRITE(6,440)
126 440  FORMAT(20X,'*',31X,'ULTIMATE VALUES',32X,'*')
127      WRITE(6,445)
128 445  FORMAT(20X,'*',78X,'*',/,20X,'*',78X,'*')
129      WRITE(6,441)Y(1),Y(2)
130 441  FORMAT(20X,'*',7X,'VERTICAL DISTANCE=',F9.3,10X,'HORIZONTAL DISTAN
131      -CE=',F9.3,5X,'*')
132      WRITE(6,446)
133 446  FORMAT(20X,'*',78X,'*',/,20X,'*',78X,'*')
134      WRITE(6,442)E,X
135 442  FORMAT(20X,'*',7X,'SEPARATION=',F9.3,17X,'TIME=',F9.3,20X,'*')
136      WRITE(6,447)
137 447  FORMAT(20X,'*',78X,'*',/,20X,'*',78X,'*')
138      WRITE(6,500)COLLE
139 500  FORMAT(20X,'*',24X,'COLLISION EFFICIENCY=',F9.3,24X,'*')
140      WRITE(6,401)
141 401  FORMAT(20X,'*',78X,'*',/,20X,'*',78X,'*')
142      WRITE(6,443)
143 443  FORMAT(20X,'*****')
144      ?*****')
145      WRITE(6,448)
146 448  FORMAT(////////,20X,'NOTE:',8X,'DISTANCES AND SEPARATION ARE IN MICR
147      SONS')
148      WRITE(6,449)
149 449  FORMAT(19X,'-----',7X,'TIME IS DIMENSIONLESS (REFERENCE TIME=BU
150      BBLE RADIUS/BUBBLE TERMINAL VELOCITY)')
151      GO TO 100
152  C
153  C      AS THE FULL TRAJECTORY HAS NOW BEEN CHARTED, WE CAN MOVE ON TO THE NEXT
154  C      RUN.
155  C
156 40  WRITE(6,41)
157 41  FORMAT(///,40X,'PARTICLE WITHIN .75 MICRONS OF BUBBLE AXIS')
158      WRITE(6,42)
159 42  FORMAT(30X,'-----')
160      Y(1)=Y(1)*R1
161      Y(2)=Y(2)*R1
162      S=S*R2
163      WRITE(6,43)Y(1),Y(2),S
164 43  FORMAT(//,20X,'VERTICAL DISTANCE =',F8.3,10X,'HORIZONTAL DISTANCE
165      ?=',F8.3,///,30X,'SEPARATION =',F8.3)
166      WRITE(6,44)
167 44  FORMAT(//,20X,'NOTE :',10X,'ABOVE DISTANCES ARE IN MICRONS',/,19X,
168      @'-----')
169      GO TO 100
170  C
171  C      AGAIN RECTIFICATION IS REQUIRED, AS THE SEPARATION HAS BECOME NEGATIVE,
172  C      AND WE CONTINUE ON TO THE NEXT SET OF DATA.
173 50  Y(1)=Y(1)*R1
174      Y(2)=Y(2)*R1

```

```

175      S=S*R2
176      WRITE(5,52)Y(1),Y(2),S
177 52   FORMAT(///,40X,'LESS THAN 1% CHANGE IN VERTICAL DISTANCE ',///,20X
178      -,'VERTICAL DISTANCE =',F9.3,///,20X,'HORIZONTAL DISTANCE =',F9.3,///
179      ,20X,'SEPARATION =',F9.3,///,20X,'NOTE :',10X,'ARCVF DISTANCES ARE
180      & $ MICRONS',/,19X,('-----'))
181 100  CONTINUE
182 303  CONTINUE
183      STOP
184      END
185      SUBROUTINE MERSON(X,DELX,DX,DXMIN,IFAIL,ITS,N,L1,L2,L3,L4)
186 C      INTEGRATES FROM X TO (X+DELX)                                MERSON02
187 C      DX IS ESTIMATE FOR INTEGRATION STEP NECESSARY              MERSON03
188 C      DXMIN IS MINIMUM STEP LENGTH TO BE PERMITTED              MERSON04
189 C      TOLKM IS REQUIRED ACCURACY                                  MERSON05
190 C      N IS NUMBER OF DEPENDENT VARIABLES                        MERSON06
191 C      CONTROL TRANSFERRED TO FIRST LABEL IF INTEGRATION FAILS: X AND Y(I) MERSON07
192 C      1 THEN CONTAIN NEW VALUES                                MERSON08
193 C      CONTROL TRANSFERRED TO SECOND LABEL IF INTEGRATION FAILS: X AND Y(I) THEN CONTAIN MOST RECENT CORRECT VALUES
194 C      IN EITHER CASE, DX CONTAINS CURRENT STEP LENGTH          MERSON10
195 C      DIMENSION Y(10),YOLD(10),FK(5,10),DY(10),DFR(10)
196      COMMON /DEP/Y/GRAC/DY/ACC/TOLKM(10)
197      COMMON K(25,5),R1,R2,S,B,RATIO,TOL,YRMIN,YIN
198      REAL K
199      TOL1=30.
200      IFS=0
201      FINTS=DELX/DX*0.5
202      INTS=IFIX(FINTS)
203      IF(INTS.LT.1)INTS=1
204      DX=DELX/INTS
205      FMULT=DX/3.
206      GO TO 4
207 C      ERROR CHECK
208 C      DO 172 I=1,2
209 C      IF(ERR(I).GT.(TOLKM(I)*5.0)) GO TO 20
210 C      CONTINUE
211 C      DO 173 I=1,2
212 C      IF(ERR(I).GT.(TOLKM(I)/32.0)) GO TO 174
213 C      CONTINUE
214 C      GO TO 21
215 C      CONTINUE
216 C      INTEGRATION SATISFACTORY: CALCULATE NEW POINTS
217 C      DO 2 I=1,N
218 C      Y(I)=YOLD(I)+0.5*FK(1,I)+2.0*FK(4,I)+0.5*FK(5,I)
219 C      ITS=ITS+1
220 C      IF(Y(I).LT.YIN) GO TO 202
221 C      GO TO 203
222 C      L3=30
223 C      L2=0
224 C      L1=0
225 C      L4=0
226 C      RETURN 1
227 C      IF(INTS.EQ.1) GO TO 201
228 C      GO TO 6
229 C      L1=10
230 C      L2=0
231 C      L3=0
232

```



```

291      GO TO 10
292 C      CORRECTOR FOR (X+DX/3,)
293      12 Y(I)=YOLD(I)+.5*(FK(1,I)+FK(2,I))
294      GO TO 10
295 C      ADVANCE TO (X+DX/2,)
296      13 Y(I)=YOLD(I)+.375*FK(1,I)+1.125*FK(3,I)
297      GO TO 10
298 C      ADVANCE TO (X+DX)
299      14 Y(I)=YOLD(I)+1.5*FK(1,I)-4.5*FK(3,I)+6.0*FK(4,I)
300      10 CONTINUE
301      IF (IS.EQ.5) GO TO 16
302 C      EVALUATE DERIVATIVES
303      CALL DERIVS(X,N,L4)
304      IF (L4.EQ.40) RETURN 5
305      GO TO 14
306 C      ON LAST INTEGRATION, EVALUATE ERROR
307      16 DO 17 I=1,2
308      17 ERR(I)=ABS(FK(1,I)-4.5*FK(3,I)+4.0*FK(4,I)-6.5*FK(5,I))
309      18 CONTINUE
310      GO TO 1
311      END
312 C
313 C      DERIVS IS THE SUBPROGRAM WHICH CALCULATES THE DIFFERENTIALS DY(I)'S
314 C      GIVEN Y(I)'S AND X.
315 C
316      SUBROUTINE DERIVS(X,N,L4)
317      DIMENSION Y(10),DY(10),T(30)
318      COMMON /DERV/Y/GRAL/DY/ACC/TOL/KV(10)
319      COMMON K(25,5),R1,R2,S,R,RATIO,TOL,Y2MIN,YIN
320      REAL X
321      R=SQRT((Y(1)+Y(1)+Y(2)+Y(2)))
322      COST=ABS(Y(1))/R
323      SINT=Y(2)/R
324      S=R*(R1/R2-1)/R2-1.
325      IF (Y(2).LT.Y2MIN) GO TO 100
326      SLOG=ALOG10(S)
327      SLC=ALOG(S)
328      DO 1 I=1,4
329      T(I)=K(I,1)+K(I,2)*SLC+K(I,3)*SLOG**2+K(I,4)*SLC**3+K(I,5)*SLOG**4
330      T(I)=EXP(T(I))
331      IF (I.EQ.1) GO TO 3
332      IF (I.EQ.4) GO TO 3
333      GO TO 1
334      3 T(I)=-T(I)
335      1 CONTINUE
336      DO 2 I=5,20
337      T(I)=K(I,1)+K(I,2)*SLOG+K(I,7)*SLOG**2+K(I,4)*SLC**3
338      2 CONTINUE
339      P=((T(3)+T(4)-H*(T(1)+T(2)))/(T(1)*T(4)-T(2)*T(3)))*COST
340      Q=((T(1)-T(20)-T(19)*T(14))+(T(9)+T(12)-(T(5)+T(6))+H
341      ? +(T(7)+H-T(11))*T(20)*(T(13)+T(14))-T(10)*(T(17)+T(18)))
342      ? +(T(8)+H-T(12))*(-T(19)*(T(13)+T(14))+T(15)*(T(17)+T(18))))*SINT
343      ? /((T(15)+T(20)-T(19)*T(14))-(T(5)*T(10)-T(9)*T(6))
344      ? +(T(11)+T(20)-T(19)*T(12))*(T(13)+T(6)-T(5)*T(14))
345      ? +(T(11)*T(16)-T(15)*T(12))*(T(7)-T(13)-T(17)*T(6))
346      ? +(T(7)*T(20)-T(19)*T(4))*(T(9)+T(14))-T(13)*T(10))
347      ? +(T(7)+T(16)-T(15)*T(4))*(T(17)+T(10))-T(9)*T(18))
348      ? +(T(7)*T(12)-T(11)*T(8))*(T(13)+T(18)-T(17)*T(14)))

```

```

MERSNC79
MERSNC80
MERSNC81
MERSNC82
MERSNC83
MERSNC84
MERSNC85
MERSNC86
MERSNC87
MERSNC88
MERSNC89
MERSNC90
MERSNC92
MERSNC93
MERSNC99
MERSNC100
MERSNC101

```

```
349      DY(1)=-P*COST-Q*SINT
350      DY(2)=-P*SINT+Q*COST
351      DY(1)=-DY(1)
352      IF(Y(1).LE.0.0) GO TO 4
353      DY(2)=-DY(2)
354      4 RATIO=DY(2)/DY(1)
355      L4=0
356      RETURN1
357 10    L4=40
358 C
359 C      L4=40 INDICATES THAT SEPARATION HAS BECOME NEGATIVE. AND RETURNS
360 C      TO SUBROUTINE MEWSON.
361 C
362      RETURN 2
363      END.
```

Exhibit D.4

VISCOUS INTERACTION MODEL; SAMPLE OUTPUT WITH  
FORWARD INTEGRATION

RUN NUMBER 341

R1= 22.00 MICRONS

R2= 7.33 MICRONS

R1/R2 = 3.00

DENSITY OF PARTICLE = 1.05 GMS/ML

INITIAL Y(1) = 880.000 MICRONS

INITIAL Y(2) = 0.500 MICRONS

VERTICAL DISTANCE	HORIZONTAL DISTANCE	SEPARATION	TIME
464.981	0.515	435.644	20.000
265.128	0.554	235.788	30.568
160.163	0.608	130.828	36.593
102.753	0.672	73.385	40.233
70.599	0.746	41.254	42.569
52.330	0.835	23.003	44.173
41.936	0.947	12.623	45.363
36.146	1.089	6.845	46.316
33.067	1.270	3.774	47.137
31.515	1.492	2.228	47.889
30.750	1.755	1.472	48.605



11.978	27.449	0.61 <sup>a</sup>	62.167
10.378	28.093	0.61 <sup>a</sup>	62.439
8.934	28.585	0.61 <sup>a</sup>	62.675
7.653	28.954	0.61 <sup>a</sup>	62.878
6.532	29.227	0.61 <sup>a</sup>	63.052
5.559	29.428	0.61 <sup>a</sup>	63.200
4.721	29.573	0.61 <sup>a</sup>	63.327
4.004	29.679	0.61 <sup>a</sup>	63.434
3.392	29.755	0.61 <sup>a</sup>	63.525
2.871	29.810	0.61 <sup>a</sup>	63.607
2.428	29.849	0.61 <sup>a</sup>	63.667
2.053	29.877	0.61 <sup>a</sup>	63.723
0.781	29.937	0.61 <sup>a</sup>	63.909
0.296	29.946	0.61 <sup>a</sup>	63.980
0.112	29.947	0.61 <sup>a</sup>	64.007
0.043	29.948	0.61 <sup>a</sup>	64.017
0.016	29.947	0.61 <sup>a</sup>	64.021
-0.220	29.947	0.61 <sup>a</sup>	64.023
-0.357	29.946	0.61 <sup>a</sup>	64.043
-0.578	29.943	0.61 <sup>a</sup>	64.075
-0.937	29.933	0.61 <sup>a</sup>	64.128
-1.518	29.910	0.61 <sup>a</sup>	64.213

-2.456	29.847	0.618	64.351
-2.835	29.813	0.618	64.407
-3.271	29.769	0.618	64.471
-3.771	29.709	0.618	64.545
-4.346	29.631	0.618	64.631
-5.005	29.527	0.618	64.730
-5.756	29.389	0.618	64.844
-6.612	29.209	0.618	64.974
-7.581	28.972	0.618	65.125
-8.671	28.665	0.617	65.297
-9.888	28.268	0.617	65.494
-11.232	27.761	0.617	65.719
-12.697	27.123	0.617	65.974
-14.267	26.330	0.617	66.262
-15.919	25.366	0.617	66.587
-17.613	24.220	0.617	66.949
-19.306	22.893	0.617	67.349
-20.946	21.402	0.616	67.788
-22.483	19.780	0.616	68.264
-23.877	18.072	0.615	68.775
-25.099	16.331	0.614	69.317
-26.137	14.610	0.613	69.888

LIBRARY UNIVERSITY OF CALIFORNIA

-26.993	12.955	0.611	70.482
-27.683	11.401	0.608	71.095
-28.225	9.971	0.604	71.724
-28.642	8.679	0.598	72.366
-28.958	7.525	0.590	73.017
-29.191	6.506	0.577	73.675
-29.358	5.613	0.560	74.338
-29.471	4.837	0.536	75.005
-29.541	4.165	0.503	75.675
-29.574	3.586	0.461	76.347
-29.579	3.090	0.410	77.019
-29.566	2.665	0.356	77.691
-29.546	2.303	0.305	78.363
-29.529	1.993	0.266	79.034
-29.520	1.727	0.241	79.706
-29.519	1.497	0.227	80.376
-29.522	1.299	0.220	81.047
-29.525	1.127	0.217	81.718
-29.529	0.978	0.215	82.389
-29.533	0.849	0.215	83.060
-29.535	0.737	0.215	83.732
-29.538	0.639	0.214	84.403

1948 JAN 20 10 10 AM '50

-29.539	0.555	0.214	85.074
-29.540	0.482	0.214	85.745
-29.541	0.418	0.214	86.417
-29.542	0.363	0.214	87.088
-29.543	0.315	0.214	87.760
-29.543	0.273	0.214	88.431
-29.543	0.237	0.214	89.102
-29.544	0.206	0.214	89.774
-29.544	0.178	0.214	90.445
-29.544	0.155	0.214	91.117
-29.544	0.134	0.214	91.788
-29.544	0.117	0.214	92.460
-29.544	0.101	0.214	93.131
-29.544	0.088	0.214	93.803
-29.544	0.076	0.214	94.474
-29.544	0.066	0.214	95.145
-29.544	0.057	0.214	95.817

PARTICLE WITHIN .05 MICRONS OF BUBBLE AXIS

VERTICAL DISTANCE = -29.544

HORIZONTAL DISTANCE = 0.050

SEPARATION = 0.214

NOTE :

ABOVE DISTANCES ARE IN MICRONS

Exhibit D.5

COLLISION EFFICIENCY WITH UNSTEADY  
STATE DRAG TERMS;  
COMPUTER PROGRAM

```

0001 DIMENSION Y(10),DY(10)
0002 COMMON /DEF/Y/GRAD/DY/ACC/TOLKM(10)
0003 COMMON FLU,K,G,RPS,RHOPF,B,FFIN,MH,S,NUM,L1,L2,L3,L4,L5,NSS
0004 INTEGER FLU*
0005 INTEGER DN,0,DP
0006 REAL K
0007 READ(5,7)HIGH,HIGL,M0,M01
0008 3 FORMAT(A1,10X,A1,10X,I2,10X,I3)
0009 TOLY=.005
0010 FAC1=0.001
0011 FAC2=0.001
0012 DC 100 L=1,M0
0013 MOT=0
0014 JP=0
0015 READ(5,5)G,K,RHOPF,RPS,YIN,FLOW,NSS
0016 5 FORMAT(SF10.4,I1,9X,I1)
0017 LIN=L+M0-1
0018 176 WRITE(6,173)LIN
0019 173 FORMAT('1',//////////%60X,'PUN NUMBER',I4)
0020 WRITE(6,174)
0021 174 FORMAT(5-X,'-----')
0022 IF(NSS.NE.1) GO TO 178
0023 WRITE(6,177)
0024 177 FORMAT(//,20X,'STEADY STATE DRAG ONLY')
0025 GO TO 180
0026 174 IF(NSS.E.2) GO TO 1178
0027 WRITE(6,179)
0028 179 FORMAT(//,20X,'UNSTEADY STATE DRAG TERMS INCLUDED')
0029 GO TO 180
0030 1178 WRITE(6,1179)
0031 1179 FORMAT(//,20X,'PRESSURE GRADIENT TERM INCLUDED')
0032 180 IF(FLU.NE.0) GO TO 171
0033 WRITE(6,405)K,G,RPS
0034 405 FORMAT(////,20X,'FLU# TYPE= POTENTIAL',/,32X,'-----',/,20X,'K
_=.F7.3,/,20X,'G=.F7.3,/,20X,'PARTICLE RADIUS/BUBBLE RADIUS=.F
67.3)
0035 GO TO 172
0036 171 WRITE(6,407)K,G,RPS
0037 407 FORMAT(////,20X,'FLU# TYPE= STOKES ',/,32X,'----- ',/,20X,'K
_=.F7.3,/,20X,'G=.F7.3,/,20X,'PARTICLE RADIUS/BUBBLE RADIUS=.F
67.3)
0038 172 CONTINUE
0039 WRITE(6,406)RHOPF,TOLY,FAC1
0040 406 FORMAT(//,20X,'FLUID DENSITY/PARTICLE DENSITY=.F7.3,/,20X,'FRACTI
ONAL TOLERANCE ON Y(2)=.F8.4,/,20X,'INTEGRATION TOLERANCE=.F8.4
)
0041 WRITE(6,250)
0042 250 FORMAT(10X,////////,11X,'Y(2)C',15X,'H OR L',15X,'Y(1)F',15X,'Y(2)F
0',15X,'SEPARATION',15X,'TIME')
0043 WRITE(6,251)
0044 251 FORMAT(10X,'-----',13X,'-----',13X,'-----',13X,'-----',13
X,'-----',13X,'-----')
0045 NUM=0
0046 Y(2)=0.65

```

ORIGINAL DOCUMENT

```

0047      28      IF(OP.EQ.0) GO TO 128
0048      902      WRITE(6,902)
0049      900      FORMAT('1',////,11X,'Y(1)',20X,'Y(2)',16X,'SEPARATION',20X,'TIME'
          3,14X,'HX',14X,'HY')
0050      WRITE(6,901)
0051      901      FORMAT(10X,'-----',19X,'-----',14X,'-----',18X,'-----',1
          82X,'-----',12X,'-----')
0052      128      Y(1)=YIN
0053      YINT=Y(2)
0054      IF(YINT-LT.0.01) GO TO 100
0055      O=1
0056      ON=1
0057      HX=0.0
0058      HY=0.0
0059      NUM=NUM+1
0060      IF(NUM.EQ.1) GO TO 50
0061      RATIO=(Y2H-Y2L)/Y2H
0062      IF(RATIO.EQ.1) GO TO 50
0063      IF(RATIO.LT.TOLY) GO TO 70
0064      50      CONTINUE
0065      TOLKM(1)=FAC1
0066      TOLKM(2)=FAC1
0067      TOLKM(3)=FAC2
0068      TOLKM(4)=FAC2
0069      EFIN=0.001
0070      X=0.0
0071      N=4
0072      A=Y(1)*Y(1)+Y(2)*Y(2)
0073      B=SQRT(A)
0074      Z=1/B
0075      C=A-1
0076      D=2*A-3*Y(2)
0077      F=4**5.0
0078      S=B-1-RPS
0079      IF(OP.EQ.0) GO TO 128
0080      542      WRITE(6,18)Y(1),Y(2),S,X,HX,HY
0081      18      FORMAT(//,9X,F7.3,17X,F7.3,16X,F7.3,20X,F7.3,10X,F7.3,9X,F7.3)
0082      128      CONTINUE
0083      IF(FLOW.EQ.1) GO TO 80
0084      UX=-1+D/(2*F)
0085      GO TO 4
0086      80      UX=-1+Z+C*D/(4*F)
0087      4      Y(3)=UX-G
0088      Y(4)=0.0
0089      DX=Y(1)/20
0090      DXMIN=Y(1)/5000
          C
          C      INITIAL VALUES OF Y(3),Y(4),DX,DXMIN ARE SET HERE.
          C
0091      8      IF(Y(1).GT.3.00) GO TO 15
0092      IF(Y(1).GT.0.25) GO TO 415
0093      IF(Y(1).GT.0.025) GO TO 215
0094      DELX=Y(1)
0095      GO TO 13

```

```

0096      15      DELX=Y(1)/2
0097      GO TO 13
0098      415     DELX=Y(1)/4
0099      GO TO 13
0100      215     DELX=Y(1)/4
0101      13      CONTINUE
0102      L1=0
0103      CALL MERSON(X,DELX,DX,DXMIN,IFAIL,ITS,N,O,ON,HX,HY)

C
C      L1=10 INDICATES THAT INTEGRATION OVER THE INTERVAL X TO X+DELX HAS
C      BEEN SUCCESSFULLY COMPLETED.
C      L2=20 INDICATES THAT INTEGRATION OVER THE INTERVAL X TO X+DELX FAILED
C      DUE TO LARGE DXMIN OR SMALL TOLKM.
C      L3=30 OCCURS WHEN WE HAVE A GRAZING TRAJECTORY.
C      L4=40 OCCURS WHEN WE HAVE A HIGH TRAJECTORY.
C      L5=50 OCCURS WHEN WE HAVE A LOW TRAJECTORY.
C
0104      IF(L1.EQ.10) GO TO 10
0105      IF(L2.EQ.20) GO TO 20
0106      IF(L3.EQ.30) GO TO 30
0107      IF(L4.EQ.40) GO TO 40
0108      IF(L5.EQ.50) GO TO 51
0109      10      CONTINUE
0110      IF(OP.EQ.9) GO TO 29
0111      547     S=3-1-RPS
0112      WRITE(5,12)Y(1),Y(2),S,X,HX,HY
0113      12      FORMAT(//,9X,F7.3,17X,F7.3,16X,F7.3,20X,F7.3,10X,F7.3,9X,F7.3)
0114      20      GO TO 3

C
C      AS THE TRAJECTORY IS NOT COMPLETED YET, WE RETURN TO MERSON WITH
C      A NEW VALUE OF DELX.
C
0115      20      WRITE(5,21)
0116      21      FORMAT(//,5X,'SMALLER DXMIN OR LARGER TOLKM REQUIRED FOR SUCCESSFU
0117      22      WRITE(5,22)Y(1),Y(2),B,IFAIL
0118      22      FORMAT(//,10X,'Y CO-ORDINATE =',F9.6,10X,'X CO-ORDINATE =',F9.6,
0119      23      //,10X,'SEPARATION =',F9.6,10X,'THE VARIABLE WHICH FAILS=',I3)

C
C      AS THE INTEGRATION FAILS AT THE POINT X, WE SIMPLY STOP AT THIS
C      POINT AND CONTINUE WITH THE NEXT RUN.
C
0119      GO TO 100
0120      30      WRITE(5,31)
0121      31      FORMAT('1',////,20X,'SUCCESSFUL TRAJECTORY')
0122      32      WRITE(5,32)Y(1),Y(2),B
0123      33      FORMAT(//,10X,'VERTICAL DISTANCE=',F9.6,10X,'HORIZONTAL DISTANCE='
0124      34      //,F9.6,10X,'SEPARATION=',F9.6)

C
C      THE TRAJECTORY BEING SUCCESSFULLY PLOTTED, WE MOVE ON TO THE NEXT RUN.
C
0124      GO TO 100
0125      40      S=3-1-RPS
0126      IF(OP.EQ.1) GO TO 260

```

```

C
C      MOT=1 INDICATES THAT THE RATIO TEST (BETWEEN HIGH AND LOW VALUES OF
C      INITIAL Y(2) ) HAS BEEN SUCCESSFUL, AND THAT THE PROCEDURE FOR LOCATING
C      A NEW VALUE OF Y(2) CAN STOP.
C
0127      WRITE(6,41)YINT,HIGH,Y(1),Y(2),S,X
0128      41  FORMAT(//,10X,F7.4,16X,A1,14X,F9.3,12X,F9.3,14X,F9.3,15X,F7.3)
0129      Y2H=YINT
C
C      SET THE HIGH VALUE OF Y(2) AT THE INITIAL VALUE OF Y(2).
C
0130      IF(NUM.LE.1) GO TO 200
C
C      ON THE FIRST LOOP GO TO 200.
C
0131      GO TO 201
0132      200  Y2L=0.0
C
C      ON THE FIRST LOOP, SINCE A VALUE FOR Y2L HAS NOT BEEN GENERATED, WE
C      SET IT EQUAL TO ZERO.
C
0133      201  Y(2)=(Y2L+Y2H)*0.5
C
C      A NEW VALUE OF INITIAL Y(2) IS GENERATED BY HALVING THE DISTANCE
C      BETWEEN THE LOW AND THE HIGH VALUES.
C
0134      GO TO 28
0135      51  S=9-1/RPS
0136      IF(MOT.EQ.1) GO TO 260
0137      WRITE(6,52)YINT,HIGH,Y(1),Y(2),S,X
0138      52  FORMAT(//,10X,F7.4,16X,A1,14X,F9.3,12X,F9.3,14X,F9.3,15X,F7.3).
C
C      WHEN WE HAVE A LOW TRAJECTORY, A SIMILAR PROCEDURE IS USED AS FOR A
C      HIGH TRAJECTORY EXCEPT THAT Y2L IS SET HERE INSTEAD OF Y2H.
C
0139      Y2L=YINT
0140      IF(NUM.LE.1) GO TO 202
0141      GO TO 203
0142      202  Y2H=2*Y2L
0143      203  Y(2)=(Y2L+Y2H)*0.5
0144      GO TO 29
0145      70  Y(2)=(Y2L+Y2H)*0.5
0146      DP=1
0147      MOT=1
C
C      WHEN THE RATIO TEST IS SATISFIED, WE GENERATE A NEW VALUE FOR Y(2) AND
C      OPEN THE SWITCHES FOR PRINT OUT BY SETTING DP=1 AND MOT=1 AND SENDING
C      THE PROGRAM BACK TO 28 WHERE THE TRAJECTORY IS THEN CHARTED.
C
0148      GO TO 28
C
C      WHEN THE FINAL TRAJECTORY IS PRINTED OUT, 260 TAKES OVER AND PRINTS OUT
C      THE COLLISION EFFICIENCY.
C

```





```

0001      SUBROUTINE MERSON(X,DELX,DX,DXMIN,IFAIL,ITS,N,D,CN,HX,HY)
          C      INTEGRATLS FROM X TO (X+DELX)
          C      DX IS ESTIMATE FOR INTEGRATION STEP NECESSARY
          C      DXMIN IS MINIMUM STEP LENGTH TO BE PERMITTED
          C      TOLKM IS REQUIRED ACCURACY
          C      N IS NUMBER OF DEPENDENT VARIABLES
          C      CONTROL TRANSFERRED TO FIRST LABEL IF INTEGRATION FAILS: X AND Y(I)M
          C      1 THEN CONTAIN NEW VALUES
          C      CONTROL TRANSFERRED TO SECOND LABEL IF INTEGRATION FAILS: X AND
          C      2Y(I) THEN CONTAIN MOST RECENT CORRECT VALUES
          C      IN EITHER CASE, DX CONTAINS CURRENT STEP LENGTH
          DIMENSION Y(10),YOLD(10),FK(5,10),DY(10),ERR(10)
          COMMON /DEP/Y/GRAD/DY/ACC/TOLKM(10)
          COMMON FLOW,K,G,RPS,RHOPF,B,CFIN,MH,S,NJM,L1,L2,L3,L4,L5,NSS
          INTEGER FLOW
          INTEGER DN,D,CP
          REAL K
          TOLK=0.001
          ITS=0
          FINTS=DELX/DX+0.5
          INTS=IFIX(FINTS)
          IF(INTS.LT.1)INTS=1
          DX=DELX/INTS
          FMULT=DX/3.
          GO TO 4
          C      ERROR CHECK
          DO 172 I=1,4
          0016      IF(ERR(I).GT.((TOLKM(I)*5.0)) GO TO 20
          0017      IF(ERR(I).GT.((TOLKM(I)/32.9)) GO TO 174
          0018      CONTINUE
          0019      DO 173 I=1,4
          0020      IF(ERR(I).GT.((TOLKM(I)/32.9)) GO TO 174
          0021      CONTINUE
          0022      GO TO 21
          0023      CONTINUE
          C      INTEGRATION SATISFACTORY: CALCULATE NEW POINTS
          3 DO 2 I=1,N
          0024      Y(I)=YOLD(I)+C.5*FK(1,I)+2.0*FK(4,I)+0.5*FK(5,I)
          0025      ITS=ITS+1
          0026      CALCULATE AND TESTS
          C      IF(B.LE.(1+RPS+EFIN).AND.ABS(Y(I)).LE.TOLK) GO TO 202
          C      IF(3.LT.(1+RPS).AND.Y(I).GT.0.0C) GO TO 209
          GO TO 203
          0027      202 L3=30
          0028      L1=0
          0029      L2=0
          0030      L4=0
          0031      L5=0
          0032      RETURN
          0033      209 L5=50
          0034      L1=0
          0035      L2=0
          0036      L3=0
          0037      L4=0
          0038      RETURN
          0039
          0040
          0041

```



```

0085      ON=ON+1
0086      IF(L4.EQ.40) GO TO 73
0087      DO 19 IS=1,5
0088      GQ TO (31,30,32,33,30),IS
0089      71 X=X+FMULT
0090      GO TO 30
0091      32 X=X+0.5*FMULT
0092      GO TO 30
0093      73 X=XOLD+DX
      C
0094      30 DO 10 I=1,N
0095      FK(IS,I)=FMULT*OY(I)
0096      CO TO (11,12,13,14,10),IS
      C
0097      11 Y(I)=YOLD(I)+FK(1,I)
0098      GO TO 10
      C
0099      12 Y(I)=YOLD(I)+0.5*(FK(1,I)+FK(2,I))
0100      GO TO 10
      C
0101      13 Y(I)=YOLD(I)+0.375*FK(1,I)+1.125*FK(3,I)
0102      GO TO 10
      C
0103      14 Y(I)=YOLD(I)+1.5*FK(1,I)-4.5*FK(3,I)+6.0*FK(4,I)
0104      15 CONTINUE
0105      IF(IS.EQ.5) GO TO 16
      C
0106      EVALUATE DERIVATIVES
0107      CALL DERIVS(X,N,0,ON,HX,HY)
0108      ON=ON+1
0109      IF(L4.EQ.40) GO TO 73
0110      GO TO 18
      C
0111      ON LAST INTEGRATION, EVALUATE ERROR
0112      16 DO 17 I=1,4
0113      ERR(I)=ABS(FK(1,I)-4.5*FK(3,I)+4.0*FK(4,I)-0.5*FK(5,I))
0114      18 CONTINUE
0115      GO TO 1
0116      73 L4=40
0117      L1=0
0118      L2=0
0119      L3=0
0120      L5=0
      RETURN
      END

```

\*OPTIONS IN EFFECT\* NOTERM, ID, ERCDIC, SOURCE, NOLIST, NODECK, LOAD, NOMAP, NOTEST

\*OPTIONS IN EFFECT\* NAME = MERSON , LINECNT = 50

\*STATISTICS\* SOURCE STATEMENTS = 120, PROGRAM SIZE = 3168

\*STATISTICS\* NO DIAGNOSTICS GENERATED

```

0001 SUBROUTINE DERIVS(X,N,D,ON,HX,HY)
0002 DIMENSION Y(10),DY(10),U+X(100),URY(100),TS(100),T(100)
0003 COMMON /CSP/Y/GRAD/DY/ACC/TCLNM(10)
0004 COMMON FLOW,K,G,RPS,RHOPF,H,CFIN,MH,S,NUM,L1,L2,L3,L4,L5,NSS
0005 INTEGER FLOW
0006 INTEGER ON,D,CP
0007 REAL K
0008 TOL=.00001
0009 A=Y(1)*Y(1)+Y(2)*Y(2)
0010 H=SQRT(A)
0011 Z=1/3
0012 IF(Y(1).LE.TOL) GO TO 10
0013 IF(Y(2).GT.(1+RPS)) GO TO 10
0014 C=A-1
0015 D=2*A-3*Y(2)
0016 E=Y(1)*Y(2)
0017 F=.5*45.0
0018 H=7*7.0
0019 Q=-(3*3.0)
0020 IF(FLOW.EQ.1) GO TO 1
0021 UX=-1+D/(2*F)
0022 UY=3+E/(2*F)
0023 DUX=Y(1)*(2/F-5*D/(2*H))
0024 DUY=1.5*(Y(1)/F-5*E*Y(2)/H)
0025 GO TO 4
0026 1 UX=-1+Z+C*D/(4*F)
0027 UY=2*E*C/(4*F)
0028 DUX=Y(1)*(1/3+(2*C+D)/(2*F)-5*C*D/(4*H))
0029 DUY=.75*((C*Y(1)+2*E*Y(2))/F-(5*E*C*Y(2)/H))
0030 4 DY(1)=Y(3)
0031 DY(2)=Y(4)
0032 IF(NSS.NE.1) GO TO 89
0033 DY(3)=(-G+UX-Y(3))/K
0034 DY(4)=(UY-Y(4))/K
0035 GO TO 22
0036 80 IF(FLOW.EQ.1) GO TO 90
0037 PX=0
0038 PY=0
0039 GO TO 91
0040 90 H1=.5*9.0
0041 V1=1/3+(2.5*C+1*D)/(2*F)-1.25*C*D/H
0042 V2=7/F-(10*C+5*D)/(1*H)+8.75*C*D/H1
0043 V3=1/3+(-1*C+1*D)/(2*F)-1.25*C*D/H
0044 V4=1/F+(3.5*C-5*D)/(1*H)+8.75*C*D/H1
0045 DUXXX=V1+Y(1)*Y(1)*V2
0046 DUXYY=V3+Y(2)*Y(2)*V4
0047 DUYXX=.75*(5*E/F-(15*E*C+20*Y(1)*Y(1)*E)/H+35*Y(1)*Y(1)*E*C/H1)
0048 DUYYY=.75*(5*E/F-(15*E*C+20*Y(2)*Y(2)*E)/H+35*Y(2)*Y(2)*E*C/H1)
0049 CUN=2*U+RPS/4
0050 P=CUN*(DUXXX+DUXYY)
0051 PY=CUN*(DUYXX+DUYYY)
0052 91 CONTINUE
0053 IF(ON.NE.1) GO TO 44
0054 DY(3)=0.0

```

```

0055      DY(4)=0.0
0056      23  URX(1)=-G
0057      URY(1)=-UY
0058      TS(1)=J
0059      44  CONTINUE
0060      IF(NS5.F0.3) GO TO 20
0061      22  DY(3)=[-G+UX-Y(3)+K*Y(3)*DUX*RHOPF]/K-PX/K
0062      DY(4)=[(UY-Y(4)+K*Y(4)*DUY*RHOPF)/K-PY/K
0063      GO TO 22
0064      20  IF(L1.EQ.10) GO TO 24
0065      GO TO 25
0066      24  U=J+1
0067      URX(J)=Y(3)-UX
0068      URY(J)=Y(4)-UY
0069      TS(J)=X
0070      DO 100 J=2,U
0071      T(J)=SQRT((2*TS(J)-TS(J-1)))
0072      100  CONTINUE
0073      SIGX=C.0
0074      SIGY=0.0
0075      DO 101 J=2,U
0076      SIGX=SIGX+((URX(J)-URX(J-1))/T(J))
0077      SIGY=SIGY+((URY(J)-URY(J-1))/T(J))
0078      101  CONTINUE
0079      QUE=1.69*SQRT((RHOPF/K))
0080      MX=-QUE*SIGX
0081      HY=-QUE*SIGY
0082      GO TO 22
0083      25  DY(3)=[(-G+UX-Y(3))/K+RHOPF*1.5*Y(3)*DUX+MX-PX/K]/(1+0.5*RHOPF)
0084      DY(4)=[(UY-Y(4))/K+RHOPF*1.5*Y(4)*DUY+HY-PY/K]/(1+0.5*RHOPF)
0085      22  L4=J
0086      RETURN
0087      10  L4=40
0088      RETURN
0089      END

```

\*OPTIONS IN EFFECT\* NOTERM, ID, EBCDIC, SOURCE, NOLIST, NODECK, LOAD, NOMAP, NOTEST

\*OPTIONS IN EFFECT\* NAME = DERIVS , LINECNT = 56

\*STATISTICS\* SOURCE STATEMENTS = 89, PROGRAM SIZE = 4286

\*STATISTICS\* NO DIAGNOSTICS GENERATED

\*STATISTICS\* NO DIAGNOSTICS THIS STEP

Exhibit D.6

COLLISION EFFICIENCY WITH UNSTEADY  
STATE DRAG TERMS;  
SAMPLE OUTPUT

RUN NUMBER 22

UNSTEADY STATE DRAG TERMS INCLUDED.

FLOW TYPE= POTENTIAL

K= 1.000

G= 0.015

PARTICLE RADIUS/BUBBLE RADIUS= 0.100

FLUID DENSITY/PARTICLE DENSITY= 0.400

FRACTIONAL TOLERANCE ON Y(2)= 0.0050

INTEGRATION TOLERANCE= 0.0010

<u>Y(2)O</u>	<u>H OR L</u>	<u>Y(1)F</u>	<u>Y(2)F</u>	<u>SEPARATION</u>	<u>TIME</u>
0.6500	L	0.706	0.819	-0.018	29.092
<del>0.9750</del>	H	0.761	1.100	0.238	28.968
0.8125	L	0.279	1.063	-0.001	29.445
0.8937	H	0.385	1.105	0.070	29.347
0.8531	H	0.241	1.101	0.027	29.476
0.8328	H	0.150	1.101	0.011	29.551
0.8227	H	0.103	1.101	0.005	29.589
0.8176	L	0.165	1.087	-0.000	29.539

<u>Y(1)</u>	<u>Y(2)</u>	<u>SEPARATION</u>	<u>TIME</u>	<u>HX</u>	<u>HY</u>
30.000	0.819	28.911	0.0	0.0	0.0
14.776	0.819	13.699	15.000	-0.000	-0.000
7.283	0.820	6.229	22.388	0.000	0.000
3.608	0.823	2.601	26.030	0.002	0.002
1.836	0.842	0.920	27.834	0.014	0.032
1.619	0.850	0.729	28.064	0.016	0.065
1.432	0.861	0.571	28.266	0.014	0.094
1.268	0.875	0.440	28.445	0.006	0.129
1.124	0.892	0.334	28.603	-0.009	0.164
0.996	0.911	0.250	28.744	-0.031	0.194
0.881	0.932	0.182	28.868	-0.057	0.211
0.777	0.954	0.130	28.978	-0.083	0.208
0.682	0.976	0.090	29.075	-0.104	0.180
0.595	0.996	0.060	29.161	-0.116	0.128
0.517	1.015	0.039	29.235	-0.118	0.056
0.446	1.031	0.024	29.300	-0.112	-0.027
0.383	1.046	0.014	29.355	-0.100	-0.113
0.328	1.058	0.007	29.403	-0.084	-0.195



E. FLUID VELOCITIES AND ACCELERATIONS

E.1 Stokes Flow

In polar coordinates  $(r, \theta)$  centred at the sphere centre:

$$u_{fr} = U \cos \theta \left[ 1 - \frac{3}{2} \left( \frac{R}{r} \right) + \frac{1}{2} \left( \frac{R}{r} \right)^3 \right]$$

where  $u_{fr}$  = fluid radial velocity;

$U$  = fluid velocity at an infinite distance from the sphere;

$R$  = sphere radius.

$$u_{fr}^* = \frac{u_{fr}}{U} = \cos \theta \left[ 1 - \frac{3}{2} \left( \frac{R}{r} \right) + \frac{1}{2} \left( \frac{R}{r} \right)^3 \right].$$

In dimensionless Cartesian coordinates  $(x, y)$  as used in Chapter 11 (reference length  $R$ ) the dimensionless velocities are:

$$u_x^* = \frac{u_x}{U} = - \left[ 1, - \frac{1}{(x^2 + y^2)^{3/2}} - \frac{(x^2 + y^2 - 1)(2x^2 - y^2)}{4(x^2 + y^2)^{5/2}} \right]$$

$$u_y^* = \frac{u_y}{U} = \frac{3(x^2 + y^2 - 1)xy}{4(x^2 + y^2)^{5/2}}$$

The free stream velocity  $U$  is in the minus  $x$ -direction.

$$\text{Let } A = x^2 + y^2$$

$$B = A^{3/2}$$

$$C = A - 1$$

$$D = 2A - y^2$$

$$E = xy$$

$$F = B^5$$

$$H = B^7$$

$$J = B^9$$

$$Q = -B^3$$

Then 
$$u_x^* = -1 + B + \frac{CD}{4F}$$

$$u_y^* = \frac{3EC}{4F}$$

It is easily shown by differentiation that:

$$\frac{\partial u_x^*}{\partial x} = x \left[ \frac{1}{B} + \frac{2C+D}{2F} - \frac{5CD}{4H} \right]$$

$$\frac{\partial u_y^*}{\partial y} = \frac{3}{4} \left[ \frac{Cx + 2Ey}{F} - \frac{5ECy}{H} \right]$$

$$\frac{\partial^2 u_x^*}{\partial x^2} = \frac{1}{Q} + \frac{2C+D}{2F} - \frac{5CD}{4H} + x^2 \left[ \frac{7}{F} - \frac{5(2C+D)}{H} + \frac{35CD}{4J} \right]$$

$$\frac{\partial^2 u_x^*}{\partial y^2} = \frac{1}{Q} + \frac{D-C}{2F} - \frac{5CD}{4H} + y^2 \left[ \frac{1}{F} + \frac{5(C+D)}{H} + \frac{35CD}{4J} \right]$$

$$\frac{\partial^2 u_y^*}{\partial x^2} = \frac{3}{4} \left[ \frac{6E}{F} - \frac{5E(3C+4x^2)}{H} + \frac{35x^2 EC}{J} \right]$$

$$\frac{\partial^2 u_y^*}{\partial y^2} = \frac{3}{4} \left[ \frac{6E}{F} - \frac{5E(3C+4y^2)}{H} + \frac{35y^2 EC}{J} \right]$$

E.2 Potential Flow

Symbols have the same meaning as in E.1.

In polar coordinates:

$$u_{fr}^* = \cos \theta \left[ 1 - \left( \frac{R}{r} \right)^3 \right]$$

In dimensionless Cartesian coordinates:

$$u_x^* = -1 + \frac{D}{2F}$$

$$u_y^* = \frac{3E}{2F}$$

$$\frac{\partial u_x^*}{\partial x} = x \left[ \frac{2}{F} - \frac{5D}{2H} \right]$$

$$\frac{\partial u_y^*}{\partial y} = \frac{3}{2} \left[ \frac{x}{F} - \frac{5Ey}{H} \right]$$